IMPERIAL COLLEGE LONDON

Department of Chemical Engineering and Chemical Technology

Organic Solvent Nanofiltration in the peptide industry

Academic supervisor: Prof. Andrew G. Livingston

Industrial supervisor: Dr. Alessandro Butté

By

Patrizia MARCHETTI

CID 00625273

A thesis submitted in fulfilment of the requirements for the degree of

Doctor of Philosophy of Imperial College London

2013

I certify that the work in this thesis is my own and that the work of others is appropriately acknowledged

"The copyright of this thesis rests with the author and is made available under a Creative Commons Attribution Non-Commercial No Derivatives licence. Researchers are free to copy, distribute or transmit the thesis on the condition that they attribute it, that they do not use it for commercial purposes and that they do not alter, transform or build upon it. For any reuse or redistribution, researchers must make clear to others the licence terms of this work"

Abstract

In recent years the application of membrane technology to molecular separation processes has stimulated interest and showed great potential in a number of industrial fields. Ultrafiltration membranes have been successfully applied to downstream separation of therapeutically active peptides, to overcome some of the limitations of the conventional techniques in terms of costs, scale-up, selectivity and solvent recovery. In this research project, Organic Solvent Nanofiltration of peptide solutions is studied, and this understanding is applied to the development of innovative membrane-based purification strategies for industrial case studies. Basic understanding of transport mechanisms was approached by investigating solvent transport through ceramic nano- and ultrafiltration membranes, and developing a predictive phenomenological model for the transport of solvents and solvent mixtures. Effects of solvent-membrane interactions strongly affected the solvent permeation through nanofiltration membranes, while they were found to be negligible in the ultrafiltration range. The effect of the organic solvent on the permeation of neutral and charged solutes (monovalent salts, a small molecule and peptides) in organic/water mixtures was studied, with particular attention to the role of preferential solvation in the solvent mixture. It was found that the solvent composition and the complex association of counter-ions and buffers highly affect membrane permeation and rejection of organic molecules. It is proposed that all these components change the relative solute-membrane affinity. Since permeation of peptides in organic/water mixtures is affected by complicated matrices of input parameters, a Design of Experiment approach was proposed to efficiently investigate the nanofiltration of model peptides in acetonitrile/water solutions. Statistical models for solvent flux, peptide and ion rejection were obtained by Analysis of Variance and interpreted from a phenomeno-

logical point of view. The statistical models were used to asisst process development for two industrial case studies: (1) concentration and salt/solvent exchange of a first therapeutic peptide were optimised, based on the integration of the statistical DoE models with the process simulation for concentration and diafiltration; (2) the nanofiltration-assisted synthesis of a second therapeutic peptide, based on the coupling between nanofiltration and reaction in one unique process, was developed and compared to the established process by techno-economical analysis. The so-called "Reactive Peptide Nanofiltration" was found to be advantageous in terms of economics, efficacy, impact on the market, and on the environment.

In conclusion, nanofiltration was found to be a solid and competitive technique for application to peptide processes. On the basis of the results of this research, Lonza decided to invest in a new nanofiltration plant for the downstream of peptides with ceramic membranes. The advantages of nanofiltration technology, in terms of development of more efficient materials (stable in critical solvents and harsh acid/basic conditions), improvement of membrane performances (selectivity, lifetime) and integration of nanofiltration with other techniques in hybrid processes seem therefore promising in overcoming the hesitancy of industries to modify the established processes and invest in new nanofiltration plants, by making the payback period for the return of investment more attractive. It is plausible to think that this technology will shortly become a primary choice for new separation and purification processes.

Acknowledgments

I would like to thank all the people, who have contributed to the development and completion of this work.

First of all, I would like to thank my academic supervisor, Prof. Andrew Livingston, and my industrial advisor, Dr. Alessandro Butté, for their guidance and constant encouragement. Their kind advice at many stages of the work has been fundamental for the shape of the project.

I wish to acknowledge the 7^{th} Framework Programme of the European Commission Marie Curie Initiative (Grant agreement no.: 214226-2, NEMOPUR project) for funding a studentship which enabled the conduction of this work and also thank all the colleagues from the research project, for the kind collaboration and the valuable friendship.

I would like to thank all the colleagues in Lonza and, particularly, the colleagues of the Tides group. Very special thanks to Iris, who was my "reference point" for every kind of technical issues. Thanks to Wen, for the nice time together, the moral support when I was stressed for a deadline, and the free Chinese lessons!

Thanks to Gaetano, Oriana, Marco, Stefan and Anna, my volleyball and dancing mates, and all my friends in Wallis, for the very pleasant time together during my three Swiss years. Thanks to Andrea, Danilo, and all the friends in Italy, for their "remote" support and their frequent visits.

Finally, extremely special gratitude to my family, to whom I dedicate my thesis. Thanks to my mum, Maria Rosa, and my grandparents, Antonia and Vigilio, who have always accepted and supported my decisions. Thank you for your love, comprehension and patience. Thanks to my uncle, Umberto, my aunt, Laura and my little cousin, Irene, for all the in-

terest in what I have been doing and the encouragement for many important decisions in my life. Grazie!!!

Publications

P. Marchetti, A. Butté, A. G. Livingston, An improved phenomenological model for prediction of solvent permeation through ceramic NF and UF membranes, J. Membr. Sci. 415-416 (2012) 444-458

P. Marchetti, A. Butté, A. G. Livingston, Reactive Peptide Nanofiltration, in: Sustainable Nanotechnology and the Environment: Advances and Achievements, N. Shamim, S. Virender (Eds.), ACS Symp. Ser. (2013)

P. Marchetti, A. Butté, A. G. Livingston, NF in organic/water mixtures: role of preferential solvation, J. Membr. Sci., http://dx.doi.org/10.1016/j.memsci.2013.04.069 (2013)

P. Marchetti, A. Butté, A. G. Livingston, Quality by Design for peptide nanofiltration: fundamental understanding and process selection, Chem. Eng. Sci. (accepted, 2013)

G. Székely, **P. Marchetti**, M. F. Jimenez-Solomon, A. G. Livingston, Nanofiltration Membranes in Organic Solvents, in: Encyclopedia of Membrane Science and Technology, E. M. V. Hoek and V. Tarabara (Eds.), John Wiley & Sons, Inc. (2013)

Contents

Abstract **III**

Acknowledgments **V**

Publications **VII**

Contents **1**

List of Figures **5**

List of Tables **9**

Symbols and Abbreviations **13**

1 Introduction **17**

2 Literature review **21**

2.1 Peptides 21

2.1.1 Physico-chemical properties 21

2.1.2 Synthesis 23

2.1.3 Purification/separation strategies 24

2.2 Membranes and membrane processes 25

2.2.1 Membranes 25

2.2.2 Membrane processes 27

2.2.3 Characterisation of membrane performance 29

2.3 Solute and solvent transport through membranes 29
2.3.1 Classification of transport models 30
2.3.2 Solvent and solute transport in OSN 39
2.4 Process development, or Quality by Design (QbD) 51
2.4.1 Statistical modelling by Design of Experiments (DoE) 52

3 Research strategy **57**

4 Solvent permeation through ceramic NF and UF membranes **61**
4.1 Introduction 61
4.2 Model development 63
4.2.1 Nanofluidics 63
4.2.2 Capillary rise in nanopores: Lucas-Washburn equation 65
4.2.3 The correction factor f_C 66
4.2.4 Parameter estimation and prediction 70
4.2.5 Modelling for solvent mixtures 71
4.3 Experimental 72
4.3.1 Materials 72
4.3.2 Methods 74
4.4 Results and discussion 77
4.4.1 Permeability measurements of pure solvents 77
4.4.2 Modelling for pure solvents 79
4.4.3 Permeability measurements of solvent mixtures 86
4.4.4 Modelling for solvent mixtures 88
4.5 Conclusion 93

5 Filtration in organic/water mixtures: role of preferential solvation **97**
5.1 Introduction 97
5.2 Experimental 98
5.2.1 Materials 98

5.2.2 Methods . . . 99
5.3 Results and discussion . . . 101
5.3.1 NF of salts and acids in organic/water mixtures . . . 101
5.3.2 NF of a small neutral organic molecule: case of Npys . . . 113
5.3.3 NF of a case-study peptide: PEP_1 . . . 118
5.4 Conclusion . . . 120

6 Peptide permeation through ceramic NF membranes 125
6.1 Introduction . . . 125
6.2 Experimental . . . 128
6.2.1 Materials . . . 128
6.2.2 Methods . . . 129
6.3 Results and discussion . . . 132
6.3.1 Nanofiltration of PEP_1 through Inopor Nano 750 . . . 132
6.3.2 Nanofiltration of P3 through Inopor Nano 450 . . . 138
6.3.3 Nanofiltration of P2-S-SH through Inopor Nano 750 . . . 141
6.3.4 Summary of the effects of operating parameters . . . 144
6.4 Conclusion . . . 147

7 Case-study 1: peptide concentration and diafiltration 149
7.1 Introduction . . . 149
7.2 Experimental . . . 151
7.2.1 Materials . . . 151
7.2.2 Methods . . . 153
7.3 Results and discussion . . . 155
7.3.1 Numerical optimization of DoE models . . . 155
7.3.2 Diafiltration experiments and model validation . . . 155
7.3.3 Extension of results from looser (Inopor Nano 750) to tighter membrane (Inopor Nano 450) . . . 162
7.3.4 Simulation and process selection . . . 163

7.4 Conclusion 166

8 Case-study 2: Reactive Peptide Nanofiltration 169

8.1 Introduction 169

8.2 Fragment condensation by disulfide bond 170

8.2.1 Conventional production 170

8.2.2 Reactive Peptide Nanofiltration 172

8.3 Experimental 173

8.3.1 Materials 173

8.3.2 Methods 174

8.4 Results and discussion 176

8.4.1 Reaction kinetics 176

8.4.2 Calculation of kinetic constants 177

8.4.3 Rejection tests for membrane selection 180

8.4.4 Reactive Peptide Nanofiltration feasibility 185

8.4.5 Process modelling and cost evaluation 188

8.5 Conclusion 193

9 Conclusions and future perspectives 195

Bibliography 201

A Calculation of the preferential solvation parameter - Quasi-Lattice Quasi-Chemical (QLQC) theory 213

B Experimental design and results of peptide nanofiltration (cf. Chapter 6) 219

List of Figures

2.1 Structure of the peptide bond that links individual amino acids to form a protein polymer. 22

2.2 Schematic representation of ceramic membrane. 26

2.3 Schematic representation of membrane filtration processes for liquid applications. 27

2.4 Dead-end and cross-flow lab-scale modules. 28

2.5 Chemical potential, pressure, and solvent activity profiles for permeation of a one-component solution through a membrane according to solution-diffusion and pore-flow transport models (adapted from Wijmans and Baker [23]). . . 33

2.6 Competition between solute-membrane and solvent-membrane affinities. . . . 46

2.7 Interfacial water near the surface of a hydrated solute (adapted from Collins [70]). 49

2.8 Full Factorial Experimental and Fractional Factorial Experimental designs. . 54

4.1 Schematic representation of the fluid velocity profile in confined geometries. (a) Velocity profile without slip; (b) velocity profile with slip. 64

4.2 Relationship between dielectric constant and dipole moment for different classes of solvent polarity. 68

4.3 Natan cross-flow system (Natan GmbH, CH). Close loop for permeation tests. 76

4.4 Experimental permeability of organic solvents and water in the NF range and best linear fitting (R^2). 78

4.6 Prediction of permeability by Hagen-Poiseuille, coupled series-parallel resistance and new models in the NF and UF range. 84
4.7 Profiles of permeability and viscosity vs. solvent composition of aqueous mixtures. Membrane: Inopor Nano 750 Da. 87
4.8 Profiles of permeability and viscosity vs. solvent composition of organic mixtures. Membrane: Inopor Nano 750 Da. 87
4.9 Profiles of permeability and viscosity vs. solvent composition for the ACN/water mixture. Membrane: Inopor Nano 750 Da. 88
4.10 Prediction of permeability of aqueous mixtures by the new model in the NF range. (—) ethanol/water; (– –) methanol/water; (· · ·) DMF/water. 89
4.11 Prediction of permeability of ACN/water mixtures by the new model. 89
4.12 Prediction of permeability of organic mixtures by the new model. (– –) Inopor Nano 450 Da; (—) Inopor Nano 750 Da; (· · ·) Sulzer 1000 Da; (– · –) Inopor Nano 2000 Da. 91
4.13 Profile of the solvent radius for ACN/water mixtures as function of the composition. 93
4.14 Prediction of permeability of ACN/water mixtures by the new model taking into account the formation of complexes between ACN and water molecules. (—) prediction without considering complexes; (– –) prediction with considering complexes. 94

5.1 Structure of Npys at pH 2 to 6. 99
5.2 NaCl rejection and permeability during NF of NaCl in water (c_{NaCl} = 1 mM). 103
5.3 Effect of NaCl concentration on NaCl rejection and permeability (P = 6 bar). 106
5.4 Effect of solvent on NaCl rejection % (values for rejection in brackets). Membrane: Inopor Nano 450 Da. 109
5.5 Rejection of Npys in different ACN/water mixtures. c_{Npys} = 1 mM. 113
5.6 Effect of HCl and TFA concentration on Npys rejection. c_{Npys} = 1 mM; $c_{NaCl} = c_{HCl} = c_{TFA}$ = 10 mM. 115

5.7 Interfacial water near the surface of hydrated Nyps, as a function of the ion nature. . . . 116
5.8 Rejection of HCl and TFA-H during NF of Npys solutions. c_{Npys} = 1 mM; $c_{HCl} = c_{TFA-H}$ = 10 mM. . . . 117
5.9 Interfacial water near the surface of hydrated PEP_1, as a function of the ion nature. . . . 121

6.1 Peptide charge as a function of pH ($pK_{COOH} < pK_r < pK_{NH_3^+}$) and schematic representation of a spherical micelle. . . . 126
6.2 Interaction B-E for PEP_1 rejection by Design Expert Software (actual factors: $C_{peptide}$ = 3.00; Pressure = 6.00; Pump frequency = 35.00). . . . 135

7.1 Downstream process for PEP_1. . . . 150
7.2 Natan cross-flow system (Natan GmbH, CH). Open loop for diafiltration tests. 152
7.3 Concentration + diafiltration sequence. . . . 153
7.4 Schematic representation of filtration process. . . . 154
7.5 Actual concentration + diafiltration sequence, due to TFA-H rejection. . . . 157
7.6 Concentration step (A → A') for PEP_1 through Inopor Nano 750 Da. P = 8 bar. . . . 158
7.7 Diafiltration 1 (a' → b') for PEP_1 through Inopor Nano 750 Da. P = 8 bar. 158
7.8 Diafiltration 2 (b' → c') for PEP_1 through Inopor Nano 750 Da. P = 8 bar. 159
7.9 Diafiltration 3 (c' → d') for PEP_1 through Inopor Nano 750 Da. P = 8 bar. 159
7.10 Diafiltration 4 (d' → e') for PEP_1 through Inopor Nano 750 Da. P = 8 bar. 160
7.11 Diafiltration 5 (e' → b') for PEP_1 through Inopor Nano 750 Da. P = 8 bar. 160
7.12 Possible diafiltration paths for salt and solvent exchange. . . . 163

8.1 Conventional process for the production of P3. . . . 171
8.2 Reactive Peptide Nanofiltration for the synthesis of P3. . . . 172
8.3 Batch production of P3 as function of pH. (o) experimental data; (–) complete kinetics; (- -) simplified kinetics. . . . 179
8.4 k_{main} as function of pH. (o) experimental data; (–) fitting function 8.17 . . . 179

8.5 Effect of pH during Reactive Peptide Nanofiltration through Inopor Nano 450 Da. 186
8.6 Reaction and flux profiles for the Reactive Peptide Nanofiltration at pH = 4 through Inopor Nano 450 Da. 187
8.7 Rejection of SM during Reactive Peptide Nanofiltration through Inopor Nano 450 Da. 188
8.8 Effect of pH during Reactive Peptide Nanofiltration through Inopor Nano 450 Da. (o) experimental data; (-) simulation. 189
8.9 Effect of peptide concentration and organic content during Reactive Peptide Nanofiltration through Inopor Nano 450 Da. (o) experimental data; (-) simulation. 190

List of Tables

2.1 Summary of the solvent, membrane and interaction parameters in the models from literature 40

4.1 Solvents used in this study and their characteristics 73
4.2 Solvent mixtures used in this study 74
4.3 Membranes used in this study and their characteristics, as provided by the supplier 75
4.4 Contact angle values for water (θ_w) and glycerol (θ_g) and surface tension values for the materials according to the theory of surface induced polarity . 75
4.5 Hagen-Poiseuille proportionality constants and coefficient of determination (R^2) of the linear fitting 78
4.6 Fitting parameters for Hagen-Poiseuille, coupled series-parallel resistance and new models 81
4.7 Capillary, dipole and steric membrane parameters 81
4.8 Capillary, dipole, steric and global correction terms for water 82
4.9 Capillary, dipole, steric and global correction terms for toluene 82
4.10 Standard deviations, σ_{L_p} of coupled series-parallel resistance, Hagen-Poiseuille and new model 85

5.1 NaCl rejection vs. Na^+ and Cl^- preferential solvation parameters and Hansen solubility parameters. P = 6 bar; C_{NaCl} = 1 mM. 104
5.2 Effect of pore dimension on NaCl rejection and permeability (70%v ACN/water; c_{NaCl} = 100 mM; P = 8 bar). 108

5.3 Effect of cation on salt rejection and permeability in 70%v ACN/water ($S_{Hansen,bulk}$ = 31.4) through Inopor Nano 450 Da. Common anion: Cl^-, salt concentration = 100 mM, P = 8 bar. 111

5.4 Effect of anion on salt rejection and permeability in 70%v ACN/water ($S_{Hansen,bulk}$ = 31.4) through Inopor Nano 450 Da. Common cation = Na^+, salt concentration = 10 mM, P = 8 bar. 111

5.5 Effect of anion on salt rejection and permeability in water and 70%v ACN/water ($S_{Hansen,bulk}$ = 31.4) through Inopor Nano 450 Da. Common cation = H^+, salt concentration = 10 mM, P = 8 bar. 112

5.6 Permeability [l m^{-2} h^{-1} bar^{-1}] during NF of Npys solutions through Inopor Nano 450 Da. P = 12 bar. In brackets rejection % of the corresponding acid. 114

5.7 Effect of %v ACN on PEP_1 rejection %, TFA^- rejection % and solvent permeability through Inopor Nano 750. %v TFA = 0.02; P = 10 bar. 119

5.8 Effect of %v TFA on PEP_1 rejection %. c_{PEP_1} = 1 g l^{-1}; c_{ACN} = 2%v; P = 4 bar. 119

6.1 Physico-chemical properties of the peptides studied in this work. 128

6.2 Experimental design for nanofiltration of PEP_1 solutions through Inopor Nano 750. 130

6.3 Experimental design for nanofiltration of P3 solutions through Inopor Nano 450. 131

6.4 Experimental design for nanofiltration of P2-S-SM solutions through Inopor Nano 750. 131

6.5 Statistical analysis of the models for PEP_1 rejection, TFA-H rejection and solvent flux. 133

6.6 ANOVA result for Rej_{PEP_1} 134

6.7 Statistical analysis of the models for P3 rejection, TFA-H rejection and solvent flux. 139

6.8 Statistical analysis of the models for P2-S-SH rejection and flux. 142

6.9 Summary of the effects of the main operating parameters on peptide rejection and flux for PEP_1, P3 and P2-S-SM (ns = not significant). 145

6.10 Effect of the main operating parameters on TFA-H rejection. 146

7.1 Optimised set of operating parameters and corresponding responses. 156

7.2 Rejection and permeability at the end of each diafiltration test. 162

7.3 Effect of pore dimension. C_{PEP_1} = 17.5 g l^{-1}; P = 8 bar; Pump frequency = 35 Hz; %v ACN = 30; %v TFA = 0.1. 162

7.4 Simulation of constant volume diafiltration for Inopor Nano 750. V = 1 l; C_{PEP_1} = 15 g l^{-1}. 164

7.5 Simulation of constant volume diafiltration for Inopor Nano 450. V = 1 l; C_{PEP_1} = 15 g l^{-1}. 165

7.6 Operating time [min] for constant volume and variable volume diafiltration. . 166

8.1 Physico-chemical properties for the species involved in the reaction. 171

8.2 Kinetic constant as function of organic content and temperature (pH = 4). . 180

8.3 Rejection of P1-SH in ACN/water solutions. 181

8.4 Rejection of P2-S-SM in ACN/water solutions. 182

8.5 Rejection of P3 in ACN/water solutions. 182

8.6 Rejection of SM in ACN/water solutions. 184

8.7 Conventional process and relative working conditions. 191

8.8 Reactive Peptide Nanofiltration and relative working conditions. 192

8.9 Cost comparison of conventional process with Reactive Peptide Nanofiltration (CHF = Swiss francs). 193

A.1 Standard molar Gibbs energies of transfer of ions [kJ mol^{-1}] from water to non-aqueous solvents at 298.15 K. For TFA^-: simulation in COSMOthermX. 215

A.2 The binary solvent systems studied and their excess Gibbs free energy of mixing 217

B.1 Experimental design and results for nanofiltration of PEP_1 solutions through Inopor Nano 750. 220
B.2 Experimental design and results for nanofiltration of P3 solutions through Inopor Nano 450. 221
B.3 Experimental design and results for nanofiltration of P2-S-SM solutions through Inopor Nano 750. 222

Symbols and Abbreviations

b_i	estimated constant of DoE model
c_i	concentration of species i [mol m^{-3}]
C_i	empirical fitting parameter
d_s	solvent molecular diameter [m]
f_1	membrane parameter characteristic of the NF layer [m s^{-1}]
f_2	membrane parameter characteristic of the UF layer [m s^{-1}]
$f_{C,i}$	correction factor for solvent i [-]
$f_{C,mix}$	correction factor for solvent mixtures [-]
J	solvent flux [l m^{-2} h^{-1}]
k_i	empirical fitting parameter
K_{HP}	Hagen-Poiseuille proportionality constant [m]
$K_{i,a}$	equilibrium constant of reaction i [-]
$k_{i,(d/i)}$	kinetic constant of direct and inverse reaction i [l mol^{-1} min^{-1}]
k_{pol}	membrane polarizability [-]
l	membrane thickness [m]
L_p	solvent permeability [l m^{-2} h^{-1} bar^{-1}]
m_i	mass of species i [mol]
MW	solvent molecular weight [g mol^{-1}]
p_C	capillary pressure [bar]
Δp	transmembrane pressure [bar]
Q_i	volumetric flow rate of species i [m^3 s^{-1}]

Rej_i	rejection of species i [%]
r	reaction rate [mol m^{-3} s^{-1}]
r_p	pore radius [m]
r_s	solvent radius [m]
R_i	reaction rate of species i [mol m^{-3} s^{-1}]
$S_{Hansen,i}$	Hansen solubility parameter of species i [-]
t	time [s]
V	volume [m^3]
V_m	solvent molar volume [m^3 mol^{-1}]
x_i	mole fraction of component i
X_{sm}	friction factor [-]
X_i	independent parameter of DoE model
$\hat{Y}$	response value of DoE model

γ_{SV}	solid surface tension [mN m^{-1}]
γ_{LV}	liquid surface tension [mN m^{-1}]
δ	slip length [m]
δ_p	dipole moment [D]
$\delta x_{s,i}$	preferential solubility parameter of species i
ϵ	porosity [-]
ϵ_L	solvent dielectric constant [-]
ϵ_S	membrane dielectric constant [-]
μ	solvent viscosity [mPa s]
ν_i	stoichiometric coefficient of species i [-]
ρ_L	solvent density [g ml^{-1}]
τ	tortuosity [-]
ϕ	solvent sorption value [-]
σ	reflection coefficient [-]

σ_{L_p}	percentage standard deviation [-]
θ	contact angle [°]

ACN	Acetonitrile
API	Active Pharmaceutical Ingredient
DoE	Design of Experiments
DMF	Dimethylformamide
DMSO	Dimethylsulfoxide
HPLC	High Performance/Pressure Liquid Chromatography
ICH	International Conference of Harmonization
MWCO	Molecular weight Cut-Off
NF	Nanofiltration
Npys	3-Nitro-2-pyridinethiol
OSN	Organic Solvent Nanofiltration
QbD	Quality by Design
RO	Reverse osmosis
TFA-H	Trifluoroacetic acid
UF	Ultrafiltration

Chapter 1

Introduction

Spending on R&D into new medicines for improving human health and quality of life has enormously increased over the past decades. The economics of the pharmaceutical industry are relentlessly applying pressure to shorten timelines for new chemical entities, in order to make new medicines reach the patients faster. Expectations of patients regarding the efficacy, safety and purity of medicines have surged in parallel.

Peptides are attractive targets for drug discovery because they have been shown to be diagnostically and therapeutically important in many areas of biomedical research [1]. The increasing interest in peptides as pharmaceuticals has been challenging the peptide industry to develop economically competitive methods for manufacturing peptides in large quantities. Chemical syntheses and purifications for peptides are usually carried out in organic solvents (such as acetonitrile, dimethylformammide, N-methylpyrrolidone, tetrahydrofuran and different alcohols) or their aqueous mixtures. Syntheses are carried out in batch reactors and comprise different chemical steps, normally separated by intermediate purifications and isolations. Among the various steps belonging to development and manufacturing of peptides and their intermediates, separation and purification are often the most critical in terms of time and costs: 50 to 90% of the capital investment costs in the chemical industry involve separation processes [2]. Conventional separation techniques include chromatography on silica or other polymeric supports, crystallization and phase separations (such as extraction). These techniques are widely employed and commercially available, but have

limitations in costs, scale up, applicability, selectivity and solvent recovery. New technologies based on membrane separation have been proposed to meet the challenge, in order to perform concentration, separation, salt and solvent exchange of peptide solutions. Additionally, some authors have proposed to use NF to assist organic synthesis, enhance the production of target compounds [3], and assist in the production of peptides [4].

Membrane science technology made big progress in the '80s with the commercialization of inorganic membranes, membranes that, thanks to their intrinsic peculiarities, enlarged the application range of this technology to new areas, in which polymeric membranes were not suitable. Inorganic membranes are suitable for applications to peptide processes, due to their good thermal and chemical stability, long lifetime (years) and resistance to multiple and/or aggressive washing. Typical processes for concentrating and purifying peptides are characterised by complicated matrices of input and output parameters. Peptide retention strongly depends on the mixture composition, since organic solvents and salts in the mixture affect the hydrophilic/phobic properties of the peptide and, in turn, the affinity between the peptide and the membrane. Additionally to steric exclusion, ternary solute-solvent-membrane interactions govern peptide and solvent permeation.

Describing, and possibly predicting, fluxes and rejections for a certain membrane requires the understanding of the transport mechanism of solutes and solvents through the membranes. This knowledge is fundamental for the application of mathematical models, which can give a clear, physico-chemically correct image of the transport mechanism and allow process development and optimization. Different models have been identified to describe the transport through membranes, however the understanding of the transport through porous structures is still open research.

From the point of view of industrial applications, the advantages of NF over conventional techniques are still not enough attractive to persuade industries to undertake modification of many established processes. Improvement of membrane performances (selectivity, lifetime) and integration of NF with other techniques in hybrid processes could address this hesitancy, by making the payback period for the return of investment more attractive for the chemical and pharmaceutical industries. Process development, at large scale, is largely improved

by fundamental research at lab scale and integration of transport modelling with process modelling should become the key point for an efficient process development. Fundamental research supporting process development is addressed in this work.

Chapter 2

Literature review

2.1 Peptides

2.1.1 Physico-chemical properties

Peptides are polyamides composed of α-amino acids joined together by peptide bonds between the carboxyl and amino groups of adjacent amino acid residues. Whether the resultant polymer is classified as a peptide or a protein is not clearly defined; some authors [5] assume that a chain length more than 20-30 residues confers protein status, whilst the term (poly)peptide can be used to cover all chain lengths. Other authors [6] attribute the term protein to a complete biological molecule in a stable conformation and the term (poly)peptide to a linear chain of amino acids lacking a stable three-dimensional structure. Other authors [7], finally, eliminate the "barrier" between peptides and proteins, because from the point of view of the synthesis or biological function of these compounds, such a barrier does not exist.

Although superficially similar, peptides display a wide variety of biological functions and physiological properties. Generally speaking, peptides can be (i) structural molecules in tissue, with structural or mechanical functions; (ii) enzymes, which catalyze biochemical reactions; (iii) antigens to raise antibodies; (iv) neurotransmitters, with functions in cell signalling and immune responses; (v) hormones, with functions in controlling physiological

processes. Their different functions depend on the sequence of amino acids and the specific nature of individual side-chains in the molecule.

All amino acids possess common structural features, including an α-carbon to which an amino group, a carboxyl group, and a variable side chain are bonded. The simplest amino acid is glycine, for which the side chain is an hydrogen atom, so there are no streochemical conformations of glycine. For all the other amino acids, two arrangements of substituents around the central α-carbon atom are possible, so they exist in two enantiomeric forms, known as L-isomers for the natural amino acids and D-isomers for those with the opposite configuration. Once linked in the protein chain, an individual amino acid is called a residue, and the linked series of carbon, nitrogen, and oxygen atoms are known as the main chain or protein backbone, as shown in Figure 2.1. The end of the protein with a free carboxyl group is known as the C-terminus or carboxy terminus, whereas the end with a free amino group is known as the N-terminus or amino terminus.

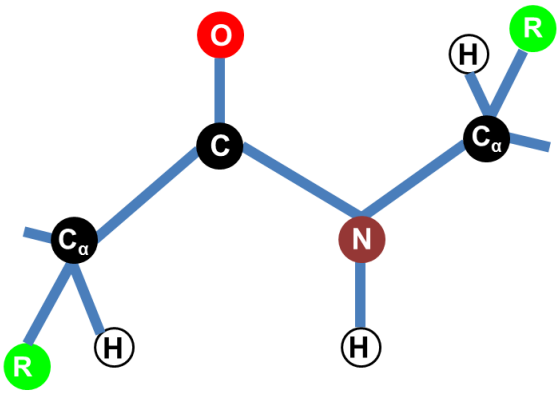


Figure 2.1: Structure of the peptide bond that links individual amino acids to form a protein polymer.

Each functional group of the amino acids exists in the protonated or unprotonated form. The ionic state of a functional group is dictated by two parameters: its chemical nature and the pH of the environment. For practical purposes, chemists characterise their acid-base behaviour in terms of the logarithm of the acid dissociation constant of the group, designated pK_a, which corresponds to the pH at which one-half of the molecules are protonated and one-half are not protonated. The pK_a of the functional groups are influenced by adjacent groups and groups in proximity - that is, the environment [8]. Organic and

inorganic salts are often present in the peptide mixture as counter-ions, associated with the charged sites of the peptide.

The isoeletric point (pI) of a polypeptide is of practical importance in many separation procedures, both analytical and preparative [9]. The pI is defined as the pH at which the net charge of the peptide is zero. Contributing to the net charge are terminal amino acids and charged side-chains within the sequence. A theoretical pI value can be calculated by using the primary structure and incluing positive and negative contributions from charged amino acids, as proposed by Skoog et al. [9].

2.1.2 Synthesis

Although peptide drugs have been on the market for decades, it is only in the last 10 to 15 years that the pharmaceutical industry really started to work seriously on the development of a new generation of peptide-based therapeutics, prompted by advances in the understanding of the genetics of diseases. The number of chemically synthesised peptide therapeutics on the market has grown from less than ten in 1990 to more than 40 a decade later [10]. In 2011, about 65 peptide-based drug products have reached approval [11] and several hundred peptides are in various stages of preclinical and clinical development. Small peptides composed of fewer amino acids can be efficiently prepared in solution, using orthogonally protected amino acids which allow for the construction of the peptide with protecting groups on the reactive side chain, or with the newer technique of solid-phase peptide synthesis, developed by Merrifield in 1963 [12]. Although the solid-phase peptide synthesis is currently the most widely used technology, since it solves the critical purification problems encountered in solution phase synthesis, it faces serious challenges including mass transfer, steric hindrance and resin handling. Furthermore, it is difficult to scale-up due to the presence of swelling effects within the solid resin. For this reason, a number of authors [13, 14] have proposed a return to solution phase synthesis, and suggested soluble polymers (polyethylenglycol or polyethylenglycol derivatives) as supports for the chain growth. They attempted to solve the purification problems coupling membrane separation to solution phase synthesis [14], in order to combine the advantages of “classical” solution

phase synthesis with the ease of purification of the solid phase method [13].

Stepwise elongation, in which the amino acids are connected step-by-step, is ideal for small peptides containing few amino acid residues, while fragment condensation of medium-short peptide chains (usually pre-synthesised by stepwise elongation) is more suitable for longer peptides. One particular type of fragment condensation reaction is the one between the thiol groups of cysteine residues, which creates a disulfide bond (S-S) via nucleophile attack. Thiol protecting, or activating, groups are normally used to inhibit, or activate, the sulfur reactivity of one of the two reacting fragments [15], and are released as side products of the fragment condensation reaction. The issues concerning this kind of fragment condensation, and its improvement by integrating nanofiltration technology with a chemical reaction, are presented for one industrial case study in Chapter 8.

2.1.3 Purification/separation strategies

Purification/separation strategies are usually based on a combination of separation methods which exploit the physiochemical properties of the synthetic molecule: size, charge, hydrophilicity/hydrophobicity. Among the classical techniques for peptide concentration, purification and recovery there are high performance/pressure liquid chromatography (HPLC) processes (such as size-exclusion chromatography, ion-exchange chromatography, partition chromatography and reverse-phase chromatography), extraction and crystallization / precipitation processes. In the chemical and pharmaceutical industries, conventional separations are often material and energy intensive, and difficult to achieve at large scale. Furthermore, the majority of industrial separation processes involve thermal operations, such as distillation, which are deleterious for heat-sensitive molecules, such as peptides. For these reasons, solvent nanofiltration represents a competitive alternative with benefits in terms of economy, environment and safety [2]. The incentives to apply nanofiltration are numerous: thermal damage can be minimised during the separation, due to the low operating temperature, compared with distillation; it is possible to recycle solvents and/or valuable compounds; energy consumption is low with respect to alternative unit operations such as distillation and crystallization; athermal solvent exchange can be performed,

permitting the solvent exchange from a high-boiling to a low-boiling solvent; concentration/purification and solvent exchange can be performed at the same time by means of diafiltration; NF can be easily installed in a continuous process or combined with existing processes into a hybrid process; finally, upscaling is simpler than for other conventional techniques, such as crystallization and chromatography [16].

Although the advantages of membrane technology over conventional techniques are clear, there is a general hesitancy of the chemical industry to implement this new technology at a large scale. The three main reasons are probably the lack of robustness of commercial membranes in organic solvents, the lack of tools to model/predict nanofiltration performance, compared to conventional purifications, and the need of investment costs to install nanofiltration systems. Designing and preparing membranes with the required nanostructure to allow molecular scale separations is an on-going challenge and currect research is towards the development of new membranes, stable in organic solvents and more selective for solutes with similar size and physico-chemical properties. Furthermore, research is towards the improvement of nanofiltration processes, in order to overcome some of the intrinsic mass-transfer limitations of the technique, such as concentration polarization, [17], and the integration of nanofiltration units with conventional separation techniques in hybrid processes [18], in order to enhance the overall purification/separation performance. The improvement of nanofiltration performance is necessary to make the payback period for the return on the investment attractive and stimulate the chemical and pharmaceutical industries to invest in new filtration plants.

2.2 Membranes and membrane processes

2.2.1 Membranes

Membranes are generally classified according to their materials and applications. According to the material which constitutes the membrane, membranes are divided into polymeric, ceramic, and mixed inorganic-organic. Common polymeric materials are cellulose acetate, polyamides, polysulfones, polyimide, poly-ethersulfone, poly-ether ether ketone,

poly-vinylidene fluoride and poly-acrylonitrile. According to the preparation, polymeric membranes can be symmetric, asymmetric or thin-film composite asymmetric. Symmetric and integrally skinned asymmetric membranes are composed of a single material; composite membranes, on the other hand, are obtained from two different materials connected at an interface.

Membrane science technology made a big progress in the '80s with the commercialization of inorganic membranes, membranes that, thanks to their intrinsic peculiarities, enlarged the application range of this technology to new areas, in which polymeric membranes were not suitable [19]. Inorganic membranes are usually fabricated with a tubular shape, with one single channel or with complex multichannel geometries. The feed flows inside the channels, while the permeate goes out in a radial direction through the porous support and the active layer, in order to be finally collected at the outside, as shown in Figure 2.2.

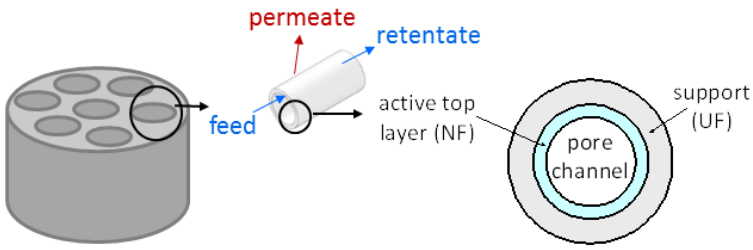


Figure 2.2: Schematic representation of ceramic membrane.

The most interesting aspect is that these membranes comprise highly versatile materials (usually aluminum oxide (Al_2O_3), zirconium oxide (ZrO_2), titanium oxide (TiO_2), silicon oxide (SiO_2) and silicon carbide (SiC)), which can overcome many of the disadvantages associated with polymeric materials, such as application in conditions of high temperature, high pressure and backflushing. Further advantages of these membranes are inertness to chemical agents and solvents; applicability over wide ranges of temperature and pH and at medium-high pressure; good thermal and chemical stability; long lifetime (years) and resistance to multiple and/or aggressive washing; ability to work in backflushing conditions (possibility to operate backflushing during cleaning); and possibility of dry storage after use. Their surface charge can be easily modulated by modifying the pH of the external solution

and their intrinsic hydrophilicity can be adjusted by chemically modifying the nature of the surface, usually with silane or silane derivatives [20, 21]. Disadvantages are connected to their intrinsic fragility (they can break if subjected to vibrations or collisions, therefore cavitations and quick pressure increases have to be avoided), their usually larger minimum pore dimension compared to polymeric membranes, and their high cost [19].

A module housing serves as a container for one or several filter elements. According to the needs of the application, the housing is made of stainless steel or other corrosion resistant materials.

2.2.2 Membrane processes

Membrane applications in liquids can be grouped in three main categories: (i) concentration; (ii) separation/purification; and (iii) constant-volume or variable-volume diafiltration, as shown in Figure 2.3.

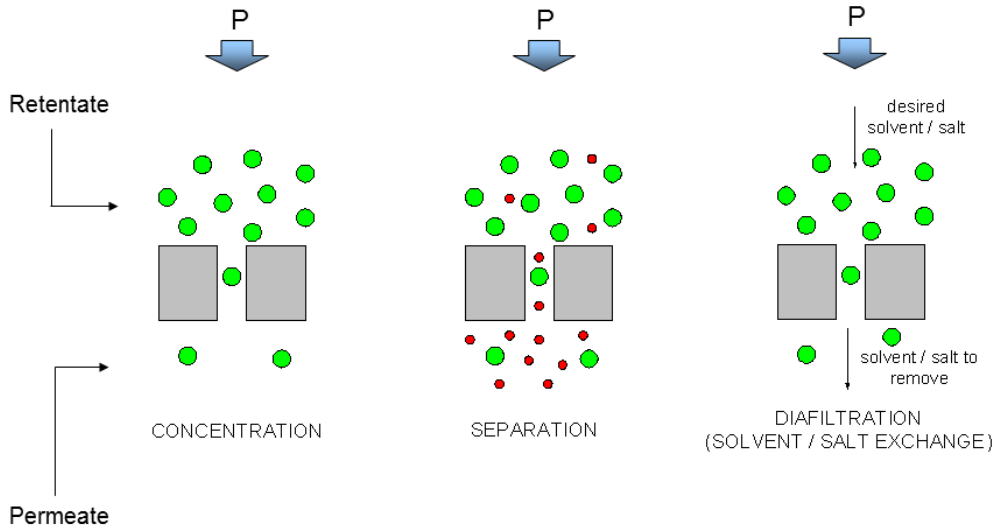


Figure 2.3: Schematic representation of membrane filtration processes for liquid applications.

Separation processes are affected by the effectiveness of the membrane in separating solutes of determined properties. Diafiltration is used to perform salt and solvent exchange, often required in the downstream of pharmaceutical and chemical production.

The two main lab-scale configurations of a NF system are the dead-end and the cross-flow modes, shown in Figure 2.4.

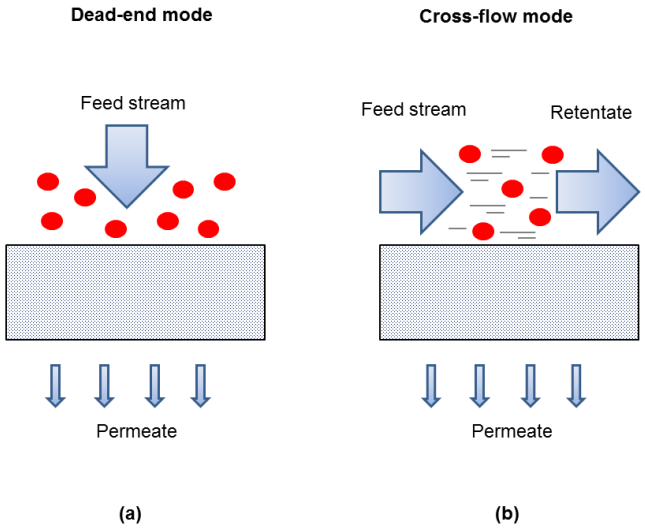


Figure 2.4: Dead-end and cross-flow lab-scale modules.

The dead-end filtration mode (cf. Figure 2.4(a)) is characterised by fluid flow in the same direction as the applied pressure; it is useful for membrane screening and proof of concept work. In dead-end cells, concentration polarization can significantly affect the membrane performance even at low solute concentration values. Concentration polarization occurs in a thin film layer at the membrane surface, when the back diffusion of the solute towards the bulk of the retentate, caused by the difference in concentration between film layer and bulk, cannot balance the convective flow of the solute towards the surface, caused by the applied pressure. A consequence is the accumulation of solute at the membrane surface and a larger effective retentate concentration at the membrane-fluid interface, as compared to the fluid bulk. Cross-flow filtration mode (cf. Figure 2.4(b)), in which the flux flows tangentially over the membrane surface and perpendicularly to the applied pressure, allows better operating conditions, as it can reduce the extent of concentration polarization by increasing the shear rate at the membrane surface. In both modes, however, osmotic pressure, gel layer formation, or other boundary layer related phenomena have to be taken into account, when working at significant solute concentrations [22]. High cross-flow velocity is normally

desired, to minimise the occurence of concentration polarization and adsorption; however it cannot be increased indefinitely for peptide applications, since peptides are shear-sensitive molecules. Typical cross-flow velocity for peptide applications is 2 - 4 m s^{-1}.

2.2.3 Characterisation of membrane performance

Membranes are usually characterised by their nominal Molecular Weight Cut-Off (MWCO), which is defined as the smallest globular solute molecular weight for which the membrane has at least a 90% rejection ($\mathrm{Rej}_i(\%) > 90$):

$$Rej_i = 100\left(1 - \frac{c_{i,P}}{c_{i,R}}\right) \tag{2.1}$$

$c_{i,P}$ and $c_{i,R}$ are the concentrations of species i in the permeate and in the retentate, respectively.

Although the MWCO is the most common way to characterise the membranes in water, for the majority of processes in organic solvents, it is not sufficient alone to describe the membrane behaviour. Since the solute retention is influenced by the organic solvent, different rejection profiles for the same molecules in different organic solvents have been observed, compromising the usefulness of the MWCO as a general descriptor for the membrane. Unification of testing systems (solute and solvent mixtures) is strongly suggested, to allow a proper comparison of commercial membranes.

2.3 Solute and solvent transport through membranes

Describing, and possibly predicting, fluxes and rejections for a specific membrane requires the understanding of the transport mechanism of solutes and solvents through porous or dense membranes. This knowledge is fundamental for the development of mathematical models, which can give a clear, physico-chemically correct image of the transport mechanism. Three kinds of models have been identified to describe transport through membranes. The first group originates from irreversible thermodynamics and treats the membrane as a black-box. It does not account for any membrane property. The two other groups account

for membrane properties and describe the transport of solutes as function of structural and physico-chemical parameters. These models are the solution-diffusion [23] and pore-flow models [24, 25], respectively. Transient transport mechanisms have also been developed, which have the characteristics of both pore-flow and solution-diffusion models [26]. A review of the main classes of models is presented here, with particular attention given to their applicability to solute and solvent transport in non-aqueous solutions.

2.3.1 Classification of transport models

Irreversible thermodynamics

In this class of models, transport is considered as an irreversible process during which free energy is dissipated continuously and entropy is produced. The first two models based on irreversible thermodynamics were the Kedem-Katchalsky [27] and the Spiegler-Kedem [28] models, which were also the first models giving description of ion transport through NF membranes [16]. They described the process by means of phenomenological equations, considering the membrane as a black box containing no description of ion transport. Thus, it is not possible to characterise the structural and electrical properties of the membrane itself.

According to the Kedem-Katchalsky model:

$$V = L_p \left(\Delta p - \sigma \Delta \pi\right) \tag{2.2}$$

$$J_i = P_i \Delta c_i + (1 - \sigma) V \bar{c}_i \tag{2.3}$$

V and J_i are the solvent velocity and the solute flux, respectively. L_p is the mechanical filtration coefficient of the membrane, or local permeability, and P_i is the permeability of the solute i. σ is the reflection coefficient, corresponding to the solute fraction rejected by the membrane. $\bar{c}_i$ is the average solute concentration in the membrane and $\Delta\pi$ is the osmotic pressure.

According to the Spiegler - Kedem model:

$$J_i = -P_i l \left(\frac{dc_i}{dx}\right) + (1-\sigma)V\bar{c}_i \tag{2.4}$$

The first and second term represent the contributions of diffusion and convection, respectively. The permeability of species i, P_i, and the reflection coefficient, σ, are obtained by fitting of experimental rejection vs. flux, according to the following equation:

$$Rej = \frac{(1-F)\sigma}{1-\sigma F} \tag{2.5}$$

where:

$$F = e^{\left[-\frac{V(1-\sigma)}{\bar{P}_i}\right]} \tag{2.6}$$

$$\bar{P}_i = \frac{P_i}{l} \tag{2.7}$$

l is the membrane thickness. The contributions of convection and diffusion in Equation 2.4 can be singularly quantified and compared. The model can be easily extended to all kinds of solvent systems, since σ and P_i are fitting parameters.

Concentration and pressure gradients in the membrane

In the class of models that account for membrane properties, the overall driving force producing movement of a permeant is the gradient in its chemical potential [23]. Thus, the flux, J_i, of the component i, becomes:

$$J_i = -L\frac{d\mu_i}{dx} \tag{2.8}$$

where L is the coefficient of proportionality (not necessarily constant) between flux and driving force and μ_i the total chemical potential of species i. μ_i can be subdivided in a chemical potential depending on pressure, temperature and concentration gradients and an electrochemical potential depending on electromotive force. This unifying approach is very useful for processes that involve more than one driving force, for example, pressure

and concentration in RO and NF. Restricting the study to driving forces generated by concentration and pressure gradients, the chemical potential is given by:

$$d\mu_i = RTdln(\gamma_i c_i) + V_i dp \tag{2.9}$$

where c_i is the molar concentration, γ_i the activity coefficient, V_i the molar volume of species i, and p the pressure. For incompressible phases the equation can be further simplified:

$$\mu_i = \mu_i^0 + RTln(\gamma_i c_i) + V_i \Delta p \tag{2.10}$$

where Δp is the differential pressure across the membrane.

Equilibrium is assumed between fluids and solutes with the membrane materials at the interface, which implies a continuous gradient of chemical potential from one side of the membrane to the other. The solution-diffusion and pore-flow models differentiate in the way the chemical potential is described (cf. Figure 1): the solution-diffusion assumes that the chemical potential is due to the concentration gradient (cf. Figure 1(a)), while the pore-flow model assumes that the chemical potential across the membrane is expressed as a pressure gradient only (cf. Figure 1(b)).

The two classes of models are discussed in the following paragraphs.

Solution-diffusion models

The solution diffusion model, introduced by the studies of Lonsdale et al. [29], Barrie et al. [30], Meares et al. [31], Yasuda and Peterlin [32], and finally reviewed by Mason and Lonsdale [33] and Wijmans and Baker [23] in the 1990s, has emerged over the past 20 years as the most widely accepted explanation of transport in dialysis, reverse osmosis, gas permeation and pervaporation [23]. The solution diffusion model assumes that the pressure within a membrane is uniform, and that the chemical potential gradient across the membrane is expressed only as a concentration gradient. Therefore, the primary assumption made in the model development is that the flux of the solute and the solvent are independent from each other.

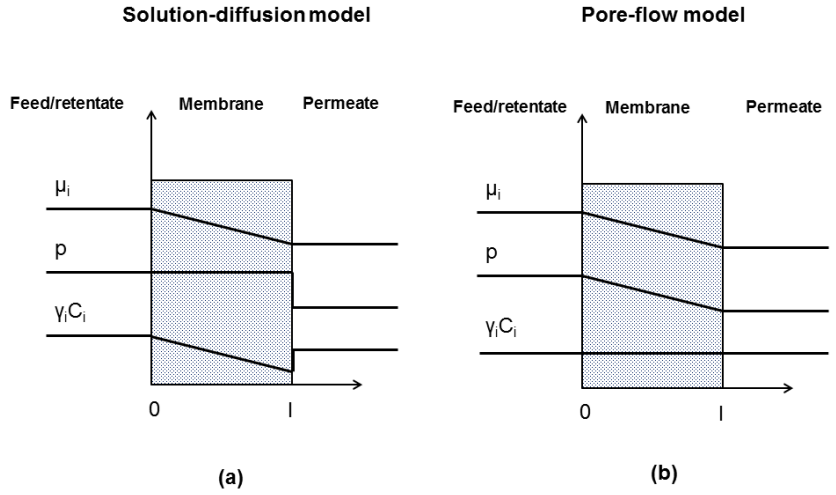


Figure 2.5: Chemical potential, pressure, and solvent activity profiles for permeation of a one-component solution through a membrane according to solution-diffusion and pore-flow transport models (adapted from Wijmans and Baker [23]).

This model is usually adopted for transport through dense membranes. In this kind of membrane, free volume elements are present as statistical fluctuations that appear and disappear at about the same time scale as the motions of permeants through the membrane. These free-volume elements are different from the pores, which are supposed to be fixed in time and space. Because no pressure gradient exists across the membrane, Equation 2.8 for the solute flux becomes:

$$J_i = -\frac{RTL}{c_i}\frac{dc_i}{dx} = -D_i\frac{dC_i}{dx} \tag{2.11}$$

This equation has the same form as Fick's law, where the term RTL/c_i is replaced by the diffusion coefficient D_i.

The basic flux equation is finally:

$$J_i = \frac{D_i}{l}(c_{i,0(m)} - c_{i,l(m)}) \tag{2.12}$$

where $c_{i,0}$ and $c_{i,l}$ are the solute concentration at the retentate and permeate side, respectively, and l the membrane thickness (cf. Figure 2.5). Subscript (m) refers to the

membrane side of the interface.

Equation 2.12 can be further developed for reverse osmosis processes [23], which generally deal with two components, salt and water. At the feed interface, pressure in the feed solution and within the membrane are identical, therefore equating the chemical potential gives:

$$\mu_{i,0} = \mu_{i,0(m)} \rightarrow c_{i,0(m)} = K_i^{SD} c_{i,0} \tag{2.13}$$

where K_i^{SD} is the sorption coefficient, or partitioning coefficient, of species i, according to the solution-diffusion theory. At the permeate interface, a pressure difference exists from p_0 within the membrane and p_l in the permeate solution. Equating the chemical potentials across the interface gives:

$$\mu_{i,l} = \mu_{i,l(m)} \rightarrow ln(\gamma_{i,l} c_{i,l}) = ln(\gamma_{i,l(m)} c_{i,l(m)}) + \frac{v_i(p_0 - p_l)}{RT} \tag{2.14}$$

where the expression for the chemical potential of an incompressible fluid (cf. Equation 2.10) has been used. Rearranging Equation 2.14 and introducing the sorption coefficient, K_i^{SD}, yields:

$$c_{i,l(m)} = K_i^{SD} c_{i,l} e^{-\frac{v_i(p_0 - p_l)}{RT}} \tag{2.15}$$

Equation 2.15 can be inserted in Equation 2.12 for the Fick's law:

$$J_i = \frac{D_i K_i^{SD}}{l} \left(c_{i,0} - c_{i,l} e^{-\frac{v_i(p_0 - p_l)}{RT}} \right) \tag{2.16}$$

Equation 2.16 is valid for both solute and solvent fluxes across the membrane in terms of the pressure and concentration difference across the membrane. The equation can be further simplified for the two species, respectively. For the solvent, at the point of osmotic equilibrium, J_i=0 (i.e. the applied hydrostatic pressure balances the water activity gradient); therefore:

$$c_{i,l} = c_{i,0} e^{\frac{v_i \Delta\pi}{RT}} \tag{2.17}$$

The solvent flux results:

$$J_i = \frac{D_i K_i^{SD} c_{i,0}}{l} \left(1 - e^{-\frac{v_i(\Delta p - \Delta\pi)}{RT}}\right) \tag{2.18}$$

where Δp = p_0 - p_l. If $(v_i(\Delta p - \Delta\pi))/(RT)$ is small, as in the majority of the cases for water applications, the simplification $1 - exp(-x) \rightarrow x$ for x $\rightarrow$ 0 can be used and the solvent and solute fluxes reduce to:

$$J_i = \frac{D_i K_i^{SD} c_{i,0}}{l} \frac{v_i(\Delta p - \Delta\pi)}{RT} = A(\Delta p - \Delta\pi) \tag{2.19}$$

$$J_i = \frac{D_i K_i^{SD}}{l}(c_{i,0} - c_{i,l}) = B(c_{i,0} - c_{i,l}) \tag{2.20}$$

where A and B are the solvent and solute permeability constants, respectively.

To account for occurrence of viscous flow and the interactions between the partial fluxes of the permeating species, the solution diffusion model can be extended to the solution diffusion with imperfections model [26, 34]. The interactions between solvent and solute are taken into account by the Maxwell-Stefan multicomponent diffusion [35, 34]. The Maxwell-Stefan equation [36, 37, 38] predicts a fully general diffusive coupling via composition dependent multicomponent diffusion coefficients in systems of three or more components. This equation relies on inter-species force balances. More precisely, it is assumed that the thermodynamical driving force d_i of species i is in local equilibrium with the total friction force. The driving force under isothermal conditions is given as:

$$\bar{d_i} = \frac{x_i}{RT} \nabla \mu_i \tag{2.21}$$

where the chemical potential is $\mu_i = \mu_i^0$ + RT ln a_i and the activity is $a_i = \gamma_i$ x_i. The activity coefficient γ_i depends on the mixture composition.

The mutual friction force between species i and j is assumed to be proportional to the relative velocity as well as to the amount of molar mass. Together with the assumption of balance of forces this leads to the relation:

$$\mathbf{d}_i = -\sum_{j \neq i} f_{ij} x_i x_j \left(\mathbf{u}_i - \mathbf{u}_j\right) \tag{2.22}$$

f_{ij} are the drag coefficients ($f_{ij} = f_{ji}$).

Introducing of the so-called Maxwell-Stefan diffusivities $D_{ij} = \frac{1}{f_{ij}}$ yields:

$$\frac{x_i}{RT} \nabla \mu_i = -\sum_{j \neq i} \frac{x_j \mathbf{J}_i - x_i \mathbf{J}_j}{c_{tot} D_{ij}} \tag{2.23}$$

The set of equations 2.23 forms the Maxwell-Stefan equations of multicomponent diffusion.

Pore-flow models

Pore flow models assume that the concentrations of solvent and solute within a membrane are uniform and that the chemical potential gradient across the membrane is expressed only as a pressure gradient [16]. The transport through macroporous membranes in the absence of a concentration gradient, based on a pure hydrodynamic analysis, can be described by Darcy's law (from Equation 2.9):

$$J_i = k \frac{p_0 - p_l}{l} \tag{2.24}$$

k is the permeability coefficient, function of structural factors, such as membrane pore size, r_p, surface porosity, ϵ, and tortuosity, τ. In the case of pure solvent flux, for which no concentration gradient is present across the membrane, flux equation 2.24 becomes the well known Hagen-Poiseuille model:

$$V = \frac{\epsilon r_p^2}{8 \mu \tau} \frac{\Delta p}{l} \tag{2.25}$$

According to this model, the viscosity, μ is the only solvent parameter affecting permeation.

For the solute flux, several empirical pore-flow models have been developed. These models originate from the Nernst-Planck equation for transport of solutes through narrow charged pores, and correlate the diffusive and convective hindrance factors with the ratio of

solute radius (r_s) to pore radius (r_p). These models indicate that the solute flux comprise three terms: diffusion driven by a concentration gradient, electromigration driven by an electric potential, and convection with the total volume flux.

Bowen et al. [24, 25] developed a hybrid model based on the extended Nernst-Planck equation, named the Donnan Steric Pore-flow Model (DSPM). This model couples steric hindrance and Donnan exclusion effects for the generic solute. The solute flux is described by Equation 2.26.

$$J_i = -K_{i,d} D_i \frac{dc_i}{dx} - \frac{z_i c_i K_{i,d} D_i}{RT} F \frac{d\psi}{dx} + K_{i,c} c_i V \tag{2.26}$$

$K_{i,d}$ and $K_{i,c}$ are the diffusion and convective hindrance factors, respectively, z_i is the solute valence and ψ the electrical potential.

Based on RO, where solute-membrane interactions are important, two models were developed: (1) the Surface Force Pore-Flow (SF-PF) model [39] and (2) the Finely Porous model [40]. In the SF-PF model a distribution of solutes at the membrane surface is considered, involving interfacial forces between the solute and the membrane material. In the Finely Porous model a kinetic effect, concerning the mobility of the solute relative to that of solvent is considered while permeating through the membrane pores. They are both described by the same differential equation:

$$J_i = \frac{RT}{\chi_{i,m} b} \frac{dc_i}{dx} + \frac{c_i u}{b} \tag{2.27}$$

u is the solvent velocity inside the pore and b the friction parameter, function of the friction coefficients between solute and solvent, $\chi_{i,s}$ and between solute and membrane, $\chi_{i,m}$:

$$b = \frac{\chi_{i,s} + \chi_{i,m}}{\chi_{i,m}} \tag{2.28}$$

The solute flux is composed of two fractions: a diffusion flux caused by a concentration gradient, and convection of solutes with the total volume flux. The friction coefficients are related to the diffusion coefficients of the solute in the solvent, $D_{i,s}$, and in the membrane,

$D_{i,m}$, respectively. The Surface Force Pore-Flow model and the Finely Porous model differ in the distribution of solute at the membrane-feed solution interface. For the Finely Porous model the solute distributes according to a partitioning equilibrium from a purely steric interaction:

$$\begin{cases} x = 0: & c_{i,m}(0) = K_i c_{i,R} \\ x = l: & c_{i,m}(l) = K_i c_{i,P} \end{cases} \tag{2.29}$$

Subscript m refers to membrane, R to retentate and P to permeate.

For the SF-PF model the equilibrium partitioning is influenced by interactions between the solute and the membrane, and is a function of the radial position:

$$\begin{cases} x = 0: & c_{i,m}(0) = c_{i,R} e^{-\frac{\phi(r)}{RT}} \\ x = l: & c_{i,m}(l) = c_{i,P} e^{-\frac{\phi(r)}{RT}} \end{cases} \tag{2.30}$$

$\phi(r)$ represents a potential function expressing the force exerted on the solute molecule by the pore wall or the membrane surface. A positive value means repulsive force, a negative value attractive force, depending on the charge of both membrane and solute. $\phi(r)$ is assumed independent of axial position and determined by the electrical double layer for electrolytic solution, or by dispersion or Van der Waals forces in the case of organic solutes. The solute concentration in the pore has the typical Boltzmann distribution:

$$c_i(r, x) = c_i(0, x) e^{-\frac{\phi(r)}{RT}} \tag{2.31}$$

The Surface- Force Pore-Flow model was further revised and the mass balance corrected. This lead to the formulation of the Modified Surface Force Pore-Flow (MD-SF-PF) model [41]. The main differences between the original and the modified versions of the model lay in the formulation of the potential function to describe the solute distribution in the pore and in the description of the concentration at the pore outlet.

The last class of pore-flow models developed from the extended Nernst-Planck equation is the class of Space-Charge (SC) models [42]. These models describe the pores as straight capillaries having charge on their surface. The basic equation of the SC models for the

radial distribution of electrical potential and ion concentration is the Poisson-Boltzmann equation. The electrical potential, $\bar{\psi}$, is divided into two parts:

$$\bar{\psi} = \psi_1(r, x) + \psi_2(x) \tag{2.32}$$

where $\psi_1(r, x)$ originates from the surface charge of capillaries, and $\psi_2(x)$ is a component due to a streaming potential in the axial direction. The potential function varies with both x and r, and thus the concentration in the capillary. The radial distribution of the solute has the typical Boltzmann distribution:

$$c_i(r, x) = c_i(0, x)e^{-\frac{z_i F \bar{\psi}}{RT}} \tag{2.33}$$

Equation 2.33 has the same structure as Equation 2.31. The only difference is in the definition of the potential function. In SC models, the potential function considers only electrostatic effects (i.e. effects due to solute and membrane charge), in the SF-PF models the potential function considers both electrostatic effects and dispersion, or van der Waals, interactions.

2.3.2 Solvent and solute transport in OSN

The transport models reviewed in the previous paragraph have been mainly developed for reverse osmosis / nanofiltration processes in aqueous systems. Application of the classical transport models to solvent and solute permeation in OSN will be discussed below for solvent and solute transport, respectively.

Solvent permeation

Different models have been developed for the description of the solvent flux through NF membranes. Three different mechanistic approaches are suggested by the literature [43]: the solution-diffusion approach [23], in which the transport of a solvent is directly proportional to its chemical potential gradient across the membrane; the pore flow approach [25, 16], in which the solvent transport is related to the convective-flow through membrane pores;

and the resistances-in-series approach [44, 45], which assumes that the overall resistance for the permeation through a NF membrane can be represented by addition of individual resistances.

These models are characterised by specific model parameters. The model parameters are classified in Table 2.1 into three groups: membrane, solvent and solvent-membrane interaction parameters. The table lists the parameters introduced by the models described below.

Table 2.1: Summary of the solvent, membrane and interaction parameters in the models from literature

Model	**Type of transport**	**Membrane parameters**	**Solvent parameters**	**Solvent-membrane interaction parameters**
Hagen-Poiseuille	convective	r_p, ϵ, τ, l	μ	-
Jonsson and Boesen [46]	convective	r_p, ϵ, τ, l	μ, M	$X_s m$
Machado [45]	resistances in series	d_p, γ_{SV}, f_1, f_2	μ, γ_{LV}	ϕ
Bhanushali [47]	solution-diffusion	γ_{SV}, K_{Bh}	μ,V_m	ϕ
Geens [48]	convective	γ_{SV}, K_{Geens}	μ,V_m, γ_{LV}	-
Darvishmanesh [49]	resistances in series-parallel	r_p, k_m, k_s, k_p ϵ_S, γ_{SV}	r_s, μ, γ_{LV}, ϵ_L	-
Darvishmanesh [50]	convective + diffusive	a_0, b_0, ϵ_S, γ_{SV}	μ, γ_{LV}, ϵ_L	-

In the Hagen-Poiseuille model, introduced in Equation 2.25 and re-written in terms of solvent flux, J_{HP}, in Eq. 2.34, the only solvent property taken into account to describe the permeability is the viscosity, μ. The proportionality factor, K_{HP} between solvent permeability and solvent viscosity is function of membrane properties only.

$$J_{HP} = \frac{\epsilon \pi r_p^4}{8\tau l \mu} \Delta p = \frac{K_{HP}}{\mu} \Delta p \tag{2.34}$$

The influence of the membrane is represented by the pore size, r_p, the porosity, ϵ, the tortuosity, τ, and the membrane thickness, l. No solvent-membrane interaction parameters are used to describe the flow. The Hagen Poiseuille model is generally agreed to accurately describe UF processes [51], but is not sufficient in the NF domain, where interactions between solvent and membrane are expected to play a much bigger role.

Jonsson and Boesen [46] modified the Hagen-Poiseuille model to obtain a combined viscous flow and frictional model, initially developed for the description of transport of solutes through reverse osmosis membranes:

$$J_{JB} = \frac{\epsilon \pi r_p^4}{8\mu\tau} \left[\frac{1}{1 + \frac{r_p^2}{8\mu} \frac{X_{sm} C}{MW}} \right] \frac{\Delta p}{l} \tag{2.35}$$

X_{sm} is a friction factor between the molecule and the pore wall and C the concentration, as the model was developed for solute transport. Jonnsson and Boesen's model can be adapted to the description of pure solvent flux, assuming M as the solvent molecular weight. Note that the friction factor, X_{sm}, must be fitted experimentally for each solvent-membrane combination.

Machado et al. [45] developed a resistance-in-series model for the permeation of pure solvents and solvent mixtures to extend the predictability of the Hagen-Poiseuille model:

$$J_M = \frac{\Delta p}{\phi \left[(\gamma_{SV} - \gamma_{LV}) + f_1 \mu \right] + f_2 \mu} \tag{2.36}$$

The authors introduced the difference in surface tension between membrane and solvent, $\Delta\gamma = \gamma_{SV} - \gamma_{LV}$, and the solvent-membrane interaction parameter, ϕ, in addition to viscosity. f_1 and f_2 are solvent-independent parameters characterising the NF and UF sublayers. The main disadvantage of this model is the use of the empirical parameter, ϕ, to be determined for each solvent-membrane combination.

Bhanushali et al. [47] developed a model based on the solution-diffusion theory for RO membranes:

$$J_{Bh} = K_{Bh} \left(\frac{V_m}{\mu} \right) \left(\frac{1}{\phi^n \gamma_{SV}} \right) \tag{2.37}$$

The authors introduced the molar volume, V_m, as measure of the molecular size and the surface energy of the membrane, γ_{SV}, as membrane parameter. K_{Bh} is the proportionality constant of the model. This model takes into consideration two solvent parameters, viscosity for the momentum transport and the molar volume for the molecular size effects; and a solvent-membrane interaction parameter, ϕ^n, where n is an empirical constant to obtain the best fitting from the experimental data.

Geens et al. [48] developed a model starting from all the considerations of the previous literature. They observed the inconsistency of the model by Bhanushali et al. [47] in describing the solvent-membrane interaction, due to the choice of using the interaction parameter ϕ^n and membrane surface tension only. Geens et al. [48] suggested the model described by Eq. 2.38.

$$J_G = K_G \frac{V_m}{\mu \Delta\gamma} \Delta p = J_{HP} \frac{V_m}{\Delta\gamma} \tag{2.38}$$

where K_G is a constant for the membrane and $\Delta\gamma$ is the difference in surface tension between membrane and solvent. The authors took the dependences on molar volume, V_m, and viscosity, μ, from Bhanushali et al. [47] and the dependence on the difference in surface tension between solvent and membrane, $\Delta\gamma$, from Machado et al. [45]. The model introduces a correction for the viscous behaviour described by the Hagen-Poiseuille approach, however the correction factor ($\frac{V_m}{\Delta\gamma}$) is not function of the membrane pore dimension. This does not allow the model to cross the continuum from nano- to ultrafiltration, as in the latter case the flux is expected to tend to J_{HP}.

Darvishmanesh et al. [49] continued the studies of Geens et al. [48] and of Machado et al. [45]. The authors adopted the idea of a semi-empirical model based on resistance in series and parallel to describe the transport of solvents through NF membranes. The permeation of the solvent, according to Darvishmanesh et al. [49] consists of three main steps: (1) transfer of solvent molecules from the bulk to the top active layer, which is characterised by a surface resistance, R_s, (2) viscous flow through NF nanopores, which is characterised as pore resistance, R_p, (3) diffusive flow through the membrane material, which is characterised by a matrix resistance, R_m. The functional form of the model is (Eq.

2.39):

$$J_D = \frac{1}{R_{overall}} \Delta p \tag{2.39}$$

where the overall resistance, $R_{overall}$, is defined as (Eq. 2.40):

$$R_{overall} = R_s + \frac{R_m R_p}{R_m + R_p} \tag{2.40}$$

and the three single resistances as (Eqs. 2.41-2.43):

$$R_s = k_s \frac{r_s}{r_p} exp(1 - \beta) \tag{2.41}$$

$$R_m = k_m \left(\frac{\mu}{\alpha} \right) \tag{2.42}$$

$$R_p = k_p \left(\frac{r_s}{r_p} \right)^2 \mu \tag{2.43}$$

with the coefficients α and β given by Eqs. 2.44 and 2.45:

$$\alpha = \frac{\epsilon_L}{\epsilon_S} \tag{2.44}$$

$$\beta = \frac{\gamma_{LV}}{\gamma_{SV}} \tag{2.45}$$

This model takes into account four solvent parameters, which are viscosity, dielectric constant, surface tension and effective molecular radius. Polarity and surface effects are considered by the ratio of solvent to membrane dielectric constant, ϵ_L and ϵ_S, and by the ratio of solvent to membrane surface tensions, γ_{LV} and γ_{SV}, (the subscript L is for liquid, S for solid and V for vapor, respectively). The solvent radius represents the effect of the steric hindrance. As one can see, at least the definition of the single resistance is highly empirical and not supported by theoretical observations.

As in Geens et al. [48], the model does not cross the continuum from nano- to ultrafiltration for large pore sizes.

Clearly, this model does not describe a pure viscous flux when r_p is large, i.e. J_D is not proportional to μ^{-1}. In addition to this, the structure of this model does not allow an easy extension to solvent mixtures and no guidance is given on how to make estimations for mixtures.

Darvishmanesh et al. [50] developed a second model to describe the solvent permeation though organic and inorganic nanofiltration membranes, based on simultaneous effects of convective and diffusive transport mechanisms. The equation used to describe the flux is presented in Eq. 2.46.

$$J_D = \frac{a_0 \alpha}{\mu e^{(1-\beta)}}(\Delta p - \Delta \pi) + \frac{b_0}{\mu e^{(1-\beta)}}\Delta p \tag{2.46}$$

a_0 and b_0 are specific diffusivity and permeability values, α and β were defined in the previous model (Eqs. 2.44 and 2.45, respectively). When the model is applied to solute free solvents, the osmotic pressure, $\Delta\pi$, is zero and the equation can be simplified to give Eq. 2.47.

$$J_D = \frac{a_0 \alpha + b_0}{\mu e^{(1-\beta)}}\Delta p \tag{2.47}$$

This model does not explicitly account for the dependence of fluxes on the pore radius, therefore it is not possible to understand the effect of an increase in the pore dimension on the solvent permeation.

Ranging from the oldest Hagen-Poiseuille model to the recent models by Darvishmanesh et al. [49, 50], the tendency is clearly towards an increase in the number of solvent and membrane parameters taken into account in the model. This tendency corresponds to the necessity for incorporating further parameters to describe the permeation at the nanoscale. In order to overcome some of the limitations of the current models, a new phenomenological and predictive model is developed and discussed in Chapter 4.

Solute permeation

Various attempts have been made to use the classical solution-diffusion and pore-flow models for permeation in Organic Solvent Nanofiltration. Peeva et al. [17] successfully de-

scribed the permeation of docosane and tetraoctylammonium bromide (TOABr) in toluene through Starmem 122 by the solution-diffusion model coupled with the film theory for mass transfer. Han et al. [52], similarly, found that solution-diffusion type models may be more appropriate than pore-flow models for describing transport of aqueous solutions of phenol and toluene through polymeric OSN membranes. The solution-diffusion model has, however, limitations when used in NF. Paul [35] pointed out that the original solution-diffusion theory appropriately accounts for effects important in typical desalination applications, but fails in describing the separation of various types of organic systems, as it does not account for any kind of coupling between solute and solvent fluxes [35]. Namely he observed that, in the classical solution-diffusion model: (i) flux is expected to increase linearly with pressure, according to Equation 2.19, which is opposite to experimental observations at high pressure; (ii) rejection is predicted to approach unity as the driving pressure increases and no permselectivity of the membrane is considered; (iii) rejection must always be positive, but clearly negative values have been observed experimentally [53]. This limitation comes from neglecting the effect of pressure on the solute transport, that may be acceptable for desalination processes, but not in the presence of some organic solutes or solvents. Paul [35] adapted the transport equations of the classical solution-diffusion theory to consider potential effects of coupling (frictional or convective) between solvent and solute transport within the membrane, and to include convective effects. Specifically, he adjusted the solution-diffusion model by including the effect of pressure on the transport of both solute and solvent and by using the Maxwell-Stefan equation to describe the concentration dependence of the diffusion coefficients.

According to the pore-flow models for aqueous applications, the main mechanisms affecting permeation are steric hindrance, diffusive transport and electrostatic (or Donnan) interactions. Occurrence of charge interaction has been questioned for OSN. Bhanushali et al. [54] identified the effects of charge for solute retention in methanol, and Zhang et al. [55] explored the surface charge on polymeric membranes in aqueous solutions of methanol and ethanol by streaming potential measurements. On the other side, Zhao et al. [56] observed no charge effects during the NF of charged solutes in methanol through polymeric mem-

branes. It is plausible that the charge does not play a significant role in organic solvents, like ACN or DMF, or their aqueous mixtures: hydrophobic solvents cannot contribute to the formation of hydroxyl groups on the membrane surface, and their low dielectric constant would decrease significantly the electrical potential experienced by the charges in solution.

In the presence of organic solvents, solute-membrane and solvent-membrane interactions, different from charge effects, may also occur [54]. These interactions are due to hydrophilic/hydrophobic and polar properties of solute, solvent and membrane and affects the ternary interactions among them. As a consequence, competition between solute-membrane and solvent-membrane affinities becomes critical and can affect the pressure-driven transport of solute and solvent through the membrane. In the case of negligible steric exclusion (i.e. the solute is small enough to pass easily through the pore, and therefore only its interaction with the membrane affects its flux), two cases could be identified, as a function of the relative solute-membrane vs. solvent-membrane affinities (cf. Figure 2.6):

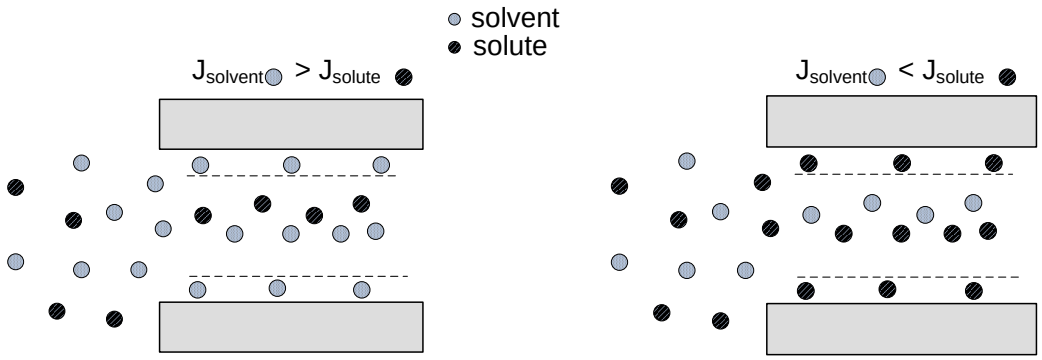


Figure 2.6: Competition between solute-membrane and solvent-membrane affinities.

(i) when the solvent-membrane affinity is larger than the solute-membrane affinity (cf. Figure 2.6(a)), solvent molecules accumulate preferentially at the pore wall, and the solvent flux ($J_{solvent}$) is finally larger than the solute flux (J_{solute}) , determining a positive solute rejection (in other words, the less affine solute is excluded from the pore and its concentration

in the permeate can be lower or equal the concentration in the retentate);

(ii) when the solute-membrane affinity is larger than the solvent-membrane affinity (cf. Figure 2.6(b)), solute molecules accumulate at the pore wall, and the solute flux is finally larger than the solvent flux. In this case, the concentration of the solute in the permeate can be higher than the concentration in the retentate, thus resulting in a negative solute rejection.

In the intermediate case, when solvent-membrane and solute-membrane affinities are comparable, solute rejection is governed by the the relative importance of the two affinities. It is worth to specify that this phenomenon is significant in small pores (such as in the NF membranes, characterised by a high specific surface) and less significant in larger pores (such as in the UF membranes, where bulk effects largely dominate over surface effects) [57]. Significant negative rejection values, found by Darvishmanesh et al. (Sudan II / Sudan Black / Sudan 408 in hexane through polyimide membranes [58]), and Koops et al. (docosanoic aid in hexane through cellulose acetate membranes [59]), have been explained by stronger solute-membrane than solvent-membrane interactions, which determine an increase in the solute flux relative to the solvent flux. In the cases of significant solute-membrane affinity, and negligible solvent-membrane affinity, the applicability of the transport models developed for aqueous environments is questionable, due to the significant differences in the solvent properties. Bhanushali et al. [54] observed that the classical description of solute flux, as in the DSPM or SC models (cf. Paragraph 2.3.1), cannot account for the acceleration of solute with respect to the solvent and therefore cannot describe negative rejection for solutions of single solutes. In their opinion, the most suitable pore-flow model to describe solute transport in non-aqueous environments (organic solvents or organic/water mixtures) is the Surface-Force Pore-Flow model, which describes the solute-membrane interactions by a potential function, which depends on solute-membrane molecular affinity.

Preferential solvation in organic/water mixtures

Understanding rejection is even more complicated in organic/water mixtures, since their physico-chemical properties lie between those of purely aqueous and purely organic so-

lutions. When a solute is dissolved in a mixture of two or more solvents, solute-solvent interactions may differ in strength for each solvent. This may cause the composition of the solvation shell to be different from that of the bulk solution. In this case, the solute is said to be preferentially (or selectively) solvated by one of the two solvents [60]. Preferential solvation is well known to occur for inorganic salts [61, 62, 63, 64], organic molecules [60, 65], and peptides [66], and can alter the specific properties of the solute, as it modifies its immediate surroundings. In other words, if preferential solvation occurs, the solute-membrane affinity depends on the composition of the solvent mixture itself.

In a typical peptide/organic solvent/water mixture, ions are often present. Ions come from the dissociation of salts or acids in solution and are finally present in the mixture as either counter-ions bonded to the peptide chain (as is often the case for chloride, acetate and trifluoreacetate anions) or free ions in solution (as buffering agents, such as ammonium sulfate or ammonium acetate). Ions are characterised by hydrophilic/phobic properties, according to their preferential solvation in water or in the organic solvents, and affect in turn the preferential solvation of the peptides, by modifying their degree of hydration (or solvation).

Two possible situations occur when ions are present in a mixture of organic solutes, and namely ions can associate with the molecule as counter-ions, as in the case of organic solutes with charged sites, or they can remain free in solution, as in the case of neutral organic solutes. In the latter case, ions are responsible for increasing ionic strength or buffering the solution pH. The effect of salts on the rejection of neutral molecules has been studied for NF in water solutions. Bouranene et al. [67], for example, studied the effect of hydrophilic salts, such as NaCl, on the rejection on polyethylenglycol (PEG) in water through ceramic NF membranes. They found that PEG rejection decreased with the salt concentration, and explained that as an effect of dehydration caused by ions and corresponding change in the Stokes radius of PEG. The effect of ions has been observed also on the rejection of charged molecules in water. The most significant example is the occurrence of salting-out [68, 69], as a consequence of changes in solubility of a molecule in the environment due to the presence of salts. Salting - out by addition of hydrophilic salts to a protein

mixture occurs because, at a certain ionic strength, water cannot support the charge of both protein and ions and the protein molecules precipitate by forming hydrophobic interactions with each other. Different authors studied the effects of salts on protein solubility and stability, in correlation with their kosmotropic or chaotropic behaviour [70, 71]. Parmar and Muschol [71] investigated whether addition of either chaotropic or kosmotropic salt ions at concentrations up to 1M would alter lysozyme hydration or the hydrodynamic interaction among the lysozyme molecules. By measuring the Stokes radius (hydrodynamic radius) of the protein in the presence of ions, they clearly observed that the radius (and therefore the hydration shell) remains the same, independent of salt and salt concentration. Apparently, neither chaotropic nor kosmotropic ions are able to alter the extent of the hydration layer around lysozyme. Collins [70] introduced a three-layer theory to explain the protein hydration and the chaotropic/kosmotropic ion effects. The mechanism by which ions modulate the ability of an aqueous solution to solvate a polar surface is illustrated in Figure 2.7.

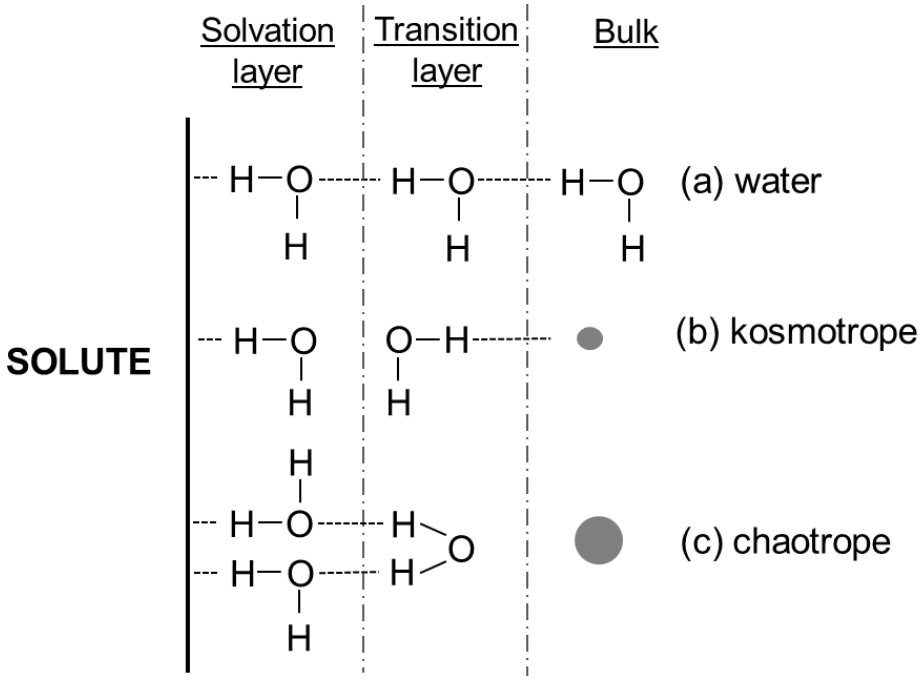


Figure 2.7: Interfacial water near the surface of a hydrated solute (adapted from Collins [70]).

He divided the interfacial region near a solute into three layers, each layer being one water molecule thick. The first water layer immediately adjacent to the protein surface was designated as the "solvation layer"; the second water layer was designated as the "transition layer"; and the third layer was the bulk surface [70]. The solvation layer and bulk surface both compete for hydrogen bonding interactions with the transition layer. Ions inserted into the third water layer modulate the interaction of the second water layer with the first water layer, for the solvation of the solute surface. This was explained by the fact that a water molecule cannot achieve the maximum pairwise enthalpy of interaction with each of its immediate neighbors simultaneously; it will therefore "choose" to interact most strongly with the neighbor for which it has the most favorable pairwise enthalpy of interaction [70]. In the absence of ions, the first, second and third water layers are connected via hydrogen bond between water molecules (case a of Figure 2.7). When a strongly hydrated anion (kosmotrope) is inserted into the third water layer, the second water layer solvates the kosmotrope and cannot help the first layer solvate the solute surface (cf. Figure (case b of Figure 2.7). In contrast, when a weakly hydrated anion (chaotrope) is inserted into the third water layer, the second water layer is left free to help the first water layer solvate the solute surface more effectively (case c of Figure 2.7).

This explanation concerns the case of water-mediated ion-pair formation between polar (hydrated) groups and ions. On the other hand, when the solute has charged sites and the bond between charged sites and counter-ions is strong, ions can bind directly to the protein, without mediation of the water molecules [70]. In such cases, the ions that come from the dissociated salt associate as counter-ions with the solute. In organic/water mixtures, this association contributes to an increase in the solute hydration, if the ions are hydrophilic, or to a decrease in the solute hydration, if the ions are hydrophobic (since hydrophobic ions contribute to the increase of the organic solvent concentration in the solute solvation shell). LoBrutto et al. [72] studied the effect of the concentration of hydrophobic counter-anions on HPLC retention of protonated analytes, and found that the HPLC retention increased with increasing counter-ion concentration. This was associated with ionic interactions of hydrophobic anions (salt or acid) with positively charged analyte molecules, which led to

the disruption of the analyte hydration shell, the increase of analyte hydrophobicity, and a corresponding increase in retention on the chromatographic column (hydrophobic C18, in their study). As expected, this process showed a "saturation" limit, when the counter-anion concentration was high enough to associate with the charged sites of the analyte. A further increase of counter-anion concentration did not produce any noticeable effect on the analyte retention on the HPLC column. After the "saturation" limit, any further addition of ions would result in a water-mediated ion pairs formation, as explained for the former case of ions in the presence of neutral organic molecules.

Effects of preferential solvation in ACN/water mixtures and ion (Cl^- and TFA^-) content on the permeation of a neutral organic molecule (Npys) and a model peptide are shown in Chapter 5.

2.4 Process development, or Quality by Design (QbD)

It is evident from the previous literature review on transport modelling (cf. Paragraph 2.3) that the struggle to describe and understand phenomena connected with transport across membranes has a long history [33]. This has not been an easy task, because the systems often contain many components and the mixtures differ widely in their properties. This is the case of typical processes for concentrating and purifying peptides, characterised by complicated matrices of input parameters. These parameters include Critical Process Parameters, which affect in turn Critical Quality Attributes of the desired product. Typical Critical Quality Attributes for NF are specifications regarding concentration of the main product, impurities, ionic and solvent composition. To support new initiatives and provide guidance for pharmaceutical process development, the International Conference on Harmonisation (ICH) of Technical Requirements for Registration of Pharmaceuticals for Human Use introduced the Quality by Design (QbD) concept. This concept was defined as "a systematic approach to development that begins with predefined objectives and emphasises product and process understanding and process control, based on sound science and quality risk management" [73] and it became the answer to assisting the industry to move towards a

more scientific approach to pharmaceutical development.

According to the conventional regulatory framework for generic drugs, or Quality by Testing, little or no emphasis is placed on how the design of efficient and effective processes can ensure product quality. Under QbD, consistency comes from the design and control of the process. Effort is made to understand all the possible effects of the Critical Process Parameters on the quality of a final drug product, and, as a result of all this knowledge, the company can (i) select the best process conditions with a limited number of experimental data; (ii) continually monitor the process to assure consistent product quality; and (iii) update the process without requiring further experimental effort.

No agreement about a unified transport theory has been reached yet, and this makes the employment of fundamental models questionable for a reliable mathematical description of the transport, and impractical for supporting process development. Although less elegant from the point of view of fundamental understanding, statistical models provide good data description and reliable predictive capability in the experimental range.

2.4.1 Statistical modelling by Design of Experiments (DoE)

Design of Experiments (DoE) methods are extensively applied in process design to help engineers understand the effects of possible combinations and interactions of various parameters on the final drug quality [74, 75]. The purpose of statistically designing an experiment is to collect the maximum amount of relevant information with the minimum expenditure of time and resources. Application of DoE provides scientific understanding of the effects of multiple process parameters on the product Critical Quality Attributes and lead to the establishment of a "design space" and a manufacturing control strategy. Within QbD, design space is defined as "the multidimensional combination and interaction of input variables and process parameters that have been demonstrated to provide quality assurance" [76]. DoE methods are much more efficient than the classical "one-factor-at-a-time" approach. The traditional approach demands considerable material expense and is more time consuming, since, to determine the effect of each factor, experiments may be designed to investigate one factor at a time so that all other independent variables (factors) are held

constant. DoE, on the other side, is characterised by reduction or minimization of the total number of trials by the simultaneous variation of all potential influencing factors.

When planning the design, the choice of the experiments and their order are based on the principles of randomization (so that the conditions in one run neither depend on the conditions of the previous run nor predict the conditions in the subsequent runs); replication (to estimate the random error independent of any lack of fit error); and orthogonality (to assure statistical independence of each run). Influencing factors must be controllable and of high measurement precision (i.e. adjustable at different levels and maintained at that level with enough precision), singular (i.e. not a function of other factors), and concordant (i.e. all the possible factor combinations should be possible). These factors are defined by their domains, which in turn define the experimental range.

The unknown response function is, in principle, approximated by a polynomial function where regression coefficients are estimated on the basis of experimental results. First and second order mathematical models are considered in this research. First-order models are obtained by performing a Full Factorial Experimental design or a Fractional Factorial Experimental design, which is a definite part of the Full Factorial Experimental design. The Full Factorial Experimental design is the experiment where all possible combinations of levels of factors are realised and experimental results are processed by applying statistical analysis. The number of Full Factorial Experimental design points-trials, N, is determined from the following relation:

$$N = p^k \tag{2.48}$$

where factors (k) are varied on two levels (p). The Full Factorial Experimental design is therefore called the design experiment of type 2k. In the case of large number of factors, the Full Factorial Experimental design requires a large number of trials, so that the Fractional Factorial Experimental design is more advantageous (cf. Figure 2.8). The Fractional Factorial Experimental design permits the reduction of the experimental set to the points in Figure 1(b).

The first-order model, obtained from the Full Factorial Experimental and Fractional

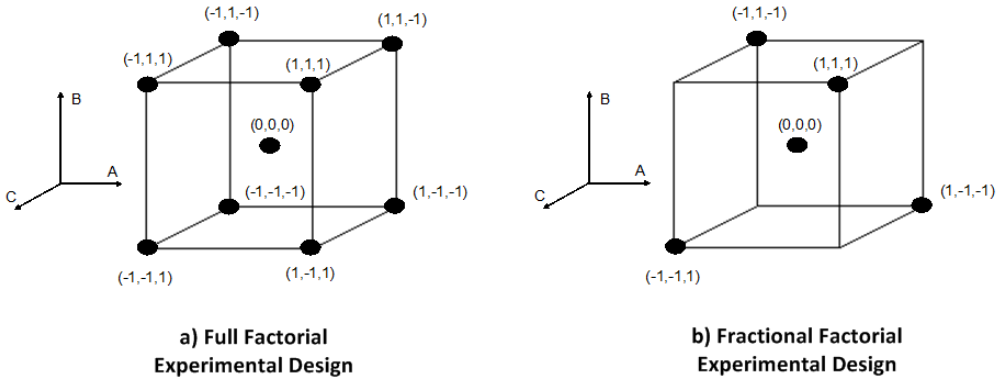


Figure 2.8: Full Factorial Experimental and Fractional Factorial Experimental designs.

Factorial Experimental designs, is defined as:

$$\hat{Y} = b_0 + \Sigma_i^k b_i X_i + \Sigma_{i,j}^k b_{ij} X_i X_j \tag{2.49}$$

where $\hat{Y}$ is the response value, X_i and X_j the independent parameters and b_i and b_{ij} the estimated constants for the single effects and the interaction effects, respectively.

Second-order models, also called Response Surface Models, are based on a computer-aided D-optimal design, with a non-orthogonal matrix of design points. In contrast to the Fractional Factorial Experimental design, points are not only on the vertices of the cube delimiting the design space, but also on the edges, or eventually outside, the design space. The second-order model, obtained from the D-Optimal design, is:

$$\hat{Y} = b_0 + \Sigma_i^k b_{1,i} X_i + \Sigma_{i,j}^k b_{ij} X_i X_j + \Sigma_i^k b_{2,i} X_i^2 \tag{2.50}$$

Analysing the magnitude of the linear regression coefficients of Equations 2.49 and 2.50, it is possible to understand the strength of the influence of associated factors on the response. The higher the value of the associated factor, the more intensively it affects the response. The sign of the coefficients has to be accounted for too: the sign is positive, if an increase in the associated factor causes an increase in the response; on the contrary, with a negative sign of the coefficient, an increase in the associated factor value causes a decrease in the response. The analysis of the results allows the identification of interactions among process parameters (impossible for the 1-factor-at-a-time approach). Interactions show an

effect when the combined change in two factors produces an effect greater (or less) than the additive effect expected from the factors alone. The quality of the model is evaluated by ANalysis Of VAriance (ANOVA) in terms of R^2 value and Lack of fit. The R^2 value (or squared multiple correlation coefficient or coefficient of determination) describes the quality of the fit. The Lack of Fit represents the probability that the difference between experimental points and predictions is due to noise. An R^2 close to 1 and a non-significant Lack of Fit are desired for models that properly fit experimental data.

DoE have been successfully employed for the development of chromatographic techniques, to identify the important factors affecting the retention performance and optimise the separation [77, 78]. Studies of NF by DoE are, on the other hand, few. An example of the application of DoE techniques to NF have been reported by Ahmad et al. [79], who investigated the separation of dye/salt/water solutions by porous ceramic membranes by DoE. Temperature, feed concentration, pressure and pH, examined by Response Surface Methods, were found to statistically affect the quality of the separation. The polynomial equations for the responses, developed by DoE, can be used to formulate objective functions for numerical optimization, in order to find the best operating conditions for achieving the separation of interest, as shown by Polom and Szaniawska [80] for the nanofiltration of acid lactic solutions. Finally, only few studies show how information from DoE can be used to support process modelling for process selection. One good example is the work by Roman et al. [81], in which concentration-dependent solute rejection obtained by experimental design was used to describe the dynamics of different membrane filtration processes and select the most appropriate filtration technique for the demineralization of acid whey.

The advantages of studying peptide NF by DoE and ANOVA are further presented and discussed in Chapter 6, for some model peptides, and the application of statical modelling to process development is shown in Chapters 7 and 8, for two industrial case studies.

Chapter 3

Research strategy

The scope of this research is twofold:

(1) to investigate the permeation mechanism of peptide solutions in Organic Solvent Nanofiltration (OSN);

(2) to develop innovative membrane-based purification strategies, which are applicable to peptide processes and can avoid some of the major drawbacks of the current production technologies or successfully integrate them. Fundamental information from permeation studies (i.e. transport modelling) is integrated with process development (i.e. process modelling).

The research strategy is reported below.

In **Chapter 4**, permeation of water and organic solvents through ceramic NF and UF membranes is investigated and a predictive model for solvent permeability is proposed. The development of the model starts from the Hagen-Poiseuille equation, which assumes the viscosity as the main parameter influencing permeation, and introduces several correction factors to account for the surface phenomena that arise in a nanotube due to solvent-membrane surface interactions: capillarity, polarity and steric hindrance. The correction terms are functions of the pore size, so that the model can be applied to both UF and NF membranes. The model is compared to the Hagen-Poiseuille model and to the Coupled Series-Parallel Resistance model by Darvishmanesh et al. [49] and shows better predictive capability for pure solvent permeation in both filtration ranges. The model is successfully

extended to aqueous and organic solvent mixtures. Only the physical parameters of the single solvents are needed to have good predictions, with the exception of the mixture viscosity. The model has the potential to be used for design calculations and to predict pure solvent and mixture fluxes for a specific membrane by obtaining a limited number of experimental data for pure solvents (necessary to obtain the fitting parameters characteristic of the membrane).

In **Chapter 5**, permeation fluxes of common monovalent salts, a small neutral organic molecule (Npys) and a model peptide (conventionally named PEP_1) in organic/water mixtures are investigated, with particular attention to the role of preferential solvation. When a substance is dissolved in a mixture of two or more solvents, the solute-solvent interactions which account for the solution process may differ in strength for each solvent. This may cause the composition of the solvation shell to be different from that of the bulk solution, and the solute is said to be preferentially (or selectively) solvated by one of the two solvents [60]. Preferential solvation can alter the properties of the solute, as it modifies its immediate surroundings. The effect of organic solvent on salt permeation is explained by the Hansen solubility parameter of the solvent, as representative of the solvent-membrane interactions, and by the preferential solvation parameter of the ion in solution, as representative of the solute-membrane affinity. Negative rejection of salts in an ACN/water mixture is attributed to solute-membrane affinity being higher than solvent-membrane affinity. The relative importance of solute-membrane vs. solvent-membrane interactions influences the permeation, with a more significant effect in NF than in UF. This is ascribed to the larger specific surface that characterises NF membranes, with respect to UF membranes, and is consistent with what is observed for the solvent permeation. The effect of salts on the rejection of Npys and the model peptide is explained by the hydrophilic/phobic (ot kosmo-/chaotropic) nature of the ions, which in turn affects the hydrophilic/phobic properties of the organic molecules.

It is evident from the studies presented in Chapters 4 and 5 that complicated matrices of input parameters characterise typical processes for concentrating and purifying peptides. In industrial R&D of NF processes, an efficient investigation of the permeation of peptide

solutions is associated with an understanding of the effect of the operating parameters on the process performance. This understanding has to be translated into mathematical models, able to predict process performances, thus fulfilling the requirements of the so-called Quality by Design (QbD) concept. Fundamental models often do not take into account the effect of mixture composition on the peptide retention, as those models were developed mainly for aqueous solutions and the extension to organic solvents is still under investigation. Design of Experiments (DoE) and Analysis of Variance (ANOVA) are normally used to design the experimental set and obtain statistical models from the experimental data. Statistical modelling is efficient, reliable and the experimental set is designed to obtain the maximum amount of information with the minimum experimental effort. Statistical modelling is a valid alternative when In **Chapter 6**, the permeation of three model peptides (conventionally named PEP_1, P3 and P2-S-SM) through two ceramic NF membranes is studied by DoE. Two peptides, one with preferential solvation for ACN over water (PEP_1), and the other with preferential solvation for water over ACN (P3), are studied in conditions largely below the isoelectric point, and the third peptide is studied in conditions close to its isoelectric point. For each peptide, peptide rejection, flux and TFA-H rejection are modelled as a function of five operating parameters (peptide concentration, %v TFA/pH, pressure, cross-flow velocity, and %v ACN). Effects of solute-solvent-membrane interactions are identified for all the peptides. Solvent composition (%v ACN/water) and salt content (%v TFA-H) affected the peptide permeation by changing the hydrophilic/phobic properties of the peptides and thus the relative solute-membrane affinity, in agreement to what was observed in Chapter 5. In operating conditions close to the peptide pI, reversible formation of micelles, which contribute to an increase in the peptide rejection and decrease in solvent flux, is observed.

Finally, the application of NF to two industrial case studies is presented, and the statistical models obtained from the DoEs of Chapter 6 are used to assist process development. In **Chapter 7**, the integration of NF in the downstream process (DSP) of one therapeutic peptide (PEP_1) is studied. NF is required to perform concentration and salt/solvent exchange between the preparative chromatography and the lyophilisation. The best conditions to

perform concentration, found by numerical optimization of the DoE models for rejection and flux, correspond to high TFA-H and ACN content (as expected from the larger hydrophobicity of the peptide in these conditions, which leads to higher exclusion from the pore). Results are extended from looser membrane (Inopor® Nano 750 Da) to tighter membrane (Inopor® Nano 450), as similar performances for the two are found to occur at high peptide concentration. DoE models, obtained in steady-state conditions, are used to simulate the dynamic diafiltration process and select the best operating conditions (i.e. shorter operating time) to perform the salt and solvent exchanges.

In **Chapter 8**, the NF-assisted synthesis of a second therapeutic peptide (P3), based on the coupling of NF and reaction in one unique process, is proposed and developed. This strategy is called "Reactive Peptide Nanofiltration". Permeation studies of P3 through ceramic NF membranes, carried out by DoE (cf. Chapter 6), are employed to select the best process conditions in terms of product recovery and operating time. The new strategy is compared to the established process in terms of economics (design complexity, scale-up feasibility), efficacy (process performances), impact on the market (time and costs), and on the environment (solvent consumption). Shortened production time and lower solvent consumption characterise this scheme, with evident advantages from technological, economical and environmental points of view.

Chapter 4

Solvent permeation through ceramic NF and UF membranes

4.1 Introduction

Membrane technology for the processing of aqueous solutions has a long history. Membrane processes in non aqueous media, particularly with nano- (NF) and ultrafiltration (UF) membranes, are more recent. Non aqueous processes are characterised by the increase in the number of solvent-membrane (and solute) interactions, compared to aqueous systems. These interactions play a determining role in the understanding and prediction of both solvent fluxes and solute rejection through nano- and ultrafiltration membranes, and are of great importance for the choice of suitable membranes.

A predictive mathematical model, based on understanding the interactions occurring between solvent and membrane, can reduce the number of experiments necessary to characterise an application, and consequently allows considerable savings in terms of time and money. This is of high importance for industrial applications. A number of authors have investigated the transport through membranes, in order to develop models able to predict the permeation of different classes of solvents [45, 47, 48, 49, 50, 82]. Unfortunately, some of these do not suggest a strategy to generalise the predictions [45, 47], while some others are highly empirical in the choice and arrangement of the functional dependences between va-

riables [49, 50] or fail in comparison with experimental data when trying to use them across the continuum from NF to UF [48, 49]. For instance, Bhanushali et al. [47] and Machado et al. [45] developed models that contain specific model parameters for a given membrane-solvent (or solvent mixture) combination, which by definition cannot be extended to other solvents without further experiments. On the other hand, Darvishmanesh et al. [49, 50] developed two models which, although highly empirical, contain model parameters specific to the membrane and solvent individually; once the membrane parameters are determined, predictions can in principle be made for any solvent based on its properties, without new data being required, although this possibility was not tested. A more complete discussion on the models available in literature was presented in Chapter 2.

Little research has been reported for solvent mixtures. Silva et al. [82] studied the permeation of two binary systems, toluene/methanol and toluene/ethylacetate, through polymeric NF membranes. Acceptable predictions for the permeability of the mixtures were obtained by knowing the permeability of the corresponding pure solvents and by using the solution-diffusion model. Geens et al. [83] investigated the permeation of ethanol/water, methanol/water and ethanol/methanol through polymeric membranes, and identified the key parameters that affected the flux, but did not suggest a model that can be used for predictions. Note that solvent mixtures are ubiquitous in industry, and so predicting mixture fluxes is important. Considering that the collection of experimental data for all the possible solvent combinations would be prohibitively time consuming, it would be useful to be able to predict the flux of any solvent mixture by knowing the composition and the flux of the pure solvents.

The aim of this work is to develop a model which can be used to predict the permeation flux of different solvents and their combinations. As the definition of membrane properties is not possible using literature data, it will be suggested how to define the membrane characteristics using a limited number of experiments only. In order to have a general model, only physical parameters of each solvent must be used. In particular, the model includes interaction phenomena between solvent and membrane which have been suggested by other authors and which can be directly correlated to the physical properties of each

solvent.

4.2 Model development

4.2.1 Nanofluidics

For microporous structures and pressure-driven processes, the viscosity of the solvent plays a significant role and the importance of the convective term seems to be greater than that of the diffusive term. The literature supporting pore-flow models suggests that the laws of classical fluid dynamics are applicable to describe the flow through pores of nanoscale dimensions, even if the fundamental properties of the fluid at the micro/nanoscale may differ significantly from those in larger devices. For instance, Bowen and Welfoot [25] used the Hagen-Poiseuille model to describe the velocity of water solutions through microporous membranes. In addition to this, they suggested a correction to take into account the effect of pore size on the effective viscosity inside the pore, as compared to that in the bulk.

Some authors [84, 85] consider that phenomena at the micro- and nanoscale can still be described using the continuum theory, even through the decrease of pore size makes the surface forces more important than at larger scales. In particular, when entering the region of nanofluidics, where the surface-to-volume ratio is high, the no-slip boundary condition typical of classical fluid dynamics, which assumes the absence of relative motion between the fluid and the membrane, does not fully hold [84]. This implies that the Navier-Stokes differential equation has to be integrated with the appropriate boundary conditions, namely, with velocity at the interface, due to the presence of interactions between solvent and membrane. Note that the Reynolds number (Re), which represents the ratio of inertial forces to viscous ones, is at least one order of magnitude smaller than unity in micro- and nanopores; therefore, in the "bulk" of the pore and in the presence of a pressure-driven flow, the regime is laminar with a well established parabolic velocity profile inside the channel.

The Hagen-Poiseuille model (Eq. 2.25) can be derived from the integration of the Navier-Stokes differential equation with no-slip boundary conditions (zero velocity at the interface). A schematic representation of the velocity profile in confined geometries, such

as pores, is shown in Figure 4.1(a).

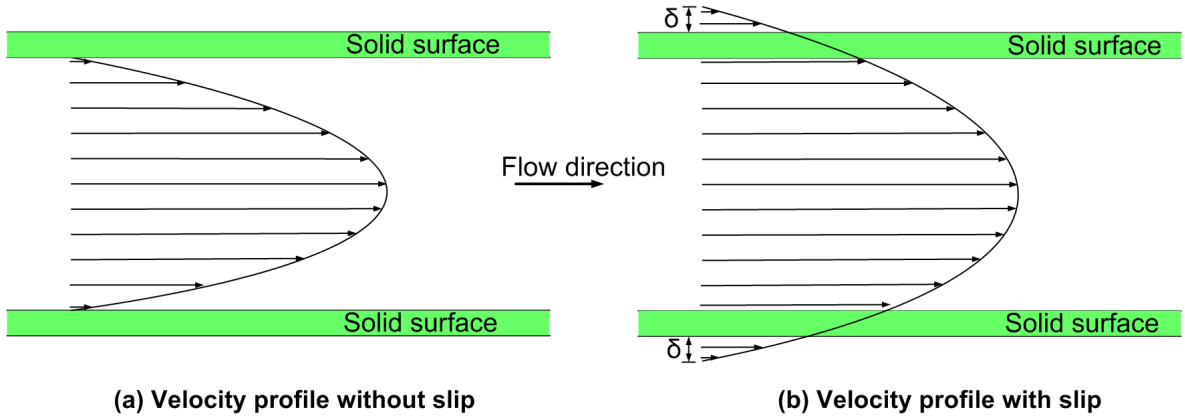


Figure 4.1: Schematic representation of the fluid velocity profile in confined geometries. (a) Velocity profile without slip; (b) velocity profile with slip.

Fluid flow in confined geometries can be significantly affected by slip at the liquid/solid interface. The measure of slip is the so-called "slip length", which is defined as an extrapolated distance relative to the wall where the tangential velocity component vanishes (cf. Figure 4.1(b)). Assuming the presence of a slip-length, δ, the integration of the transport equations with the appropriate boundary conditions 4.1 results in a modified Hagen-Poiseuille relationship (Eq. 4.2):

$$\begin{cases} \frac{dv}{dr} = 0, & \mathrm{r} = 0 \\ v(r) = -\delta \frac{dv}{dr}, & \mathrm{r} = \mathrm{r}_p \end{cases} \tag{4.1}$$

$$J = J_{HP}\left(1 + \frac{4\delta}{r_p}\right) = J_{HP}\left(1 + f_C\right) \tag{4.2}$$

or in terms of permeability, $\mathrm{L}_p = \frac{J}{\Delta p}$:

$$L_p = L_{p,HP}\left(1 + f_C\right) \tag{4.3}$$

The slip-length is a function of the several types of interactions occurring between solvent and membrane. This observation provides a theoretical background for the presence of a correction factor, f_C, to the classical Hagen-Poiseuille model for flow in nanopores. The

aim of the following section is to discuss a reliable correction factor as a function of solvent and membrane properties and to test the plausibility of Eq. 4.3 as a general model for a robust description of the solvent transport.

4.2.2 Capillary rise in nanopores: Lucas-Washburn equation

It is well known that the spontaneous motion of a solvent inside a small tube is described by capillarity. Since the membranes used in this study all have pores with nanoscale dimensions, the occurrence of capillary effects inside the pores is possible.

Dimitrov et al. [86, 87] studied capillarity at the nanoscale, using the penetration of fluids into fine pores with wettable walls by both spontaneous and forced imbibition. They supported the validity of the Lucas-Washburn equation at the nanoscale [86, 87]. This equation describes the capillary rise in small pores and follows from integration of the differential equation describing steady state flow, where the capillary force inside the pore is balanced by the viscous drag, with the assumption that the Navier-Stokes equation and the no-slip boundary conditions are valid. The capillary force determines a capillary pressure, p_C, inside the nanotube (cf. Eq. 4.4), proportional to the liquid surface tension, γ_{LV}, the contact angle between the two phases, θ, and the inverse of the pore radius, r_p.

$$p_C = \frac{2\gamma_{LV} cos\theta}{r_p} \tag{4.4}$$

Note that p_C can be either positive or negative, depending on the contact angle θ, i.e. on the affinity between membrane and solvent.

Dimitrov et al. [87] extended the studies to the effect of external pressure on the imbibition process, referring to the so-called "forced" imbibition. They extended the original Lucas-Washburn approach to include the external pressure, Δp, in the total effective pressure, as driving force of the process (cf. Eq. 4.5):

$$\Delta p_{eff} = p_C + \Delta p = \frac{2\gamma_{LV} cos\theta}{r_p} + \Delta p \tag{4.5}$$

It is interesting to note that the effects of external and capillary pressures were found to

be additive. This implies that the combination of spontaneous and forced motion of a fluid inside a nanopore can be described by considering the total effective pressure, given by the sum of the externally applied pressure plus a term governed by purely surface interactions. Similarly, when referring to the Hagen-Poiseuille model (cf. Eq. 2.25), the flux can be written as function of the effective pressure, Δp_{eff}, as in Eq. 4.6:

$$J = K_{HP}\frac{\Delta p_{eff}}{\mu} = K_{HP}\frac{(\Delta p + \tilde{p_C})}{\mu} = \frac{K_{HP}\Delta p}{\mu}\left(1 + \frac{\tilde{p_C}}{\Delta p}\right) \tag{4.6}$$

where K_{HP} is the constant of the Hagen-Poiseuille model and the factor $\frac{\tilde{p_C}}{\Delta p}$ becomes the correction factor f_C. It is worth noting that K_{HP} can be considered constant for ceramic materials, because it depends on membrane structural parameters only. It was assumed that the pore structure remains unchanged for ceramic membranes exposed to organic solvents.

Note that $\tilde{p_C} = \mathrm{C_1}\ p_C$ has been used in the formula above instead of p_C. In fact, it is clear that the phenomenon of capillary rise is not fully equivalent to the permeation of a solvent under forced conditions into a nanopore. However, it is believed that in both cases a major role is played by the correction term p_C derived by the Lucas-Washburn equation, which quantifies the interactions of the solvent with the pore walls. The correction constant $\mathrm{C_1}$ emphasises the similarity between the two phenomena.

4.2.3 The correction factor f_C

The correction factor should account for all the dependences that affect the permeability through nanopores, apart from viscosity, which is already included in the Hagen-Poiseuille term, $\mathrm{L}_{p,HP}$ (cf. Eq. 4.3). It was assumed that the gap between the experimental permeability and the permeability given by the viscous flow is due to interactions between solvent and pore walls only. In other words, for larger pores the correction factor becomes negligible and the permeability is easily reduced to the Hagen-Poiseuille permeability.

The main solvent, membrane and interaction parameters identified by the literature are summarised in Table 2.1. They are, briefly: the solvent and membrane surface tensions, the solvent and membrane polarities (mainly as dielectric constants), and the solvent and pore dimensions.

The Lucas-Washburn equation points to the importance of the liquid-vapour surface tension and the contact angle (which in turn determine the interfacial tension between a solvent and a solid surface), on the solvent transport both by spontaneous and forced imbibition. That is, the affinity between the liquid and the solid phases is described by means of contact angle values. Similar approaches were used by other authors. Geens et al. [48] introduced the effect of the surface tension as an influencing parameter, and they assumed that the permeability was proportional to the difference between the solvent and membrane surface tension values; Darvishmanesh et al. [49] introduced the same effect as the ratio between solvent and membrane surface tension values (cf. Eq. 2.45). In the new model the surface tension was introduced as a component of the capillary pressure term (cf. Eq. 4.4). The correction factor was assumed proportional to the capillary pressure, which can be positive or negative, according to the sign of the cosine of the contact angle (i.e. according to the affinity between solvent and membrane phases).

Polarity was considered as a further contribution. Polarity effects were introduced by Geens et al. [48] and by Darvishmanesh et al. [49] by including the dielectric constant in the model. However, the dielectric constant is only one of the possible descriptors for the polarity; the dipole moment is another possibility. The two parameters are not linearly correlated (cf. Figure 4.2), and it is interesting to note that they are characterised by clearly separated behaviours for different classes of solvents (apolar, polar protic and polar aprotic solvents). The main difference between the two descriptors, to which the lack of proportionality between the two is ascribed, is that the dielectric constant is a bulk property, while the dipole moment is a molecular property.

An effect of the presence of a dipole moment in the solvent is the possible obstruction effect due to the orientation of the molecules at the pore walls. A high degree of orientation can cause the formation of layers of highly interacting molecules, which in turn can cause a restriction of the effective pore radius [88], [89]. The dipole moment is, therefore, a better candidate for the correction factor, as it is consistent with the choice of f_C comprising only terms representing the interactions of the solvent molecules with the pore walls. Accordingly, a term which is proportional to $|\delta_s - k_{pol}|$, where δ_s is the dipole moment of the

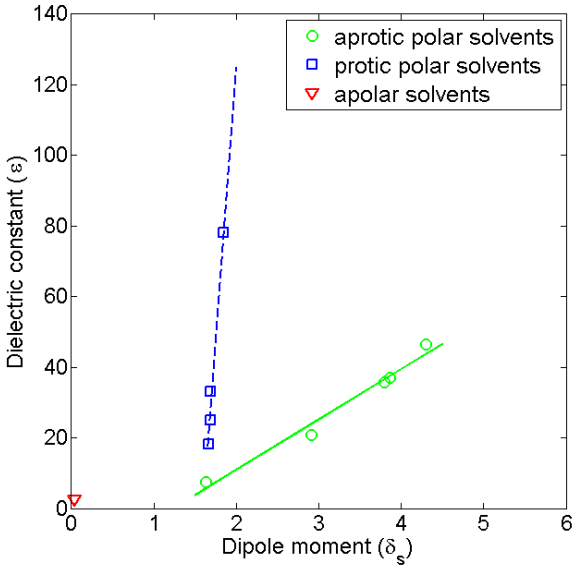


Figure 4.2: Relationship between dielectric constant and dipole moment for different classes of solvent polarity.

solvent and k_{pol} the polarizability of the membrane has been introduced in the correction factor. The description of the calculation of k_{pol} is given below (cf. Paragraph 4.2.3), where both k_{pol} and the contact angle, θ, needed for the Washburn term of the correction factor, are computed in the frame of the surface polarizability theory [88] as a function of the surface tension components of the solvents.

At the nanoscale, the dimension of the solvent molecules is comparable with the dimension of the pore. Steric hindrance is therefore plausible. As in Darvishmanesh et al. [49], this effect is introduced via the correction factor as the ratio of molecular radius to pore radius, since it is representative of the molecular steric hindrance in the pore.

In conclusion, the proposed model incorporates the following solvent, membrane and interaction parameters: (i) viscosity, as the governing factor; (ii) surface tension and contact angle between solvent and membrane, inside the capillary pressure term; (iii) polarity; and (iv) effective molecular dimension. The correction factor is defined in Eq. 4.7 for the generic solvent:

$$f_C = f_{C_{capillary}} + f_{C_{dipole}} + f_{C_{steric}} = C_1 \frac{2\gamma_{LV} cos\theta}{r_p} + C_2|\delta_s - k_{pol}| + C_3 \left(\frac{r_s}{r_p}\right)^2 \quad (4.7)$$

r_s and r_p are the solvent and pore radii, and C_1, C_2 and C_3 are the three fitting parameters (or proportional factors) characteristic of the membrane. The sign of the global correction factor, f_C, depends on the sum of the three single contributions. Capillary forces can be either positive or negative. Therefore, the sign of $f_{C_{capillary}}$ depends on the sign of the cosine of the contact angle. Negative cosine values of contact angles represent lack of affinity, while positive cosine values represent high affinity. For this reason, C_1 is expected to have a positive value, so that the higher the affinity, the higher the positive contribution to the increase in permeability, and vice versa. On the other hand, both dipole and steric effects are expected to decrease permeation. In particular, it is expected that solvent orientation is proportional to the difference in dipole moment between solvent and membrane only, independently of the sign of such difference. For this reason, both C_2 and C_3 are expected to assume negative values only, as in both cases the main argument of the correction factor can be only positive. Note that during the parameter fitting (see the Experimental Result section), all the three coefficients C_i are left free to take any value, positive or negative. This will be used as an indirect test of the validity of our model.

Calculation of k_{pol} and θ

The polarity of the solvent molecules was compared to the polarity of the membrane. The membrane itself , in fact, possesses the capability to be polarised. Giovambattista et al. [89] studied the relationship between surface polarity, hydrophilicity and water contact angle for silica surfaces by carrying out molecular dynamics simulations. They found that the surface polarity is quantified by the dipole moments of the SiOH groups at the wall surface. Each of the these groups contributes with a dipole moment given by $p = p_{SiO} + p_{OH}$, where p_{SiO} is the dipole moment due to the charge of the Si atom and a compensating partial charge on the O atom. Similarly, p_{OH} is the dipole moment due to the charge of the H atom and a corresponding compensating partial charge on the O atom. It was assumed that the

same phenomenon occurs for TiO_2 and ZrO_2 surfaces. The adsorption of water and organic solvents on the membrane walls can change the contribution of the surface charged groups, therefore changing the contribution of the polar component of the surface free energy.

This theory of the surface polarizability, based on the hypothesis of solid surface polarity induced by the liquid in contact, was proposed by Carré et al. [88], and is a modification of the standard theory of the surface components developed by Owens et al. [90]. This theory introduces a new parameter, not commonly recognised in the theory of the permanent polarity, which is defined as membrane polarizability, k_{pol} (cf. Eq. 4.8):

$$k_{pol} = 2\sqrt{\frac{\gamma_{SV}^{p}}{\gamma_{LV}^{p}}} \tag{4.8}$$

where γ_{SV}^{p} and γ_{LV}^{p} are the polar components of the solid and liquid surface tension, respectively. According to this theory, the contact angle is a function of the solid and the liquid surface tension components, as described in Eq. 4.9.

$$cos\theta = \left(2\sqrt{\gamma_{SV}^{d}} + k_{pol}\frac{\gamma_{LV}^{p}}{\sqrt{\gamma_{LV}^{d}}}\right)\frac{\sqrt{\gamma_{LV}^{d}}}{\gamma_{LV}} - 1 \tag{4.9}$$

γ_{SV}^{d} and γ_{LV}^{d} are the dispersion components of the solid and liquid surface tension, respectively. This equation was adopted to calculate firstly the solid surface tension components, by knowing the experimental contact angles of two given solvents, and then the contact angle of all the other solvents. In this work the difference between the solvent dipole moment and the membrane surface polarizability, k_{pol}, was chosen to take into account the possible effect of the polarity.

4.2.4 Parameter estimation and prediction

K_{HP} was obtained by linear regression of experimental permeability data vs. inverse of viscosity for five solvents with different physico-chemical properties. C_1, C_2 and C_3 were obtained by non-linear regression of experimental permeability data for the same five solvents. The least squares (OLS) approach was adopted, i.e. the best-fit curve which minimises the sum of squared residuals was found. Both linear and non-linear regressions were

carried out using suitable functions in Matlab2008a [91].

The model including the estimated parameters was then used to make predictions for six further solvents and solvent mixtures. The performance of the model was evaluated by calculating the standard deviation.

4.2.5 Modelling for solvent mixtures

The structure of the new model permits an easy extension to the case of solvent mixtures. The formulation of the new model for a generic mixture of solvents i and j is presented in Eq. 4.10.

$$L_{p,mix} = \frac{K_{HP}}{\mu_{mix}}(1 + f_{C,mix}) \tag{4.10}$$

The solvent permeability, viscosity and correction factors were substituted by the corresponding terms for the mixture ($L_{p,mix}$, μ_{mix}, $f_{C,mix}$, respectively). K_{HP} remained unchanged, as it is a function of membrane structural parameters only. The mixture viscosity is normally accessible from either simple experimental data or theoretical prediction by suitable mixing rules. The correction factor for a mixture, in contrast, is not easily evaluable in an independent manner, since it contains physical properties that are not commonly accessible for the solvent mixtures. The assumption that viscosity plays a central role in describing the solvent permeation has two consequences: (i) the highly non-linear profile of the mixture viscosity as a function of the composition has to be taken into account; and (ii) it is plausible to make simplifying hypotheses to calculate the correction factor, in order to use the model as a practical and effective predictive tool.

In this work, an easy mixing rule for the correction factor was tested, that is to obtain mixture correction factors from the weighted average with the molar composition, according to Eq. 4.11.

$$f_{C,mix} = x_i f_{C,i} + (1 - x_i) f_{C,j} \tag{4.11}$$

The correction factor for the mixture $i + j$ was calculated from the correction factors for

the pure solvents, $f_{C,i}$ and $f_{C,j}$, respectively. These are accessible for any solvent through an a priori calculation.

4.3 Experimental

4.3.1 Materials

Solvents

Feed solvents and solutions were selected in order to cover a broad range of properties (viscosity, surface tension, polarity and molecular dimension). The solvents used in this study were water, acetonitrile (ACN), methanol, ethanol, toluene, dimethylformamide (DMF), isopropanol, tetrahydrofuran (THF), dimethyl sulfoxide (DMSO), acetone, and N-methylpyrrolidone (NMP) (supplied by Sigma Aldrich or Scharlau, with purity $\geq 99\%$) . Their properties are listed in Table 4.1. Viscosity, molecular weight, density, dielectric constant, dipole moment and surface tension of the solvents were taken from the literature (atmospheric pressure and 25°C, [49, 92, 93]).

In membrane filtration processes, the size of a molecule significantly affects its transport through nanopores [94]. Different size descriptors are generally available: the molecular weight, the Stokes diameter and other size descriptors which take into account the molecular geometry. In this work the effective molecular dimension, d_s, is estimated by evaluating the steric hindrance of the molecule in the molar volume. The liquid phase represents the state at which the molecules are separated by the minimum possible distance (which is reflected by relative incompressibility), while still remaining able to move with respect to each other. The volume occupied by one molecule in the volume is comparable to the steric hindrance of the molecule. By assuming a regular packing of the molecule in the molar volume, V_m, and by assuming that each molecule could be inscribed in a cube, the molecular dimension was assumed as the dimension of the cube that circumscribes the molecule:

$$d_s = \left(\frac{V_m}{N_A}\right)^{\frac{1}{3}} \tag{4.12}$$

Table 4.1: Solvents used in this study and their characteristics

solvent	μ **[cP]**	MW **[Da]**	ρ_L **[g ml^{-1}]**	ϵ_L **[-]**	δ_s **[D]**	γ_{LV} **[mNm^{-1}]**	d_s **[nm]**
ACN	0.34	41.1	0.78	35.7	3.49	28.66	0.44
water	1	18	1	78.2	1.85	72.8	0.31
methanol	0.54	32	0.78	33	1.69	22.12	0.41
DMF	0.92	73.1	0.946	37	3.86	36.3	0.50
ethanol	1.08	46.1	0.78	24.9	1.69	21.99	0.46
NMP	1.7	99.1	1.027	32.2	4.09	40.7	0.54
acetone	0.3	58.1	0.88	20.7	2.91	23.3	0.48
isopropanol	1.96	60.1	0.786	18.23	1.66	21.7	0.50
THF	0.46	72.1	0.89	7.5	1.63	24.98	0.51
toluene	0.55	92.1	0.86	2.4	0.36	27.92	0.56
DMSO	1.999	78.1	1.095	46.4	3.96	42.98	0.49

The comparison of the effective molecular dimensions calculated from molar volume data (Table 4.1) and the kinetic diameters from literature [95] showed a good agreement.

Solvent mixtures

Four aqueous and four organic mixtures were investigated over the whole composition range. The mixtures used in this study are summarised in Table 4.2.

The composition of the mixtures was controlled by gas chromatography before and after the NF experiments. The viscosity of the mixtures was calculated using the mixing rule suggested by Teja and Rice [96], with the interaction parameter evaluated from the fitting of literature data.

Table 4.2: Solvent mixtures used in this study

Organic/aqueous mixtures	Organic/organic mixtures
ACN/water	methanol/ethanol
methanol/water	methanol/ACN
ethanol/water	toluene/DMF
DMF/water	toluene/ACN

Membranes

The cross-flow filtration system used in this study contained a tubular module, suitable for multichannel tubular membranes with a length of 250 mm and an outer diameter of 25 mm. Four commercial ceramic membranes were used in this study, with two different active layers, TiO_2 and ZrO_2, respectively, on Al_2O_3 and different MWCOs. Three of them were prepared by Inopor (Germany) under the commercial names of Inopor® Nano 750 Da, Inopor® Nano 450 Da, and Inopor® Ultra 2000 Da. The fourth membrane was provided by Sulzer, with a nominal MWCO of 1000 Da. All the membranes had 19 channels with an internal diameter of 3.5 mm and filtration area of 516 cm^2. The MWCO values and the nominal pore dimensions of the active top layer were measured by the manufacturer. The nominal properties of the membranes are summarised in Table 4.3.

4.3.2 Methods

Contact angle and surface tension measurements

Contact angle measurements were carried out on flat samples of the same material as the active top layer inside the membrane channels; the samples were kindly provided by Inopor (Germany). Measurements were done using two standards: water and glycerol, on a OCA-15 plus equipment (DataPhysics). A drop of each solvent was put on the top layer of the

Table 4.3: Membranes used in this study and their characteristics, as provided by the supplier

Membrane/Supplier	Material	MWCO [Da]	Range	Pore dimension [nm]
Inopor® Nano	TiO_2	450	NF	0.9
Inopor® Nano	TiO_2	750	NF	1
Sulzer	TiO_2	1000	UF	2.5
Inopor® Ultra	ZrO_2	2000	UF	3

sample and the contact angle between the drop and the surface layer was calculated by the instrument. The membrane surface tension was calculated afterwards from the contact angle measurements using the theory of the surface tension components, discussed above (cf. Eq. 4.9).

Contact angle values and membrane surface tension components calculated by the theory of surface induced polarity [88] are given in Table 4.4. The properties are assumed to be valid for all membranes of the same material, irrespective of their pore size. Porosity of these surfaces is supposed to be too small to influence the measure of the contact angle.

Table 4.4: Contact angle values for water (θ_w) and glycerol (θ_g) and surface tension values for the materials according to the theory of surface induced polarity

Membrane material	$\theta_w[^\circ]$	$\theta_g[^\circ]$	γ^d_{SV} [mN m^{-1}]	k_{pol} [-]	$\gamma^p_{SV,w}$ [mN m^{-1}]
TiO_2	45	50	27.1	1.5	28.2
ZrO_2	80	82	13.5	1.0	12.8

The value of the solid polarizability, k_{pol}, and of the polar component of the surface

free energy induced by the contact with water, $\gamma^p_{SV,w}$, are larger for the more hydrophilic material, TiO_2, as expected.

Solvent permeation

The permeation experiments were carried out in a Natan cross-flow system (Natan GmbH, CH), shown in Figure 4.3.

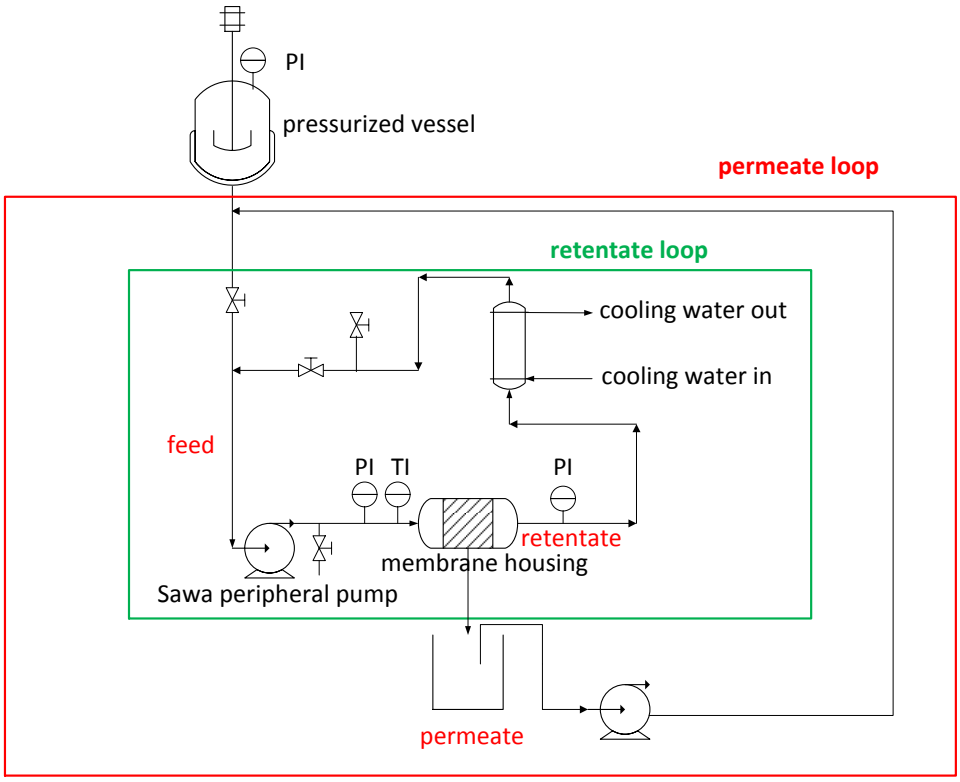


Figure 4.3: Natan cross-flow system (Natan GmbH, CH). Close loop for permeation tests.

The permeate was collected in a graduated cylinder and the flux monitored. Different cross-membrane pressures were tested for each solvent and membrane, from 1 to 6 bar. The permeation flux increased linearly with applied pressure, therefore the permeability, L_p (in [l $m^{-2}h^{-1}bar^{-1}$]) was constant in this pressure range. The membranes were conditioned for at least 10 h in the solvent before measurement, to allow any adsorption of solvent

molecules to the surface, so to reach steady state. The temperature was maintained at 19-20°C in all experiments, and the flux was monitored until a constant value was reached at this temperature (by recycling both retentate and permeate in a close loop). Water flux was used as a reference value and it was checked in between measurements of solvent flux for each membrane. The water flux was found to be constant during the investigation, with an experimental error of ±10%. As the membranes tested always remained within these limits, they were not changed during the investigation. Thus each data set was obtained using a single membrane piece.

4.4 Results and discussion

4.4.1 Permeability measurements of pure solvents

The validity of the Hagen-Poiseuille model implies the linearity of the profile of the experimental permeability, L_p, against the inverse of viscosity, μ^{-1}. In Figure 4.4, the permeability of a wide class of solvents is plotted against the inverse of viscosity for the UF and NF range, respectively.

A linear regression was done on the experimental data for each membrane to obtain a line through the origin with slope K_{HP} (cf. Figure 4.4). The fitted slopes correspond to the Hagen-Poiseuille constants and are reported in Table 4.5 for the four membranes.

The quality of the fitting, R^2, increases with the pore radius. This was expected, as UF membranes are expected to behave according to the Hagen-Poiseuille model, i.e. correction factors are small in this case. Viscosity, the only solvent parameter taken into account by the Hagen-Poiseuille model, explains most of the data variability. In other terms, it is confirmed that permeation is driven by viscosity and that in NF pores correction factors are needed to take into account the interactions of each solvent with the membrane.

As in Tsuru et al. [51] and in Dobrak et al. [97], the experimental results were interpreted by comparison with the Hagen-Poiseuille theory. In this case, the permeability, L_p, multiplied by the viscosity μ is constant, irrespective of type of solvent [51] (cf. Eqs. 2.25 and 4.3):

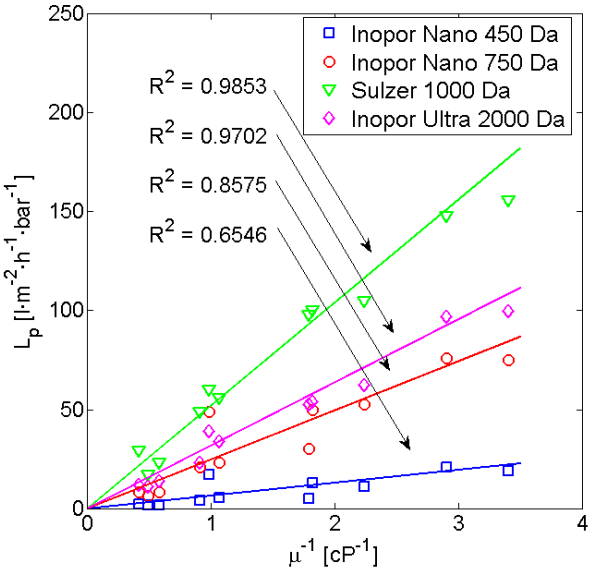


Figure 4.4: Experimental permeability of organic solvents and water in the NF range and best linear fitting (R^2).

Table 4.5: Hagen-Poiseuille proportionality constants and coefficient of determination (R^2) of the linear fitting

Model	**Inopor Nano® 450 Da**	**Inopor Nano® 750 Da**	**Sulzer 1000 Da**	**Inopor Ultra® 2000 Da**
K_{HP} [10^{-14} m]	1.8	6.9	14.5	8.9
R^2	0.6546	0.8575	0.9853	0.9702

$$K = L_p \mu \tag{4.13}$$

This is shown in Figures 4.5(a) to 4.5(d).

For Inopor® Nano 450 and 750 Da, the product of permeability by viscosity changed significantly with the solvent (cf. Figures 4.5(a) and 4.5(b), respectively). The product K, defined in Eq. 4.13, was much higher for water in comparison to the value of all the other solvents used in the investigation. In contrast, the values of K for toluene, NMP, DMSO and isopropanol were much lower than the values of all the other solvents. Note that the dashed lines in Figures 4.5(a-d) represent the value of K_{HP} from Table 4.5.

For Inopor® Ultra 2000 Da and Sulzer 1000 Da (cf. Figures 4.5(c) and 4.5(d), respectively), the K values are relatively similar for the different solvents, and closer to the corresponding K_{HP}. This shows that for membranes in the UF range, solvent transport could be adequately described by viscous flow [97], in contrast to the NF range. The gap between the actual K values and the regressed K_{HP} values, in the NF range, must be explained by some factors other than viscosity.

In conclusion, the viscosity plays a major role in explaining most of the permeation behaviour of water and organic solvents but it is not sufficient to describe it with the desired precision, especially in NF membranes.

4.4.2 Modelling for pure solvents

Model parameters

Three transport models were evaluated on the experimental data: the Hagen-Poiseuille model [25, 16], the Coupled Series-Parallel Resistance (CSPR) model [49] and the model of this work. The three models contain specific fitting parameters, summarized in Table 4.6.

The fitting parameters were evaluated with the same procedure for all the models: the numerical fitting of the experimental data was done using a least square fit to obtain the value of the unknown parameters (Matlab2008a, Mathworks [91]). The model parameters were regressed on data for permeation of five solvents with different physical characteristics:

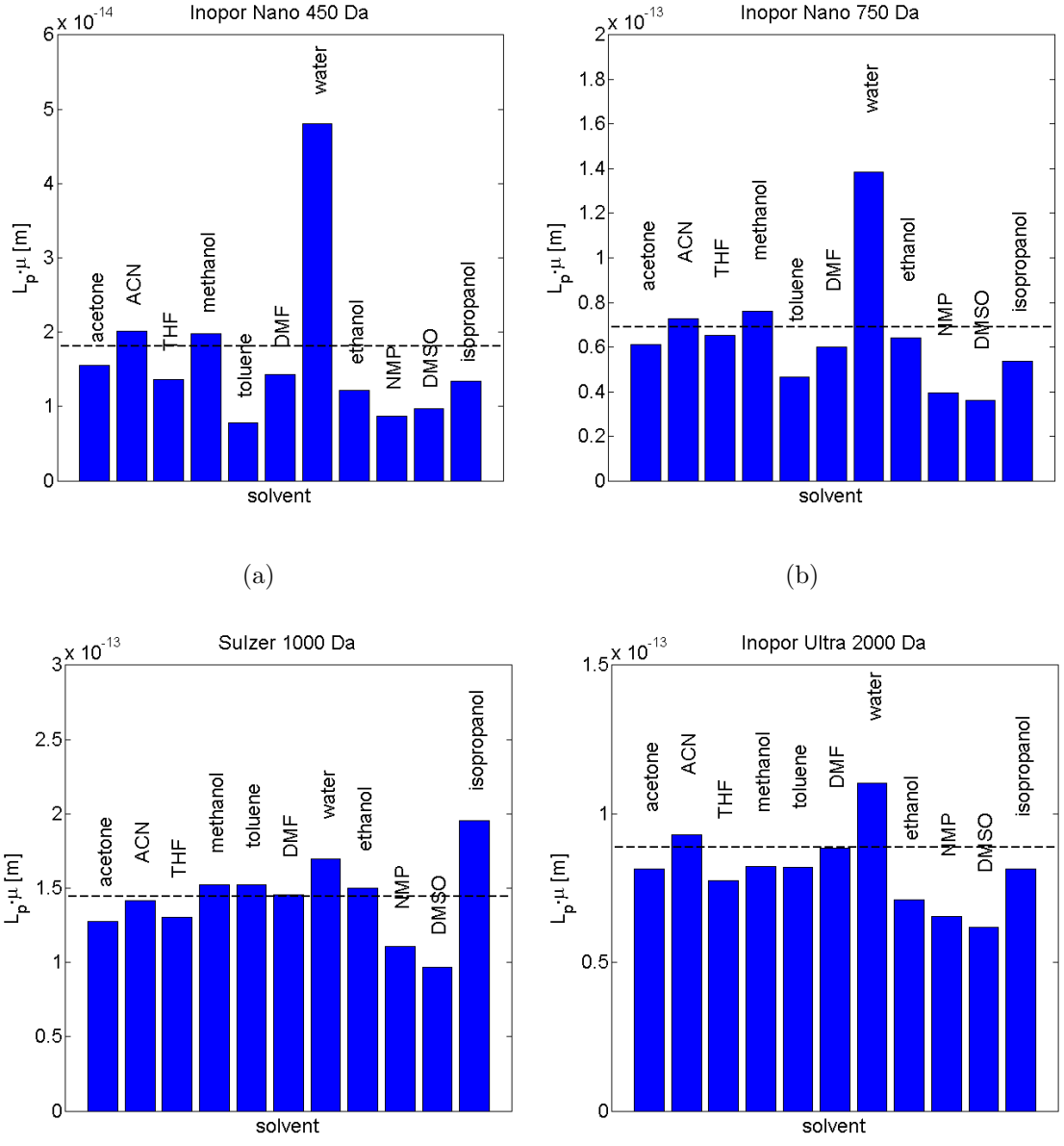


Figure 4.5: Product of permeability by viscosity (Eq. 4.13) for NF and UF membranes.

Table 4.6: Fitting parameters for Hagen-Poiseuille, coupled series-parallel resistance and new models

Model	Fitting parameters	Regression
Hagen-Poiseuille model	K_{HP}	linear
CSPR model	k_s,k_m, k_p	non-linear
New model	K_{HP}	linear
	C_1, C_2, C_3	non-linear

water, ACN, ethanol, DMF and toluene. Looking at Table 4.1, the choice of the five solvents was made to cover a broad range of values of viscosity, dielectric constant and surface tension.

The values of the three non-linear fitting parameters are reported in Table 4.7. As discussed above, the contribution of the capillary term is dependent on the sign of the cosine of the contact angle, C_1 being a positive constant, while the contribution of the other two terms is always negative, C_2 and C_3 being negative constants.

In Tables 4.8 and 4.9, the values of the correction factors for the different membranes are reported when working with water and toluene, respectively.

Table 4.7: Capillary, dipole and steric membrane parameters

Membrane parameter	Inopor Nano® 450 Da	Inopor Nano® 750 Da	Sulzer 1000 Da	Inopor Ultra® 2000 Da
C_1	$9.13\ 10^{-4}$	$6.43\ 10^{-4}$	$2.36\ 10^{-4}$	$8.89\ 10^{-4}$
C_2	$-3.86\ 10^{-2}$	$-4.48\ 10^{-2}$	$-3.13\ 10^{-2}$	$-4.83\ 10^{-3}$
C_3	$-4.24\ 10^{0}$	$-3.09\ 10^{0}$	$-1.36\ 10^{0}$	$-2.14\ 10^{0}$

Table 4.8: Capillary, dipole, steric and global correction terms for water

Correction term	Inopor Nano® 450 Da	Inopor Nano® 750 Da	Sulzer 1000 Da	Inopor Ultra® 2000 Da
$f_{C_{capillary}}$	2.09 10^{0}	1.33 10^{0}	1.94 10^{-1}	1.49 10^{-1}
$f_{C_{dipole}}$	-1.42 10^{-2}	-1.16 10^{-2}	-1.15 10^{-2}	-2.86 10^{-3}
$f_{C_{steric}}$	-5.04 10^{-1}	-2.97 10^{-1}	-2.09 10^{-2}	-2.28 10^{-2}
f_{C}	1.57 10^{0}	1.01 10^{0}	1.62 10^{-1}	1.24 10^{-1}

Table 4.9: Capillary, dipole, steric and global correction terms for toluene

Correction term	Inopor Nano® 450 Da	Inopor Nano® 750 Da	Sulzer 1000 Da	Inopor Ultra® 2000 Da
$f_{C_{capillary}}$	1.09 10^{0}	6.96 10^{-1}	1.02 10^{-1}	-4.91 10^{-2}
$f_{C_{dipole}}$	-4.32 10^{-2}	-5.03 10^{-2}	-3.51 10^{-2}	-4.35 10^{-3}
$f_{C_{steric}}$	-1.65 10^{0}	-9.76 10^{-1}	-6.87 10^{-2}	-7.51 10^{-2}
f_{C}	-5.99 10^{-1}	-3.29 10^{-1}	-1.72 10^{-3}	-1.29 10^{-1}

The importance of the correction factors decreased with the nominal pore size, becoming nonessential in the UF range. Among the three terms, the dipole moment contribution was small compared to the capillary and the steric terms in both NF and UF range. Both capillary and steric terms were higher in the NF range and than in the UF range, even working with toluene, where the difference with the membrane polarizability is greater. Capillary forces and steric effects have a much larger impact in the NF membranes than

in the UF ones for both solvents. It is also interesting to notice that for water capillary forces are more important than steric effects as compared to toluene. This is expected, as both TiO_2 and ZrO_2 are hydrophilic. Interestingly, for toluene on ZrO_2, the capillarity contribution to the correction term is negative (very low affinity) and, summed up to the other two correction factors, contributes in lowering the global correction factor to about the same absolute value as for water on the same membrane.

In conclusion, capillary and steric effects play a determining role in the permeation of solvents through NF and UF membranes. The dipole correction term makes a less important contribution.

Model validation

The predictive capability of the three models was tested by using the regressed parameters, K_{HP}, C_1, C_2 and C_3, to predict the permeation of the six remaining solvents. The predictions of the three models are shown in Figures 4.6(a-b) for the NF membranes and in Figures 4.6(c-d) for the UF membranes for the three models considered above.

The standard deviations, σ_{L_p}, of the three models were calculated from the predicted permeability values, according to Eq. 4.14, and they are presented in Table 4.10.

$$\sigma_{L_p} = \sqrt{\frac{1}{N-1}\sum_i \left(\frac{L_{p,i} - L_{p,i}^{exp}}{L_{p,i}^{exp}}\right)^2} \tag{4.14}$$

$L_{p,i}$ and $L_{p,i}^{exp}$ are the calculated and experimental permeabilities, respectively, and N is the total number of experimental points.

As expected, the Hagen-Poiseuille model shows high correlations with experimental data in the UF range and large deviations in the NF range.

The predictions of the CSPR model show a general good agreement with experimental data. The experimental error is lower than that from the Hagen-Poiseuille model for both Inopor® 750 Da and Inopor® 450 Da. Interestingly, larger deviations of the CSPR model were observed in the UF range compared to the Hagen-Poiseuille model. The CSPR model failed, therefore, to consistently predict flux across the continuum from the UF to the NF

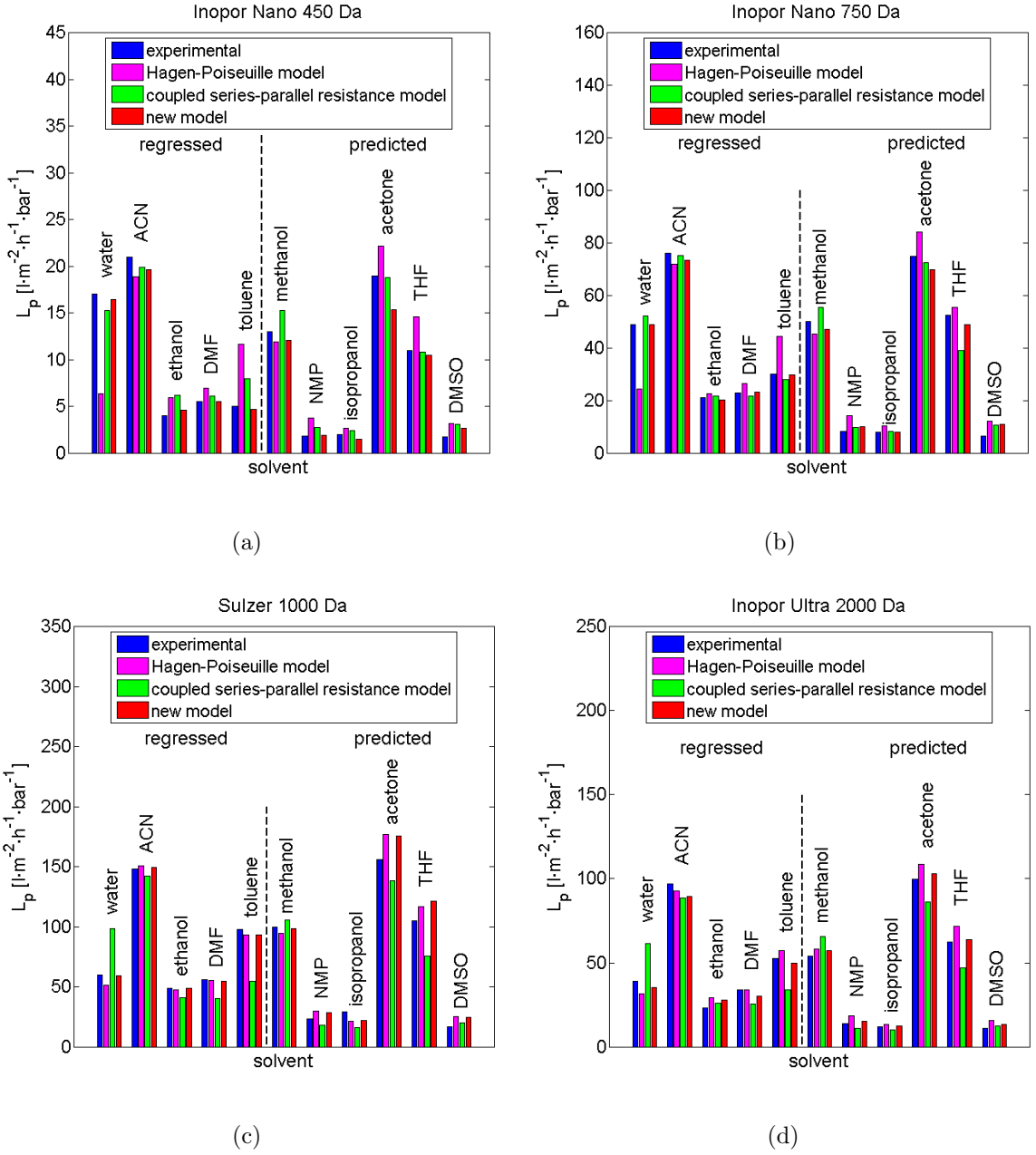


Figure 4.6: Prediction of permeability by Hagen-Poiseuille, coupled series-parallel resistance and new models in the NF and UF range.

Table 4.10: Standard deviations, σ_{L_p} of coupled series-parallel resistance, Hagen-Poiseuille and new model

Model	Inopor Nano® 450 Da	Inopor Nano® 750 Da	Sulzer 1000 Da	Inopor Ultra® 2000 Da
Hagen-Poiseuille model	0.68	0.44	0.22	0.22
CSPR model	0.41	0.24	0.33	0.27
New model - three fitting parameters (C_1, C_2, C_3)	0.22	0.24	0.19	0.11
New model - two fitting (parameters C_1, C_3)	0.25	0.28	0.22	0.12

range. This can be ascribed to an arbitrary incorporation of the functional dependences, without taking into account the governing role of the viscosity as the main influencing parameter for the permeation through both NF and UF membranes. It is also interesting to notice that the highest σ_{L_p} value was actually obtained for the tighter membrane.

Finally, the model proposed in this work shows good correlations with experimental data in both NF and UF range. It is clear from the comparison of the standard deviations that this model represents an improvement to both the Hagen-Poiseuille and the CSPR model.

The model can be simplified with only two fitting parameters in the correction factor, i.e. by removing the correction term for polarity. The simulation with two parameters (C_1 and C_3) is consistent and gives experimental errors similar to those obtained using the three-parameters version of the model (C_1, C_2 and C_3), as shown in Table 4.10.

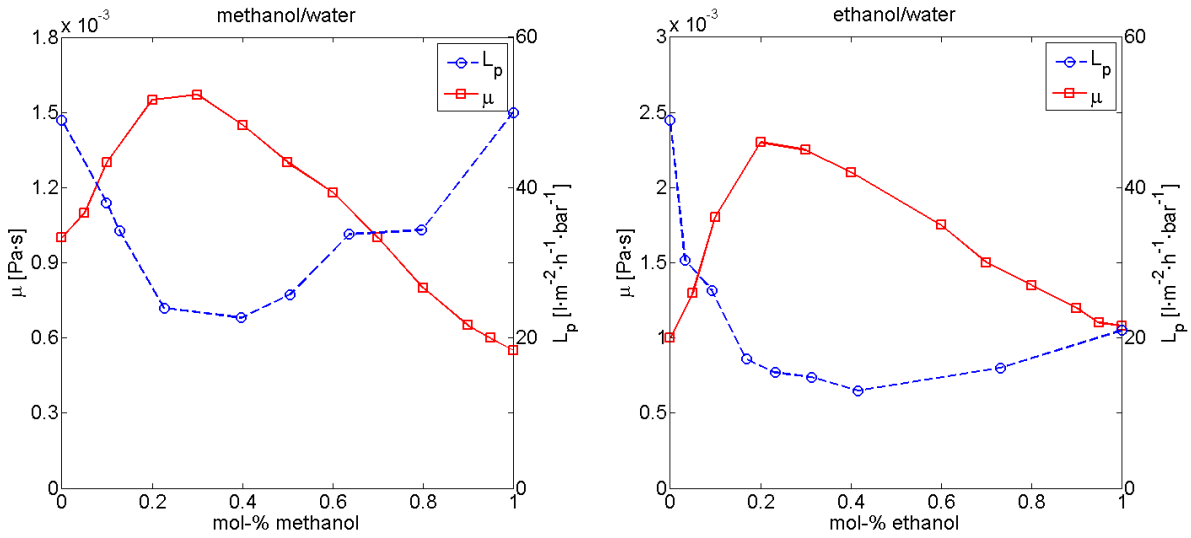
4.4.3 Permeability measurements of solvent mixtures

A key factor that can distinguish the pore-flow from the solution-diffusion transport mechanism is the degree of solvent separation [82]. In the pore-flow model, no solvent separation is expected, while the solution-diffusion model predicts a small solvent separation, according to the values of diffusivity of the two species (the extent to which this is possible is very concentration dependent). In this work, the composition of the mixtures was controlled by gas chromatography. GC-analyses of feed, retentate and permeate samples showed that no significant differences in composition occurred (the difference in composition was always less than the experimental error of the measurement; data not shown). This indicated that liquid transport occurred mainly by convection, therefore, for the membranes used in this study, the liquid mixtures were considered as bulk liquids.

Some organic/water and organic/organic mixtures were investigated over the whole range of composition. For the majority of the cases, it was immediately observed that the profile of the permeability against the composition followed the opposite of the profile of the experimental viscosity for the same mixture: the permeability profile showed a minimum where the viscosity profile showed a maximum, and vice versa. The viscosity profiles were taken by different sources available in literature (methanol/water, ethanol/water and methanol/ethanol from [48], DMF/water from [98], ACN/water from [99], methanol/ACN from [100], toluene/ACN from [101], toluene/DMF from [102]). The profiles of permeability and viscosity for two aqueous and two fully organic solvent mixtures are shown in Figures 4.7 and 4.8, respectively. The permeability values correspond to the Inopor® 750 Da.

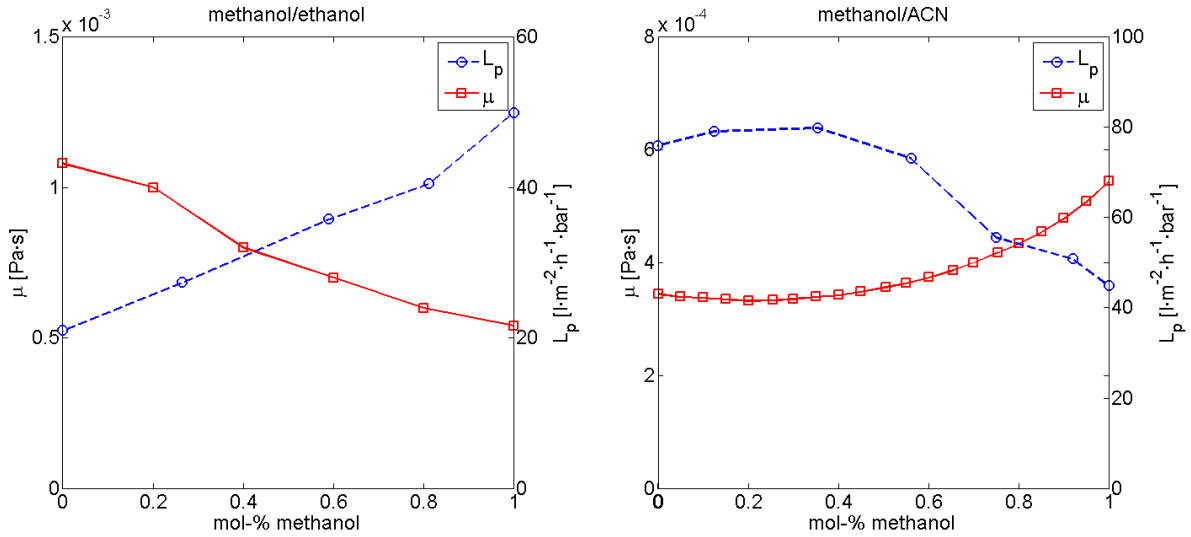
The similarity between the permeability and the viscosity profiles suggested that the viscosity again plays a fundamental role in influencing the permeation of solvent mixtures, as was the case for pure solvents.

The only significant exception to this behaviour is the ACN/water mixture, which showed a permeability profile different from the viscosity profile measured by Moreau et al. [99] (cf. Figure 4.9). The anomalous behaviour of this mixture will be approached later (cf. Paragraph 4.4.4).



(a) (b)

Figure 4.7: Profiles of permeability and viscosity vs. solvent composition of aqueous mixtures. Membrane: Inopor Nano 750 Da.



(a) (b)

Figure 4.8: Profiles of permeability and viscosity vs. solvent composition of organic mixtures. Membrane: Inopor Nano 750 Da.

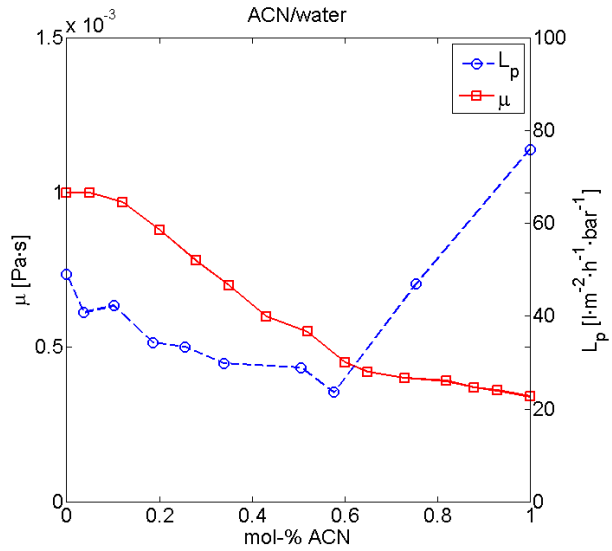


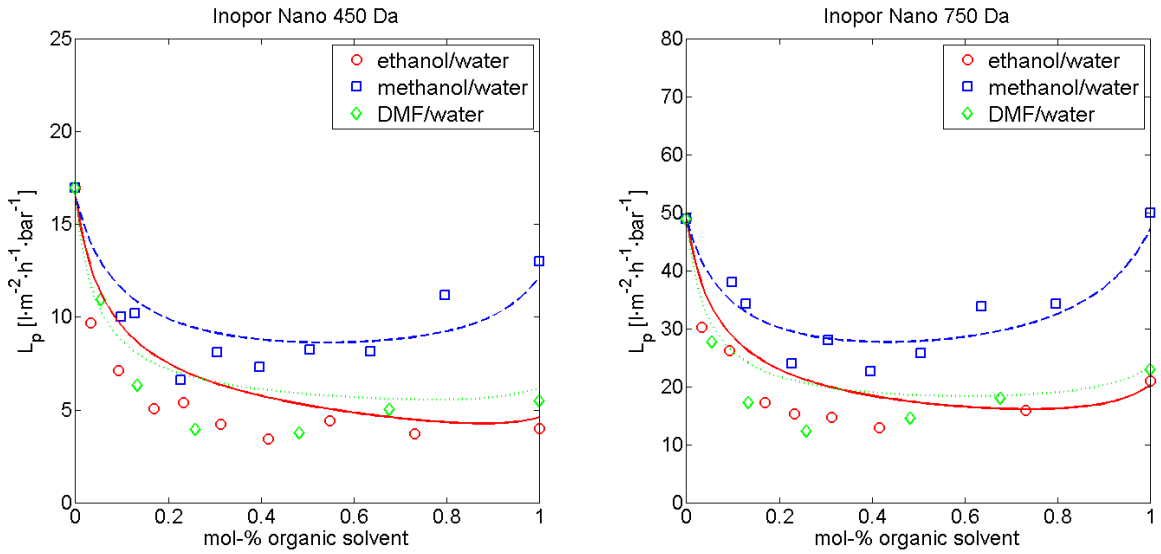
Figure 4.9: Profiles of permeability and viscosity vs. solvent composition for the ACN/water mixture. Membrane: Inopor Nano 750 Da.

4.4.4 Modelling for solvent mixtures

The model was tested on the experimental data for the aqueous and organic mixtures in a purely predictive way. Firstly, the permeability values of the pure solvents were calculated using the new model and subsequently the permeability for all intermediate compositions were calculated using the hypothesis of a weighted average of the correction factor on the solvent composition (cf. Eq. 4.11). The K_{HP} value is typical of the membrane and therefore was kept constant (cf. Table 4.5).

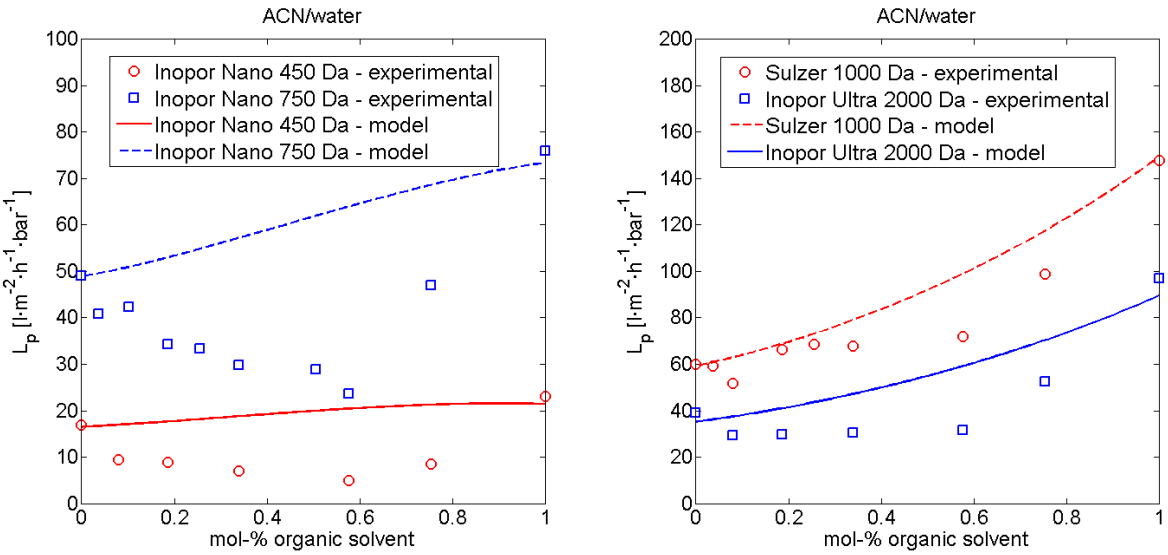
The predictions of the model for the four aqueous mixtures and the four membranes are shown in Figures 4.10 and 4.11. Figures 4.10(a-b) show the profiles for the aqueous mixtures of methanol, ethanol and DMF in the NF range. For all these mixtures the prediction of the new model is in good agreement with the experimental data. In contrast, the model fails to describe the profiles of ACN/water for the NF range (cf. Figure 4.11(a)). In the UF range, the model showed good predictions for the aqueous mixtures of ethanol, methanol and DMF (not shown), and also better (but still poor) predictions for ACN/water compared to the NF range (cf. Figure 4.11(b)).

The prediction of the model for the different organic mixtures is shown in Figure 4.12.



(a) (b)

Figure 4.10: Prediction of permeability of aqueous mixtures by the new model in the NF range. (—) ethanol/water; (– –) methanol/water; (· · ·) DMF/water.



(a) (b)

Figure 4.11: Prediction of permeability of ACN/water mixtures by the new model.

The prediction by the new model is in very good agreement with the experimental data for all the organic mixtures, supporting the simplifying hypothesis of linear correlation between correction factor and composition.

ACN/water mixtures

In the NF range the permeability profile shows a significant minimum, for both Inopor® Nano 750 and 450 Da, around 60-70%v ACN/water. The model is not able to capture the minimum, since it is based on the assumption that both the permeability and the viscosity depend on the composition in the same way.

The anomalous behaviour of the ACN/water mixture in the NF range could be attributed to the strong tendency of ACN and water to form complexes [99, 103]. ACN is a typical aprotic solvent and exhibits a strong complexation tendency due to the free electron pair of the nitrogen atom, responsible for the solvation of acceptor bonds. Kinart et al. [103] thoroughly studied the internal structures that ACN and water assume. They suggested the formation of intermolecular complexes, such as ACN·H_2O, ACN·$2H_2O$, 2ACN·$3H_2O$ and 2ACN·H_2O types. They carried out ^{1}H-NMR spectral studies and recorded the values of the chemical shifts differences δ_{NMR}(ACN-H_2O) at 298 K, between the center of the ^{1}H-NMR signals of the -OH group of water and the center of the ^{1}H-NMR signals of -CH_3 group of ACN molecules over the whole range of composition. The location of the maximum of this parameter refers to the composition with the strongest intermolecular interactions between the components, where hydrogen bonds are involved [103]. The profile showed a maximum around 67%mol ACN. The most stable complex formed at this composition suggested by the authors is 2ACN·H_2O. Furthermore, Moreau et al. [99] studied physical, thermodynamic and excess properties of acetonitrile + water mixtures and they distinguish three interaction regions between the components of the binary system:

- Region 1: in the water-rich region ($0 \leq x_{ACN} \leq 0.2$), the voids of the aqueous structure are progressively filled by the organic molecules, without enhancement of this structure;

- Region 2: the geometry of ACN cannot fit exactly to the aqueous network. In the intermediate region ($0.2 \leq x_{ACN} \leq 0.75$-$0.8$), a progressive break of the precedent structure

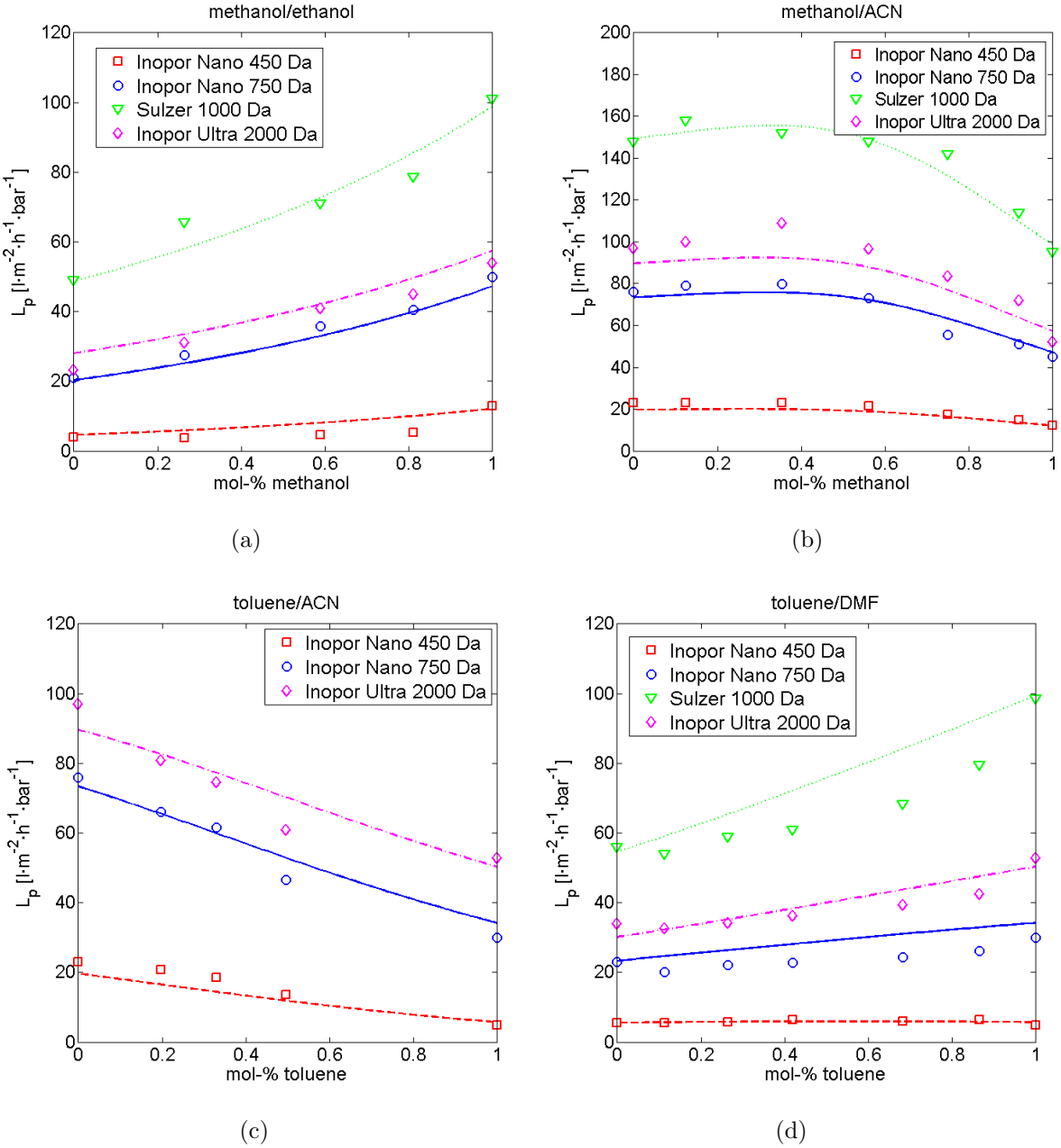


Figure 4.12: Prediction of permeability of organic mixtures by the new model. (– –) Inopor Nano 450 Da; (—) Inopor Nano 750 Da; (· · ·) Sulzer 1000 Da; (– · –) Inopor Nano 2000 Da.

occurs. This range of concentration has been called "micro-heterogeneity region";

- Region 3: the third region (0.75-0.8 $\leq x_{ACN} \leq 1$) can be compared to some extent with the water-rich region, since the initial structure of the organic solvent is progressively disturbed by the addition of water molecules.

The formation of complexes in the "microheterogeneity" region (region 2) affects the average molecular dimension. It is not the purpose of this work to study in detail the changes in molecular dimensions due to the occurrence of complexation between ACN and water; however, this mixture is an interesting case-study to understand the effect of the molecular dimension as an influencing parameter in the model. A profile of the solvent radius vs. solvent composition was hypothesised to carry out the simulation. It is plausible that the concentration of the solvents in the mixture affects the complexation tendency in a way that the stronger complexes increase the mean solvent molecular dimension. The complexation does not involve all the molecules in the mixtures, therefore complexes are coexisting with free molecules. A mean solvent molecular dimension was adopted as a steric parameter to describe the mixture, and described by a parabolic profile as function of the solvent composition. This choice is supported by the analogy between the profile of the proposed mean molecular dimension and the profile of the chemical shift, representing the intensity of the interactions between the two molecules. It was assumed for the average radius of the solvent the molecular radius of water, r_{H_2O}, and ACN, r_{ACN} as boundary limits, i.e. at concentrations of 0%m and 100%mol ACN, and maximum around 60%mol ACN, similar to the composition at which the strongest molecular interactions occur. At this composition, the average radius of the mixture has been computed as $\alpha\,(r_{ACN} + r_{H_2O})$, where α is a fitting parameter. This is shown in Figure 4.13, where the curve has $\alpha = 0.8$.

The remaining terms of the correction factors were calculated with the hypothesis of linear dependence on the composition, since it was demonstrated to be effective for the other aqueous and organic mixtures.

The prediction of the model for the ACN/water mixtures, considering the mean solvent molecular dimension as explained above, is shown in Figure 4.14. The value $\alpha = 0.8$ returned the best agreement between model and experimental data. This value is realistic,

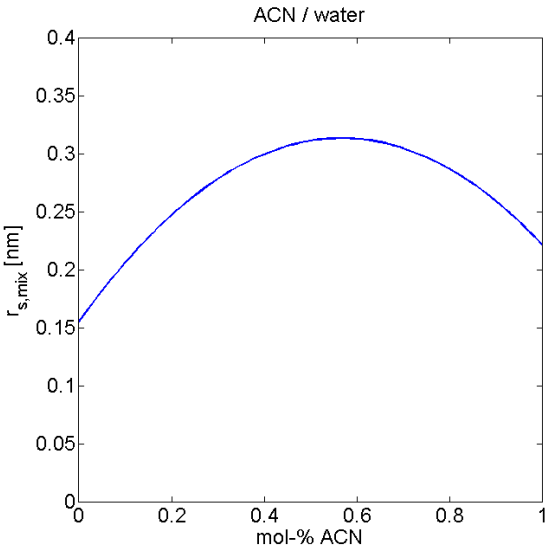


Figure 4.13: Profile of the solvent radius for ACN/water mixtures as function of the composition.

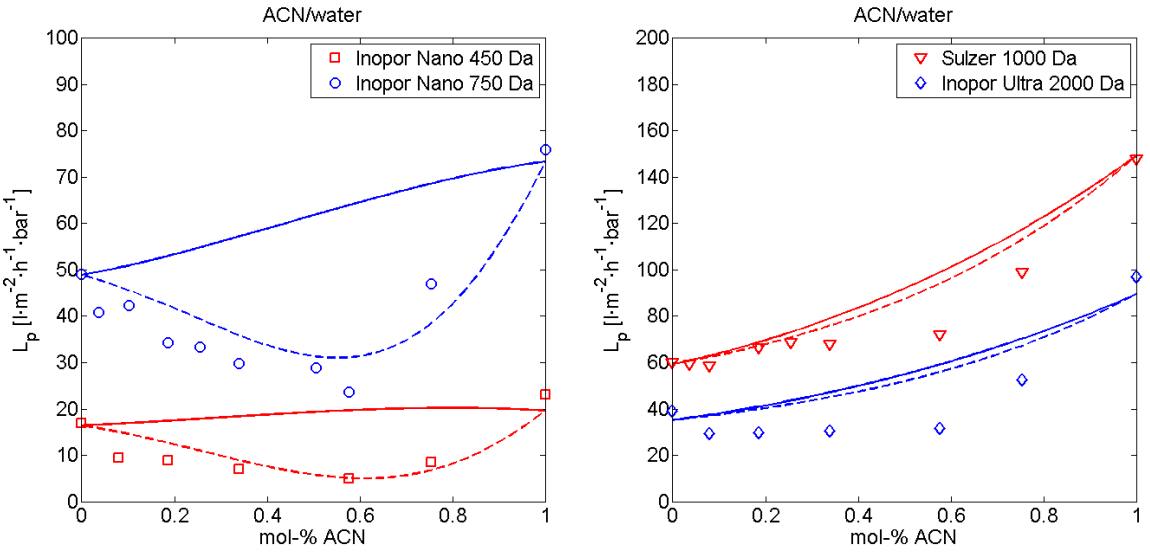
as the most common complex in the mixture is $2ACN \cdot H_2O$.

The prediction improved strongly in the NF range (cf. Figure 4.14(a)) and slightly in the UF range (cf. Figure 4.14(b)). Clearly, the good agreement between model and data does not prove alone the assumption that the peculiar behaviour of the ACN/H_2O mixture is due to the formation of complexes, which are giving more steric hindrance to the flow. However, the behaviour of the ACN/water mixture permitted to demonstrate the importance of the steric term in the model and the possible significant role of the complexes in affecting permeation.

4.5 Conclusion

Permeation of water and organic solvents through ceramic nanofiltration and ultrafiltration membranes was investigated.

Experimental results clearly indicated that the Hagen-Poiseuille equation fails in describing solvent permeation through NF membranes, whereas it is able to describe the experimental permeability through UF membranes. The coupled series-parallel model was able to describe the experimental permeability in the NF range, but was not easily able to cross



(a) (b)

Figure 4.14: Prediction of permeability of ACN/water mixtures by the new model taking into account the formation of complexes between ACN and water molecules. (—) prediction without considering complexes; (– –) prediction with considering complexes.

the continuum from the UF to the NF range.

A model was proposed to describe solvent permeation through NF and UF membranes. The development of the model started from the Hagen-Poiseuille equation, which assumes viscosity as the key parameter influencing permeation. Several correction factors were considered, to account for the surface phenomena that arise in a nanotube due to solvent-membrane surface interactions. These corrections terms, namely the capillary pressure, the dipole and the steric term, were found to be functions of the pore size, so that the model could be applied to both UF and NF ranges. The dipole term was revealed to be non-significant, therefore the model could be simplified from a three-parameter to a two-parameter model.

The model was also applied to selected aqueous and organic mixtures in a simplified version. To test its predictive power, mixture fluxes were predicted from pure solvent regression parameters. It was observed that viscosity was again the key influencing factor, with the permeability profiles following the viscosity profiles of the corresponding mixtures. The

hypothesis of linear dependence of the correction factor on the solvent composition was found to be reasonable for all the aqueous and organic solvent mixtures, apart from the ACN/water mixture. The formation of some complexes between ACN and water molecules was ascribed as the cause of such deviations. For the exceptional case of the ACN/water mixture, a parabolic distribution of solvent radius as function of the composition was hypothesised and the model afterwards tested on the experimental data. The agreement between model prediction and experimental data demonstrated the importance of the steric term as an influencing parameter in the model and the significant effect that the formation of complexes between the solvent molecules can exert on the permeation of the mixture through pores of nanoscale dimensions.

The model has the potential to make design calculations and predict pure solvent and mixture fluxes for a specific membrane by obtaining a limited number of experimental data for pure solvents (necessary to obtain the fitting parameters characteristic of the membrane). Taking a wider perspective, this tool can find interesting application both in the lab scale and in the industrial environment. It is suggested to use the model according to the following procedure:

- Step 1: collect experimental permeability data for five solvents with different physico-chemical properties (water, acetonitrile, ethanol, DMF and toluene were suggested);

- Step 2: carry out the linear regression of the experimental permeability data from Step 1 versus inverse of viscosity to obtain the Hagen-Poiseuille constant, K_{HP};

- Step 3: carry out a non-linear regression of the experimental permeability data from Step 1 versus inverse of viscosity to obtain the fitting constants for the correction factor (C_1 - C_3).

After these preliminary steps, the model can be used to:

(I) predict the permeability for pure solvent/s of interest: the physico-chemical properties of the solvents required to use the model are normally available in literature or accessible experimentally;

(II) predict the permeability for solvent mixtures of interest: the sole mixture property required to use the model is the solvent viscosity, available in literature or accessible expe-

rimentally. Caution should be paid when solvent mixtures are highly not ideal and undergo complexation.

The description of solvent-membrane interactions by means of the new model represents the basis for the future development of a more generalised model for the combined description of solvent flux and solute rejection.

Chapter 5

Filtration in organic/water mixtures: role of preferential solvation

5.1 Introduction

When a solute is dissolved in a mixture of two or more solvents, solute-solvent interactions may differ in strength for each solvent. This causes the composition of the solvation shell to be different from that of the bulk solution and the solute is preferentially (or selectively) solvated by one of the two solvents [60]. Preferential solvation is well known to occur for inorganic salts [61, 62, 63, 64], organic molecules [60, 65] and peptides [66] and alters the specific properties of the solute, as it modifies its immediate surroundings. When preferential solvation occurs, the solute-membrane affinity depends on the composition of the solvent mixture itself.

Ions are often present in a typical peptide/organic solvent/water mixture, as either counter-ions associated to the peptide chain (as is often the case for chloride, acetate and trifluoreacetate anions) or free ions in solution (as buffering agents such as ammonium sulfate or ammonium acetate). The effect of the hydrophilic/phobic properties of the ion on the preferential solvation of organic molecules in solution has been reviewed in Chapter 2. Briefly, two possible situations occur when ions are present in a mixture of organic solutes, and namely ions can associate with the molecule as counter-ions, as in the presence

of organic solutes with charged sites, or they can remain free in solution, as in the presence of neutral organic solutes. This has, in turn, an effect on the transport of the organic solutes through the membrane.

Aim of this work is to study the effect of the solute-solvent competition, in terms of relative affinity with the membrane, on the NF performance. Permeation of single salts and acids (NaCl, KCl, LiCl, NaI, NaF, HCl and trifluoroacetic acid, TFA-H) in organic/water mixtures through hydrophilic ceramic membranes (TiO_2/Al_2O_3) was firstly investigated, in order to demonstrate the role of preferential solvation in affecting NF and UF in organic/water mixtures. Using salts was advantageous for two reasons. Firstly, salts are not affected by steric retention, and therefore affinity effects could be isolated and analyzed separately. Afterwards, preferential solvation data for common inorganic ions are either available in the literature or easily derivable from theoretical models. Availability of these data permits one to look for a correlation between permeation performances and solvation characteristics.

Afterwards, rejections of one small organic molecule, Npys (governed by affinity effects only), and one model peptide, PEP_1 (governed by both steric exclusion and affinity effects), through the same hydrophilic ceramic membranes, were studied as a function of solvent composition (%v ACN/water) and ion content (Na^+, H^+, Cl^-, and TFA^-,). The effects of the influencing factors on the NF performance are presented and discussed.

5.2 Experimental

5.2.1 Materials

The salts used in this study are NaCl, NaI, NaF, KCl, and LiCl, and the acids are HCl and trifluoroacetic acid (TFA-H), all supplied by Sigma Aldrich. 3-Nitro-2-pyridinethiol (Npys) (cf. Figure 5.1) was purchased from Bionet and used as a representative of a neutral solute. Although Npys can assume different charge conformations, according to the pH of the solution, the neutral conformation of Figure 5.1 is the favourite one in the experimental range of this study (pH 2 to 6). This information was obtained by simulation

of the molecular structure in MarvinSketch (ChemAxon).

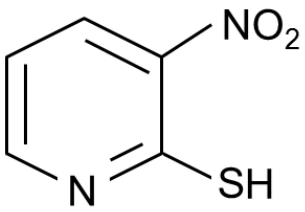


Figure 5.1: Structure of Npys at pH 2 to 6.

A peptide produced in Lonza was used as a representative of a charged solute. The case-study peptide, named PEP_1 in this work, has a molecular weight of 3000 g mol^{-1}, an isoelectric point of 4, and a large water solubility (> 10 g $\cdot$ l^{-1}).

The solvents used in this study are distilled water, ethanol, methanol, ACN, acetone, DMF and DMSO, supplied by Sigma Aldrich or Scharlau. The cross-flow filtration system used in this study contained a tubular module, suitable for multichannel tubular membranes with a length of 250 mm and an outer diameter of 25 mm. Three commercial ceramic membranes were used in this study, with the same active layer, TiO_2 on Al_2O_3 and different MWCOs. Two of them were prepared by Inopor (Germany) under the commercial names of Inopor® Nano 750 Da, and Inopor® Nano 450 Da. The third membrane was provided by Sulzer, with a nominal MWCO of 1000 Da. All the membranes had 19 channels with an internal diameter of 3.5 mm and filtration area of 516 cm^2. The MWCO values and the nominal pore dimensions of the active top layer were measured by the manufacturer. The nominal properties of the membranes were summarised in Table 3.3.

5.2.2 Methods

Rejection and permeation tests

Solutions of (i) pure salts/acids, (ii) pure Npys, (iii) Npys + salts/acids and (iv) PEP_1 + TFA-H in water and organic solvent/water mixtures of different compositions were prepared. Solute rejection and permeation were tested in a Natan cross-flow system (Natan

GmbH, CH; cf. Figure 3.2). Samples of retentate and permeate were taken at regular intervals. Npys and PEP_1 concentrations were analyzed by HPLC measurements, and ion concentration measured by conductivity meter and ion chromatography. The permeate was collected in a graduated cylinder and the flux monitored. Each test was repeated at least two times, and the values of rejection and flux averaged. The error was always less than 10%.

Calculation of the preferential solvation parameter- Quasi-Lattice Quasi-Chemical (QLQC) theory

The Quasi-Lattice Quasi-chemical theory was developed by Marcus [64] to describe the standard Gibbs free energy of transfer of an ion, X, from a reference solvent to a mixture of solvents, and the solvent composition in the vicinity of the ion, quantified by the so-called preferential solubility parameter, δx_s [64].

The preferential solvation of X by one of the two solvents in the mixture A+B, say A, is defined as the difference between the local mole fraction x_A^L and the bulk mole fraction x_A, and is calculated as in Equation 5.1 (for more details about this theory, see reference [64] and Appendix A).

$$\delta x_A = x_A^L - x_A = \frac{(1 - x_A) \cdot \left[1 - y \cdot exp\left(\frac{\Delta}{2}\right)\right]}{1 + (1 - x_A) \cdot y \cdot x_A^{-1} \cdot exp\left(\frac{\Delta}{2}\right)} \tag{5.1}$$

For the case of transfer of ions from water as the reference solvent (solvent A) into aqueous solvent mixtures (solvent B), the factor Δ of Equation 5.1 takes the form:

$$\Delta = \frac{-\Delta G_t^0(X, W \rightarrow B)}{Z \cdot R \cdot T} \tag{5.2}$$

Standard molar Gibbs energies of transfer, ΔG_t^0, from water to non-aqueous solvents are available in literature [61, 104] and are reported in Appendix A. The factor y in Equation 5.1 is defined as:

$$y = \frac{x_A}{(1 - x_A)} \cdot \left(\frac{N_{B,B}}{N_{A,A}}\right)^{\frac{1}{2}} \tag{5.3}$$

where $N_{B,B}$ and $N_{A,A}$ represent the number of (i, j) neighbours for the ion X (see Appendix A for more detail).

The theory was applied to calculate the preferential solubility parameters of the ions used in this study, and the profiles compared with the available data from literature [62, 63]. The slight disagreement (less than 10%) between the profiles calculated in this study and the literature data was accepted, as the data in [62] and [63] were calculated by using a different theoretical approach. The trend of the preferential solvation parameter with concentration was satisfactorily reproduced for all ions, confirming that the QLQC method suggested by Marcus [64] can be applied to calculate the preferential solvation parameters for a generic ion, knowing its standard molar Gibbs energy of transfer. This method can be extended to organic molecules too, knowing the standard molar Gibbs energy of transfer, as shown by Marcus for certain drugs and polycyclic aromatic hydrocarbons [105]. In this chapter, the method was not extended to Npys and PEP_1, due to lack of information about their ΔG_t^0. Considerations of their preferential solubility were undertaken by analyzing their molecular structure and comparing it with standard reference molecules with known preferential solvation. Preferential solvation of Npys in ACN over water was assumed from the similarity of Npys with phenol, which has a larger affinity with ACN than water [65] and preferential solvation of PEP_1 in ACN was assumed by the larger percentage of hydrophobic over hydrophilic amino acids present in its chain (cf. Gekko et al. [66]). Availability of simulation tools could improve this qualitative analysis and help in the quantification of the preferential solvation parameter for organic molecules. In this study, knowledge of qualitative preferential solvation in either organic solvent or water is enough to carry on the discussion.

5.3 Results and discussion

5.3.1 NF of salts and acids in organic/water mixtures

In this paragraph, the NF of some inorganic salts and common acids in organic/water mixtures is presented. The aim of this work was to understand which are the important

factors governing rejection in presence of organic solvents, and namely, to understand the relative importance of electrostatic interaction vs. molecular affinity interactions for small (i.e. non-sterically hindered) charged solutes. Molecular affinity was expected to play a role in terms of solute-solvent competition for the transport through the membrane. The following procedure was followed:

- the NF of salts/acids was studied in water and in organic solvent/water mixtures, in order to demonstrate an effect of the solvent composition on charge and molecular affinity interactions;

- the NF of salts/acids was studied through different membranes of the same material and different pore dimensions, in order to investigate the effect of the specific surface area (affinity effects are expected to be proportional to the membrane specific surface area);

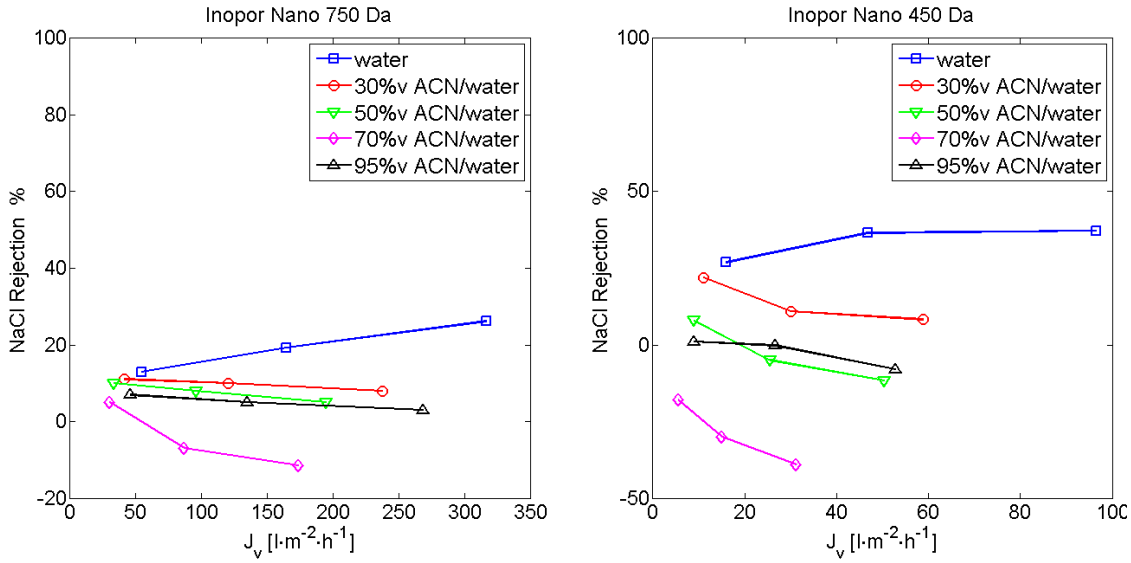
- the NF of salts/acids was studied in aqueous mixtures of different solvents, in order to demonstrate the effect of the solvent nature, in terms of Hansen solubility parameter;

- the NF of salts/acids was studied for different anions and cations, in order to demonstrate the effect of the solute nature, in terms of preferential solvation parameter.

NF of NaCl in water and ACN/water mixtures

NaCl rejection and solvent permeation in water and ACN/water mixtures are shown in Figure 5.2(a-b) for the cases of Inopor® Nano 450 Da and Inopor® Nano 750 Da, respectively. Pressure values used in this study were 1, 3 and 6 bar.

Two different rejection profiles were found in water and in ACN/water mixtures. In the case of pure water, NaCl rejection increases with flux for both membranes (cf. Figures 5.2(a-b)), as normally observed in literature for NF of salts in water [25]. This is the characteristic behaviour of a system governed by strong solvent-membrane affinity [106]. This situation occurs when the increase in pressure favours the passage of solvent molecules more than the passage of the solute, since solvent is the species with larger affinity with the membrane. This is normally explained by the Donnan theory of the electrostatic repulsion [25]: both solute and membrane are charged and solute rejection occurs via electrostatic repulsion between the two charged bodies [25]. In this case, both rejection and flux increase



(a) (b)

Figure 5.2: NaCl rejection and permeability during NF of NaCl in water (c_{NaCl} = 1 mM).

with pressure. Flux may be affected by osmotic effects, which decrease the permeation at high solute concentrations [106]. Water flux in Figures 5.2(a-b) is only slightly lower than that of pure water; pure water permeability was 55 l m^{-2} h^{-1} bar^{-1} for Inopor® Nano 450 Da and 17 l m^{-2} h^{-1} bar^{-1} for Inopor® Nano 750 Da, respectively. This means that, as NaCl concentration was very low, osmotic effects were negligible at this salt concentration.

Opposite to what was observed in water, NaCl rejection profiles in ACN/water mixtures decrease with the flux (cf. Figures 5.2(a-b)). According to Mehdizadeh et al. [106], this trend of rejection vs. flux (or, in turn, pressure) suggests that these systems are governed by solute-membrane affinity (i.e. an increase in pressure favours the passage of the solute, as it is the species with larger affinity with the membrane). Significant negative rejection was observed for the case of NaCl in 70%v ACN/water through Inopor ® Nano 450 Da (cf. Figure 5.2(b)). It is interesting to note that both NaCl rejection and flux are larger in 95%v ACN than in 70%v ACN for both membranes (cf. Figures 5.2(a-b)). NaCl rejection and solvent flux are, therefore, not directly proportional to the %v ACN/water.

Reduction of charge effects may explain the decrease in rejection with %v ACN/water. Reduction of charge, however, cannot explain the occurrence of negative rejection and the

fact that rejection in 95%v ACN/water is higher (less negative) than in 70%v ACN/water. It was observed in a previous study [57] that pure solvent flux of 95%v ACN/water mixture was higher than that of 70%v ACN/water mixture (the permeability profile of ACN/water mixtures over the whole composition range showed a minimum around 75%v ACN). This was attributed to higher solvent-membrane affinity for the 95%v ACN mixture than for the 70%v. Formation of hydrophobic complexes between ACN and water molecules was causing such a low affinity at 70%v ACN, while 95%v ACN was outside the so-called "microheterogeneity" region [103]. It is plausible, therefore, that another kind of solute-membrane molecular affinity is responsible for this anomalous behaviour, which causes NaCl in 70%v ACN to have a larger affinity with the membrane than in 95%v ACN (as it permeates faster than the solvent mixture). The trend of NaCl rejection is compared with that of preferential solvation and Hansen solubility parameter of both Na^+ and Cl^- ions (cf. Table 5.1).

Table 5.1: NaCl rejection vs. Na^+ and Cl^- preferential solvation parameters and Hansen solubility parameters. $P = 6$ bar; $C_{NaCl} = 1$ mM.

	30%v ACN	**50%v ACN**	**70%v ACN**	**95%v ACN**
Rej_{NaCl} % by Inopor® Nano 450	8.2	- 11.7	- 39.1	- 8.0
Rej_{NaCl} % by Inopor® Nano 750	8.1	5.2	- 11.5	3.5
$S_{Hansen,bulk}$	40.78	36.1	31.42	25.57
$\delta x_{ACN,Cl^-}$ / S_{Hansen,Cl^-}	- 0.11 / 43.4	- 0.17 / 40.1	- 0.32 / 38.9	- 0.27 / 30.25
$\delta x_{ACN,Na^+}$ / S_{Hansen,Na^+}	- 0.02 / 41.2	- 0.05 / 37.3	- 0.08 / 33.3	- 0.07 / 27.2

The preferential solvation of the ions were calculated as the difference between ACN concentration in the ion solvation shell and in the solvent bulk:

$$\delta x_{ACN,i} = x^L_{ACN,i} - x_{ACN,i} \tag{5.4}$$

Hansen solubility parameter (S_{Hansen}) is useful in predicting if one material will dissolve in another and form a solution [107]. This parameter quantifies the affinity between two materials, and can be extended to liquid-solid interactions too. Hansen solubility parameters for the mixture (i,j) were calculated as a molar weighted average of the values of the pure solvents (i and j, respectively), taken from literature [107], according to Equation 5.5:

$$S_{Hansen,(i,j)} = x_i \cdot S_{Hansen,i} + (1 - x_i) \cdot S_{Hansen,j} \tag{5.5}$$

where x_i is the molar fraction of component i. They are referred to as $S_{Hansen,bulk}$ in Table 5.1. The preferential solvation parameters of the ions, calculated according to QLQC theory [108], were used to calculate the actual composition of the ion solvation shell, and that composition used the calculate the Hansen solubility parameter corresponding to that composition. The assumption that the Hansen solubility parameter of the ions (S_{Hansen,Cl^-} and S_{Hansen,Na^+}) was proportional to the Hansen solubility parameter of the solvation shell in their immediate surrounding was made.

The trend of preferential solvation parameter for both ions Na^+ and Cl^- follows that observed for NaCl rejection, as is clear from Table 5.1. Both preferential solvation parameters and rejection decrease from water to 70%v ACN, and they increase from 70%v to 95%v ACN (cf. Table 5.1). This means that both ions are more hydrophobic at 95%v than at 70%v ACN and their exclusion from the membrane is more pronounced in the former case. $S_{Hansen,ion}$ for the ions is always higher than $S_{Hansen,bulk}$ (meaning that the ions are always hydrated, and therefore more affine to the membrane than the bulk solvent). The larger ratio $S_{Hansen,ion}$ / $S_{Hansen,bulk}$ (i.e. the larger difference between composition of the solute molecular shell and the bulk solvent) is for the %70v ACN/water mixture. In conclusion, decrease of importance of membrane charge and both larger solvent-membrane affinity and lower solute-membrane affinity at 95%v ACN than at 70%v ACN/water could be ascribed to the larger NaCl rejection in 95%v ACN/water mixtures.

The effect of NaCl concentration was studied for both NF membranes in water and ACN/water mixtures. The results are shown in Figures 5.3(a-d).

The effect of concentration is the same in water and ACN/water mixtures and, namely,

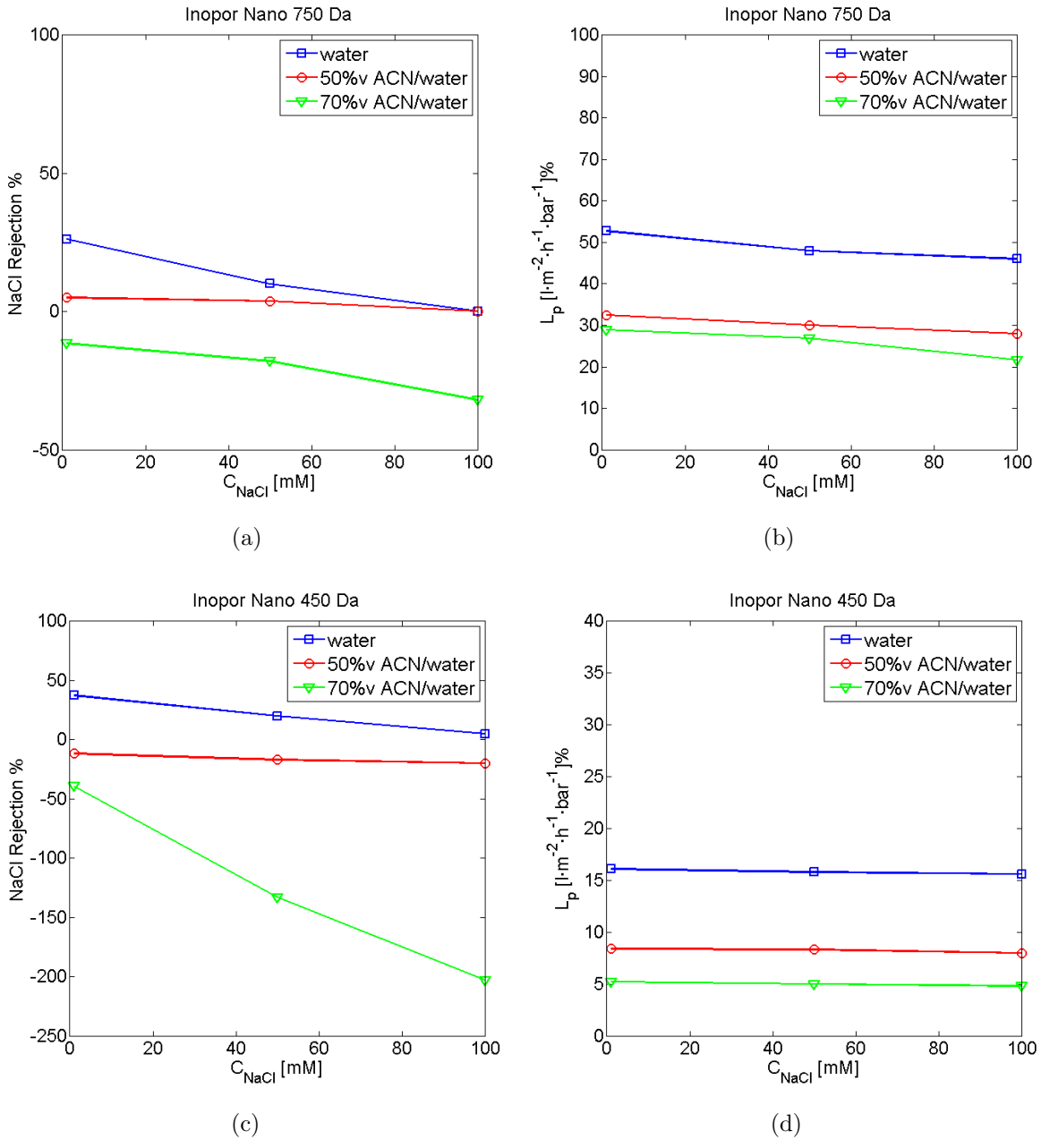


Figure 5.3: Effect of NaCl concentration on NaCl rejection and permeability (P = 6 bar).

NaCl rejection decreases with NaCl concentration for both membranes (cf. Figures 5.3(a) and (c), respectively). Decreasing profiles of rejection with solute concentration are normally explained by the increased compression of the electrical double layer, caused by the increase in the ionic strength of the solution. Small charge effects are expected at high ionic strength. Increasing solute flux determines also incresing friction in the pore. The lower rejection may be, therefore, responsible for the decreasing profile of the permeability against the salt concentration (cf. 5.3(b) and (d)).

Effect of pore dimension on the solute-solvent-membrane surface interactions

The effect of pore dimension on the solvent-membrane affinity during solvent permeation through ceramic NF and UF membranes was presented in a previous chapter (cf. Chapter 4). Intermolecular affinity between solvent and membrane was found to affect the solvent permeation through NF membranes [57], since surface effects cannot be neglected with respect to bulk effects in high specific surface systems. The pore dimension (i.e. NF vs. UF) was expected to affect salt rejection too.

Three membranes of the same material but different pore dimension and MWCO were compared in terms of filtration performances of NaCl/ACN/water solutions. NaCl rejection and permeability for the three membranes are shown in Table 5.2. 70%v ACN was chosen as a reference composition, as the most significant solute-membrane affinity effects were identified at this concentration value.

Rejection was negative for all three membranes and increasing (i.e. becoming less negative) with the MWCO. Surprisingly, rejection was negative in the UF range (Sulzer) too, even if to a much more limited extent. This means that the pore dimension of all these membranes is small enough to let solute-membrane affinity affect the permeation. Permeability increased with the MWCO, as expected from the fact that affinity effects become less important when incresing pore dimension (cf. Chapter 4).

Table 5.2: Effect of pore dimension on NaCl rejection and permeability (70%v ACN/water; c_{NaCl} = 100 mM; P = 8 bar).

Membrane	**Filtration range/ MWCO [Da]**	**Rej$_{NaCl}$ %**	**Permeability [l m^{-2} h^{-1} bar^{-1}]**
Inopor® Nano 450 Da	NF / 450	- 220.1	5.5
Inopor® Nano 750 Da	NF / 750	- 37.2	21.2
Sulzer	UF / 1000	- 13.0	27.0

Effect of the organic solvent: Hansen solubility parameter and solute preferential solvation

Surprising negative rejection for NaCl was found in ACN/water solutions, and explained in terms of negligible electrostatic effects and larger solute-membrane than solvent-membrane affinity, due to the occurrence of preferential solvation of both ions in the solvent mixture. Since the nature of the organic solvent is also one of the factors that affects the preferential solvation of the ions, NaCl rejection in other common organic solvents was also investigated. Six different organic solvents were studied, and a composition of 45%mol organic solvent/water was chosen (since this corresponds to the critical value of 70%v ACN/water). Results for NaCl rejection by Inopor® Nano 450 are shown in Figure 5.4 for the different solvents, together with the Hansen solubility parameters of the corresponding solvent mixtures and the two ions (Cl^- and Na^+) in the same mixture.

In the case of pure water, the Hansen solubility parameter of the hydrated ions is the same as that of water. At high salt concentration (100 mM) the charge effects in water were found to be negligible, and therefore NaCl rejection is very low. In the presence of organic solvent, rejection changes significantly. It can be observed, in the first place, that Hansen solubility parameter alone (blue bars in Figure 5.4) cannot explain the trend of NaCl rejection observed in the different mixtures. All Hansen solubility parameters are

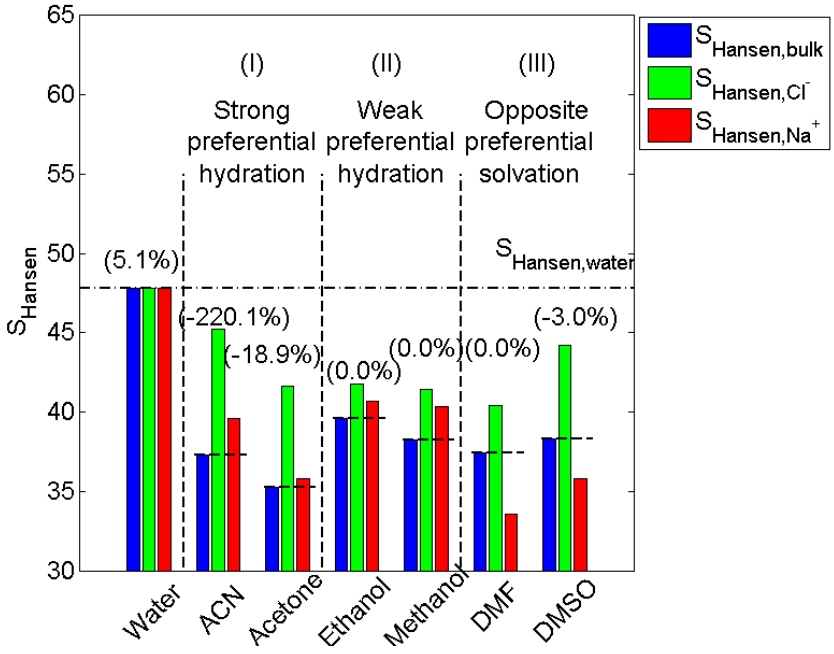


Figure 5.4: Effect of solvent on NaCl rejection % (values for rejection in brackets). Membrane: Inopor Nano 450 Da.

lower than that for water ($S_{Hansen,water} = 47.8$). By taking into account the preferential solvation of the ions, it can be observed that there is a large difference in the behaviour of the ions in the different solvents. Cl^- is largely hydrated in ACN and acetone (i.e. $S_{Hansen,Cl}$ is closer to $S_{Hansen,water}$ than $S_{Hansen,bulk}$), and Na^+ is slightly hydrated. Higher hydration of the ions determines in turn higher solute-membrane affinity, with respect to solvent-membrane affinity, and finally enhanced permeation of NaCl. This corresponds to significantly negative NaCl rejection (cf. Figure 5.4). NaCl rejection is more negative in ACN than in acetone, as expected from the larger hydration of Cl^- in the former solvent. In ethanol and methanol, both Cl^- and Na^+ are slightly hydrated , but this effect is too small to enhance the permeation of the ions over that of the solvent. NaCl rejection in these two solvents was found to be almost zero (cf. Figure 5.4). Finally, in DMF and DSMO, Cl^- is hydrated , but Na^+ is not. The solvation shell around Na^+ in DMF and DMSO is richer in organic solvent than in water. Since the two ions permeate together, the enhanced hydrophilicity of Cl^- ($S_{Hansen,Cl} > S_{Hansen,bulk}$) is balanced by the enhanced hydrophobicity

of Na^+ ($S_{Hansen,Cl} < S_{Hansen,bulk}$), and finally the salt rejection is around zero (cf. Figure 5.4). Three cases can be outlined from all the previous observations (as shown in Figure 5.4):

(I) strong preferential hydration of the salt: if anion and cation have $S_{Hansen,i} > S_{Hansen,bulk}$ (which corresponds to significantly negative preferential solubility parameter, $\delta x_{s,i}$), global salt permeation is favoured and rejection can be negative;

(II) weak preferential hydration of the salt: if both ions have $S_{Hansen,i} \sim S_{Hansen,bulk}$ (which corresponds to negligible $\delta x_{s,i}$), salt rejection is low or zero. This means that the ions are different to the environment and do not show preferential affinity with the membrane compared to the solvent;

(III) opposite preferential solvation of the two ions: if one of the two ions has $S_{Hansen,i} > S_{Hansen,bulk}$ (which corresponds to negative $\delta x_{s,i}$) and the other has $S_{Hansen,i} < S_{Hansen,bulk}$ (which corresponds to positive $\delta x_{s,i}$), the global salt permeation depends on the relative importance of the two conflicting contributions.

Effect of cation and anion: ion preferential solvation

Further validation of the importance of preferential solvation in affecting salt permeation through NF membranes was obtained by studying the effect of different cations and anions (characterised by different preferential solvation parameters) in the same solvent mixture (70%v ACN/water) through the Inopor® Nano 450 Da. The effect of cation is reported in Table 5.3. The common anion for all the cations was Cl^-.

The preferential solvation parameter, $\delta x_{ACN,+}$, of all cations is negative and the Hansen solubility parameter slightly higher than the Hansen solubility parameter of the bulk ($S_{Hansen,bulk} = 31.4$). Rejection and permeability slightly increase with $\delta x_{ACN,+}$, but rejection is almost constant and significantly negative. The effect of the cation on the NF performance is therefore not significant.

The effect of anion is reported in Tables 5.4 and 5.5. In Table 5.4 the common cation for all the anions is Na^+. In Table 5.5 the common cation is H^+ (this comparison is therefore between rejection of two acids, hydrophilic HCl vs. hydrophobic TFA-H).

Table 5.3: Effect of cation on salt rejection and permeability in 70%v ACN/water ($S_{Hansen,bulk}$ = 31.4) through Inopor Nano 450 Da. Common anion: Cl^-, salt concentration = 100 mM, P = 8 bar.

Cation	$\delta x_{ACN,+}$ / $\mathbf{S}_{Hansen,+}$	$\mathbf{Rej}_{salt}$ %	**Permeability** [l $\mathbf{m^{-2}}$ $\mathbf{h^{-1}}$ $\mathbf{bar^{-1}}$]
H^+	- 0.31 / 38.7	-230.3	5.40
Li^+	- 0.22 / 36.6	-221.0	5.51
Na^+	- 0.10 / 33.8	- 220.1	5.60
K^+	- 0.05 / 32.6	- 199.8	5.69

Table 5.4: Effect of anion on salt rejection and permeability in 70%v ACN/water ($S_{Hansen,bulk}$ = 31.4) through Inopor Nano 450 Da. Common cation = Na^+, salt concentration = 10 mM, P = 8 bar.

Anion	$\delta x_{ACN,-}$ / $\mathbf{S}_{Hansen,-}$	$\mathbf{Rej}_{salt}$ %	**Permeability** [l $\mathbf{m^{-2}}$ $\mathbf{h^{-1}}$ $\mathbf{bar^{-1}}$]
F^-	- 0.34 / 39.4	- 186.7	5.60
Cl^-	- 0.32 /38.9	- 115.0	5.92
I^-	- 0.14 / 34.7	- 39.2	6.19

Table 5.5: Effect of anion on salt rejection and permeability in water and 70%v ACN/water ($S_{Hansen,bulk}$ = 31.4) through Inopor Nano 450 Da. Common cation = H^+, salt concentration = 10 mM, P = 8 bar.

Anion	**Solvent**	$\delta x_{ACN,-}$ / $\mathbf{S}_{Hansen,-}$	$\mathbf{Rej}_{salt}$ %	**Permeability** [l $\mathbf{m}^{-2}$ $\mathbf{h}^{-1}$ $\mathbf{bar}^{-1}$]
Cl^-	water	-	35.3	16.80
TFA^-	water	-	19.2	17.10
Cl^-	70 %v ACN/water	- 0.32 /38.9	- 116.7	5.60
TFA^-	70 %v ACN/water	0.42 / 21.6	4.1	8.41

For the cases in Table 5.4, the preferential solvation parameter, $\delta x_{ACN,-}$, of all anions is significantly negative, the Hansen solubility parameter higher tha that of the solvent bulk ($S_{Hansen,bulk}$ = 31.4), and rejection and permeability increased with $\delta x_{ACN,-}$. For the cases in Table 5.5, rejection of the two acids in water is positive, as expected by occurrence of electrostatic repulsion, and significantly lower in the presence of ACN, as expected by the lower importance of charge effects in 70 %v ACN/water mixtures. Rejection is strongly negative for HCl and slightly positive for TFA-H in 70 %v ACN/water. HCl dissociates in a strongly hydrophilic anion (Cl^-), with a significantly negative $\delta x_{ACN,-}$ and $S_{Hansen,-} \sim S_{Hansen,water}$, while TFA-H dissociates in a hydrophobic anion (TFA^-), with a significantly positive $\delta x_{ACN,-}$ and $S_{Hansen,-} << S_{Hansen,water}$. Flux is larger in the presence of TFA^- anions than Cl^- ions. This is explained by the larger friction caused by the enhanced passage of Cl^- through the pore, with respect to TFA^-, in the same operating conditions. Both results from Table 5.4 and Table 5.5 demonstrate a significant effect of the anion on the global NF performance. From this analysis, the lower importance of charge effects in the presence of organic solvents is further supported by the two following experimental observations:

- the rejection of two acids, HCl and TFA-H, in 70 %v ACN/water (acid pH), is negative

for the former and negligible for the latter acid (cf. Table 5.5);

- the rejection of NaCl (neutral pH) and HCl (acid pH) is similar (cf. Tables 5.4 and 5.5).

5.3.2 NF of a small neutral organic molecule: case of Npys

Results from rejection of salts and acids demonstrated that preferential solvation affects rejection and flux through NF membranes in the presence of organic solvents. This study was extended to a small organic molecule, Npys, commonly used in peptide processes as protecting group for some amino acid side chains. Although the molecule can assume different conformations, according to the pH of the solution, the preferred conformation in the experimental range (pH 2 to 6) is the neutral one, shown in Figure 5.1. Preferential solvation of the molecule in a generic ACN/water mixture is expected to be in favour of ACN. Npys contains an aromatic ring, therefore the solvation shell around the molecule is expected to be richer in ACN than in water (as observed for phenol in the work of Wakisaka et al. [65]). Rejection of Npys in water and different ACN/water mixtures is shown in Figure 5.5.

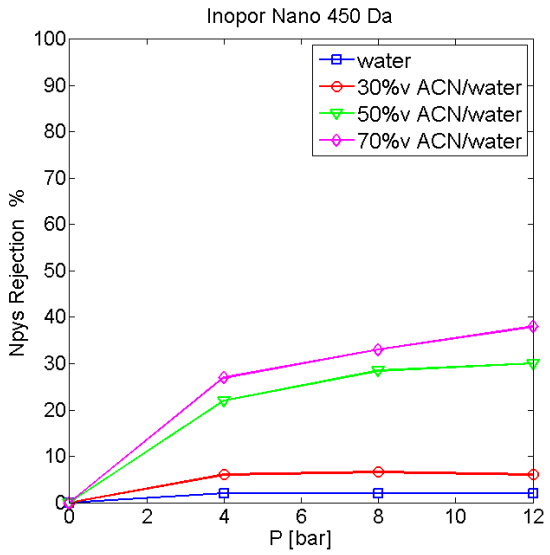


Figure 5.5: Rejection of Npys in different ACN/water mixtures. $c_{Npys} = 1$ *mM.*

Rejection is almost zero in water and increases significantly with the organic content.

Negligible rejection in water was expected, as Npys has a small MW (156 g mol^{-1}), compared to the membrane MWCO (450 g mol^{-1}) and a negligible electrical charge. The trend of Npys rejection with the %v ACN/water demonstrates the hydrophobic nature of the molecule: an increase of the ACN concentration in the bulk causes the increase of the ACN concentration in the solvation shell, and therefore the larger exclusion of the solute from the membrane.

Permeation fluxes of Npys solutions are similar to those of the corresponding neat solutions (i.e. same solvent composition without Npys), as reported in Table 5.6.

Table 5.6: Permeability [l m^{-2} h^{-1} bar^{-1}] during NF of Npys solutions through Inopor Nano 450 Da. P = 12 bar. In brackets rejection % of the corresponding acid.

%v ACN/water	Permeability solvent mixture	Permeability Npys solutions	Permeability Npys+HCl	Permeability Npys+TFA
0	13	12.9	12.7 (13%)	12.9 (5%)
30	9.5	9.6	9.2 (13%)	9.4 (12%)
50	6.9	7.6	6.7 (- 25%)	7.5 (20%)
70	5.6	6	3.8 (-182%)	6.2 (21%)

The effect of ions (Na^+, H^+, Cl^- and TFA^-) on rejection and flux of Npys solutions is reported in Figure 5.6.

Rejection of Npys in water is small (cf. Figure 5.6(a)) and not significantly affected by the presence and the nature of the anions (Cl^- vs. TFA^-). The presence of Cl^- anions, from NaCl (neutral pH) and from HCl (acid pH) increases the Npys rejection, while the presence of TFA^- decreases it. This can be explained by the different preferential solvation of the ions, and in turn the different hydration effect on the organic molecule, as schematically represented in Figure 5.7.

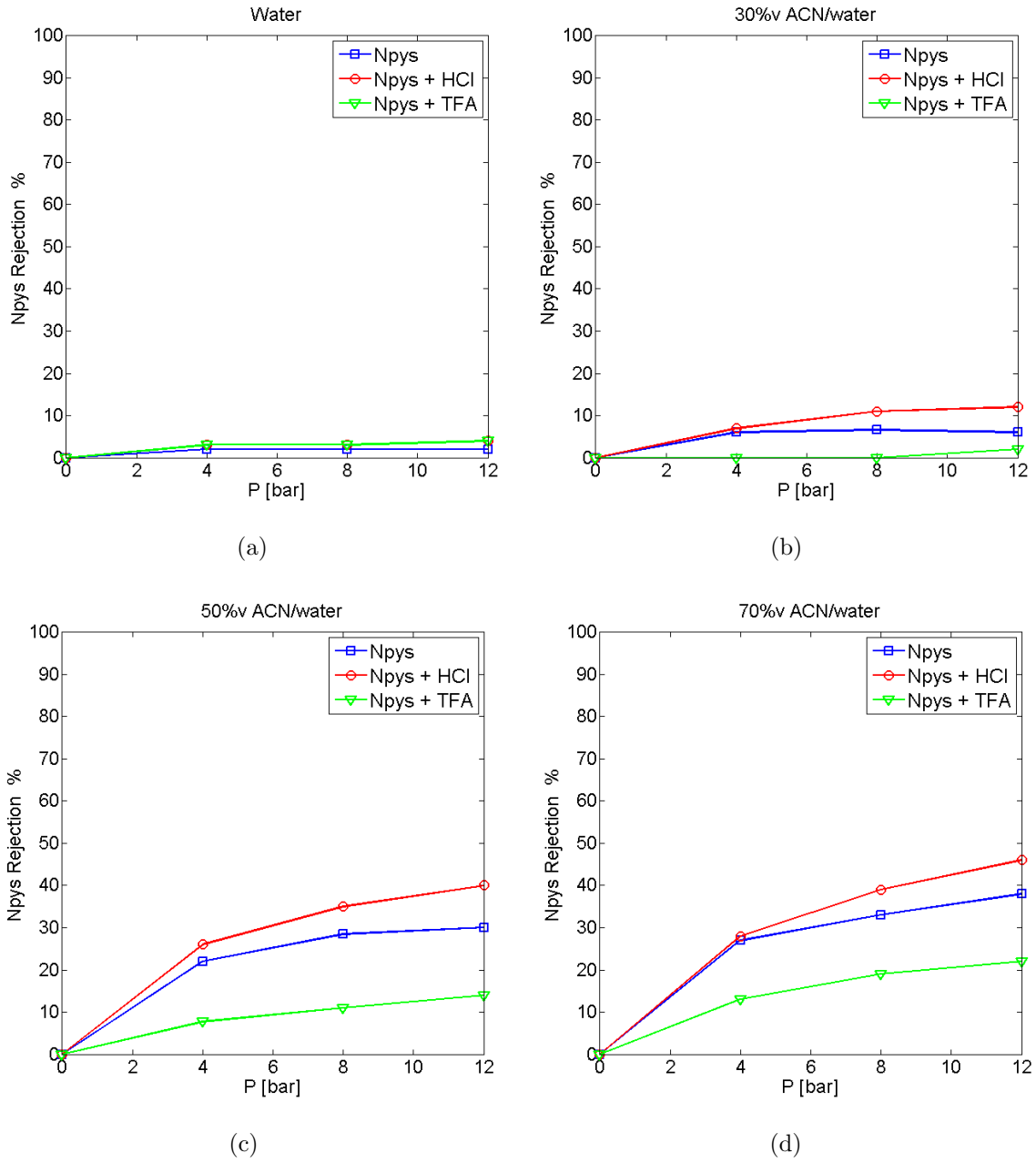


Figure 5.6: Effect of HCl and TFA concentration on Npys rejection. c_{Npys} *= 1 mM;* $c_{NaCl} = c_{HCl} = c_{TFA}$ *= 10 mM.*

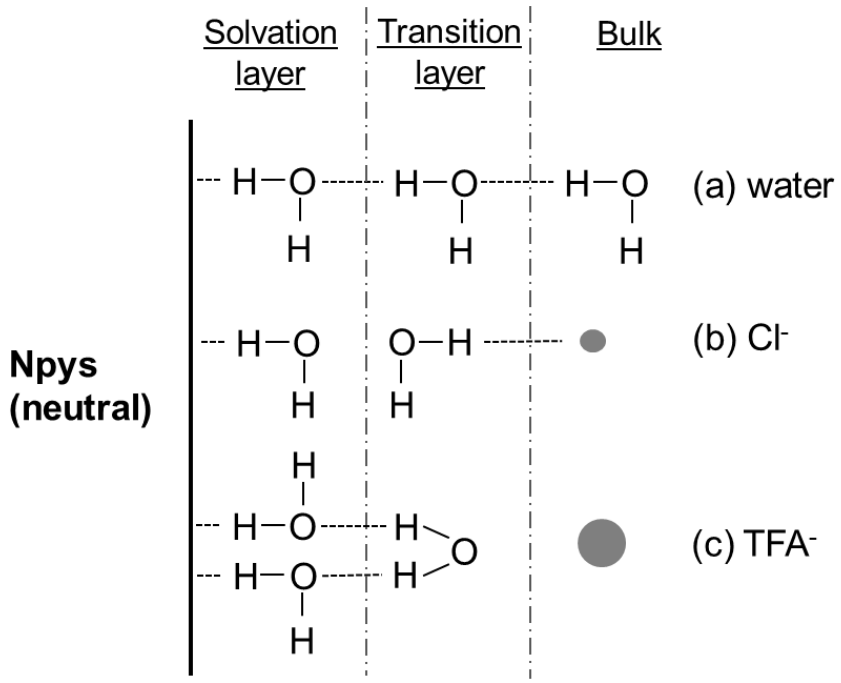
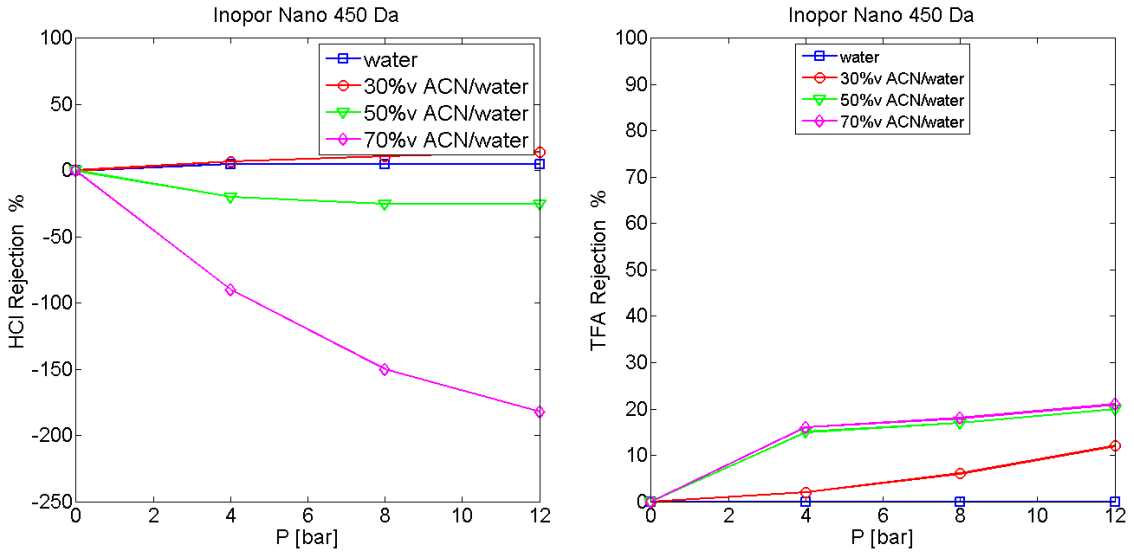


Figure 5.7: Interfacial water near the surface of hydrated Nyps, as a function of the ion nature.

Addition of hydrophilic Cl^- in the third ("bulk") layer (case b in Figure 5.7) causes the water molecules in the second layer to preferentially hydrate the anions rather than Npys. This decreases the Npys hydrophilicity and, in turn, its affinity with the membrane, and increases its rejection. Cl^- behaves therefore as a kosmotropic ion for Npys. Same effect of NaCl and HCl was expected, as the effects of cation (H^+ vs. Na^+) and pH were demonstrated to be negligible, with respect to the effect of the anion (Cl^-) (cf. Tables 5.3 and 5.4). The opposite situation was observed in the presence of TFA^-, which is preferentially solvated by ACN over water, and behaves as a chaotropic ion for Npys. Namely, TFA^- ions allow the water to solvate Npys, thus favouring the Npys affinity with the membrane (case c in Figure 5.7).

Rejections of HCl and TFA-H as function of the organic content are reported in Figure 5.8(a-b), respectively.

HCl rejection is low and positive in water and in 30% ACN, and decreases with the ACN content (cf. Figure 5.8(a-b)). In water, rejection of HCl in the presence of Npys is



(a) (b)

Figure 5.8: Rejection of HCl and TFA-H during NF of Npys solutions. $c_{Npys} = 1$ *mM;* $c_{HCl} = c_{TFA-H} = 10$ *mM.*

lower than that of pure HCl (cf. Table 5.5). This could be due to an effect of Npys on the pure electrostatic repulsion of HCl, possibly due to the formation of water-mediated ion pairs, which decrease the degree of freedom of Cl^- anions in solution. Similar results in water and in 30 %v ACN/water demonstrate that the presence of ACN is not significantly affecting the hydrophobicity of Npys and HCl in this range. Rejection of HCl becomes significantly negative as soon as the %v ACN in the mixture increases (as observed also in Paragraph 5.3.1). The same was found for NaCl (data not shown). This effect has been previously explained as due to the larger hydration of Cl^- ions in the solvent mixture, and therefore their preferential permeation over the solvent. In conclusion, the increase of %v ACN/water causes the increase of Npys rejection and the decrease of the HCl rejection, thus improving the membrane selectivity. Again, the opposite behaviour was observed for TFA^- ions. In water and 30%v ACN, rejection of TFA-H is almost zero and decreases with the ACN content (cf. Figure 5.8(a-b)). As observed for HCl, rejection of TFA-H in water is slightly lower in the presence of Npys, than in pure water (cf. Table 5.5). The preferential solvation of TFA-H in ACN over water is responsible for the increase in rejection with the

%v ACN/water.

Fluxes during NF of Npys solutions are reported in Table 5.6. In water and 30%v ACN/water, no significant decrease in the flux is noted, compared to the solution of pure Npys. Differently, in 50%v and 70%v ACN/water, the effect of ion rejection on the solvent flux is more evident. Corresponding to significant negative ion rejection, flux decreases (case of Npys + HCl), differently in the case of significantly positive ion rejection, flux remains almost constant (case of Npys + TFA-H). Since friction due to Npys is negligible (as is clear from the comparison of second and third columns in Table 5.6), the decrease of the flux is explained by the friction created by the enhanced permeation of the Cl^- ions (which causes their negative rejection). Differently, TFA^- permeation does not influence significantly the flux, since the flux of TFA^- ions is slower than the solvent flux. Similar effects of Cl^- and TFA^- on the solvent flux were observed in Table 5.5 for the NF of the single ions.

5.3.3 NF of a case-study peptide: PEP_1

The effects of preferential solvation and presence of ions in the mixture (i.e. %v ACN/water and %v TFA-H) were studied also on the rejection of a model peptide through ceramic membranes (TiO_2/Al_2O_3). The effect of %v ACN on PEP_1 rejection, TFA^- rejection and solvent permeability is shown in Table 5.7.

PEP_1 rejection increases with the organic content, at both PEP_1 concentration values. This is explained by the increase of the peptide hydrophobicity, due to the increase of the %v ACN in the mixture. PEP_1 preferential solvation is, in fact, in ACN, i.e. the peptide attracts preferentially ACN molecules rather than water ones into its solvation shell. This is due to the high number of hydrophobic amino acids in the chain [66]. TFA-H rejection increases with the organic content too, as extensively discussed in the previous paragraphs. Flux increases corresponding to the increase of PEP_1 and TFA-H rejections. Again, this may be explained by less friction, corresponding to higher peptide and ion rejections.

The effect of TFA^- ions on PEP_1 rejection is shown in Table 5.8 for two ceramic NF membranes and constant %v ACN.

Table 5.7: Effect of %v ACN on PEP_1 rejection %, TFA^- rejection % and solvent permeability through Inopor Nano 750. %v TFA = 0.02; P = 10 bar.

%v ACN/water	$\mathbf{c}_{PEP_1}$ [g l^{-1}]	$\mathbf{Rej}_{PEP_1}$	$\mathbf{Rej}_{TFA-H}$	**Permeability** [l m^{-2} h^{-1} bar^{-1}]
0	1	82.5	19.1	3.71
30	1	99.5	31.4	4.52
0	5	95.4	36.4	1.99
30	5	98.2	53.2	3.23

Table 5.8: Effect of %v TFA on PEP_1 rejection %. c_{PEP_1} = 1 g l^{-1}; c_{ACN} = 2%v; P = 4 bar.

%v TFA-H	$\mathbf{Rej}_{PEP_1}$ **for Inopor® Nano 450**	$\mathbf{Rej}_{PEP_1}$ **for Inopor® Nano 450**
0.02	96.5	83.0
0.1	99.1	99.1
0.5	83.5	-
5	74.8	43.3

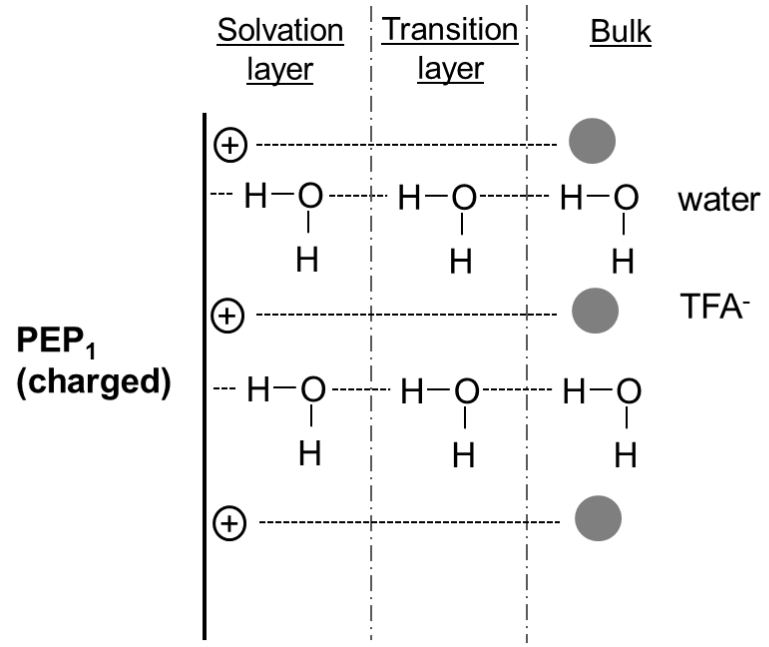
Rejection firstly increases with the acid content (from 0.02%v to 0.1%v TFA-H). In this concentration range, TFA^- associates with the peptide as a counter-ion, as schematically shown in Figure 5.9(a). The association with the hydrophobic ion increases the hydrophobicity of the peptide, thus increasing its rejection (cf. Table 5.8).

The association process has a "saturation" limit [72], beyond which the counter-ions cannot associate with the peptide anymore (cf. Figure 5.9(b)). This limit was found to be around 0.1%v TFA-H. A further increase of ion concentration leads to the increase of the concentration of free ions in solution, which eventually interact with the peptide by forming water-mediated ion pairs. In this situation, further addition of hydrophobic anions in the bulk layer allows the orientation of the water molecules in the second ("transition") layer towards the first ("solvation") layer, thus favouring the hydration of the peptide. For this reason, incresing the TFA-H concentration beyond the saturation layer leads to a decrease in the peptide rejection (cf. Table 5.8).

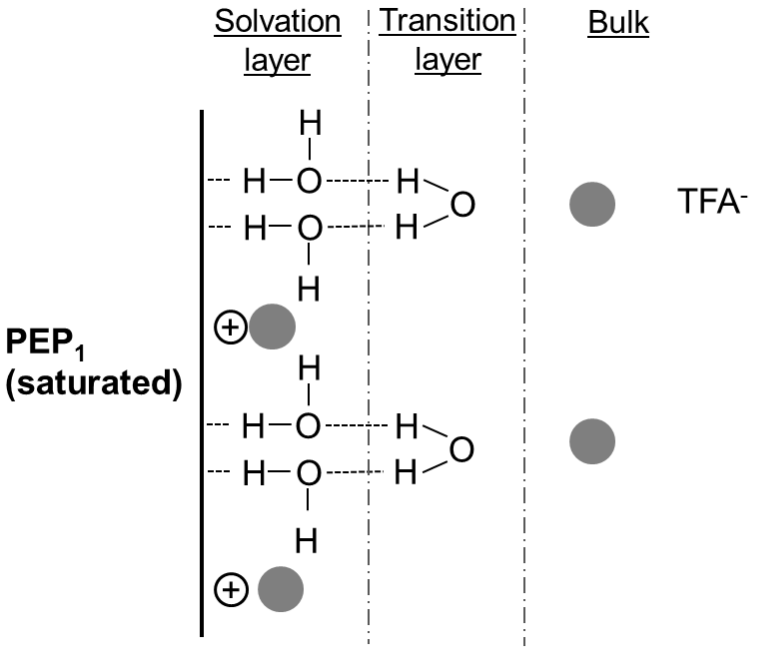
The two scenarios proposed in the introduction have been therefore identified for this peptide: (i) when the ion (TFA^-) associates as a counter-ion with the peptide, it contributes to the increase of the peptide hydrophobocity, since it increases the ACN content in the peptide solvation shell; (ii) on the other hand, when TFA^- cannot associate with the peptide anymore, due to the overcoming of the saturation limit, it behaves as a chaotropic ion, enhancing the hydration of the peptide in its second, or transition, layer.

5.4 Conclusion

In this chapter, NF in organic/solvent water mixtures was investigated, with particular attention to the role of solute-membrane and solvent-membrane competition on the molecular transport through ceramic NF membranes. NF of NaCl in water and in ACN/water mixtures was studied, in order to investigate the effects of electrostatic interaction and solute-solvent competition in terms of preferential solvation in organic/water mixtures. Different trends of the rejection profiles were observed for the two systems. In water, NaCl rejection increased with the solvent flux, which is the common trend characterising the



(a)



(b)

Figure 5.9: Interfacial water near the surface of hydrated PEP_1, as a function of the ion nature.

pressure-driven transport governed by solvent-membrane affinity. Salt rejection was well explained by the Donnan theory of electrostatic repulsion. On the other hand, NaCl rejection decreased with the solvent flux in organic/water mixtures. This profile represents the pressure-driven transport governed by solute-membrane affinity. At particular salt and organic solvent concentrations, NaCl rejection was found to be significantly negative, i.e. salt permeation was strongly enhanced with respect to solvent permeation. The solute-solvent competition had a more significant effect at low pore dimension (strong negative rejection was found in the NF range) and became more negligible for large pore dimension (UF range). This demonstrated that the affinity effects are more significant in the NF range, due to the high specific surface that characterises these membranes. The effect of the type of solvent on the ion rejection was found to be a function of the Hansen solubility parameter of the solvent ($S_{Hansen,bulk}$), the Hansen solubility parameter of the ion ($S_{Hansen,ion}$), and the preferential solubility parameters of the ion in the aqueous mixture, $\delta x_{s,i}$. Three possible cases for the solute-solvent competition were identified: (I) if anion and cation have strong affinity with the membrane ($S_{Hansen,i} > S_{Hansen,bulk}$), overall salt permeation is favoured and rejection can be negative; this case was observed for NaCl in ACN/water and acetone/water mixtures. (II) if ions are indifferent to the environment and do not show preferential affinity with the membrane compared to the solvent ($S_{Hansen,i} \sim S_{Hansen,bulk}$), rejection is low or zero; this case was observed for NaCl in ethanol/water and methanol/water mixtures. (III) if one of the two ions has strong affinity with the membrane ($S_{Hansen,i} > S_{Hansen,bulk}$), and the other a negligible one ($S_{Hansen,i} < S_{Hansen,bulk}$), the overall salt permeation depends on the relative importance of the two conflicting contributions. This case was observed for NaCl in DMF/water and DMSO/water mixtures. Finally, overall salt rejection was found to depend more on the preferential solvation parameter of the anion than on that of the cation.

Rejections of one small neutral organic molecule, Npys, and a model peptide, PEP_1, were studied, in order to understand the effect of solvent composition (%v ACN/water) and salt content (%v TFA-H). Rejections increased with the concentration of ACN, as expected from the preferential solvation of both in ACN over water. Rejection of Npys

increased in the presence of Cl^- ions, since Cl^- competed with Npys for water molecules and decreased the Npys hydrophilicity. Cl^- behaved as a kosmotropic ion for Npys. The effects of HCl (pH of the solution = 2) and NaCl (pH of the solution = 5.4) on Npys rejection were similar, meaning that the major contribution was played by the anion, Cl^-, and negligible effects could be attributed to solution pH (i.e. charge effects) and nature of the cation. On the other hand, Npys rejection decreased in the presence of TFA-H. This different behaviour was explained by the hydrophobic nature of TFA^- anions, which does not compete for water molecules and allows the water molecules in the transition shell to make hydrogen bonding with the water molecules in the first solvation shell. TFA^- behaved as a chaotropic ion for Npys.

For PEP_1, two scenarios were identified, as a function of the acid/ion concentration: in the low ion concentration range, TFA^- associated with the peptide as a counter-ion, and contributed to the increase of the peptide hydrophobicity, by favouring the solvation of the peptide in ACN, and in turn the peptide rejection; in the high ion concentration range, beyond the peptide "saturation" limit, TFA^- remained free in solution, enhancing the hydration of the peptide and therefore decreasing its rejection (chaotropic behaviour).

In conclusion, additionally to steric and electrostatic retention mechanism, it has been shown in this work that preferential solvation of both salts and organic molecules in solution affects the membrane transport, by changing the molecule hydration degree, and in turn the hydrophilic/hydrophobic interactions with the membrane. Solvent composition and ion nature and concentration are therefore significant additional effects for the pressure-driven permeation through ceramic NF membranes.

Chapter 6

Peptide permeation through ceramic NF membranes

6.1 Introduction

Typical processes for concentrating and purifying peptides are characterised by complicated matrices of input and output parameters. As shown in Chapter 5, the permeation mechanism of peptides in organic/water mixtures is influenced by the preferential solvation of both peptide and counter-ions by one of the mixture solvents. This means that the peptide retention depends on both solvent composition and salt content, which affect the hydrophilic/phobic properties of the peptide. Fundamental models often do not account for the effect of mixture composition on the peptide retention, as those models were developed mainly for aqueous solutions and tentatively extended to pure organic solvents. Furthermore, in particular working conditions, the composition of the mixture can affect the steric properties of the peptide, by favouring the aggregation of peptides in micelles. This has in turn significant consequences on NF behaviour.

Peptides are amphiphilic molecules, with charged head and more or less hydrophobic backbone (depending on the amino acid sequence constituting the peptide). The peptide charge is a function of the solution pH and the acid dissociation constants of the amino group ($pK_{NH_3^+}$), the carboxylic group (pK_{COOH}) and the side chain (pK_r), as shown in

Figure 6.1(a). Peptides can form micelles, under specific operating conditions (organic content and pH of the mixture). A typical micelle in aqueous solution forms an aggregate with the hydrophilic "head" regions in contact with surrounding solvent, sequestering the hydrophobic single-tail regions in the micelle centre, as shown in Figure 6.1(b).

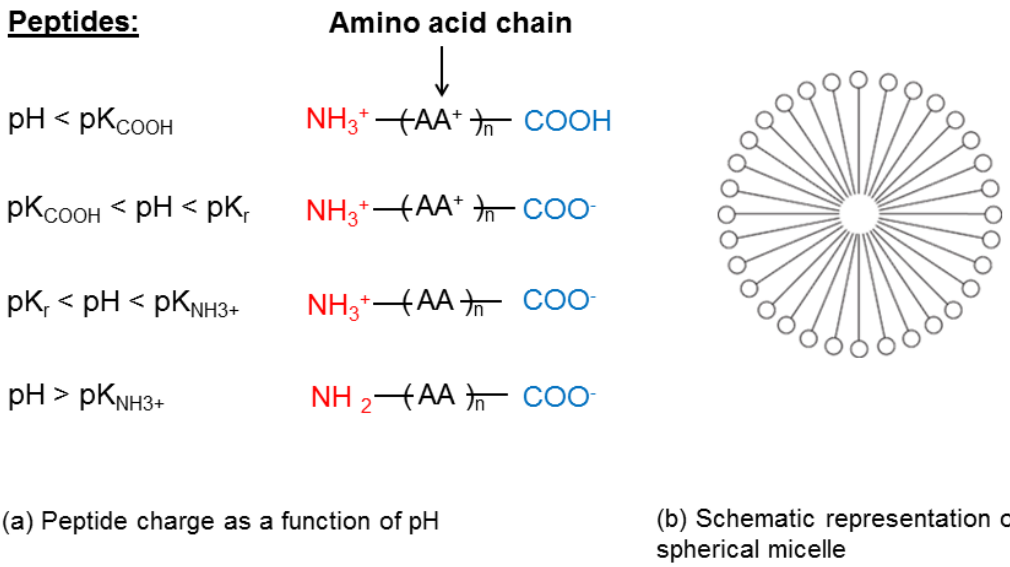


Figure 6.1: Peptide charge as a function of pH ($pK_{COOH} < pK_r < pK_{NH_3^+}$) and schematic representation of a spherical micelle.

Formation of micelles is favoured at high peptide concentration and near to the peptide isoelectric point (pI), where the global charge of the peptide chain is negligible (and in turn the natural repulsion between two peptide chains is non-existent). According to the nature of the amino acid side chains, pI can be lower or higher than pK_r. Peptide rejection and solvent flux are expected to significantly increase in the presence of micelles, due to their larger solute size and hydrophobicity.

In typical industrial R&D of nanofiltration processes, under the QbD concept, it is important to efficiently investigate the peptide permeation. Efficient investigation means the understanding of the effect of the operating parameters on the process performance and the translation of this understanding into mathematical models, able to make predictions in the design space. Design of Experiments (DoE) and Analysis of Variance (ANOVA) are

good tools to design the experimental set and obtain statistical models from that. Statistical modelling is efficient, reliable and requires low experimental effort, as the experimental set is designed to obtain the maximum amount of information with the minimum amount of experimental tests. DoE for statistical modelling was presented in more detail in Chapter 2.

In this chapter, the permeation of three model peptides produced by Lonza through two ceramic NF membranes is studied by DoE and ANOVA. Two peptides, one with preferential solvation for ACN over water (PEP_1) and the other with preferential solvation for water over ACN (P3), were studied under conditions largely below the isoelectric point; a third peptide (P2-S-SM) was studied under conditions close to its isoelectric point. For each peptide, peptide rejection, flux and TFA-H rejection were modelled as function of five operating parameters (peptide concentration, %v TFA-H/pH, pressure, cross-flow velocity, and %v ACN/water). The effect of the operating parameters was discussed in terms of positive or negative effects on the responses. Positive effects occur when the increase in the operating factor causes an increase in the response, negative effects occur when the increase in the operating factor causes a decrease in the response. Effects of interactions between operating parameters (i.e. the combined change in two factors that produces an effect greater, or less, than the additive effect expected from the factors alone) were also detected by this analysis. The statistical models obtained for the responses were commented on from a phenomenological point of view. Effects of solute-solvent-membrane interactions were identified for all the peptides, and the role of preferential solvation and effect of salt on peptide flux and rejection highlighted. For P2-S-SM, in operating conditions close to the peptide pI, reversible formation of micelles was observed and its effect on the permeation performance identified.

6.2 Experimental

6.2.1 Materials

Three peptides synthesised by Lonza were used in this study. Their properties are reported in Table 6.1.

Table 6.1: Physico-chemical properties of the peptides studied in this work.

Molecule	MW [Da]	pI	Preferential solvation	Water solubility
PEP_1	3000	4	ACN	> 10 g l^{-1}
P2-S-SM	1500	4	ACN	< 0.1 g l^{-1}
P3	4050	11	Water	> 30 g l^{-1}

All peptides in Table 6.1 are commercialised as TFA^- salts. For the first peptide, named PEP_1, NF is used to perform concentration, salt and solvent exchange, as part of the downstream process. PEP_1 has a high water solubility, however the percentage of hydrophobic amino acids in the peptide chain is higher than that of hydrophilic ones. For that reason, it is expected that the preferential solvation (i.e. the composition of the solvation shell in its immediare surrounding) is in favour of ACN over water molecules.

P2-S-SM and P3 are one reagent and the main product of a fragment condensation reaction between two pre-synthesised peptides (P1-SH and P2-S-SM, respectively). The fragment condensation reaction occurs via disulfide bond, with the release of a small molecule, SM, which is originally the protecting group of the S atom of P2-S-SM. The reaction is shown in Eq. 6.1:

$$P1 - SH + P2 - S - SM \rightarrow P3 + SM \tag{6.1}$$

P3 is largely hydrophilic and its preferential solvation is in water over ACN, while P2-S-SM is largely hydrophobic, with a significantly lower water solubility.

More detail about the application of NF to these two case studies and the reaction involved will be provided in Chapters 7 and 8, respectively.

The solvents used in this study are distilled water and ACN. The range of organic/water concentration studied for the three peptides is different, according to the specific case-study. The cross-flow filtration system used in this study contained a tubular module, suitable for multichannel tubular membranes with a length of 250 mm and an outer diameter of 25 mm. Two commercial ceramic membranes were used in this study, with the same different active layer, TiO_2 on Al_2O_3 and different MWCOs. They were prepared by Inopor (Germany) under the commercial names of Inopor® Nano 750 Da and Inopor® Nano 450 Da. All the membranes had 19 channels with an internal diameter of 3.5 mm and filtration area of 516 cm^2. The MWCO values and the nominal pore dimensions of the active top layer were measured by the manufacturer. The nominal properties of the membranes were summarised in Table 3.3.

6.2.2 Methods

Filtration tests

Solutions of pure PEP_1, P3, and P2-S-SM in ACN/water mixtures were prepared and their rejection and permeation tested in a Natan cross-flow system (Natan GmbH, CH; cf. Figure 3.2). 100 mM ammonium sulfate was added as buffer for the cases of P3 and P2-S-SM, and the pH adjusted with trifluoroacetic acid (TFA-H). Samples of retentate and permeate were taken at regular intervals, the permeate collected in a graduated cylinder and the flux monitored. Peptide concentration was measured by HPLC analysis, and salt content by conductivity and ion chromatography measurements.

Experimental design

Rejection and permeation of PEP_1 through Inopor® Nano 750, P3 through Inopor® Nano 450, and P2-S-SM through Inopor® Nano 750 were studied as function of five operating parameters: peptide concentration, %v TFA-H/pH, pressure, cross-flow velocity, and %v

ACN/water.

The operating parameters, selected as significant influencing factors for the peptide NF, were grouped in two classes:

1) parameters that affect solute-membrane interactions: they are the peptide concentration, the pressure and the pump frequency (i.e. the frequency of the pump that provides the circulation of the retentate in the NF loop; the pump frequency represents the cross-flow velocity over the membrane surface). These parameters affect the passage of the solute through the membrane by influencing accumulation/adsorption of the peptide at the membrane surface, without changing its physico-chimical properties;

2) parameters that affect solvent-solute-membrane interactions: they are the concentrations of peptide, of TFA-H, and of ACN. These parameters affect the solute physico-chemical properties (by association of TFA^- anions and ACN molecules with the peptide) and, therefore, the relative solute-membrane vs. solvent-membrane affinities. The peptide concentration is included in this group, since it affects the micellization tendency of the peptide under conditions close to its pI, thus changing the solute physico-chemical properties.

Experimental designs for PEP_1, P3 and P2-S-SM are reported in Tables 6.2, 6.4, and 6.3, respectively.

Table 6.2: Experimental design for nanofiltration of PEP_1 solutions through Inopor Nano 750.

Variable	**Operating parameter**	**Range of variation**
A	PEP_1 concentration [g l^{-1}]	1 - 5
B	%v TFA-H	0.02 - 0.1
C	Pressure [bar]	2 - 10
D	pump frequency [Hz]	25 - 45
	(cross-flow velocity [m s^{-1}])	(2 - 4)
E	%v ACN/water	0 - 30

Table 6.3: Experimental design for nanofiltration of P3 solutions through Inopor Nano 450.

Factor	Operating parameter	Range of variation
A	P3 concentration [g l^{-1}]	2 - 10
B	pH	2 - 5
C	Pressure [bar]	5 - 15
D	Pump frequency [Hz]	25 - 45
	(cross-flow velocity [m s^{-1}])	(2 - 4)
E	%v ACN / water	10 - 50

Table 6.4: Experimental design for nanofiltration of P2-S-SM solutions through Inopor Nano 750.

Factor	Operating parameter	Range of variation
A	P3 concentration [g l^{-1}]	1 - 5
B	pH	2 - 5
C	Pressure [bar]	2 - 10
D	Pump frequency [Hz]	25 - 45
	(cross-flow velocity [m s^{-1}])	(2 - 4)
E	%v ACN / water	30 - 70

The nanofiltration performances were studied by means of DoE, and specifically by using a Fractional Factorial Experimental (FRFE) design and a Response Surface Model (RSM) design for first and second order models, respectively. Experimental data for permeation flux, peptide rejection and TFA-H rejection were analyzed by ANOVA and a statistical model was found for the responses, as functions of the five influencing parameters. Both design planning and data analysis were undertaken by the software Design Expert 7.0.3.

6.3 Results and discussion

6.3.1 Nanofiltration of PEP_1 through Inopor Nano 750

FRFE design and results for PEP_1 rejection, TFA-H rejection and solvent flux, J_v, are reported in Table B.1 (Appendix B). The flux varies between 4.2 l m^{-2} h^{-1} to 52.7 l m^{-2} h^{-1}, which in turn means that the permeability is between 2.1 and 5.3 l m^{-2} h^{-1} bar^{-1}. PEP_1 rejection is between 83.3% and 99.9% and TFA-H rejection between 3.1 and 53.1%.

The statistical model for PEP_1 rejection in terms of coded factors is given by Equation 6.2. Factors are "coded" when they assume values between -1 and +1 corresponding to the minimum and the maximum actual values, respectively.

$$\begin{aligned} REJ_{PEP_1} = 95.50 + 0.85A + 3.25B - 0.1C + 0.14D + 2.21E - 1.20A \cdot B + \\ -0.56A \cdot E - 1.78B \cdot E + 1.97C \cdot D \end{aligned} \tag{6.2}$$

The model for PEP_1 rejection in terms of actual factors is:

$$\begin{aligned} REJ_{PEP_1} = +90.92 + 1.60C_{PEP_1} + 171.08\%vTFA - 1.75Pressure - 0.28PumpFreq. + \\ +0.38\%vACN - 15.04C_{PEP_1} \cdot \%vTFA - 0.02C_{PEP_1} \cdot \%vACN + \\ -2.97\%vTFA - H \cdot \%vACN + 0.05Pressure \cdot PumpFreq. \end{aligned} \tag{6.3}$$

The coefficients of correlation for peptide rejection are reported in Table 6.5.

Table 6.5: Statistical analysis of the models for PEP_1 rejection, TFA-H rejection and solvent flux.

	$\mathbf{Rej}_{PEP_1}$	$\mathbf{Rej}_{TFA-H}$	$\mathbf{J}_{v,PEP_1}$
Response transformation	none	none	$\ln(J_{v,PEP_1})$
Lack of Fit p-value	0.1486	0.5308	0.3162
R^2	0.9698	0.9132	0.9987
Predicted R^2	0.9395	0.8134	0.9952
Adjusted R^2	0.9317	0.8798	0.9979

The "Lack of Fit p-value" higher than 0.05 implies the Lack of Fit is not significant relative to the error. Non-significant lack of fit is desired for the model to properly fit the experimental data.

The significance of the model and of each operating factor is reported in Table 6.6 for the peptide rejection.

The results in Table 6.6 indicate that the model fits the observations well. This is because the fitted model is highly significant with an F-test value of 32.08. The F-test value quantifies the significance of the factor in the statistical model. Factors A, B, D, and E and interactions AB, AE, BE, and CD have high F-test value, and are therefore significant, while factors C and D, have a very low F-test value, and have therefore non-significant effect on the peptide rejection.

Peptide concentration (factor A) has a positive effect on the peptide rejection. This was attributed to the occurrence of adsorption at high peptide concentrations, which causes obstruction of the pores and blocks the passage of the peptide through the membrane. The positive effect of %v TFA-H and %v ACN (factors B and E, respectively) has been explained by the decrease in affinity between peptide and membrane caused by adsorption of TFA^- and ACN on the peptide chain. TFA^-, in fact, associates with the peptide chain as a counter-ion [72] and ACN solvates the hydrophobic amino acid side chains [66], and so they

Table 6.6: ANOVA result for Rej_{PEP_1} .

	Sum of squares	**df**[a]	**Mean square**	**F value**[b]	**Probability>F**	**Remarks**
Model	400.29	9	44.48	32.08	< 0.0001	significant
A	11.48	1	11.48	8.28	0.0183	significant
B	169.46	1	169.46	122.21	< 0.0001	significant
C	0.16	1	0.16	0.12	0.7403	non-significant
D	0.32	1	0.32	0.23	0.6443	non-significant
E	77.84	1	77.84	56.14	< 0.0001	significant
AB	23.16	1	23.16	16.70	0.0027	significant
AE	4.96	1	4.96	3.58	0.0911	significant
BE	50.94	1	50.94	36.74	0.0002	significant
CD	61.98	1	61.98	44.70	< 0.0001	significant

[a] Degrees of freedom.

[b] Fisher.

both contribute to the increase in the peptide hydrophobicity, decreasing its affinity with the hydropilic membrane, as seen in Chapter 5. The effect of pressure and pump frequency (factors C and D, respectively) are not statistically significant for peptide rejection (since the respective model coefficients in Equation 6.2 are negligible).

The interaction between peptide concentration and %v TFA-H (A-B), peptide concentration and %v ACN (A-E), %v TFA-H and %v ACN (B-E), pressure and pump frequency (C-D) are statistically significant. Figure 6.2 shows the interaction between factors B and E, as an example (since it is the most statistically significant interaction).

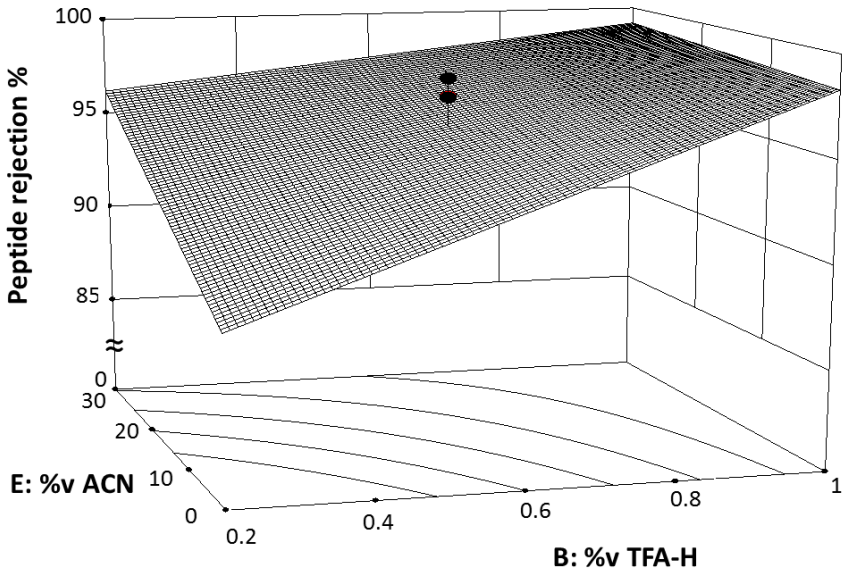


Figure 6.2: Interaction B-E for PEP_1 rejection by Design Expert Software (actual factors: $C_{peptide}$ = 3.00; Pressure = 6.00; Pump frequency = 35.00).

The surface of Figure 6.2 is not flat, as it would be in the absence of interaction between the two factors. The contribution of this interaction is negative, meaning that the combined effect of the two single variables is less than additive. From a practical point of view, this means that the effect of %v ACN on peptide rejection (due to the solvation/hydrophobization effect) is more significant at low %v TFA-H, and vice versa, %v ACN effect is less significant at larger %v TFA-H values. Interactions A-B and A-E show the same type of additive effect (data not shown).

The statistical model for the solvent flux [l m^{-2} h^{-1}] in terms of coded factors is given by Equation 6.4.

$$ln(J_{v,PEP_1}) = +2.82-0.13A+0.11B+0.70C+0.062D+0.24E+0.057A\cdot B+0.089A\cdot E \quad (6.4)$$

The model for flux in terms of actual factors is:

$$\begin{aligned} ln(J_{v,PEP_1}) = +1.60 - 0.15C_{peptide} + 0.70\%vTFA + 0.17Pressure + \\ +0.006PumpFreq. - 0.007\%vACN + 0.72C_{peptide}\cdot\%vTFA + \\ +0.003C_{peptide}\cdot\%vACN \end{aligned} \quad (6.5)$$

The coefficients of correlation for the flux are reported in Table 6.5. The transformation of the response to the natural logarithm, $\ln(J_{v,PEP_1})$ has been suggested by ANOVA, to improve the normal plot of the residuals.

Peptide concentration (A) affects the flux negatively. This is attributed to the effect of peptide concentration on concentration polarization and adsorption, favourable at large peptide concentration. The same effect was found to positively influence peptide rejection. %v TFA-H (B) and %v ACN (E) affect the flux positively, as they increase the hydrophobicity of the peptide by associating with the peptide molecule, which in turn increases the exclusion of the peptide from the pore. This decreases both peptide adsorption (i.e. pore obstruction) and solute friction through the pore, due to less solute passage. The positive effect of pressure (C) on flux is explained by the positive effects of pressure on the convective bulk flow through the membrane. The positive effect of the pump frequency (D) (i.e. flow rate in the system), is attributed to the mechanical action of the fluid stream inside the membrane channel, which reduces concentration polarization and adsorption on the membrane surface. Less accumulation/adsorption ensures in turn larger effective pore dimensions and filtration area.

The interactions between peptide concentration and %v TFA-H (A · B) and peptide concentration and %v ACN (A · E) are statistically significant. As for peptide rejection,

this means that the simultaneous variation of the factors in the pair produces an effect different from that obtained by summing the effects of the two singular variations.

As clear from Table B.1, the rejection of the small counter-ion (TFA^-) is not negligible, and can assume values up to 53%. The statistical model for TFA-H rejection in terms of coded factors is the following:

$$REJ_{TFA-H} = 24.53 + 6.58A - 9.76B - 3.54D + 5.69E - 3.82D \cdot E \tag{6.6}$$

while in terms of actual factors the model is:

$$\begin{aligned} REJ_{TFA-H} = +22.62 + 3.29C_{peptide} - 243.95\%vTFA - H + 0.028PumpFreq. + \\ +1.27\%vACN - 0.025PumpFreq. \cdot \%vACN \end{aligned} \tag{6.7}$$

TFA-H rejection is positively affected by peptide concentration. If peptide concentration is large, in fact, more TFA^- counter-ions can associate with the peptide chains and be less available for the permeation through the pore. TFA-H rejection is negatively affected by %v TFA-H. This is explained by the effect of concentration polarization of TFA^- ions in solution, which decreases ion rejection at large concentration values (as it favours the accumulation of the ions at the membrane surface), and decreases the solvent flux. The %v ACN affects TFA-H rejection positively, since ACN increases the anion hydrophobicity by adsorbing in its preferential solvation shell and, in turn, causing its preferential exclusion from the pore (cf. Chapter 5).

Occurrence of TFA-H rejection has important consequences on global diafiltration performance. It affects peptide retention and flux and the number of diafiltration volumes required for the salt exchange. Extended knowledge of how counter-ion concentration affects filtration performace is fundamental for the process selection.

6.3.2 Nanofiltration of P3 through Inopor Nano 450

FRFE design and results for P3 rejection, TFA-H rejection and flux are reported in Table B.2 (Appendix B).

The flux varies between 3.7 l m^{-2} h^{-1} to 64.2 l m^{-2} h^{-1}, which in turn means that the permeability is between 0.7 and 4.3 l m^{-2} h^{-1} bar^{-1}. The peptide rejection is always higher than 98.0%.

The statistical models for rejection of P3 in terms of coded and actual factors are given by Equations 6.8 and 6.9.

$$REJ_{P3} = 99.68 - 0.05A - 0.18B - 0.11E - 0.075A \cdot B - 0.088B \cdot E \tag{6.8}$$

$$\begin{aligned} REJ_{P3} = +99.76 + 0.03C_{P3} + 0.05pH + 4.58\%vACN - 0.01C_{P3} \cdot pH + \\ -2.92pH \cdot \%vACN + \end{aligned} \tag{6.9}$$

The statistical models for the permeation flux in terms of coded and actual factors are given by Equations 6.10 and 6.11.

$$J_{v,P3}^{0.5} = 4.34 - 1.17B + 1.06C + 0.20D + 0.13E - 0.24A \cdot B - 0.302B \cdot C - 0.59B \cdot E \tag{6.10}$$

$$\begin{aligned} J_{v,P3}^{0.5} = -0.22 + 0.45pH + 0.35Pressure + 0.02Pump.Freq. + 0.06\%vACN + \\ -0.04C_{P2-S-SM} \cdot pH - 0.042pH \cdot Pressure - 0.02pH \cdot \%vACN \end{aligned} \tag{6.11}$$

The coefficients of correlation for all models are reported in Table 6.7.

The "Lack of Fit p-value" higher than 0.05 implies the Lack of Fit is not significant relative to the error. Response transformation for flux was suggested by ANOVA.

Table 6.7: Statistical analysis of the models for P3 rejection, TFA-H rejection and solvent flux.

	$\mathbf{Rej}_{P3}$	$\mathbf{Rej}_{TFA-H}$	$\mathbf{J}_{v,P3}$
Response transformation	None	None	$J_{v,P3}^{0.5}$
Lack of Fit p-value	0.2170	0.3013	0.5283
R^2	0.8217	0.8714	0.9790
Predicted R^2	0.7532	0.7707	0.9111
Adjusted R^2	0.5573	0.8121	0.9622

The main influencing parameters for the rejection are pH and %v ACN, both with negative effect. pH shows a negative effect on the flux too, while %v ACN does not significantly affect it. The strong contribution of pH (i.e. %v TFA-H) is explained by its influence on steric and hydrophobic properties of the peptide: the increase in TFA-H content (i.e. low pH) determines the increase in peptide dimension and hydrophobicity, which in turn contributes to the exclusion of the molecule from the pore. Solvent flux is larger through the pore corresponding to higher rejection, since friction due to solute flux is less important. The negative effect of ACN content on rejection is explained by the poor solubilization of P3 by ACN. By increasing the ACN content, the hydrophobicity of the solvent increases, thus contributing to the decrease in relative solvent-membrane affinity, as compared to the solute-membrane affinity. When the solvent-membrane affinity is lower than the solute-membrane affinity, enhanced permeation of solute occurs through the membrane, thus reducing rejection [58].

Peptide concentration has no significant effect on either flux or rejection. This is limited to the investigated experimental range only. It is plausible that an increase in concentration will decrease the flux, as concentration polarization and adsorption may occur.

Pressure shows a remarkably positive effect on flux, as expected from the driving force for the process, and no significant effect on the rejection. The effect of pressure on concentration polarization is therefore negligible.

Pump frequency, which in turn represents the linear velocity over the membrane surface, has a positive effect on the flux and a non significant effect on the rejection. This is explained by the effect of linear velocity on concentration polarization [17]: the larger the linear velocity, the lower the solute accumulation at the membrane surface and the less significant the concentration polarization layer. Similarly to what was observed for the effect of pressure, changes in fluid dynamic conditions affect the flux, but not the retention performance.

Effects of interactions between pH and %v ACN and between pH and peptide concentration affect both rejection and solvent flux in the same way (i.e. negative effects), while interaction between pH and pressure affect the flux only. It is worth noting that pressure and pump frequency affect the flux and not the peptide rejection, both as single and interactions effects. These parameters, in fact, affect the fluid dynamics of the system but do not influence solute-membrane interface interactions, as pH and %v ACN/water do. In other words, it is plausible to assume that rejection of P3 is governed by solute-membrane interactions at the surface level only, while flux is influenced by both solute-membrane interactions and fluid-dynamics in the module.

As already observed for PEP_1, the rejection of the small counter-ion (TFA^-) is not negligible. It assumes values up to 37.7% (cf. Table B.2). The statistical models for TFA-H rejection in terms of coded and actual factors are given by Equations 6.12 and 6.13.

$$REJ_{TFA-H} = 18.32 + 4.27A - 2.29B + 4.02C - 5.74E - 1.15B \cdot E - 3.23C \cdot E \quad (6.12)$$

$$\begin{aligned} REJ_{TFA-H} = 4.13 + 1.07C_{P3} - 0.38pH + 1.77Pressure + 0.17\%vACN + \\ -0.38pH \cdot \%vACN - 0.03Pressure \cdot \%vACN \end{aligned} \quad (6.13)$$

The coefficients of correlation for this model are reported in Table 6.7.

As found during the NF of PEP_1 solutions, TFA-H rejection is positively affected by peptide concentration (if peptide concentration is large, in fact, more TFA^- counter-ions

can associate with the peptide chains and be less available for the permeation through the pore). TFA-H rejection is negatively affected by pH and %v ACN, similarly to the peptide rejection. It is plausible that the association between peptide and TFA^- is strong enough to determine coupled flow of the two.

6.3.3 Nanofiltration of P2-S-SH through Inopor Nano 750

For this peptide, the range of variation for the pH extended over the peptide pI value. A Response Surface Model (RSM) was therefore used to obtain a second order model, which could account for eventual non-idealities/non-linearities in the dependences, due to changes in the peptide physico-chemical properties. The second order RSM model was compared with the first order model from Factorial Design (2FI) for regression performance.

RSM design and results for P2-S-SH rejection, TFA-H rejection and flux are reported in Table B.3 (Appendix B).

The flux varies between 29.0 l m^{-2} h^{-1} to 211.1 l m^{-2} h^{-1}, which in turn means that the permeability is between 14.5 and 21.1 l m^{-2} h^{-1} bar^{-1}. Interestingly, the peptide rejection ranges from 3.6 to 98.5%. Formation of micelles was observed corresponding to high peptide concentration and low TFA-H content (in a form of turbid solution). Reversible formation of micelles was demonstrated by changing the pH of the solution.

First and second models (2FI and quadratic models, respectively) are compared for P2-S-SM rejection and solvent flux in Table 6.8.

Interestingly, for both responses, the 2FI model was suggested by ANOVA over the quadratic one. This means that second order models are not required for describing peptide rejection and solvent flux and first order models are valid in the investigated range. The formation of micelles, therefore, is not changing the effect of the operating parameters in the design space. Note that this could be different outside the design space, and extrapolation is highly risky for this peptide.

The statistical models for P2-S-SM rejection in terms of coded and actual factors are given by Equations 6.14 and 6.15.

Table 6.8: Statistical analysis of the models for P2-S-SH rejection and flux.

Response	**Model**	**Lack of Fit**	**R^2**	**Pred R^2**	**Adj R^2**	
$Rej_{P2-S-SM}$	2FI	0.1070	0.9217	0.9098	0.7373	suggested
	Quadratic	0.1628	0.9475	0.9345	0.6774	
$J_{v,P2-S-SM}$	2FI	0.2149	0.9581	0.9363	0.7712	suggested
	Quadratic	0.1575	0.9581	0.9279	0.5782	

$$REJ^{0.5}_{P2-S-SM} = 6.25 + 1.41A + 0.35B + 0.85E + 1.42A \cdot B - 0.44A \cdot E \tag{6.14}$$

$$\begin{aligned} REJ^{0.5}_{P2-S-SM} = 4.54 - 0.41C_{P2-S-SM} - 1.19pH + 0.08\%vACN + \\ +0.47C_{P2-S-SM} \cdot pH - 0.01C_{P2-S-SM} \cdot \%vACN \end{aligned} \tag{6.15}$$

The statistical models for the permeation flux in terms of coded and actual factors are given by Equations 6.16 and 6.17.

$$\begin{aligned} J_{v,P2-S-SM} = 109.23 - 12.77A - 5.39B + 56.65C + 9.96D + 18.82E - 12.97A \cdot C + \\ +8.38A \cdot D - 13.60B \cdot C + 14.94B \cdot D + 19.30C \cdot E - 8.80D \cdot E \end{aligned} \tag{6.16}$$

$$J_{v,P2-S-SM} = 58.66 - 11.32C_{P2-S-SM} - 24.84pH + 14.89Pressure - 1.54PumpFreq. + \\ +1.03\%vACN - 1.62C_{P2-S-SM} \cdot Pressure + 0.42C_{P2-S-SM} \cdot PumpFreq. + \\ -2.27pH \cdot Pressure + 0.99pH \cdot PumpFreq. + 0.24Pressure \cdot \%vACN + \\ -8.80PumpFreq. \cdot \%vACN \tag{6.17}$$

The statistical models for TFA-H rejection in terms of coded and actual factors are given by Equations 6.18 and 6.19.

$$(REJ_{TFA-H}+0.46)^{0.5} = +3.07+0.50A+0.88B+0.32D+0.51E+0.92A{\cdot}B+0.35A{\cdot}D \tag{6.18}$$

$$(REJ_{TFA-H} + 0.46)^{0.5} = 2.90 - 1.44C_{P2-S-SM} - 0.33pH - 0.02PumpFreq. + \\ +0.03\%vACN + 0.31C_{P2-S-SM} \cdot pH + 0.02C_{P2-S-SM} \cdot PumpFreq. \tag{6.19}$$

Response transformations have been suggested by ANOVA.

For this case study, the effect of peptide concentration is twofold: on one side, it affects concentration polarization at the membrane surface; on the other, it affects the steric properties of the peptide, by enhancing the formation of peptide micelles. Peptide concentration shows a positive effect on the peptide rejection, and a negative effect on the flux. At high peptide concentration, the hydrophobic peptide chains are not stable in the aqueous solutions, and tend to form micelles, which increase the peptide rejection and decrease the flux, as expected from their size and hydrophobicity. Similarly, pH showed a positive effect on peptide rejection and a negative effect on the solvent flux. At high pH value (pH $\sim$ pI, in this study), micelles form, while, at low pH values (pH $<$ pI), peptides are stabilised in solution and do not aggregate. At high peptide concentration and high pH value, flux

declines, due to the presence of large hydrophobic micelles in solution, which cause larger pore obstruction and strongly affect the concentration polarization.

The concentration of ACN affects both peptide rejection and flux positively. ACN, in fact, increases the hydrophobicity of the peptide (both as a single chain and as a micelle) by associating with it, increasing in turn the exclusion of the solute from the hydrophilic membrane pore and reducing the friction due to the solute flux.

Pressure shows a remarkably positive effect on flux, as expected from the driving force for the process, and no significant effect on the rejection. The effect of pressure on concentration polarization is therefore negligible.

Pump frequency, which in turn represents the linear velocity over the membrane surface, has a positive effect on the flux and a non-significant effect on the rejection. This is explained by the effect of the cross-flow velocity on concentration polarization, as observed for all the peptides in this study.

TFA-H rejection is positively affected by peptide concentration, as for all the case studies in this work. If peptide concentration is large, in fact, more TFA^- counter-ions associate with the peptide and remain preferentially in the retentate.

6.3.4 Summary of the effects of operating parameters

Here, the main effects of the operating parameters on peptide rejection, solvent flux and salt rejection are summarised, to unify the understanding. The summary of these effects is reported in Table 6.9.

Parameters affecting solute-membrane interactions

When statistically significant, the effect of peptide concentration is positive on the peptide rejection, and negative on the solvent flux. This is due to two different mechanisms: (i) formation of micelles, enchanced at high peptide concentration (case of P2-S-SM); (ii) concentration polarization, due to the accumulation of the solute at the membrane surface, in concentrated solutions, and the increase the resistance to the transport through the pores (case of PEP_1).

Table 6.9: Summary of the effects of the main operating parameters on peptide rejection and flux for PEP_1, P3 and P2-S-SM (ns = not significant).

	$\mathbf{J}_{v,PEP_1}$	$\mathbf{Rej}_{PEP_1}$	$\mathbf{J}_{v,P3}$	$\mathbf{Rej}_{P3}$	$\mathbf{J}_{v,P2-S-SM}$	$\mathbf{Rej}_{P2-S-SM}$
C_{PEP_1}	-	+	ns	ns	-	+
Pressure	+	ns	+	ns	+	ns
Pump frequency	+	ns	+	ns	+	ns
%v TFA-H[a]	+	+	+	+	+	-
%v ACN	+	+	+	-	+	+

[a] For P3 and P2-S-SM, %v TFA-H is used in the comparison, instead of pH, to allow the comparison with PEP_1. The sign of the effect is, therefore, the opposite as that found in Equations 6.8, 6.10, 6.14, and 6.16.

The effect of pressure is positive on the flux and not significant for the peptide rejection, for all the case studies; increasing pressure increases the driving force for the solvent flux (positive effect on $J_{v,i}$), without significantly affecting the concentration polarization (not significant effect on Rej_i).

The pump frequency (i.e. the cross-flow velocity) positively affects the flux, as it impedes concentration polarization, avoiding solute accumulation at the membrane surface, but does not significantly affect the peptide rejection.

Interestingly, these parameters have the same effects on the NF performance. This is expected, since they affect the fluid dynamics of the system, and have no effects on the solute properties (apart from the special case of P2-S-SM).

Parameters affecting solute-solvent-membrane interactions

The effects of %v TFA-H and %v ACN strongly depend on the nature of the peptide. For peptides under conditions far from their pI, the effect of %v TFA-H is on the hydropho-

bicity of the peptide, by molecular association. The increase of the peptide hydrophobicity determines higher rejection (due to exclusion from the pore) and larger flux (due to less friction in the pore). For the hydrophobic peptide close to pI (P2-S-SM), %v TFA-H has opposite effects on rejection and flux. It affects the formation of new larger entities, which causes the increase in the peptide rejection and the decrease in the solvent flux.

The effect of ACN is different for peptides with preferential solvation in ACN over water (PEP_1) and for peptides with preferential solvation in water over ACN (P3). When the peptide preferential solvation is in ACN, the increase in %v ACN led to a positive effect on both flux and peptide rejection (ACN increases the peptide hydrophobicity and exclusion from the pore). On the contrary, when the peptide preferential solvation is in water, the increase in %v ACN led to a negative effect on the peptide rejection, for the opposite reason. The concentration of ACN affects also the formation of micelles (case of P2-S-SM): low organic content favours the formation of hydrophobic micelles. For this peptide, %v ACN has a positive effect on both flux and peptide rejection.

Effects on TFA-H rejection

The main operating parameters that affect TFA-H rejection in the three case studies are the concentrations of peptide, %v TFA-H and %v ACN. In Table 6.10, the effects of the three main influencing parameters are compared for the three peptides.

Table 6.10: Effect of the main operating parameters on TFA-H rejection.

	$\mathbf{Rej}_{TFA-H}$ / $\mathbf{DoE}_{PEP_1}$	$\mathbf{Rej}_{TFA-H}$ / $\mathbf{DoE}_{P3}$	$\mathbf{Rej}_{TFA-H}$ / $\mathbf{DoE}_{P2-S-SM}$
C_{PEP_1}	+	+	+
%v TFA-H	-	+	-
%v ACN	+	-	+

It is interesting to observe that TFA-H rejection is always positively affected by the

peptide concentration; TFA^-, in fact, associates as a counter-ion with the peptides and is therefore retained with them. On the other side, effects of %v TFA-H and %v ACN are different. It seems that there is an analogy between the two peptides preferentially solvated by ACN (PEP_1 and P2-S-SM), with respect to hydrophilic one (P3). Retention of TFA-H is, however, difficult to explain, since it is coupled with the peptide retention. This means that the nature of the peptide and the effects of the operating parameters on the peptide can affect indirectly the ion retention, making its phenomenological understanding more complicated.

6.4 Conclusion

Fundamental models often do not take into account the effect of mixture composition on the peptide retention, as those models were developed mainly for aqueous solutions and tentatively extended to pure organic solvents. Under particular working conditions, however, the composition of the mixture can affect the steric and hydrophobic properties of the peptide, with significant consequences on the NF behaviour.

In this work, Design of Experiments was used to study the NF of three model peptides and understand the effect of the operating parameters on solvent flux, peptide and salt rejection. The three peptides were chosen, as representative of real Lonza case studies. Statistical models for the responses as functions of the operating parameters were obtained by statistical Analysis of Variance. Qualitative conclusions were drawn from phenomenological interpretation of the statistical models:

(i) the operating parameters affecting the solute-membrane interactions and the fluid dynamics in the system (peptide concentration for PEP_1 and P3, pressure and pump frequency) are the parameters that affect the passage of the solute through the membrane by influencing accumulation/adsorption of the peptide at the membrane surface, without changing its physico-chemical properties. They showed the same effect on all the peptides, and namely: positive effect of pressure and cross-flow velocity on the flux, and negligible effect of both on the peptide rejection;

(ii) the operating parameters affecting solute-solvent-membrane interactions (peptide concentration for P2-S-SM, TFA-H concentration, and ACN concentration) are the parameters that affect the solute physico-chemical properties (by association of TFA^- anions and ACN molecules with the peptide and by enhancing the formation of micelles for hydrophobic peptides in hydrophilic solutions) and, therefore, the relative solute-membrane vs. solvent-membrane affinities. They showed different effects for the three case studies, as a function of the peptide physico-chemical properties: preferential solvation by ACN determined an increase in hydrophobicity for the peptide, and in turn, preferential exclusion from the membrane; on the other side, association with water molecules determined the increase in the peptide-membrane affinity and relative peptide permeation. Formation of micelles caused a significant increase in the peptide rejection and, in turn, a significant flux reduction.

TFA-H rejection was found to be significant (up to 53% in some cases). Since TFA-H rejection affects peptide retention and solvent flux, it has important consequences on the overall filtration performances. Extended knowledge of how counter-ion concentration affects filtration performaces is fundamental for the understanding and process selection, as it will be shown in Chapters 7 and 8 for two Lonza's case studies.

Chapter 7

Case-study 1: peptide concentration and diafiltration

7.1 Introduction

Recently, nanofiltration techniques have been adopted by pharmaceutical industries as part of the downstream processes for peptides, to perform concentration, purification and salt/solvent exchange and have been demonstrated to be suitable to integrate conventional purification techniques, providing savings in terms of time and costs [109]. The Quality by Design (QbD) concept, introduced by the International Conference on Harmonisation (ICH) of Technical Requirements for Registration of Pharmaceuticals for Human Use to support new initiatives and provide guidance for pharmaceutical process development, became the answer to assisting the industry to move towards a more scientific approach to pharmaceutical development. Design of Experiments (DoE) methods have been extensively applied in process design under QbD to help engineers understand the effects of possible combinations and interactions of various parameters on the final drug quality [74]. The QbD concept and DoE for statistical modelling were introduced in Chapter 2 and applied to some case studies in Chapter 6. Apart from basic transport modelling for NF, information from DoE can be used to support process modelling, by using concentration-dependent solute rejection and solvent flux obtained by experimental design to descibe the dynamics of different membrane

filtration processes (concentration, constant volume diafiltration and variable volume diafiltration), providing a methodology to select the most appropriate filtration technique for a given separation problem.

In this chapter, nanofiltration is applied to perform concentration, salt and solvent exchange for the first model peptide, PEP_1, introduced in Chapter 6, as part of its downstream process (cf. Figure 7.1).

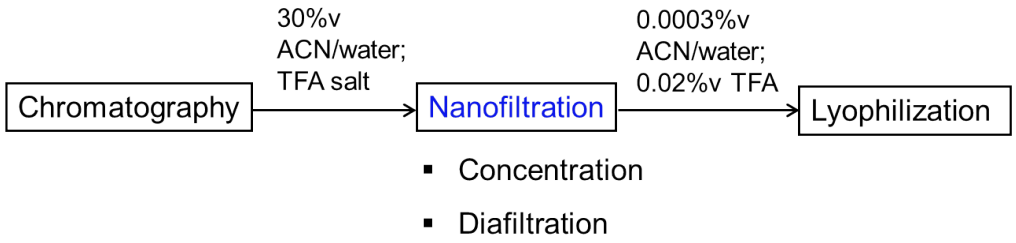


Figure 7.1: Downstream process for PEP_1.

The peptide mixture exits the preparative chromatography with a composition of 0.1%v TFA / 30%v ACN/water; concentration and diafiltration are applied to increase the peptide concentration, reduce the operating volumes and reach the composition of 0.02%v TFA / 0.003%v ACN / water before entering the lyophilization. Rejection and permeation performances of PEP_1 solutions through the Inopor® Nano 750 Da were studied by DoE and statistical models for rejection and flux obtained as a function of several operating parameters in Chapter 6.

In this study:

(1) the best operating conditions for concentration (large solvent flux and peptide rejection) were found by numerical optimization of the statistical models obtained in Chapter 6;

(2) The statistical models from DoE were included in the mathematical framework of the diafiltration process, to calculate the evolution of peptide, counter-ion (TFA^-) and solvent (ACN) concentrations in the system. The process modelling including time-dependent rejection and permeability was validated using experimental data for diafiltration at concentration values larger than that used for DoE;

(3) The best operating conditions found for Inopor® Nano 750 Da were tested for a tighter ceramic NF membrane from the same material, Inopor® Nano 450 Da. Surprisingly, the flux through the tighter membrane remained similar to that of the looser membrane, while rejection increased to almost 99.99%;

(4) The model combining the dynamic mass balance for diafiltration and time-dependent rejection and permeability was used to simulate different possible constant volume diafiltration paths to perform the salt and solvent exchanges of interest (0.1%v TFA / 30%v ACN → 0.02%v TFA / 0.003%v ACN, i.e. point D → point C in Figure 7.12);

(5) Assuming complete rejection, and the best path identified from step (4), constant volume and variable volume diafiltration modes were compared, to simultaneously perform concentration and salt/solvent exchange. Preconcentration followed by constant volume diafiltration was compared to variable volume diafiltration. The former strategy was selected, as it requires lower operating time.

7.2 Experimental

7.2.1 Materials

A peptide produced by Lonza AG (Switzerland), and named PEP_1, was used in this work. The same peptide was presented in Chapters 5 and 6 and its physico-chemical properties reported in Table 5.1. The solvents used in this study are distilled water and acetonitrile (ACN), supplied by Scharlau. The cross-flow filtration system contained a tubular module, suitable for multichannel tubular membranes with a length of 250 mm and an outer diameter of 25 mm. Two commercial ceramic membranes were used in this study, with different active layers, TiO_2 on Al_2O_3 and different MWCOs. They were prepared by Inopor (Germany) under the commercial names of Inopor® Nano 750 Da and Inopor® Nano 450 Da. All the membranes had 19 channels with an internal diameter of 3.5 mm and filtration area of 516 cm^2. The MWCO values and the nominal pore dimensions of the active top layer were measured by the manufacturer. The nominal properties of the membranes were summarised in Table 4.3.

Rejection and permeation tests

Solutions of PEP_1 in water and ACN/water mixtures of different compositions were prepared. Trifluoroacetic acid (TFA-H) was added to adjust the concentration of the peptide counter-ion (TFA^-). Solute rejection and permeation were tested in a Natan cross-flow system (Natan GmbH, CH), in the open loop configuration (cf. Figure 7.2).

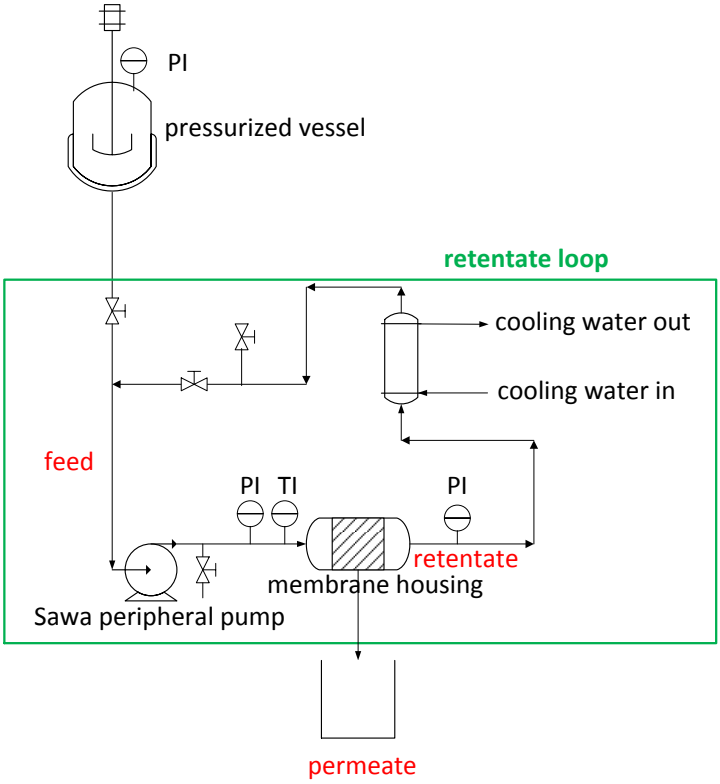


Figure 7.2: Natan cross-flow system (Natan GmbH, CH). Open loop for diafiltration tests.

For diafiltration tests, the retentate stream was recirculated and the permeate stream collected separately (cf. Figure 7.2). During this operation, the fresh diluant stream was loaded into the feed tank and entered the retentate loop at the same velocity as the permeate flux flowed from the membrane housing (this configuration is known as constant volume diafiltration mode [81]).

Six filtration experiments were performed (cf. Figure 7.3).

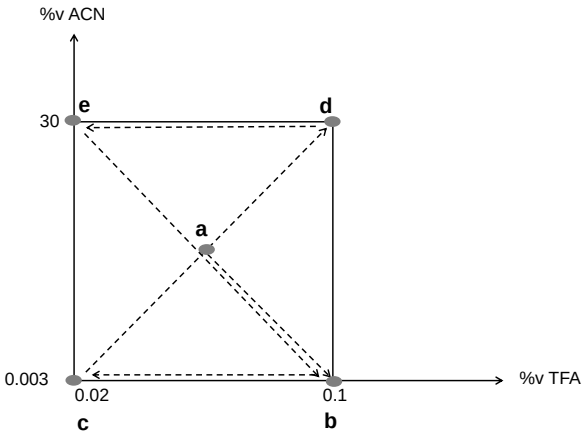


Figure 7.3: Concentration + diafiltration sequence.

The first experiment was done at point a: a solution of 1.75 g l^{-1} in 0.05%v TFA-H and 15%v ACN was prepared and concentrated down to 0.5 l. The same solution was afterwards used to perform five diafiltration experiments in sequence, as shown in Figure 7.3: a $\rightarrow$ b, b $\rightarrow$ c, c $\rightarrow$ d, d $\rightarrow$ e, e $\rightarrow$ b. Diafiltration a $\rightarrow$ b was done by adding fresh diluant solution with the composition of point b, diafiltration b $\rightarrow$ c by adding fresh diluant solution with the composition of point c, and so on. Eight diafiltration volumes (1 diafiltration volume = 0.35 l) were used for each run. The last experiment e $\rightarrow$ b was undertaken to replicate the first one and check if there were history effects on the membrane performance.

In all experiments, samples of retentate and permeate were taken at regular intervals. Peptide concentration was analyzed by HPLC measurements, and TFA-H concentration was measured by ion chromatography. The permeate was collected in a graduated cylinder to monitor the flux.

7.2.2 Methods

Describing equations for the filtration processes

The schematic representation of membrane filtration setting is shown in Figure 7.4.

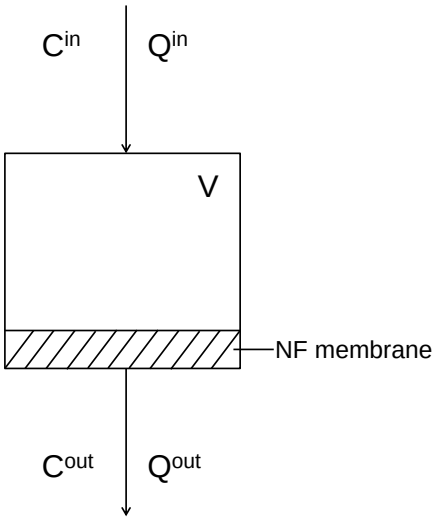


Figure 7.4: Schematic representation of filtration process.

The mass balance for the species i is given by Equation 7.1:

$$\frac{dm_i}{dt} = Q^{in}c_i^{in} - Q^{out}c_i^{out} \tag{7.1}$$

where c_i^{in} and c_i^{out} are the concentration of i entering and exiting the retentate loop, respectively. Q^{in} and Q^{out} are the inlet and outlet flows, respectively. By introducing $c_i^{out} = (1 - Rej_i)c_i$, where c_i is the concentration inside the retentate loop and the rejection, Rej_i, was introduced in Equation 2.1, and by developing the derivative for $m_i = c_i$ V, Equation 7.1 becomes:

$$V\frac{dc_i}{dt} + c_i\frac{dV}{dt} = Q^{in}c_i^{in} - Q^{out}(1 - rej_i)c_i \tag{7.2}$$

The mass balance for the volume is:

$$\frac{dV}{dt} = -Q^{out} \tag{7.3}$$

Equations 7.2 and 7.3 have to be solved together with the following initial conditions: $c_i(0) = c_i^0$ and $V_i(0) = V^0$.

In the case of concentration processes, $Q^{in} = 0$ and a combination of Equations 7.2 and 7.3 results in Equation 7.4:

$$\frac{dc_i}{dt} = \frac{1}{V(t)} Q^{out} rej_i c_i \tag{7.4}$$

For the case of the constant volume diafiltration mode, V = cost. and $Q^{in} = Q^{out} = Q$. Equation 7.2 becomes therefore:

$$\frac{dc_i}{dt} = \frac{Q}{V}[c_i^{in} - (1 - rej_i)c_i] \tag{7.5}$$

7.3 Results and discussion

7.3.1 Numerical optimization of DoE models

DoE analysis provided polynomial models for the response of interest, which are suitable to solve optimization problems (cf. Chapter 6). The process optimization for the filtration of PEP_1 in TFA-H/ACN/water mixtures has been carried out by the software Design Expert 7.0.3. The selected optimization criteria were the maximization of flux and PEP_1 rejection. The best set for the operating parameters and the corresponding responses are shown in Table 7.1.

The optimum conditions correspond to large values for PEP_1 concentration, %v TFA-H, pressure, pump frequency (i.e. cross-flow velocity) and %v ACN. At these conditions, almost complete PEP_1 rejection is obtained. TFA-H rejection of almost 20% occurs under these process conditions.

7.3.2 Diafiltration experiments and model validation

Models for PEP_1 rejection, flux and TFA-H rejection were derived by statistical analysis of experimental data (cf. Equations 6.2 and 6.4), in order to provide a phenomenological explanation for purely statistical formula and understand qualitatively how operating parameters affect the process. It was found that %v ACN and %v TFA-H positively affect

Table 7.1: Optimised set of operating parameters and corresponding responses.

Factor	Operating parameter / Response	Value
A	PEP_1 concentration [g l^{-1}]	5
B	%v TFA	0.1
C	Pressure [bar]	10
D	Pump frequency [Hz]	45
E	%v ACN / water	30
Response 1	PEP_1 rejection [%]	99.90
Response 2	Flux [l m^{-2} h^{-1}]	52.43
Response 3	TFA-H rejection [%]	19.68
Desirability [%]	-	99.70

both flux and PEP_1 rejection, and this is a general observation for all peptides that undergo association of ACN and TFA^- on their chain. The occurrence of TFA-H rejection was also observed.

The statistical models were inserted in the mathematical framework describing the diafiltration process (i.e. Equations 7.2 and 7.3) and the global filtration model validated on data obtained from constant volume diafiltration tests. Furthermore, the DoE models obtained at medium-low concentration (1 to 5 g l^{-1}) were tested on experimental diafiltration data at higher concentration (up to 17 g l^{-1}), to check extrapolation of the models up to this concentration values.

The operating path for the concentration + diafiltration sequence was shown in Figure 7.3. Pre-concentration at point a was followed by five diafiltration tests, and namely, a $\rightarrow$ b, b $\rightarrow$ c, c $\rightarrow$ d, d $\rightarrow$ e and e $\rightarrow$ b (cf. Figure 7.3). Eight diafiltration volumes were used for each test. The resulting effective path was different than the expected one (cf. Figure 7.5 vs. Figure 7.3), due to the occurrence of TFA-H rejection. As is clear from Figure 7.5, after eight diafiltration volumes, the final points for each test were shifted towards larger

TFA-H concentrations.

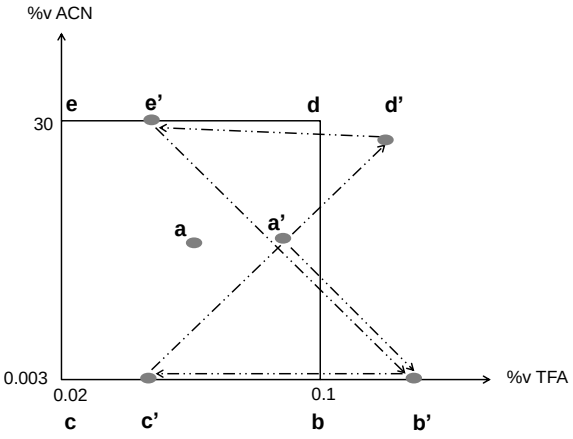
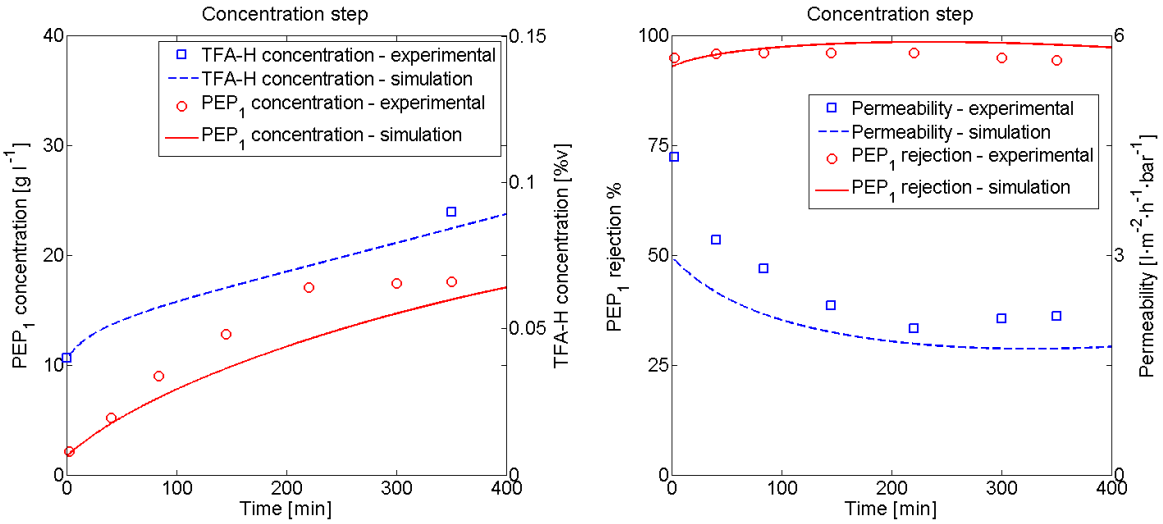


Figure 7.5: Actual concentration + diafiltration sequence, due to TFA-H rejection.

During pre-concentration at point a, the solution initially of 0.05%v TFA-H and 15%v ACN ended up as of 0.085%v TFA-H and 15%v ACN (rejection of ACN was zero). PEP_1 and TFA-H concentrations, rejection and solvent permeability for step A $\rightarrow$ A' are plotted vs. operating time in Figures 7.6(a-b). Simulations by solving Equations 7.2 and 7.3 including time-dependent flux and rejections (cf. Equations 6.4, 6.3 and 6.7) are also shown in the same graphs.

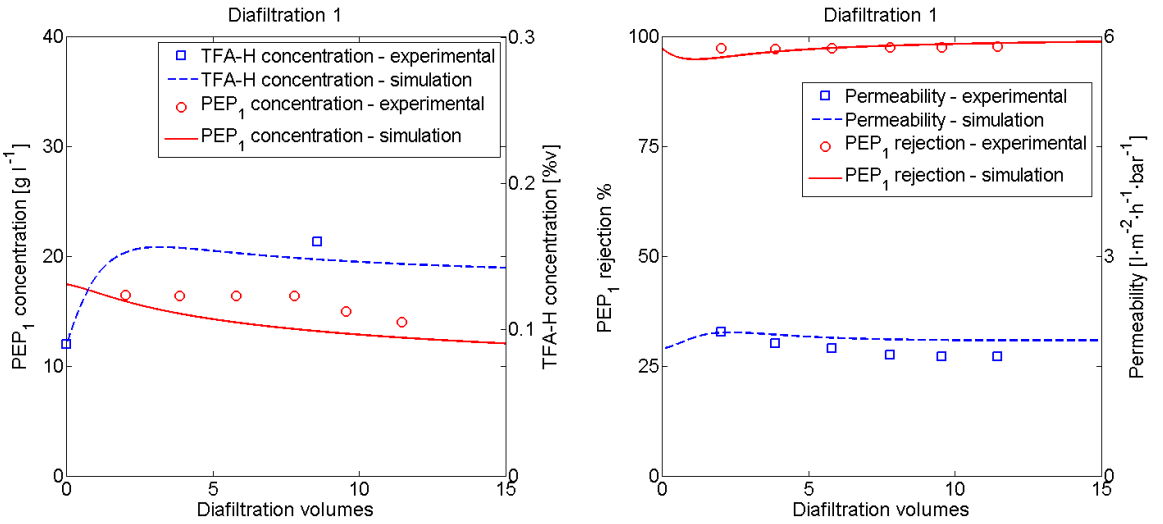
Both PEP_1 and TFA-H concentration increase with time (cf. Figure 7.6(a)), since they are both rejected by the membrane. Simulation of the concentration profiles using DoE models are satisfactory. PEP_1 rejection is large and almost constant with time. Permeability decreases with time and reaches a steady state value (cf. Figure 7.6(b)). Experimental permeability is slightly larger than the predicted values, but the trend over time is reproduced. The difference between actual and predicted flux values could be attributed to the error caused by the extrapolation of the DoE models outside the operating range.

The experimental profiles of the five diafiltration tests are shown in Figures 7.7 -7.11. PEP_1 and TFA-H concentration, PEP_1 rejection and solvent permeability are plotted vs. diafiltration volumes. Simulations by solving Equations 7.2 and 7.3 with time-dependent flux and rejections (cf. Equations 6.4, 6.3 and 6.7) are also shown on the same graphs.



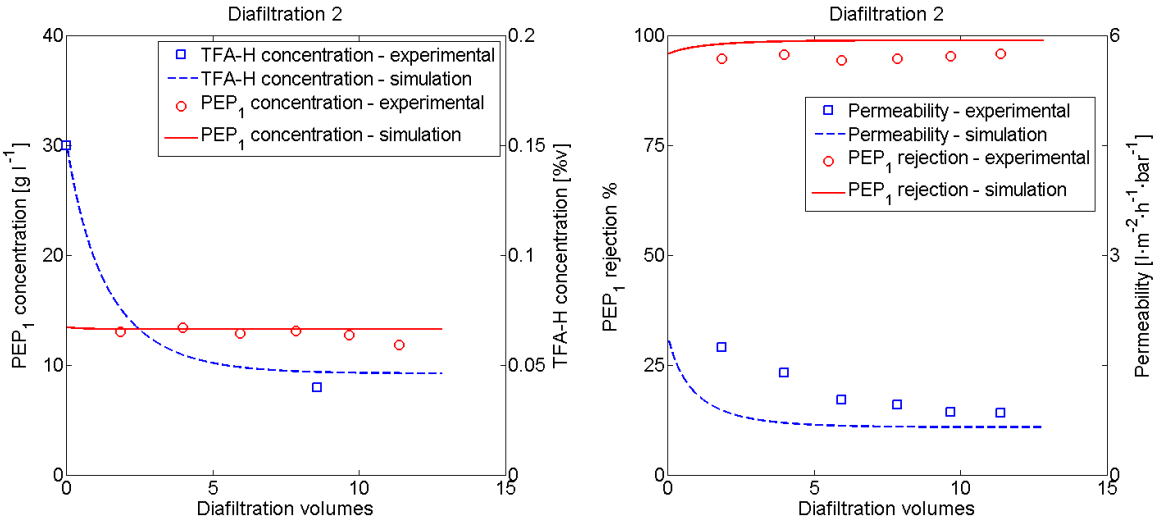
(a) (b)

Figure 7.6: Concentration step (A → A') for PEP_1 through Inopor Nano 750 Da. P = 8 bar.



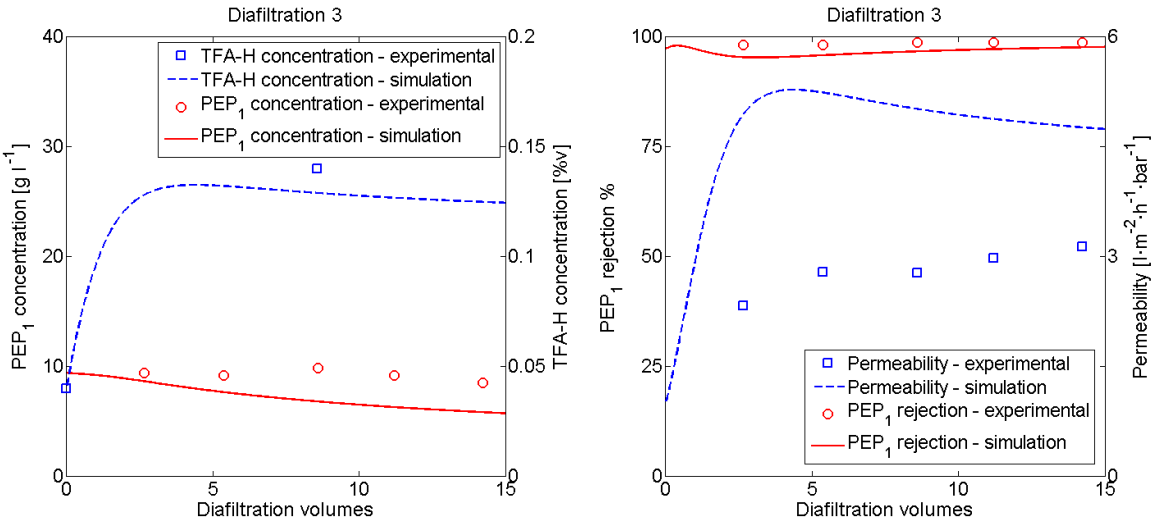
(a) (b)

Figure 7.7: Diafiltration 1 (a' → b') for PEP_1 through Inopor Nano 750 Da. P = 8 bar.



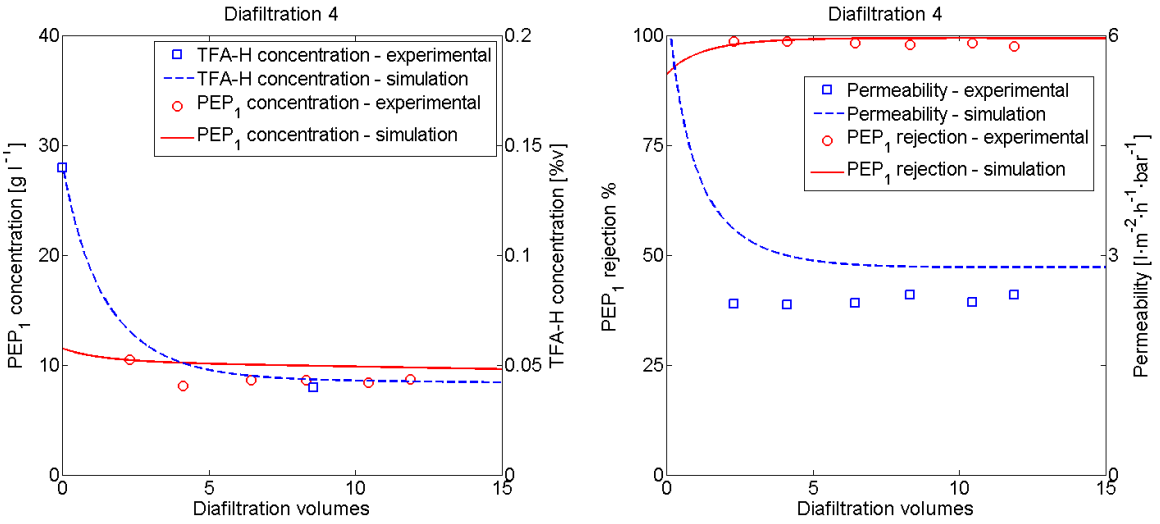
(a) (b)

Figure 7.8: Diafiltration 2 (b' → c') for PEP_1 through Inopor Nano 750 Da. P = 8 bar.



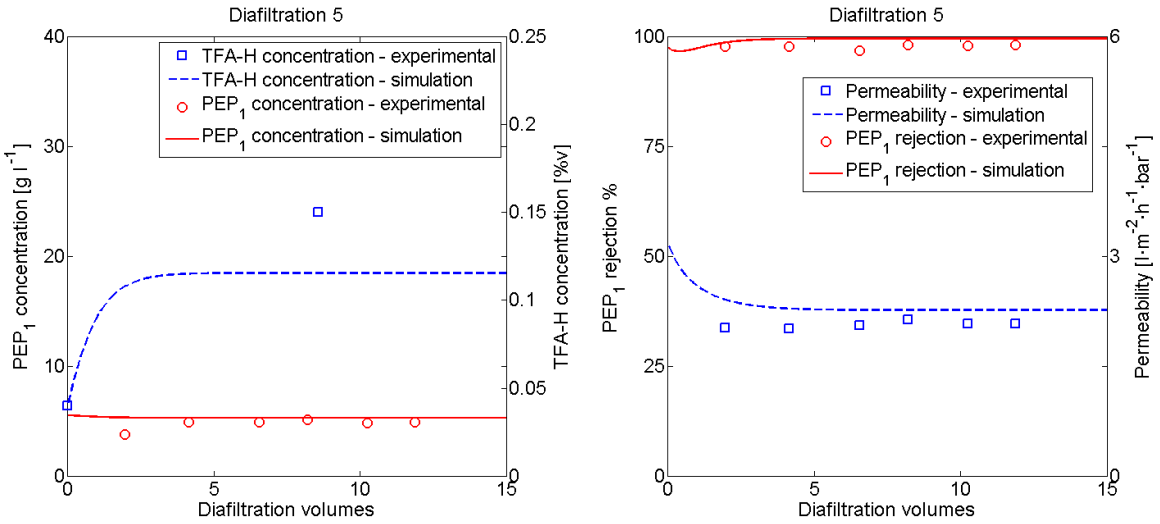
(a) (b)

Figure 7.9: Diafiltration 3 (c' → d') for PEP_1 through Inopor Nano 750 Da. P = 8 bar.



(a) (b)

Figure 7.10: Diafiltration 4 (d' → e') for PEP_1 through Inopor Nano 750 Da. $P = 8$ bar.



(a) (b)

Figure 7.11: Diafiltration 5 (e' → b') for PEP_1 through Inopor Nano 750 Da. $P = 8$ bar.

During the first diafiltration test (a' → b'; cf. Figure 7.7(a-b)), permeability does not change significantly. PEP_1 concentration slighlty decreases over time, as peptide rejection is not complete. TFA-H concentration increases up to 0.15 %v. In the second step (b' → c'; cf. Figure 7.8(a-b)), PEP_1 rejection is slightly overestimated, and this could be due to the extrapolation of the model to peptide concentration values larger than those used in the DoE. Outside the experimental range, peptide rejection is expected to increase, since peptide concentration has a positive effect on it (cf. Equation 6.2). Permeability, PEP_1 and TFA-H concentration are satisfactorily simulated. In the third step (c' → d'; cf. Figure 7.9(a-b)), permeability is overestimated. This could be due to overestimation of the interaction between %v TFA-H and %v ACN (B-E) in the mixture. Rejection, PEP_1 and TFA-H concentration are satisfactorily simulated. In the fourth and fifth steps (d' → e' and e' → b'; cf. Figures 7.10(a-b) and 7.11(a-b), respectively), simulations are in agreement with the experimental data. It is interesting to note that flux and PEP_1 rejection are similar for the first and the fifth runs (which were done under the same operating conditions), even if the actual peptide concentration was lower for the fifth run than for the first one.

From this study, it can be concluded that modelling dynamic evolution of diafiltration processes by including DoE models for flux and rejection gives reliable results. Extrapolation to high peptide concentration values, outside the experimental range, and overestimation of the interaction between %v TFA-H and %v ACN (B-E) could lead to errors in predicting the actual rejection and permeability values, however the profiles over time are well reproduced.

The experimental results at the end of each diafiltration test (i.e. corresponding to marked points in Figure 7.5) are reported in Table 7.2.

It is clear from Table 7.2 that the higher peptide rejection and permeability were obtained when performing the third diafiltration (c' → d'), which ends with large %v ACN and %v TFA-H values (point d' in Table 7.2). This is in agreement with previous observations from DoE results.

Table 7.2: Rejection and permeability at the end of each diafiltration test.

Point	**%v ACN**	**%v TFA**	**Rej**$_{PEP_1}$ [%]	**Permeability** [l m^{-2} h^{-1} bar^{-1}]
A'	15	0.09	-	-
B'	0	0.15	97.84	1.62
C'	0	0.04	96.03	0.84
D'	30	0.14	98.88	2.51
E'	30	0.04	98.32	2.46

7.3.3 Extension of results from looser (Inopor Nano 750) to tighter membrane (Inopor Nano 450)

The best operating conditions found for Inopor® Nano 750 (i.e. point d' in Table 7.2) were tested for a tighter ceramic membrane, Inopor® Nano 450. The comparison is shown in Table 7.3.

Table 7.3: Effect of pore dimension. C_{PEP_1} = 17.5 g l^{-1}; P = 8 bar; Pump frequency = 35 Hz; %v ACN = 30; %v TFA = 0.1.

Membrane	**Rej**$_{PEP_1}$ [%]	**Permeability** [l m^{-2} h^{-1} bar^{-1}]
Inopor® Nano 450	99.99	2.30
Inopor® Nano 750	98.88	2.51

It was found that rejection increased to almost 99.99% for the tighter membrane, while the flux decreased only of the 10%, compared to that of the looser membrane. This was attributed to an almost negligible effect of the pore dimension on the flux at such high

peptide concentrations, probably due to occurrence of concentration polarization. For this reason, in the following simulation section, the DoE model for solvent permeation (cf. Equation 6.5) was assumed valid for both membranes. Complete rejection was adopted to simulate the Inopor® Nano 450.

7.3.4 Simulation and process selection

Constant volume diafiltration

It has been shown in the previous section that the mathematical model for diafiltration with time-dependent rejection and permeability (obtained from statistical DoE analysis) is suitable to describe dynamic diafiltration conditions. The aim of this section is to carry out process modelling to find the best way to perform the desired diafiltration for PEP_1, i.e. salt + solvent exchange from point D to point C in Figure 7.3.

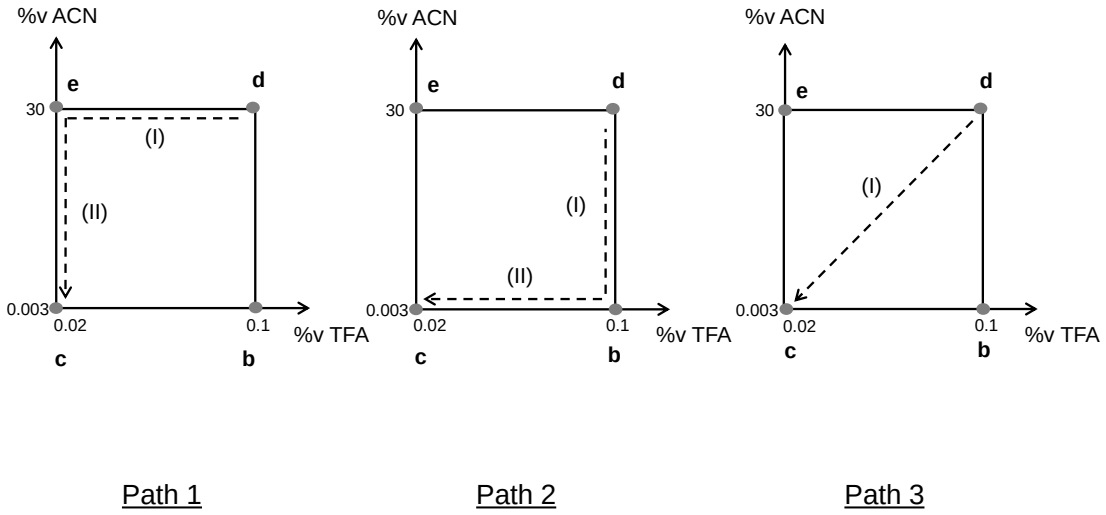


Figure 7.12: Possible diafiltration paths for salt and solvent exchange.

Three diafiltration paths were compared (cf. Figure 7.12):

(1) salt exchange (0.1 → 0.02%v TFA-H) at 30%v ACN and then solvent exchange (30 → 0.003%v ACN) at 0.02%v TFA-H (cf. Path 1 in Figure 7.12);

(2) solvent exchange (30 → 0.003%v ACN) at 0.1%v TFA-H and then salt exchange (0.1 → 0.02%v TFA-H) at 0.003%v ACN (cf. Path 2 in Figure 7.12);

(3) combined salt+solvent exchange (30 → 0.003%v ACN and 0.1 → 0.02%v TFA-H) (cf. Path 3 in Figure 7.12).

The three diafiltration paths were compared in terms of operating time, required diafiltration volumes and required amount of organic solvent (ACN). Starting peptide concentration was set at 15 g l^{-1}.

The simulation for Inopor® Nano 750 (using Equations 6.2 and 6.4 for peptide rejection and solvent flux, respectively) is reported in Table 7.4.

Table 7.4: Simulation of constant volume diafiltration for Inopor Nano 750. V = 1 l; C_{PEP_1} = 15 g l^{-1}.

Path	**From → to (%v ACN / %v TFA-H)**	**Diafiltration volumes**	**Operating time [min]**	$\mathbf{l}_{ACN}/\mathbf{l}_{feed}$	$\mathbf{C}^{fin}_{PEP_1}/\mathbf{C}^{in}_{PEP_1}$
1(I)	30 / 0.1 → 30 / 0.02	5	1011	1.5	0.95
1(II)	30 / 0.02 → 0.003 / 0.02	10	3857	0	∼ 1
2(I)	30 / 0.1 → 0.003 / 0.1	10	741	0	0.73
2(II)	0.003 / 0.1 → 0.003 / 0.02	5	1186	0	0.99
3(I)	30 / 0.1 → 0.003 / 0.02	10	3014	0	0.97

It is clear from Table 7.4 that solvent exchange requires less diafiltration volumes (DV = 10), compared to salt exchange (DV = 5). Total operating times are: 4868 min for path 1 (sum of times for 1(a) and 1(b), respectively), 1927 min for path 2 (sum of times for 2(a) and 2(b), respectively) and 3014 min for path 3. Path 2 is therefore the best one from the point of view of operating time. Path 1 requires additional ACN to perform the

diafiltration, while paths 2 and 3 do not, as they are performed by adding fresh water as a diluant. Solvent exchange during path 2(a) causes significant product loss in the system ($C^{fin}_{PEP_1}/C^{in}_{PEP_1} < 1$), due to partial rejection of the peptide. Path 3 is the best one to avoid product loss during the diafiltration.

Simulation by accounting for complete rejection (as for the case of Inopor® Nano 450) in the system gives comparable results in terms of operating time and diafiltration volumes. This is shown in Table 7.5.

Table 7.5: Simulation of constant volume diafiltration for Inopor Nano 450. V = 1 l; C_{PEP_1} = 15 g l^{-1}.

Run	**From → to (%v ACN / %v TFA-H)**	**DF volumes**	**Operating time [min]**	**l_{ACN} / l_{feed}**
1(a)	30 / 0.1 → 30 / 0.02	5	1179	1.5
1(b)	30 / 0.02 → 0.003 / 0.02	10	3857	0
2(a)	30 / 0.1 → 0.003 / 0.1	10	740	0
2(b)	0.003 / 0.1 → 0.003 / 0.02	5	1187	0
3	30 / 0.1 → 0.003 / 0.02	10	3145	0

By using the Inopor® Nano 450, it is possible to avoid the problem of product loss and to maintain at the same time similar flux performances. Path 2 is finally the most efficient path for the desired diafiltration.

Constant volume vs. variable volume diafiltration

The role of nanofiltration between chromatography and lyophilization in the downstream of PEP_1 is to concentrate the solution up to the desired value (normally given by solubility or stability limits) and reduce the amount of TFA-H and ACN in the solvent mixture (i.e. concentration + salt/solvent exchange). The two possible approaches to combine concentration and diafiltration are: (i) pre-concentration followed by constant volume diafiltration,

which was studied in the previous paragraph; (ii) variable volume diafiltration. These two strategies are compared in this paragraph.

Simulations were done, assuming a starting solution of 5 l and 5 g l^{-1} and a final desired solution of 15 g l^{-1}. Pressure was set at 8 bar. Complete peptide rejection, time-dependent solvent flux and TFA-H rejection (cf. Equations 6.4 and 6.6), and the suitable mass balance for the diafiltration (cf. Paragraph 7.2.2) were used. Comparison of the two approaches in terms of operating time is shown in Table 7.6.

Table 7.6: Operating time [min] for constant volume and variable volume diafiltration.

Step	**Constant volume diafiltration**	**Variable volume diafiltration**
Pre-concentration	126	-
Solvent exchange (d → b)	696	1425
Salt exchange (b → c)	1273	1243
Total (d → c)	2095	2668

Operating time required for pre-concentration followed by constant volume diafiltration (approach (i)) is less than that required for performing variable volume diafiltration (approach (ii)). Approach (i) has been therefore selected as best diafiltration process to perform the salt and solvent exchange of interest.

7.4 Conclusion

In this chapter, the Quality by Design concept and Design of Experiments have been applied to investigate the nanofiltration of a model peptide (PEP_1) in TFA-H/ACN/water mixtures through ceramic NF membranes. Nanofiltration was used to perform concentration and salt/solvent exchange for this peptide, as part of the downstream process between the

preparative chromatography and the lyophilization.

Statistical models for peptide rejection, flux and salt (TFA-H) rejection were obtained as a function of several operating parameters, by Design of Experiments and Analysis of Variance. The design space was selected in terms of composition of the mixture (peptide, TFA-H and ACN/water concentrations), pressure and cross-flow velocity over the membrane surface. Phenomenological interpretation of the purely statistical models was provided, in order to qualitatively understand the transport mechanism through the membrane. The best operating conditions for concentration and diafiltration (high flux and high peptide rejection) were found to correspond to high %v ACN and high %v TFA-H. This was attributed to the increase of the peptide hydrophobicity with the association of ACN molecules and TFA^- counter-ions on the peptide chain. This association dimishes the affinity of the peptide with the membrane and causes in turn stronger exclusion of the peptide from the membrane, and less friction through the pore.

The statistical models from DoE were included in the mathematical framework of diafiltration processes, to obtain the evolution of peptide, counter-ion (TFA^-) and solvent (ACN) concentrations in the system. Process modelling by including time-dependent rejection and permeability was validated on experimental data for diafiltration at concentration values larger than that used for DoE. The model combining a dynamic mass balance for diafiltration with time-dependent rejection and permeability was used to simulate different possible constant volume diafiltration paths to perform the salt and solvent exchanges of interest. Preconcentration followed by constant volume diafiltration was compared to variable volume diafiltration, in terms of operating time and solvent consumption. For the case study in this work, the former strategy (i.e. preconcentration + constant volume diafiltration) was identified as the best one.

In conclusion, this work discusses a general procedure for investigating nanofiltration for peptide concentration and diafiltration under the QbD concept. Experimental investigation by DoE allows process understanding, modelling, and optimization, and this knowledge can be applied to perform process selection, all at the expense of a limited number of experimental data.

Chapter 8

Case-study 2: Reactive Peptide Nanofiltration

8.1 Introduction

Peptide therapeutics produced by chemical synthesis represent an important class of Active Pharmaceutical Ingredients (APIs), manufactured at large scale. Long-chain peptide therapeutics are often synthesised in batch reactors, by fragment condensation of shorter chains, pre-synthesised by solution-phase or solid-phase techniques. The chemical syntheses by fragment condensation, implemented in organic solvents or aqueous-organic mixtures, often require large reaction times and subsequent precipitation of reaction mixtures to isolate the target compound from the side products and the reagents in excess, leading to discontinuous processes. Conventional organic solvent-based fragment condensations may furthermore suffer from: (i) presence of poorly soluble compounds that can precipitate or demix; (ii) high organic solvent consumption; (iii) deleterious side reactions; and (iv) poor yield of the desired product. The integration of membrane separation techniques into the reaction step can help in addressing these problems.

In this chapter, a fragment condensation model reaction is presented and discussed. The reaction between the protected sulfur atom of one fragment and the unprotected sulfur atom of the other occurs via nucleophilic attack, with the release of the protecting molecule,

as a side-product of the condensation. This side product is deleterious as its presence in the reaction mixture causes side reactions and phase separation.

This model synthesis is improved by integrating membrane technology into the reaction step, in the so-called Reactive Peptide Nanofiltration scheme. The Reactive Peptide Nanofiltration strategy is based on the separation of small side products from the reaction mixture, the recycle of the solvent after the nanofiltration, and the elimination of time-consuming steps (i.e. precipitation and drying), typical of the conventional strategy. The performance of the new strategy is compared to the conventional batch process by means of a techno-economical analysis. Shorter production time and lower solvent consumption characterise this scheme, with evident advantages from technological, economical and environmental point of view.

8.2 Fragment condensation by disulfide bond

The case study presented in this work concerns the chemical synthesis of a therapeutic peptide (P3), produced by fragment condensation of two pre-synthesised peptides (P1-SH and P2-S-SM, respectively). The reaction of fragment condensation occurs via disulfide bond, with the release of a small molecule, SM, which is originally the protecting group of the S atom of P2-S-SM. The reaction is shown in Eq. 8.1:

$$P1 - SH + P2 - S - SM \rightarrow P3 + SM \tag{8.1}$$

P1-SH and P2-S-SM are composed of almost the same number of amino acids but differ significantly in their hydrophilic/phobic properties. The physico-chemical properties of the species involved in the reaction are reported in Table 8.1.

8.2.1 Conventional production

The conventional production of P3 is composed of three main steps:

- batch reaction between P1-SH and P2-S-SM in organic solvent (ACN or THF)/water mixture;

Table 8.1: Physico-chemical properties for the species involved in the reaction.

Molecule	MW [Da]	pI	Hydrophilic / Hydrophobic	Water solubility
P1-SH	2700	12	Hydrophilic	> 30 g l^{-1}
P2-S-SM	1500	4	Hydrophobic	< 0.1 g l^{-1}
P3	4050	11	Hydrophilic	> 30 g l^{-1}
SM	150	3.5	-	n/a

- precipitation in 90%v ACN/water, followed by drying and re-solubilization in 10%v ACN/water;

- final purification by preparative chromatography.

The scheme for the conventional production is shown in Figure 8.1.

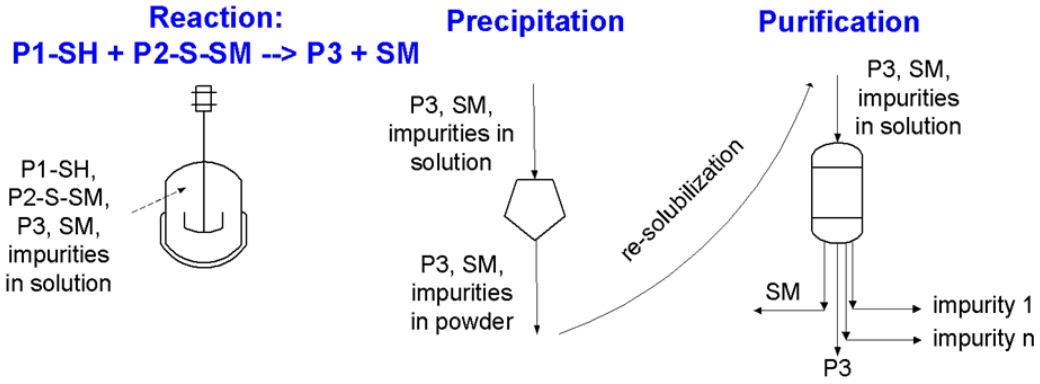


Figure 8.1: Conventional process for the production of P3.

The main issues concerning this scheme are: (1) the small molecule, SM, is continuously produced during the reaction and its presence in the mixture causes secondary reactions; (2) high content of organic solvent is needed in the reactor to solubilise P2-S-SM (hydrophobic) and to avoid its phase separation; (3) the process is overall discontinuous, with time-

consuming intermediate steps, such as precipitation, drying and re-solubilization.

8.2.2 Reactive Peptide Nanofiltration

An alternative approach to the production of P3 is proposed in this work. The scheme is named Reactive Peptide Nanofiltration, as it is based on the coupling between reaction and nanofiltration in one unique scheme, as shown in Figure 8.2.

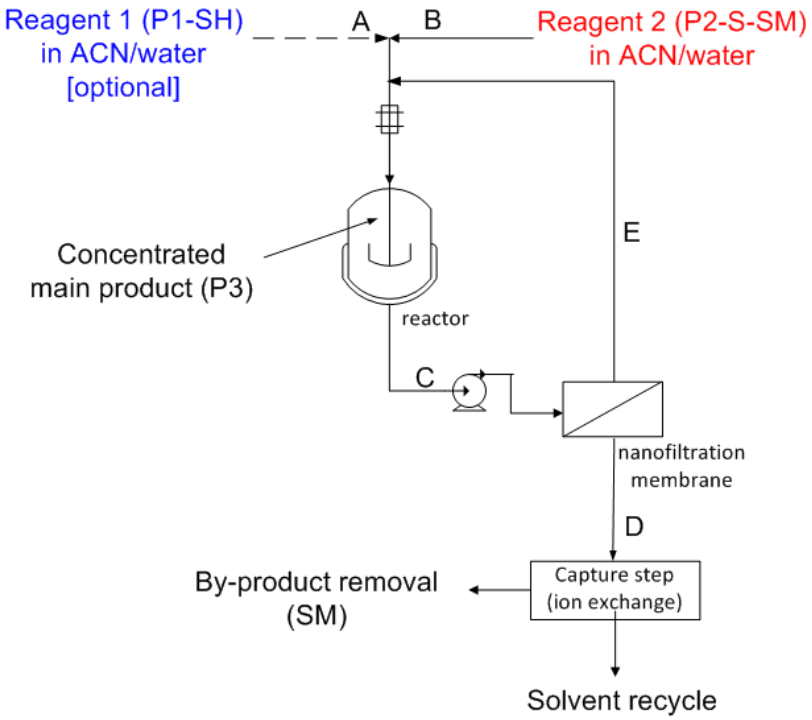


Figure 8.2: Reactive Peptide Nanofiltration for the synthesis of P3.

The process works in semi-batch mode: P1-SH (the hydrophilic reagent) is loaded into the reactor in 10%v ACN/water and P2-S-SM (the hydrophobic reagent) is slowly added by diluted stream B. The reaction mixture is pumped afterwards to the nanofiltration membrane, which separates the small molecules from the three peptides. SM permeates through the membrane in stream D, due to its small size, while P1-SH, P2-S-SM and P3 are completely retained in stream E. SM is finally captured from stream D by an ion exchange resin, in order to allow for solvent recycling. Alternatively to the semi-batch mode, it is possible to operate the system in continuous mode, by continuously adding P1 to the

reactor by stream A.

The advantages of this scheme are:

(1) SM is continuously removed by the membrane, thus minimizing secondary reactions;

(2) the organic content in the reactor can be low, since the hydrophobic reagent, P2-S-SM, is added slowly and diluted;

(3) the outgoing reaction mixture can be directly injected into the preparative chromatography for the final purification, without requiring solvent exchange (10 - 20%v ACN/water);

(4) time consuming steps, such as precipitation, drying and resolubilization, are not required.

(5) the amount of organic solvent required for the whole process is lower than for the conventional process, with consistent economical and environmental benefits.

8.3 Experimental

8.3.1 Materials

P1-SH and P2-S-SM were synthesised by solid-phase chain elongation and purified by preparative chromatography. P3 used in the feasibility experiments was produced by fragment condensation of P1-SH and P2-S-SM in liquid-phase, according to the conventional strategy (cf. Paragraph 8.2.1). Pure SM was purchased from Bionet. The physico-chemical properties of the species are reported in Table 8.1.

The solvents used in this study were distilled water and ACN. THF was additionally used for testing the reaction kinetics. The cross-flow filtration system used in this study contained a tubular module, suitable for multichannel tubular membranes with a length of 250 mm and an outer diameter of 25 mm. Two commercial ceramic membranes were used in this study, with the same different active layer, TiO_2 on Al_2O_3 and different MWCOs. They were prepared by Inopor (Germany) under the commercial names of Inopor® Nano 750 Da and Inopor® Nano 450 Da. All the membranes had 19 channels with an internal diameter of 3.5 mm and filtration area of 516 cm^2. The MWCO values and the nominal pore dimensions of the active top layer were measured by the manufacturer. The nominal

properties of the membranes were summarised in Table 4.3.

8.3.2 Methods

Reaction tests

The reaction kinetics of the fragment condensation between P1-SH and P2-S-SM were studied under batch conditions. Solutions of P1-SH and P2-S-SM of different concentrations were prepared and mixed together. The consumption rate of the reagents and the production rate of the products were monitored at regular intervals by means of HPLC analysis. Three different concentration of ACN/water (10%v, 30%v and 50%v), two different temperatures (10 and 20°C) and the effect of the solvent (ACN vs. THF) were investigated.

Rejection tests for membrane selection

Solutions of pure P1-SH, P2-S-SM, P3 and SM in ACN/water mixtures were prepared and their rejection and permeation tested in a Natan cross-flow system (Natan GmbH, CH; cf. Figure 3.2).

%v ACN/water between 20 and 40 and pH between 2 and 4 were investigated. TFA-H was used to set the pH. Samples of retentate and permeate were taken at regular intervals, the permeate collected in a graduated cylinder and the flux monitored. Each test was repeated at least two times, and the values of rejection and flux averaged (the error was always less than 10%). Rejection and permeation tests of pure substances were used to choose the best membrane to perform the separations of interest, and the membrane with the highest rejection of P1-SH, P2-S-SM and P3 and the lowest rejection of SM was chosen.

Reactive Peptide Nanofiltration feasibility

The feasibility of the Reactive Peptide Nanofiltration scheme was tested in the Natan cross-flow system in semi-batch configuration (cf. Figure 8.2). To check the effect of pH, simultaneous loading of both reagents was adopted. Solutions of P1-SH and P2-S-SM were prepared in ACN/water mixtures of different compositions and mixed together. The

reaction mixture was immediately loaded into the reaction loop (tank and nanofiltration chamber) and the NF started. The operating pressure was set at 8 bar.

To check the effects of reagent concentration and organic content, separate loading of reagents was adopted. Solutions of P1-SH and P2-S-SM were prepared in ACN/water mixtures of different composition. The solution of P1-SH was loaded in the reaction loop (tank and nanofiltration chamber) and the solution of P2-S-SM was put in an external tank. P2-S-SM was added slowly to the reaction loop, at the same velocity at which the permeate was collected in the cylinder. The operating pressure was set at 5 bar.

For both cases of simultaneous and separated loading of reagents, the temperature was fixed at 19 ± 2°C. Samples of retentate and permeate were collected at different time points, to monitor the evolution of the reaction, and the permeate collected in a graduated cylinder, to monitor the flux decline.

Model equations for the system

Both conventional process and Reactive Peptide Nanofiltration were described with model equations. The conventional process was described by the mass balance for batch reactor. The reaction rate for the species i was given by:

$$\frac{dc_i}{dt} = R_i \tag{8.2}$$

C_i is the concentration of the species ($c_i = m_i/V$, where V is the reactor volume) and R_i the reaction rate ($R_i = \nu_i r$, where ν_i is the stoichiometric coefficient of species i and r is the reaction rate).

The Reactive Peptide Nanofiltration was described by the mass balance for a semi-batch reactor. The derivative of the concentration in time for the species i was given by Equation 8.3:

$$\frac{dc_i}{dt} = Q^{in}c_i^{in} - Q^{out}c_i^{out} + R_i \tag{8.3}$$

Q_{in} and Q_{out} are the inlet and outlet volumetric flows for the semi-batch reactor, respectively. When P1-SH and P2-S-SM were loaded together into the reaction loop, no

external stream was subsequently provided and Q_{in} was set to zero. In the case of Reactive Peptide Nanofiltration, outlet flow Q_{out} is representative of the permeation rate thorugh the membrane.

Kinetic constants, volumetric flow and rejection were generally a function of the operating parameters:

$$k_r = k_r\left(c_i, pH, \%vACN/water\right) \tag{8.4}$$

$$Q^{in} = Q^{in}\left(c_i, pH, \%vACN/water\right) \tag{8.5}$$

$$rej = rej\left(c_i, pH, \%vACN/water\right) \tag{8.6}$$

Detail about the reaction kinetics will be provided in Paragraph 8.4.1, while considerations about the effects of operating parameters on flux and rejection will be discussed in Paragraph 8.4.3.

8.4 Results and discussion

8.4.1 Reaction kinetics

Kinetic scheme

The main reaction, represented by Equation 8.1, is composed of the three following steps:

$$P1 - SH \underset{k_{1,i}}{\overset{k_{1,d}}{\rightleftharpoons}} P1 - S^- + H^+ \tag{8.7}$$

$$P1 - S^- + P2 - S - SM \xrightarrow{k_{2,d}} P3 + SM^- \tag{8.8}$$

$$SM^- + H^+ \underset{k_{3,i}}{\overset{k_{3,d}}{\rightleftharpoons}} SM \tag{8.9}$$

Equations 8.7 and 8.9 are reactions at equilibrium. Their equilibrium constants are:

$$K_{1,a} = \frac{k_{1,d}}{k_{1,i}} \tag{8.10}$$

$$K_{3,a} = \frac{k_{3,d}}{k_{3,i}} \tag{8.11}$$

Equation 8.8 is an irreversible reaction, with P3 = P1-S-S-P2.

The reaction rate for reaction 8.1 is:

$$r_{main} = k_{2,d}\frac{K_{1,a}}{c_{H^+}}c_{P1-SH}c_{P2-S-SM} = k_{main}c_{P1-SH}c_{P2-S-SM} \tag{8.12}$$

k_{main}, the kinetic constant of the main reaction, is function of the acid-base equilibrium for P1-SH ($K_{1,a}$), the velocity of the nucleophile attack ($k_{2,d}$) and the pH (c_{H+}). The two main side reactions identified in this process are the permutation of SM from P2-S-SM to P1-SH (Equation 8.13) and the dimerization of P2-S-SM (Equation 8.14):

$$P1 - SH + SM \xrightarrow{k_{perm}} P1 - S - SM \tag{8.13}$$

$$P2 - S - SM + P3 \xrightarrow{k_{dim}} P1 - S - SM + P2 - S - S - P2 \tag{8.14}$$

For both side reactions 8.13 and 8.14, the same kinetic mechanism was considered as for the main reaction (i.e. nucleophile attack). The reaction rates proposed for the side reactions are therefore:

$$r_{perm} = k_{perm}c_{P1-SH}c_{SM} \tag{8.15}$$

$$r_{dim} = k_{dim}c_{P2-S-SM}c_{P3} \tag{8.16}$$

8.4.2 Calculation of kinetic constants

Solutions of P1-SH + SM and P2-S-SM + P3 were prepared and the variation of the concentration monitored during time, to test secondary reactions 8.13 and 8.14, respectively.

The kinetic constants of secondary reactions could not be obtained by fitting of experimental data, due to lack of pure material for the calibration of P1-S-SM and P2-S-S-P2. It was possible to observe, however, that secondary reaction 8.13 was negligible (from the almost negligible consumption of the reagents) and the consumption of P3 and P2-S-SM to give P2-S-S-P2 and P1-S-SM in secondary reaction and 8.14 was significantly slower in time, compared to the consumption rate of the same reagents during the main reaction. This means that k_{dim} was expected to be much smaller than k_{main}.

The variation of the concentration was monitored during time for solutions of P1-SH and P2-S-SM. The kinetic constants of reactions 8.1 and 8.14 were calculated from fitting of experimental profiles of P3 concentration vs. time.

The kinetic constant of the main reaction was a function of pH, as expected from Equation 8.12. Figure 8.3 shows the profiles of P3 for four different values of pH at constant concentrations of starting reagents (c_{P1-SH} = 1 mM and $C_{P2-S-SM}$ = 1 mM) in 50%v ACN/water. Kinetics that considered the occurrence of side reaction 8.14 (continuous line) described the experimental data better than kinetics that considered the main reaction only (dashed line). This observation allowed the fitting of k_{dim}, which was found to be 5 to 6 times slower than k_{main}.

For each profile, the corresponding k_{main} value was found. Figure 8.4 and fitting function 8.17 describe the variation of the kinetic constant with the pH.

$$k_{main}[\frac{l}{mol \cdot min}] = 0.0067 pH^{2.003} \tag{8.17}$$

The same dependency was extended to the range 10%v - 50%v ACN/ water, since no significant effect of the organic content on the reaction rate was found in this range, as shown in Table 8.2.

The kinetic constant of the main reaction was not significantly affected by temperature in the range 10 - 20°C (cf. Table 8.2). It was concluded that only the pH had a significant influence on the kinetics of the main reaction.

The production/consumption rates of all the species are described by Equations 8.18 - 8.21:

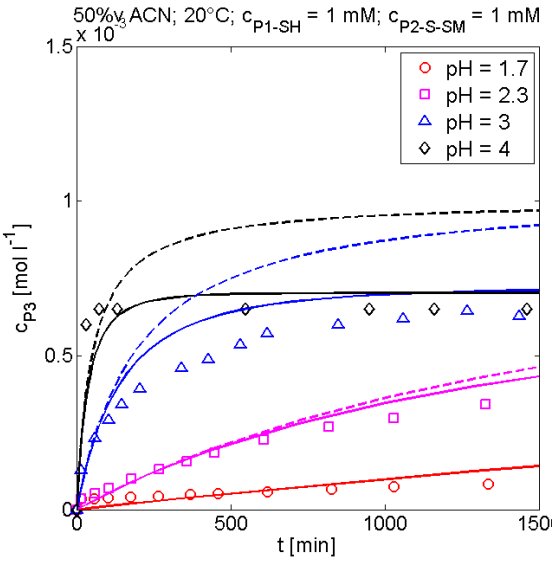


Figure 8.3: Batch production of P3 as function of pH. (o) experimental data; (–) complete kinetics; (- -) simplified kinetics.

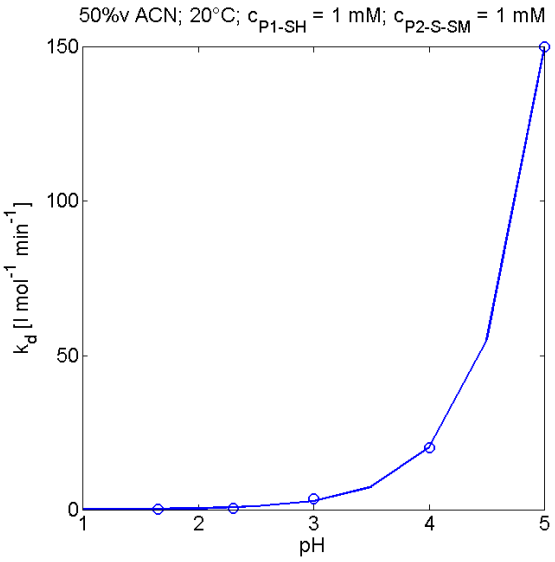


Figure 8.4: k_{main} as function of pH. (o) experimental data; (–) fitting function 8.17

Table 8.2: Kinetic constant as function of organic content and temperature (pH = 4).

$\mathbf{c}_{P1-SH}$ / $\mathbf{c}_{P2-S-SM}$	%v organic/water	T [°C]	k [l $\mathbf{mol}^{-1}$ min−1]
1 mM / 1 mM	50%v ACN	10	16
1 mM / 1 mM	50%v ACN	20	20
1 mM / 1 mM	50%v THF	10	19

$$\frac{dc_{P1-SH}}{dt} = -k_{main}c_{P1-SH}c_{P2-S-SM} - k_{perm}c_{P1-SH}c_{SM} \tag{8.18}$$

$$\frac{dc_{P2-S-SM}}{dt} = -k_{main}c_{P1-SH}c_{P2-S-SM} - k_{dim}c_{P3}c_{P2-S-SM} \tag{8.19}$$

$$\frac{dc_{P3}}{dt} = k_{main}c_{P1-SH}c_{P2-S-SM} - k_{dim}c_{P3}c_{P2-S-SM} \tag{8.20}$$

$$\frac{dc_{SM}}{dt} = k_{main}c_{P1-SH}c_{P2-S-SM} - k_{perm}c_{P1-SH}c_{SM} \tag{8.21}$$

8.4.3 Rejection tests for membrane selection

Ceramic membranes were chosen for this case study, due to the significant advantages they offer compared to polymeric membranes [4, 110] (cf. Chapter 2 for more details).

Two ceramic NF membranes were tested: Inopor® Nano 450 and Inopor® Nano 750, respectively. Rejection and flux for P1-SH, P2-S-SM, P3 and SM are reported in Tables 8.3, 8.4, 8.5 and 8.6, respectively.

Rejection and permeability of P1-SH in different operating conditions are reported in Table 8.3.

Rejections were always large for both membranes. A slight effect of pH was observed: at pH 3 and 4 the rejection was 96%, while at pH 2 the rejection was complete. This can be attributed to the larger steric dimension and hydrophobicity that the peptide has at

Table 8.3: Rejection of P1-SH in ACN/water solutions.

C_{P1-SH} [g l^{-1}]	%v ACN/water	pH	P [bar]	Membrane MWCO [Da]	Rej_{P1-SH} %	Permeability [l m^{-2} h^{-1} bar^{-1}]
1	20	2	3	750	99.0	30.5
1	30	2	3	750	99.2	31.0
1	30	3	3	750	96.1	30.9
1	30	4	3	750	95.9	29.0
1	40	2	3	750	100.0	27.5
1	30	2	3	450	100.0	9.5

lower pH (due to the association with more TFA^- anions). With the Inopor® Nano 450, the rejection was complete , but the permeability was lower, as expected from the smaller pore dimension of this membrane (last experiment in Table 8.3).

Rejection and permeability of P2-S-SM in different operating conditions are reported in Table 8.4.

An effect of the organic content on the rejection of P2-S-SM was found for both Inopor® Nano 450 and 750. The larger the %v ACN/water, the larger the rejection and the permeability, as observed from the DoE for P2-S-SM (cf. Chapter 6). pH between 2 and 3 did not affect significantly the peptide rejection. Rejection was larger and permeability lower for the Inopor® Nano 450, as observed for P1-SH.

It is worth noting that permeation fluxes are lower for P2-S-SM than for P1-SH, although P1-SH is bigger. This was explained by the higher friction experienced by the hydrophobic peptide in the hydrophilic membrane pore, compared to that experienced by the hydrophilic peptide, due to the difference in chemical affinity.

Rejection and permeability of P3 with the two NF membranes are reported in Table 7.

Rejection of P3 was large for both membranes, but in the case of Inopor® Nano 750 insufficient for the Reactive Peptide Nanofiltration: rejection of 95-97%, or in turn, perme-

Table 8.4: Rejection of P2-S-SM in ACN/water solutions.

$\mathbf{C}_{P2-S-SM}$ [g l^{-1}]	%v ACN/water	pH	P [bar]	Membrane MWCO [Da]	$\mathbf{Rej}_{P2-S-SM}$ %	Permeability [l m^{-2} h^{-1} bar^{-1}]
0.1	20	2	3	750	63.2	11.2
0.1	20	3	3	750	60.3	10.2
0.1	30	2	3	750	75.5	16.9
0.1	30	2	5	750	73.2	14.6
0.1	40	2	3	750	81.9	13.2
0.1	40	3	3	750	75.8	17.1
0.1	20	1.5	5	450	85.6	3.0
0.1	20	2	5	450	94.4	2.66
0.1	40	2	5	450	96.1	5.8
0.1	40	3	5	450	95.9	5.26

Table 8.5: Rejection of P3 in ACN/water solutions.

$\mathbf{C}_{P3}$ [g l^{-1}]	%v ACN/water	pH	P [bar]	Membrane MWCO [Da]	$\mathbf{Rej}_{P3}$ %	Permeability [l m^{-2} h^{-1} bar^{-1}]
1	30	3.5	3	750	97.1	6.6
1	30	3.5	6	750	97.3	7.9
2	30	3.5	3	750	95.2	3.2
6	30	3.5	10	450	99.8	1.5
2	10	2	5	450	99.9	2.8

ation of 3-5%, means too high product loss from the retentate loop. No significant effect of pressure on either flux or rejection was detected at constant concentration, while a slight effect of concentration was found at constant pressure: at higher concentration, both flux and rejection were slightly lower than at lower concentration. Rejection was almost complete with the Inopor® Nano 450, and not significantly influenced by concentration, pressure and organic solvent. This membrane was, therefore, suitable to perform the Reactive Peptide Nanofiltration.

It is interesting to note that the rejection of P3 was comparable with that of P1-SH under almost the same operating conditions (cf. Tables 8.3 and 8.5), although the MW of P3 was much larger. The retention mechanism, in fact, was influenced not only by the steric properties of the peptides, but also by the additional steric and hydrophobic properties caused by TFA^- anions. P3 and P1-SH can associate almost the same number of TFA^- anions (they possess an almost similar number of free sites available for adsorbing the salt). Since the contribution of P2-S-SM in terms of available adsorption sites is negligible, the presence of P2-S-SM did not influence the effect of the operating parameters on the retention mechanism of P3, and the behavior of P3 was similar to that of its hydrophilic fragment, P1-SH.

Rejection and permeability of SM with the two NF membranes are reported in Table 8. Concentration of 0.2 g l^{-1} was chosen as representative of the concentration of SM in the process.

Rejection of pure SM was always low for both membranes. No significant effect of pH was detected between pH 2 and 4. For the Inopor® Nano 450, it was observed that the rejection of SM increased and the permeability decreased with the increase of the organic content.

By comparing the data from Tables 8.3 - 8.6, it was concluded that Inopor® Nano 450 is the best membrane to perform the Reactive Peptide Nanofiltration. It provides complete rejection for P1-SH and P3, almost complete (96%) for P2-S-SM and null for SM. Inopor® Nano 750 shows larger fluxes, however rejections of P2-S-SM and P3 are not sufficiently high.

Table 8.6: Rejection of SM in ACN/water solutions.

C_{SM} [g l^{-1}]	%v ACN/water	pH	P [bar]	Membrane MWCO [Da]	Rej_{SM} %	Permeability [l m^{-2} h^{-1} bar^{-1}]
0.2	30	2	3	750	0.0	18.6
0.2	30	4	3	750	0.0	30.0
0.2	20	2	4	450	0.0	12.0
0.2	30	2	4	450	0.0	9.4
0.2	40	2	4	450	10.0	7.5
0.2	30	4	4	450	3.0	11.0

Choice of working conditions for the Reactive Peptide Nanofiltration

As discussed, reaction kinetics was found to be influenced by reagents concentration and pH, and not significantly influenced by organic content and temperature. Permeation rate through the Inopor® Nano 450 was found to be a function of peptide concentration, pH, pressure, cross-flow velocity and organic content (cf. Table 8.5 and Paragraph 5.3.2). The main observations from kinetic and permeation studies were combined together to find the best working conditions for the Reactive Peptide Nanofiltration.

The principal issue was the choice of the operating pH, which showed opposite effects on reaction and permeation: it had a positive effect on the reaction rate and a negative effect on permeation. At the desired working pH, both reaction and flux had to be sufficiently fast, in order to have high productivity. pH 4 was chosen as best compromise value.

Low organic content was advantageous for having high flux. Since the effect of the solvent on the reaction rate was negligible, 10%v ACN/water was chosen as reaction solvent. The great advantage of this choice was the possibility of exiting the Reactive Peptide Nanofiltration with a solution ready for the preparative chromatography and that minimises the solvent consumption.

The pump frequency positively affected the permeation flux and showed no significant effects on the peptide degradation. High values (45 Hz) were therefore preferred.

The concentration of P1-SH in the reactor was an adjustable parameter, while the concentration of P2-S-SM was limited by the solubility limit in 10%v ACN/water ($\leq$ 0.1 g_{crude} l^{-1}).

8.4.4 Reactive Peptide Nanofiltration feasibility

The Reactive Peptide Nanofiltration was studied in the Natan cross-flow NF system (cf. Figure 8.2) with the Inopor® Nano 450 in the range 10 - 50%v ACN/water. Firstly, the effect of pH was tested in semi-batch conditions, constant pressure (8 bar) and constant organic content (30%v ACN/water). In order to compare the occurrence of the reaction at constant pressure, simultaneous loading of P1-SH and P2-2-SM solutions was adopted. The effect of pH is shown in Figure 8.5(a-c).

It is evident that the reaction was slower at pH 2.5 than at pH 5, from both the profiles of P3 production and P2-S-SM consumption. In the case of pH = 2.5 (cf. Figure 8.5(a)), the concentration of SM increased more slowly than the concentration of P3, as expected from its lower rejection by the NF membrane. In contrast, for the case of pH = 5 (cf. Figure 8.5(b)), SM reached the maximum value after some minutes, and then started to decrease, when the reaction reached completion. Similar effects of pH were found for 10%v ACN/water (data not shown). The flux was larger at pH 2.5 than at pH 5 (cf. Figure 8.5(b)), as expected from the results of DoE (cf. Paragraph 5.3.2).

The effect of concentration was tested under semibatch conditions, with separate loading of reagents (cf. Paragraph 8.3.2 for experimental detail), at pH = 4. This test was meant to compare the reaction rate in the nanofiltration loop with that under batch conditions. Two different starting concentrations for P1-SH and P2-S-SM in 50%v ACN/water and two different solutions, 30 and 50%v ACN/water were tested. The profiles of SM, P2-S-SM and P3 at pH = 4 are reported in Figures 8.6(a-c).

The concentration of SM increased quickly at the beginning of the reaction and then more slowly over time (cf. Figure 8.6(a)), since it was continuously removed by the mem-

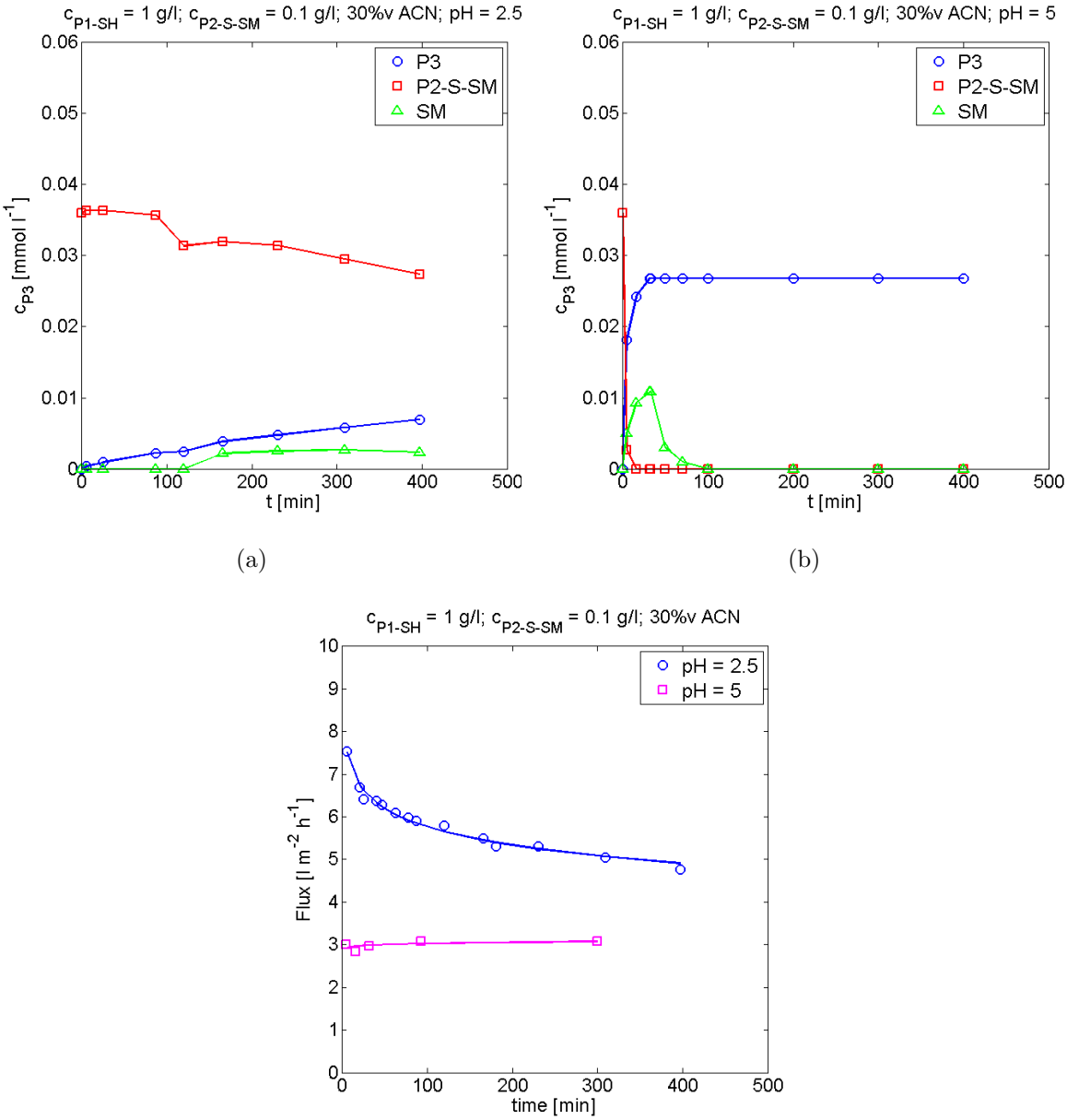


Figure 8.5: Effect of pH during Reactive Peptide Nanofiltration through Inopor Nano 450 Da.

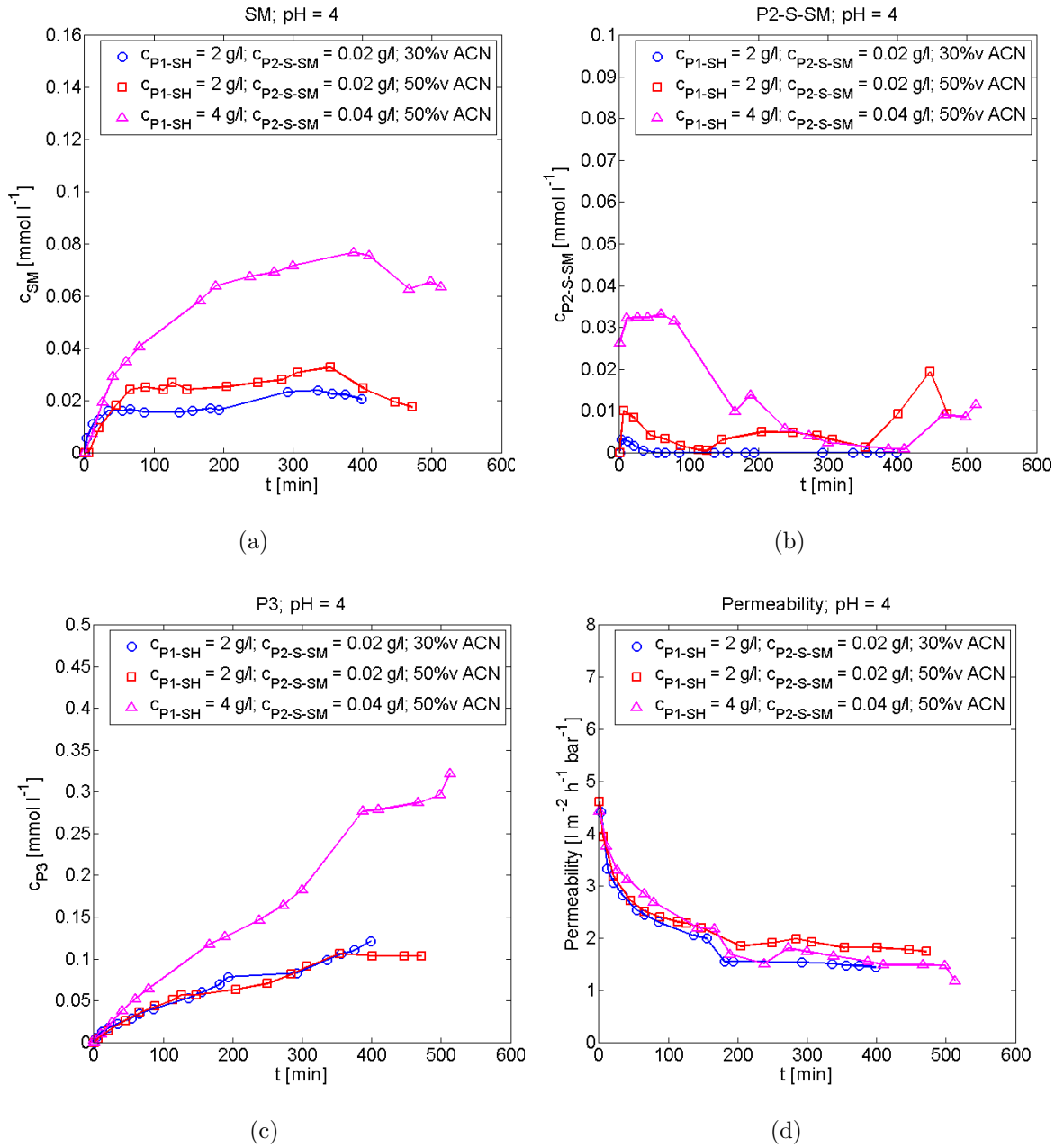


Figure 8.6: Reaction and flux profiles for the Reactive Peptide Nanofiltration at pH = 4 through Inopor Nano 450 Da.

brane. The concentration values were significantly higher for the case of higher concentration of starting reagents, and only slightly affected by the organic content. The rejection of SM was constant at 50%v ACN/water for both the concentration of starting reagents, while it was slightly lower at 30 %v (cf. Figure 8.7).

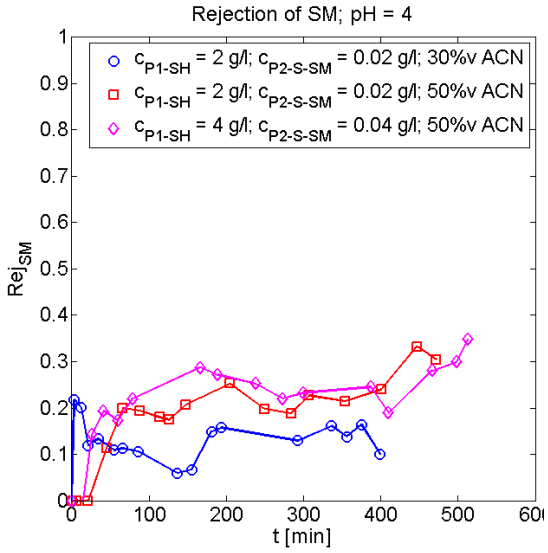


Figure 8.7: Rejection of SM during Reactive Peptide Nanofiltration through Inopor Nano 450 Da.

The concentration of P2-S-SM was always low, since this reagent was continuously added to the system and immediately consumed by the reaction (cf. Figure 8.6(b)). The concentration of P3 increased during time, together with the consumption of the reagents (cf. 8.6(c)). The rejection of P1-SH, P2-S-SM and P3 by the NF membrane was complete. The difference in concentration and organic solvent was not significant to determine a noticeable difference in the permeability decline during time (cf. Figure 8.6(d)).

8.4.5 Process modelling and cost evaluation

The mass balances for the Reactive Peptide Nanofiltration were introduced in Paragraph 8.3.2. The process model was validated on the experimental data and the Reactive Peptide Nanofiltration compared with the conventional process in terms of performances and costs.

Model validation

Firstly, the effect of pH under semibatch conditions with simultaneous loading of reagents was simulated. The kinetics described well the profiles for the cases of pH = 2.5 (cf. Figure 8.8(a)) and pH = 5 (cf. Figure 8.8(b)). Equation 8.17 was used to describe the kinetic constant as function of pH.

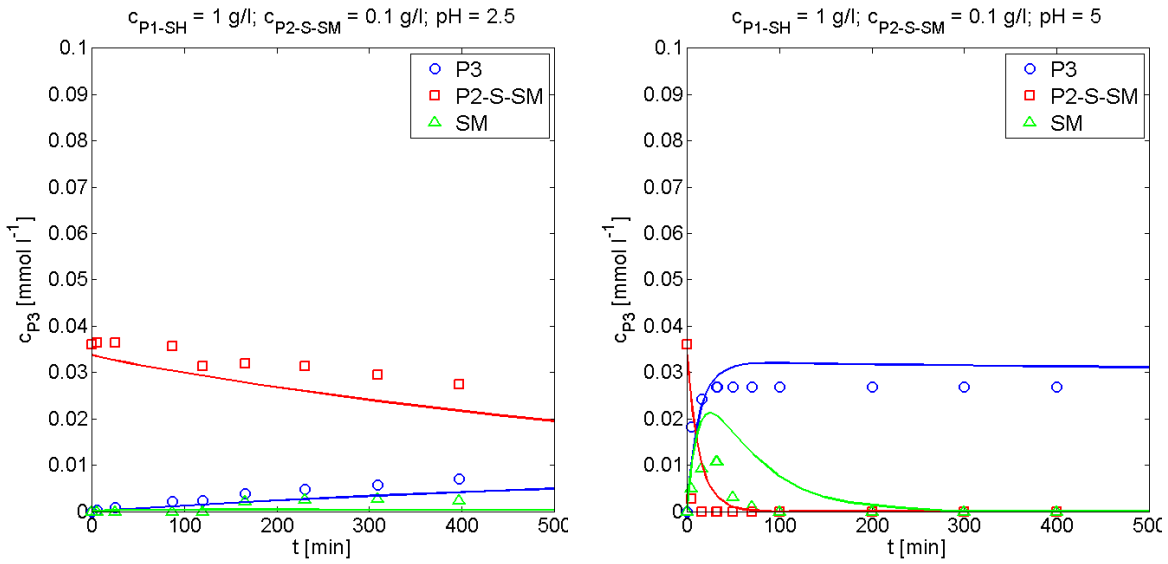


Figure 8.8: Effect of pH during Reactive Peptide Nanofiltration through Inopor Nano 450 Da. (o) experimental data; (-) simulation.

Afterwards, semibatch conditions with separated loading of reagents were simulated for the cases of two different concentrations of organic solvents (Figure 8.9(a) vs. 8.9(b)) and two different starting concentrations of reagents (Figure 8.9(b) vs. 8.9(c)).

Experimental fluxes were used for the description of the permeation rate ($Q_{in} = Q_{out}$ in Equation 8.3). They were shown in Figures 8.5(b) and 8.6(d), for the simulation of Figures 8.8 and 8.9, respectively.

The matching between simulated and experimental profiles was satisfactory. Experimental kinetics obtained under batch conditions were representative of the kinetics in the NF loop and its combination with the mass balances for the semi-batch reactor successfully

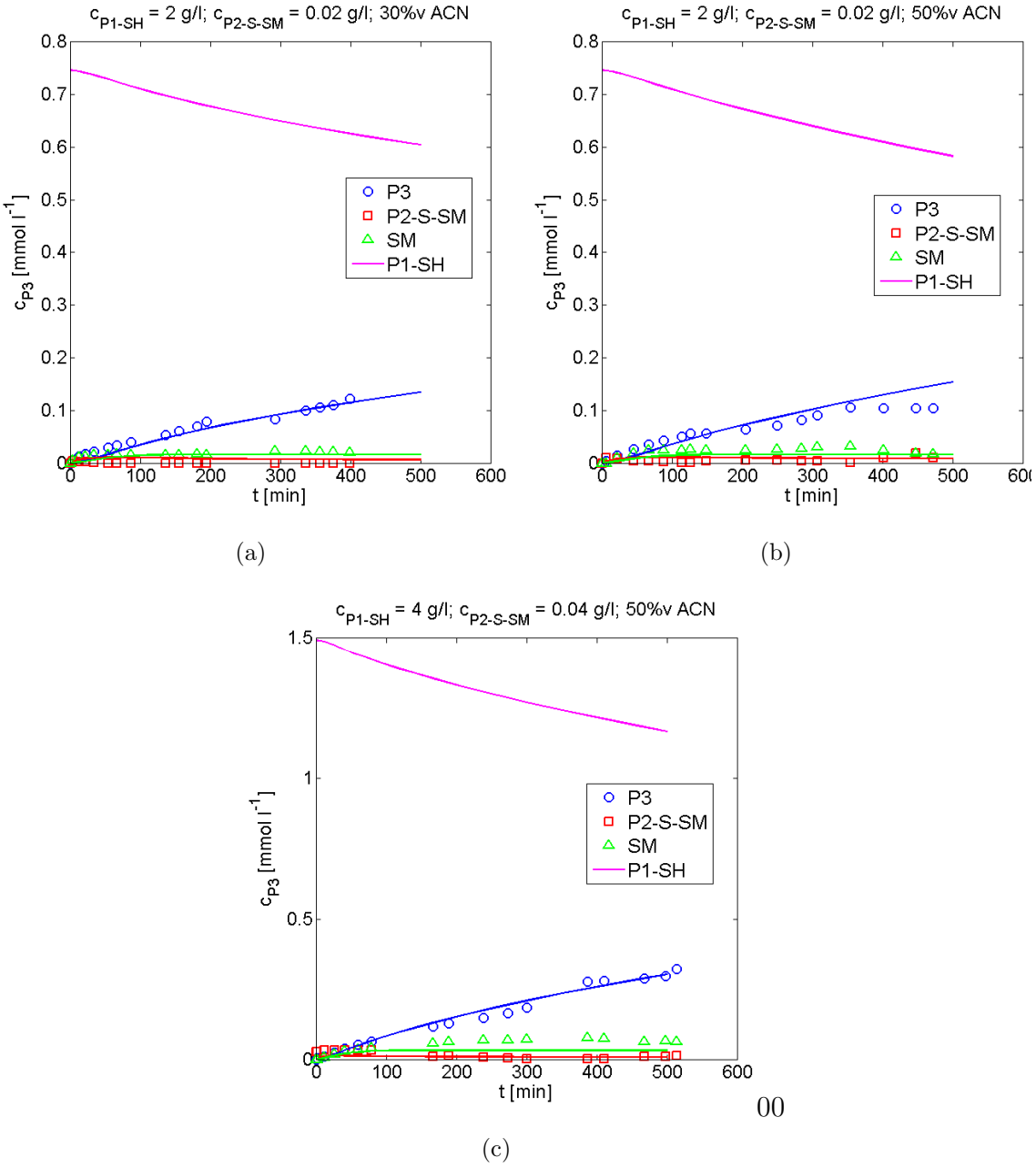


Figure 8.9: Effect of peptide concentration and organic content during Reactive Peptide Nanofiltration through Inopor Nano 450 Da. (o) experimental data; (-) simulation.

described the Reactive Peptide Nanofiltration.

Reactive Peptide Nanofiltration vs. conventional production: process performances and cost comparison

Reactive Peptide Nanofiltration and conventional process were compared to each other in terms of performance and costs. The simulation was undertaken for large scale: 26 kg of P3 was set as the goal for the production. Production steps and relative operating conditions for the conventional process are reported in Table 8.7.

Table 8.7: Conventional process and relative working conditions.

Step	Working value	Time
Preparation of THF / water = 75 / 25 solution	170 l	1 h
Addition of P2-S-SM	10.6 kg	2 h
Temperature adjustment	0° C	1 h
Addition of P1-SH	17.4 kg	4 h
Reaction		12 h
Addition of ACN for precipitation	1370 l	2 h
Wash x 3	400 l	3 h
Drying		36 h
Dissolution time for chromatography		4 h

The conventional reaction was run with P2-S-SM in slight excess, compared to P1-SH. A high load of organic solvent was necessary to solubilise P2-S-SM. The time required for the reaction was long, almost 12 h. After the reaction, ACN was added to precipitate the main product. Three steps of washing and drying followed the precipitation. The time required for the drying was significant. Finally, the product was re-solubilised for the final chromatography step. The total reaction volume was 1540 l and the total time required for

the production of P3 was 67 h. Production steps and relative operating conditions for the Reactive Peptide Nanofiltration are reported in Table 8.8.

Table 8.8: Reactive Peptide Nanofiltration and relative working conditions.

Step	Working value	Time
Preparation of ACN / water = 10 / 90 solution	1650 l	1 h
Addition of P1-SH	17.4 kg	2 h
Addition of P2-S-SM / Reaction / Dialysis	10.6 kg	15 h

The number of steps was significantly reduced for the Reactive Peptide Nanofiltration. Permeability of 2 l m^{-2} h^{-1} bar^{-1} and pressure of 20 bar were assumed as representative values for real working conditions. Filtration area of 25 m^2 was assumed as representative for commercially available ceramic modules. The time required for addition of P2-S-SM + reaction + dialysis (i.e. 15 h) was due to the necessity of having 10 dialysis volumes with permeation flow of 1000 l h^{-1} . The total time required for the production of P3 was 18 h.

The cost comparison of the conventional process with the Reactive Peptide Nanofiltration is presented in Table 8.9.

Costs for the raw materials were similar, since the same amounts of starting reagents were used. Costs for the solvents were ten times higher for the conventional process than for the Reactive Peptide Nanofiltration, since the organic solvent could not be recovered at the end of the former process, while it could be recycled at the end of the latter. Production costs were estimated to be three times higher for the conventional process, due to longer production times and higher manpower requirements. Costs for membranes are present for the Reactive Peptide Nanofiltration only, but they were not significant compared to the other cost items. According to the cost evaluation for this business case, total costs without raw materials foreseen for the Reactive Peptide Nanofiltration were almost the 50% of those for the conventional process. The advantages from technical, economical and environmental points of view were significant for this kind of technology, which was therefore demonstrated

Table 8.9: Cost comparison of conventional process with Reactive Peptide Nanofiltration (CHF = Swiss francs).

Cost Center	Traditional process $\mathbf{CHF \cdot 10^3}$	Membrane Process $\mathbf{CHF \cdot 10^3}$
Raw material	7000	7000
Solvent	34	3
Production	217	72
Membrane	0	25
C/O	67	67
Total	7318	7167
Total w/o raw materials	318	167

to be promising for application in the large-scale production of peptides.

8.5 Conclusion

Integration of membrane separation techniques into the reaction step was presented in this chapter, to address some of the drawbacks of conventional peptide production by fragment condensation. The strategy was named Peptide Reactive Nanofiltration and the main features are: (i) the incorporation of the NF unit into the reaction step; (ii) the separation of the small side product, formed as a consequence of the fragment condensation reaction; (iii) the recycle of the solvent after the nanofiltration (which means in turn lower solvent consumption for the global process); and (v) the elimination of time-consuming steps (precipitation, washing and drying), typical of the conventional strategy.

The performance of the new strategy was presented for an industrial case study. Reaction kinetics were studied as a function of the operating conditions, and rejection and permeability were investigated for the membrane selection. Permeation through the mem-

brane was studied as a function of different operating parameters (peptide concentration, pH, pressure, cross-flow velocity and ACN concentration), to select the best working conditions. Experimental kinetics obtained under batch conditions were representative of the kinetics in the NF loop, and its combination with the mass balances for the semi-batch reactor successfully described the Reactive Peptide Nanofiltration.

The Reactive Peptide Nanofiltration was compared to the conventional batch process by means of techno-economical analysis. Shorter production time and lower solvent consumption characterised this scheme, with evident advantages from technological, economical and environmental point of view.

Chapter 9

Conclusions and future perspectives

The increasing interest in peptides as pharmaceuticals has been challenging the peptide industry to develop economically competitive methods for manufacturing peptides in large quantities. Separation and purification technologies based on membrane separation have been proposed to overcome some of the limitations of the conventional processes. NF can be applied to perform concentration, separation, salt/solvent exchange of peptide solutions and assist the organic synthesis, thus enhancing the production of target compounds. Below, the research presented in this work is summarised, referring to the goals set at the beginning of this research (cf. Chapter 3), and the future perspectives in the field are outlined.

In **Chapter 4**, permeation of solvents, salts, neutral organic molecule and model peptides was studied, to improve the knowledge of the permeation mechanism of peptide solutions in Organic Solvent Nanofiltration. As a first step towards a deeper undearstanding of the transport mechanism, permeation of water and organic solvents through ceramic NF and UF membranes was investigated. Experimental results clearly indicated that solvent-membrane interactions cannot be neglected when the pore-size decreases (such as in NF). As a consequence, the Hagen-Poiseuille equation may fail in describing solvent permeation through NF membranes, as it does not account for molecular interaction effects, whereas it is able to describe the experimental permeability through UF membranes. A new phenomenological model was proposed to describe solvent permeation through NF and UF membranes. Several correction factors for the basic viscous flow were considered, to ac-

count for the surface phenomena that arise in a nanotube due to solvent-membrane surface interactions. These correction terms, namely the capillary pressure, the dipole and the steric term, were found to be functions of the pore size, so that the model could be applied to both UF and NF ranges. The model was applied to aqueous and organic mixtures in a simplified version, by using only pure solvent regression parameters. The hypothesis of linear dependence of the correction factor on the solvent composition was found to be reasonable for all the aqueous and organic solvent mixtures, apart from ACN/water mixture. The formation of some complexes between ACN and water molecules was ascribed to be one possible explanation for such deviation. The model has the potential to make design calculations and predict pure solvent and mixture fluxes for a specific membrane by obtaining a limited number of experimental data for pure solvents (necessary to obtain the fitting parameters characteristic of the membrane). Taking a wider perspective, this tool can find interesting applications both at the lab scale and in an industrial environment.

This chapter discusses the solvent permeation in confined geometries , by introducing correction factors for the bulk viscosity. The viscosity inside the channel may differ from that of the bulk solution. The modelling of solvent permeation could be also approached by modelling the effect of the channel dimension (in the NF range) on the solvent viscosity. Furthermore, this model was developed for non-swelling ceramic membranes, under the hypothesis of constant pore radius. This model could be extended to swelling polymeric membranes, by modelling the pore radius as a function of the solvent properties (i.e. sorption degree).

In **Chapter 5**, fundamental investigation was extended to NF of solutes in organic/water mixtures, which represent the typical environments found in processes involving peptides. Straight extension of steric and electrostatic separation mechanisms, typical of aqueous environments, to non-aqueous systems was found to be complex, due to the significant differences in the structures and properties of the solvents. In such complex systems, molecular affinity between the species may become critical. Molecular affinity is influenced by hydrophilic/phobic and polar properties of solute, solvent and membrane and affects the ternary interactions among them. As a consequence, competition between solute-

membrane and solvent-membrane affinities becomes critical and can affect the pressure-driven transport of solute and solvent through the membrane. Two cases were identified, as a function of the relative solute-membrane vs. solvent-membrane affinities:

(i) when the solvent-membrane affinity is larger than the solute-membrane affinity, solvent molecules accumulate preferentially at the pore wall, and the solvent flux ($J_{solvent}$) is finally larger than the solute flux (J_{solute}) , determining a positive solute rejection (in other words, the less affine solute is excluded from the pore and its concentration in the permeate can be lower or equal the concentration in the retentate);

(ii) when the solute-membrane affinity is larger than the solvent-membrane affinity, solute molecules accumulate at the pore wall, and the solute flux is finally larger than the solvent flux. In this case, the concentration of the solute in the permeate can be higher than the concentration in the retentate, thus resulting in a negative solute rejection.

In the intermediate case, when solvent-membrane and solute-membrane affinities are comparable, solute rejection is governed by the the relative importance of the two affinities.

Rejection of monovalent ions showed that solute-membrane affinity has a more significant effect at low pore dimensions (NF range) and becomes negligible for large pore dimensions (UF range), due to the high significance of surface interactions in large specific surface systems (in agreement with observations for solvent permeation). The effect of the solvent can be explained by the Hansen solubility parameter of the solvents and the preferential solubility parameters of the ions in the solvent mixture. Studying the effects of %v ACN and %v TFA-H on the rejection of one small neutral organic molecule, Npys, and one model peptide, PEP_1, the importance of preferential solvation, caused by mixture composition and salt/ion content, in affecting permeation of neutral and charged molecules in solvent mixtures was demonstrated. Affinities among solute, solvent and membrane play therefore a fundamental role in NF and should be included as a further contribution to the understanding of the membrane transport.

Fundamental models often do not take into account the effect of mixture composition on the peptide retention, as those models were developed mainly for aqueous solutions and the extension to organic solvents is still under investigation. In **Chapter 6**, Design of Experi-

ments was proposed to study the NF of three model peptides and understand the effect of the operating parameters on solvent flux, peptide and salt rejection. Statistical models for the responses as functions of the operating parameters were obtained by statistical Analysis of Variance. It was found that the operating parameters affecting the solute-membrane interactions and the fluid dynamics in the system (peptide concentration, pressure and pump frequency) showed the same effect on all the peptides, since they do not depend on the peptide physico-chemical properties. On the other hand, the operating parameters affecting solute-solvent-membrane interactions (TFA-H concentration, ACN concentration and peptide concentration in some special cases) showed different effects for the threee case studies, as a function of the peptide physico-chemical properties. This confirms the effect of the solvent mixture in affecting the solute-membrane affinity. TFA-H rejection was found to be significant. Since TFA-H rejection affects peptide retention and solvent flux, it has important consequences on the global filtration performances. Extended knowledge of how counter-ion concentration affects filtration performace is fundamental for the understanding and process selection.

The understanding of the transport mechanism through NF membranes is an important research topic, for both phenomenological understanding and process selection and a complex issue, since a large number of operating parameters can affect the process performance. Studies on solute retention in OSN have been done for some commercially available membranes. However, still no general agreement about a suitable transport mechanism (solution-diffusion, pore-flow, solute-solvent coupling) and the best mathematical model for that has been reached. Phenomenological understanding of transport processes by Design of Experiment methods and statistical modelling could provide useful information for supporting fundamental modelling. Efficient experimental techniques can help in reducing the number of experiments necessary for characterising an application and sound Analysis of Variance can confirm the significance of the operating parameters, thus guiding the choice and the formulation of the most suitable fundamental model for describing the trasport process.

In **Chapters 7** and **8**, application of NF to two real industrial case studies was pro-

posed and fundamental information from permeation studies was used to assist the process development. The first case study addressed the application of NF for concentration and salt/solvent exchange, as part of the downstream processing of a model peptide (PEP_1) in TFA-H/ACN/water mixtures. This work provides a general procedure to efficiently investigate nanofiltration for peptide concentration and diafiltration under the QbD concept. Statistical DoE models for peptide rejection and permeation as functions of several operating parameters (peptide, TFA-H and ACN/water concentrations, pressure and cross-flow velocity) were used to select the best operating conditions for concentration and salt/solvent exchange. The best conditions for concentration (i.e. high solvent flux and peptide rejection) were found to correspond to high %v ACN and high %v TFA-H, which caused an increase of the peptide hydrophobicity by molecular association of ACN molecules and TFA^- counter-ions with the peptide chain. Experimental investigation by DoE allowed process understanding, modelling, and optimization, and this knowledge was applied to perform process selection, all at the expense of a limited number of experimental data. The statistical models from DoE were, in fact, included in the mathematical framework of the diafiltration process, to obtain the evolution of peptide, counter-ion (TFA^-) and solvent (ACN) concentrations in the system. Process modelling by including time-dependent rejection and permeability was validated on experimental data for diafiltration at concentration values larger than that used for DoE. The model combining a dynamic mass balance for diafiltration with time-dependent rejection and permeability permitted to simulate different possible constant volume diafiltration paths and select the best one (i.e. the one with the lowest operating time) to perform the salt and solvent exchanges of interest.

The second case study focused on the integration of NF into the reaction step of a model fragment condensation, to address some of the drawbacks of the conventional process. The strategy, named Peptide Reactive Nanofiltration, is based on the separation of the small side product, formed as a consequence of the fragment condensation, by NF; the recycle of the solvent after the nanofiltration (which means in turn lower solvent consumption for the global process); and the elimination of time-consuming steps (precipitation, washing and drying), typical of the conventional strategy. Reaction kinetics was studied and re-

jection and permeability investigated for the membrane selection. The effect of different operating parameters (peptide concentration, pH, pressure, cross-flow velocity and ACN concentration) on the NF performance was studied by DoE, to select the best working conditions. The Reactive Peptide Nanofiltration was compared to the conventional batch process by means of techno-economical analysis. Shorter production time and lower solvent consumption characterised this scheme, with evident advantages from technological, economical and environmental point of view.

In this study, NF was found to be a solid and competitive technique for application to peptide processes. NF was found advantageous to perform concentration and diafiltration and to assist peptide synthesis, allowing improvement of global process performance and cost reduction. High rejection and permeability values validated the choice of ceramic membranes for peptide processes. On the basis of the results of this research, Lonza decided to invest in a new NF plant for the downstream of peptides with ceramic membranes. The improvement of NF technology, in terms of development of more efficient materials (stable in critical solvents and harsh acid/basic conditions), improvement of membrane performances (selectivity, lifetime) and integration of NF with other techniques in hybrid processes seem therefore promising in overcoming the hesitancy of industries to modify the established processes and invest in new NF plants, by making the payback period for the return of investment more attractive. It is plausible to think that shortly this technology will become a primary choice for new separation and purification processes.

Bibliography

[1] A. Ghosh, E. Fan, A novel method for sequence independent incorporation of activated/protected cysteine in Fmoc solid phase peptide synthesis, Tetrahedron Lett. 41 (2000) 165–168.

[2] J. Geens, B. De Witte, B. Van der Bruggen, Removal of APIs (Active Pharmaceutical Ingredients) from organic solvent nanofiltration, Separ. Sci. Technol. 42 (2007) 2435–2449.

[3] J. A. Whu, B. C. Balzis, K. K. Sirkar, Modeling of nanofiltration-assisted organic synthesis, J. Membr. Sci. 163 (1999) 319–331.

[4] J. So, L. Peeva, E. Tate, R. J. Leatherbarrow, A. G. Livingston, Organic solvent nanofiltration: a new paradigm in peptide synthesis, Org. Process Res. Dev. 14 (2010) 1313–1325.

[5] G. C. Barrett, D. T. Elmore, Amino Acids and Peptides, Cambridge University Press, 1998.

[6] M. Pusceddu Nardella, G. Testoni, BioLogica, vol.A, Trevisini Editore Milano, 2003.

[7] N. Sewald, H. D. Jakubke, Peptides: Chemistry and Biology, Wiley-VCH, 2002.

[8] N. L. Benoiton, Chemistry of peptide synthesis, Taylor & Francis, 2005.

[9] B. Skoog, A. Wichman, Calculation of the isoeletric points of polypeptides from the amino acid composition, Trends Anal. Chem. 5(4) (1986) 82–83.

[10] B. L. Bray, Large-scale manufacture of peptide therapeutics by chemical synthesis, Nature rev. 2 (2003) 587–593.

[11] R. Lax, C. Meenan, Challenges for therapeutic peptides, Part 1: On the inside, looking out. Innovations in Pharmaceutical Technology / Issue 42 (Autumn,2012). URL http://www.polypeptide.com/news/publications.htm

[12] R. B. Merrifield, Solid phase peptide synthesis. 1. The synthesis of a tetrapeptide, J. Am. Chem. Soc. 85 (1963) 2149–2154.

[13] S. So, L. G. Peeva, E. W. Tate, R. J. Leatherbarrow, A. G. Livingston, Membrane enhanced peptide synthesis, Chem. Commun. 46 (2010) 2808–2810.

[14] E. Bayer, M. Mutter, R. Uhmann, J. Polster, H. Mauser, Kinetic studies of the liquid phase peptide synthesis, J. Am. Chem. Soc. 96 (1974) 7333–7336.

[15] D. Witt, Recent developments in disulfide bond formation, Synthesis 16 (2008) 2491–2509.

[16] P. Vandezande, L. E. M. Gevers, I. Vankelecom, Solvent resistant nanofiltration: separating on a molecular level, Chem. Soc. Rev. 37 (2007) 365–405.

[17] L. G. Peeva, E. Gibbins, S. S. Luthra, L. S. White, R. P. Stateva, A. G. Livingston, Effect of concentration polarisation and osmotic pressure on flux in organic solvent nanofiltration, J. Membr. Sci. 236 (2004) 121–136.

[18] G. Székely, J. Bandarra, W. Heggie, B. Sellergren, F. C. Ferreira, A hybrid approach to reach stringent low genotoxic impurity contents in active pharmaceutical ingredients: combining molecularly imprinted polymers and organic solvent nanofiltration for removal of 1,3-diisopropylurea, Sep. Purif. Technol. 86 (2012) 79.

[19] C. Mazzoni, Caratterizazione di membrane da nanofiltrazione, PhD tesi Ciclo XX, Universitá di Bologna, 2008.

[20] M. K. Naskar, D. Kundu, M. Chatterjee, Silicalite-1 zeolite membranes on unmodified and modified surfaces of ceramic supports: A comparative study, Bull. Mater. Sci. 32 (2009) 537–541.

[21] A. Sah, H. L. Castricum, A. Bliek, D. H. A. Blank, J. E. Elshof, Hydrophobic modification of γ-alumina membranes with organochlorosilanes, J. Membr. Sci. 243 (2004) 125–132.

[22] A. G. Livingston, L. G. Peeva, S. Han, D. Nair, S. S. Luthra, L. S. White, L. M. Freitas dos Santos, Membrane separation in green chemical processing. solvent nanofiltration in liquid phase organic synthesis reactions, Ann. N.Y. Acad. Sci. 984 (2003) 123–141.

[23] J. G. Wijmans, R. W. Baker, The solution diffusion model: a review, J. Membr. Sci. 107 (1995) 1–21.

[24] W. R. Bowen, H. Mukhtar, Characterisation and prediction of separation performance of nanofiltration membranes, J. Membr. Sci. 112 (1996) 263.

[25] W. R. Bowen, J. S. Welfoot, Modelling the performance of membrane nanofiltration - critical assessment and model development, Chem. Eng. Sci. 57 (2002) 1121–1137.

[26] E. Yaroshchuk, Solution-diffusion-imperfection model revised, J. Membr. Sci. 10 (1995) 83–87.

[27] O. Kedem, A. Katchalsky, Thermodynamic analysis of the permeability of biological membranes to non-electrolytes, Biochim. Biophys. Acta 27(2) (1958) 229–246.

[28] K. S. Spiegler, O. Kedem, Thermodynamics of hyperfiltration (reverse osmosis): criteria for efficient membranes, Desalination 1 (1966) 311–326.

[29] H. K. Lonsdale, U. Merten, R. L. Riley, Transport properties of cellulose acetate osmotic membranes, J. Appl. Polym. Sci. 9 (1965) 1341.

[30] J. A. Barrie, A. S. Michaels, W. R. Vieth, Gas diffusion in glassy polymers, J. Polym. Sci. Part B 13(4) (1975) 859–861.

[31] P. Meares, J. B. Craig, J. Webster, Diffusion and flow of water in homogeneous cellulose acetate membranes, in: J. N. Sherwood, A. Y. Chadwick, W. N. Muire, F. L. Swinton (Eds.), Diffusion Processes, Vol. 2, Gordon and Breach, London, 1971.

[32] H. Yasuda, A. Peterlin, Diffusive and bulk flow transport in membranes, J. Appl. Polym. Sci. 17 (1973) 433.

[33] E. A. Mason, H. K. Lonsdale, Statistical-mechanical theory of membrane transport, J. Membr. Sci. 51 (1990) 1–81.

[34] M. F. J. Dijkstra, S. Bach, K. Ebert, A transport model for organophilic nanofiltration, J. Membr. Sci. 286 (2006) 60.

[35] D. R. Paul, Reformulation of the solution-diffusion theory for reverse osmosis, J. Membr. Sci. 241 (2004) 317–386.

[36] J. C. Maxwell, On the dynamical theory of gases, Phil. Trans. R. Soc. Lond. 157 (1867) 48.

[37] J. Stefan, Ueber das gleichgewicht und bewegung, insbesondere die diffusion von gemischen, in: N. Shamim, S. Virender (Eds.), Sitzungsberichte der Kaiserlichen Akademie der Wissenschaften Wien, 2te Abteilung a, 63, ACS Symp. Ser., 1871.

[38] R. Bird, W. Stewart, E. Lightfoot, Transport Phenomena, Second Edition., Wiley, 2007.

[39] T. Matsuura, S. Sourirajan, Reverse osmosis transport through capillary pores under the influence of surface forces, Ind. Eng. Chem. Proc. Des. Dev. 20 (1981) 273–282.

[40] H. Niemi, S. Palosaari, Flowsheet simulation of ultrafiltration and reverse osmosis processes, J. Membr. Sci. 91 (1994) 111–124.

[41] H. Mehdizadeh, J. M. Dickson, Theoretical modification of the surface force pore flow model for reverse osmosis transport, J. Membr. Sci. 42 (1989) 119–145.

[42] X. L. Wang, T. Tsuru, S. I. Nakao, S. Kimura, Electrolyte transport through nanofiltration membranes by the Space-Charge model and the comparison with Teorell-Meyer-Sievers model, J. Membr. Sci. 103 (1995) 117–133.

[43] J. Santos, A. Hidalgo, R. Oliveira, S. Velizarov, J. Crespo, Analysis of solvent flux through nanofiltration membranes by mechanistic, chemometric and hybrid modelling, J. Membr. Sci. 300 (2007) 191–204.

[44] D. R. Machado, D. Hasson, R. Semiat, Effect of solvent properties on permeate flow through nanofiltration membranes. Part I: investigation of parameters affecting solvent flux, J. Membr. Sci. 163 (1999) 93–102.

[45] D. Machado, D. Hasson, R. Semiar, Effect of solvent properties on permeate flow through nanofiltration membranes. Part II: transport model, J. Membr. Sci. 166 (2000) 63–69.

[46] G. Jonsson, C. E. Boesen, Water and solute transport through cellulose acetate reverse osmosis membranes, Desalination 17 (1975) 145–165.

[47] D. Bhanushali, S. Kloos, C. Kurth, D. Bhattacharayya, Performance of solvent-resistant membranes for non-aqueous systems: solvent permeation results and modeling, J. Membr. Sci. 189 (2001) 1–21.

[48] J. Geens, B. Van der Bruggen, C. Vandecastleele, Transport model fo solvent permeation through nanofiltration membranes, Sep. Purif. Technol. 48 (2006) 255–263.

[49] S. Darvishmanesh, A. Buekenhoudt, J. Degréve, B. Van der Bruggen, Coupled series-parallel resistance model for transport of solvent through inorganic nanofiltration membranes, Sep. Purif. Technol. 70 (2009) 46–52.

[50] S. Darvishmanesh, A. Buekenhoudt, J. Degréve, B. Van der Bruggen, General model for prediction of solvent permeation thorugh organic and inorganic solvent resistant nanofiltration membranes, J. Membr. Sci. 334 (2009) 43–49.

[51] T. Tsuru, M. Miyawaki, H. Kondo, T. Yoshioka, M. Asaeda, Inorganic porous membranes for nanofiltration of nonaqueous solutions, Sep. Purif. Technol. 32 (2003) 105.

[52] S. J. Han, S. S. Luthra, L. G. Peeva, X. J. Yang, A. G. Livingston, Insights into the transport of toluene and phenol through organic solvent nanofiltration membranes, Separ. Sci. Technol. 38(9) (2003) 1899–1923.

[53] H. K. Lonsdale, U. Merten, M. Tagami, Phenol transport in cellulose acetate membranes, J. Appl. Polym. Sci. 11 (1967) 1807–1820.

[54] D. Bhanushali, S. Kloos, D. Bhattacharayya, Solute transport in solvent-resistant nanofiltration membranes for non-aqueous systems: experimental results and the role of solute-solvent coupling, J. Membr. Sci. 208 (2002) 343–359.

[55] Y. Zhang, T. Xu, L. Z., Streaming potential across a porous charged membrane in organic - aqueous solutions, Desalination 212 (2008) 183–190.

[56] Y. Zhao, Q. Yuan, Comparison of nanofiltration with aqueous and organic solvents, J. Membr. Sci. 279 (2006) 453–458.

[57] P. Marchetti, A. Butté, A. G. Livingston, An improved phenomenological model for prediction of solvent permeation through ceramic NF and UF membranes, J. Membr. Sci 415-416 (2012) 444–458.

[58] S. Darvishmanesh, J. Degréve, B. Van der Bruggen, Mechanisms of solute rejection in solvent resistant nanofiltration: the effect of solvent on solute rejection, Phys. Chem. Chem. Phys. 12 (2010) 13333–13342.

[59] Koops, Separation of linear hydrocarbons and carboxylic acids from ethanol and hexane solutions by reverse osmosis, J. Membr. Sci. 189 (2001) 241–254.

[60] A. Bagno, M. Campulla, M. Pirana, G. Scorrano, S. Stiz, Preferential solvation of organic species in binary solvent mixtures probed by intermolecular ^{1}H NOESY NMR spectroscopy, Chem. Eur. J. 5 (1999) 1291–1300.

[61] Y. Marcus, Gibbs energies of transfer of anions from water to mixed aqueous organic solvents, Chem. Rev. 107 (2007) 3880–3897.

[62] Y. Marcus, Preferential solvation of ions in mixed solvents. 5. The alkali metal, silver and thallium(I) cations in aqueous organic solvents according to the inverse Kirkwood-Buff integral (IKBI) approach, J. Solution Chem. 36 (2007) 1385–1399.

[63] Y. Marcus, Preferential solvation of ions in mixed solvents. 6. Univalent anions in aqueous organic solvents according to the inverse Kirkwood-Buff integral (IKBI) approach, J. Chem. Thermodynamics 39 (2007) 1338–1345.

[64] Y. Marcus, Preferential solvation of ions in mixed solvents. Part 2: the solvent composition near the ion, J. Chem. Soc. Faraday Trans. 1 84 (1988) 1465–1473.

[65] A. Wakisaka, S. Takahashi, N. Nishi, Preferential solvation controlled by clustering conditions of acetonitrile-water mixtures, J. Chem. Soc. Faraday Trans 91 (1995) 4063–4069.

[66] K. Gekko, E. Ohmae, K. Kameyama, T. Takagi, Acetonitrile-protein interactions: amico acid solubility and preferential solvation, Biochim. Biophys. Acta 1387 (1998) 195–205.

[67] S. Bouranene, A. Szymczyk, P. Fievet, A. Vidonne, Effects of salts on the retention of polyethylenglycol by a nanofiltration ceramic membrane, Desalination 240 (2009) 94–98.

[68] Y. Gu, P. H. Shih, Salt-induced phase separation can effectively remove the acetonitrile from the protein sample after the preparative RP-HPLC, Enz. Microbial. Technol. 35 (2004) 592–597.

[69] C. Reichardt, Solvents and Solvent Effects in Organic Chemistry, Third Edition, WILEY-VCH Verlag & GmbH Co. KGaA, Weinheim, 2003.

[70] K. D. Collins, Ions from the Hofmeister series and osmolytes: effects on proteins in solution and in the crystallization process, Methods 34 (2004) 300–311.

[71] A. S. Parmar, M. Muschol, Hydration and hydrodynamic interactions of lysozyme: Effects of chaotropic versus kosmotropic ions, Biophys. J. 97 (2009) 590–598.

[72] R. LoBrutto, A. Jones, Y. V. Kazakevich, Effect of counter-anion concentration on retention in High Performance Liquid Chromatography of protonated basic analytes, J. Chromatography A 913 (2001) 189–196.

[73] International Conference On Harmonisation of Technical Requirements for Registration of Pharmaceuticals for Human Use, ICH Harmonised Tripartite Guideline: Pharmaceutical Development Q8(R2)., http://www.ich.org/products/guidelines/quality/article/quality-guidelines.html, August 2009.

[74] M. Shivhare, G. McCreath, Practical considerations for DoE implementation in Quality by Design, BioProcess International (2010) 22–30.

[75] Z. R. Lazic, Design of Experiments in Chemical Engineering, WILEY-VCH Verlag GmbH &Co. KGaA, Weinheim, 2004.

[76] L. X. Yu, Pharmaceutical Quality by Design: product and process development, understanding and control, Pharmaceutical Research 25 (2007) 781–791.

[77] D. B. Hibbert, Experimental design in chromatography: a tutorial review., Journal of Chromatography B 910 (2012) 2–13.

[78] A. C. Atkinson, R. D. Tobias, Optimal experimental design in chromatography., Journal of Chromatography A 1177 (2008) 1–11.

[79] A. L. Ahmad, C. P. Leo, S. R. A. Shukor, Statistical design of experiments for dye-salt-water separation study using bimodal porous silica/gamma-alumina membrane, Desalin. Water Treat. 5 (2009) 80–90.

[80] E. Polom, D. Szaniawska, Rejection of lactic acid solutions by dynamically formed nanofiltration membranes using a statistical design method, Desalination 198 (2006) 208–214.

[81] A. Román, G. Vatai, A. Ittzés, Z. Kovács, P. Czermak, Modeling of diafiltration processes for demineralization of acid whey: an empirical approach, J. Food Eng. 35 (2012) 708–714.

[82] P. Silva, S. Han, A. Livingston, Solvent transport in organic solvent nanofiltration membranes, J. Membr. Sci. 262 (2005) 49–59.

[83] J. Geens, K. Peeters, B. Van der Bruggen, C. Vandecastleele, Polymeric nanofiltration of binary water-alcohol mixtures: influence of feed composition and membrane properties on permeability and rejection, J. Membr. Sci. 255 (2005) 255–264.

[84] G. Hu, D. Li, Multiscale phenomena in microfluidics and nanofluidics, Chem. Eng. Sci. 62 (2007) 3443–3454.

[85] P. Abgrall, N. T. Nguyen, Nanofluidic devices and their applications, Anal. Chem. 80 (2008) 2326–2341.

[86] D. Dimitrov, A. Milchev, K. Binder, Capillary rise in nanopores: molecular dynamics evidence for the Lucas-Washburn equation, Phys. Rev. Lett. 99 (2007) 1–4.

[87] D. I. Dimitrov, A. Milchev, K. Binder, Forced imbibition - a tool for separate determination of Laplace pressure and drag force in capillary filling experiments, Phys. Chem. Chem. Phys. 10 (2008) 1867–1869.

[88] A. Carré, Polar interactions at liquid/polymer interfaces, J. Adhes. Sci. Tech. 21 (2007) 961–981.

[89] N. Giovambattista, P. G. Debenedetti, P. J. Rossky, Effect of surface polarity on water contact angle and interfacial hydration structure, J. Phys. Chem. B 111 (2007) 9581–9587.

[90] D. K. Owens, R. C. Wendt, Estimation of the surface free energy of polymers, J. Appl. Polymer Sci. 13 (1969) 1741–1747.

[91] T. F. Coleman, Y. Li, An interior trust region approach for nonlinear minimization subject to bounds, SIAM J. Optim. 6 (1996) 418–445.

[92] R. H. Perry, D. M. Green, J. O. Maloney, Perry's Chemical Engineer's Handbook, McGraw-Hill Book Company, New York, 1984.

[93] I. M. Smallwood, Handbook of Organic Solvent Properties, Elsevier, 1996.

[94] F. Zheng, Z. Zhang, C. Li, Q. Yuan, A comparative study of suitability on different molecular size descriptors with the consideration of molecular geometry in nanofiltration, J. Membr. Sci. 332 (2009) 13–23.

[95] D. Rébiscoul, L. Broussous, W. Puyrenier, V. Rouessac, A. Ayral, Impact of solvent and low k material surface characteristics on pore sealing efficiency and porosity measurement, J. Phys. Conf. Ser. 152 (2009) 1–8.

[96] B. E. Poling, J. M. Prausnitz, J. P. O'Connel, Properties of Gases and Liquids, fifth Ed., McGraw-Hill, New York, 2001.

[97] A. Dobrak, B. Verrecht, H. Van der Dungen, A. Buekenhoudt, I. F. J. Vankelecom, B. Van der Bruggen, Solvent flux behavior and rejection characteristics of hydrophilic and hydrophobic masoporous and microporous TiO_2 and ZrO_2 membranes, J. Membr. Sci. 346 (2010) 344–352.

[98] M. Jelinska-Kazimierczuk, J. Szydlowski, Physicochemical properties of solutions of amides in H_2O and in D_2O, J. Sol. Chem. 30 (2001) 623–640.

[99] C. Moreau, G. Douhéret, Thermodynamic behavior of water-acetonitrile mixtures, Thermo. Acta 13 (1975) 385–392.

[100] N. Saha, B. Das, D. K. Hazra, Viscosities and excess molar volumes for acetonitrile + methanol at 298.15, 308.15, and 318.15 k, J. Chem. Eng. Data 40 (1995) 1264–1266.

[101] G. Ritzoulis, N. Papadopoulos, D. Jannakoudakis, Densities, viscosities, and dielectric constants of acetonitrile + toluene at 15, 25 and 35° C, J. Chem. Eng. Data 31 (1986) 146–148.

[102] N. Tsierkezos, A. C. Filippou, Thermodynamic investigation of N,N-dimethylformamide/toluene binary mixtures in the temperature range from 278.15 to 293.15 k, J. Chem. Thermodyn. 38 (2006) 952–961.

[103] C. M. Kinart, W. J. Kinart, A. Kolasisnki, Acetonitryle-water binary mixtures and their assumed international structures, Phys. Chem. Liq. 35 (1998) 201–208.

[104] C. Kalidas, G. Hefter, Y. Marcus, Gibbs energies of transfer of cations from water to mixed aqueous organic solvents, Chem. Rev. 100 (2000) 819–852.

[105] Y. Marcus, On the preferential solvation of drugs and PAHs in binary solvent mixtures, J. Mol. Liq. 140 (2008) 61–67.

[106] H. Mehdizadeh, J. M. Dickson, Modeling of reverse osmosis in the presence of strong solute-membrane affinity, AIChE Journal 39 (1999) 434–445.

[107] C. Hansen, Hansen Solubility Parameters: A user's handbook, Second Edition, CRC Press, 2007.

[108] Y. Marcus, Preferential solvation of ions in mixed solvents. Part 4: Comparison of the Kirkwood-Buff and Quasi-Lattice Quasi-Chemical approaches, J. Chem. Soc., Faraday Trans. 1 85 (1989) 3019–3032.

[109] P. Marchetti, A. Butté, A. Livingston, Reactive Peptide Nanofiltration, in: N. Shamim, S. Virender (Eds.), Sustainable Nanotechnology and the Environment: Advances and Achievements, ACS Symp. Ser., Washington, DC, 2013.

[110] C. Martin-Orue, S. Bouhallab, A. Garem, Nanofiltration of amino acid peptide solutions: mechanism of separation, J. Membr. Sci. 142 (1998) 255–233.

[111] J. Barbosa, D. Barrón, R. Bergés, V. Sanz-Nebot, I. Toro, Prefential solvation in acetonitrile-water mixtures, J. Chem. Soc., Faraday Trans. 93 (1997) 1915–1920.

[112] Y. Marcus, Preferential solvation. Part 3: Binary solvent mixtures, J. Chem. Soc., Faraday Trans. 1 85 (1989) 381–388.

Appendix A

Calculation of the preferential solvation parameter - Quasi-Lattice Quasi-Chemical (QLQC) theory

The Quasi-Lattice Quasi-Chemical theory was developed by Marcus [64] to describe the standard Gibbs free energy of transfer of an ion from a reference solvent to a mixture of solvents and the solvent composition in the vicinity of the ion, quantified by the so-called preferential solvation parameter [64]. The theory was based on the assumptions that: (1) each particle in the dilute solution of ions X in the mixed solvent A and B is surrounded by Z neighbours; (2) the pair interaction energies between components ($e_{X,A}$, $e_{X,B}$ and $e_{A,B}$) are independent of the nature of the neighbours each particle may have; (3) there is no volume change on mixing the components; (4) the entropy of mixing is ideal.

The local mole fraction of the solvent A near the ion X is:

$$x_A^L = \frac{N_{A,X}}{N_{A,X} + N_{B,X}} \tag{A.1}$$

The quasi-chemical expression defines the number of (i,j) neighbours:

$$N_{i,j}^2 = 4N_{i,i} \cdot N_{j,j} exp\left(\frac{\Delta e_{i,j}}{k_B \cdot T}\right) \tag{A.2}$$

where $\Delta e_{i,j} = e_{i,i} + e_{j,j} - 2e_{i,j}$, k_B is Boltzmann's constant and T the absolute temperature. Application of Equation A.2 to Equation A.1 yields:

$$x_A^L = \frac{2 \cdot N_{X,X}^{\frac{1}{2}} \cdot N_{A,A}^{\frac{1}{2}} exp\left(\frac{\Delta e_{X,A}}{2 \cdot k_B \cdot T}\right)}{2 \cdot N_{X,X}^{\frac{1}{2}} \cdot N_{A,A}^{\frac{1}{2}} exp\left(\frac{\Delta e_{X,A}}{2 \cdot k_B \cdot T}\right) + 2 \cdot N_{X,X}^{\frac{1}{2}} \cdot N_{B,B}^{\frac{1}{2}} exp\left(\frac{\Delta e_{X,B}}{2 \cdot k_B \cdot T}\right)} \tag{A.3}$$

This can be simplified into:

$$x_A^L = \frac{1}{1 + (1 - x_A) \cdot y \cdot x_A^{-1} \cdot exp\left(\frac{\Delta}{2}\right)} \tag{A.4}$$

where:

$$\Delta = \frac{(\Delta e_{X,A} - \Delta e_{X,B})}{k_B T} \tag{A.5}$$

$$y = \frac{x_A}{(1 - x_A)} \cdot \left(\frac{N_{B,B}}{N_{A,A}}\right)^{\frac{1}{2}} \tag{A.6}$$

The preferential solvation of X by one of the two solvents in the mixture, say A, is defined as the difference between the local mole fraction x_A^L and the bulk mole fraction x_A:

$$\delta x_A = x_A^L - x_A = \frac{(1 - x_A) \cdot \left[1 - y \cdot exp\left(\frac{\Delta}{2}\right)\right]}{1 + (1 - x_A) \cdot y \cdot x_A^{-1} \cdot exp\left(\frac{\Delta}{2}\right)} \tag{A.7}$$

The evaluation of Δ requires the difference in standard molar Gibbs energies of transfer of the ion X from the reference solvent (normally water, W) into the pure solvents A and B, which are experimentally accessible, and the lattice parameter Z:

$$\Delta = \frac{[\Delta G_t^0(X, W \rightarrow A) - \Delta G_t^0(X, W \rightarrow B)]}{Z \cdot R \cdot T} \tag{A.8}$$

For the case of transfer of ions from water as the reference solvent (solvent A) into aqueous solvent mixtures (solvent B), Equation A.8 takes the form:

$$\Delta = \frac{-\Delta G_t^0(X, W \rightarrow B)}{Z \cdot R \cdot T} \tag{A.9}$$

Standard molar Gibbs energy of transfer from water to non-aqueous solvents are available in literature [61, 104]. The Gibbs energies of transfer of anions and cations used in this study are reported in Table A.1.

Ion	ΔG_t^0 **to ACN**	ΔG_t^0 **to ethanol**	ΔG_t^0 **to DMF**	ΔG_t^0 **to acetone**
F^-	49.3	25.8		41
Cl^-	41.9	20.3	45.9	28.5
Br^-	24.7	19	22	22.6
I^-	18.9	14	11.1	14.4
TFA^-	- 57.35	-	-	-
H^+	44.8	11.1	- 14.4	
Li^-	28.5	10.3	-22.4	
Na^-	11.9	14.9	-10.6	
K^-	6.5	16.4	-9.1	

Table A.1: Standard molar Gibbs energies of transfer of ions [kJ mol^{-1}] from water to non-aqueous solvents at 298.15 K. For TFA$^-$: simulation in COSMOthermX.

For TFA^- no literature data were available. Gibbs energy of transfer was obtained as difference between the molar Gibbs energy of TFA^- in water and that in ACN, $\Delta G^0(TFA^-, water)$ and $\Delta G^0(TFA^-, ACN)$, respectively, obtained by simulation in COSMOthermX (COSMOlogic). Since only $\Delta G^0(TFA-H, water)$ (acid form) was available in COSMOthermX, hypothesis of additivity of $\Delta G^0(TFA^-)$ and $\Delta G^0(H^+)$ was done to calculate $\Delta G^0(TFA^-)$ from$\Delta G^0(TFA-H)$.

$$\Delta G_t^0(TFA^-, water \rightarrow ACN) = \Delta G^0(TFA^-, ACN) - \Delta G^0(TFA^-, water) \qquad \text{(A.10)}$$

The total number of pairs of neighbours, S, in the system is:

$$S = \frac{Z}{2}(N_A + N_B) \tag{A.11}$$

where N_A and N_B designate the number of molecules of the components in the bulk. The number of neighbouring pairs of these molecules, according to the quasi-lattice theory, are $N_{A,A}$ and $N_{B,B}$. Since $N_{A,A} = (ZN_A - N_{A,B})/2$ and $ZN_A = 2x_AS$, and similarly for $N_{B,B}$ and ZN_B:

$$\left(\frac{N_{B,B}}{N_{A,A}}\right)^{\frac{1}{2}} = \left[\frac{1 - x_A - N_{A,B}/2S}{x_A - N_{A,B}/2S}\right]^{\frac{1}{2}} \tag{A.12}$$

$$\frac{N_{A,B}}{2S} = \frac{(1 - [1 - 4 \cdot x_A \cdot (1 - x_A) \cdot [1 - exp(-\Delta e_{A,B}/k_B \cdot T)]]^{\frac{1}{2}})}{2 \cdot [1 - exp(-\Delta e_{A,B}/k_B \cdot T)]} \tag{A.13}$$

The exponent appearing in Equation A.13 is given by:

$$exp(-\Delta e_{A,B}/k_BT) = \left[2 \cdot exp\left[-2G^E_{A,B}(x = 0.5)/\left(Z \cdot R \cdot T\right)\right] - 1\right]^{-2} \tag{A.14}$$

The QLQC theory requires the following input data: $\Delta G^\circ_t(X, A \rightarrow B)$, $G^E_{A,B}(x = 0.5)$, and Z. $\Delta G^\circ_t(X, A \rightarrow B)$ exerts the major effect: its sign determines that of $\delta_{X,A}$. A positive value of the standard Gibbs free energy of transfer $\Delta G^\circ_t(X, A \rightarrow B)$ means that the ion prefers A, and the preferential solvation $\delta_{X,A}$ is mostly positive, meaning that there is an excess of A in the vicinity of the ion over its fraction in the bulk solvent. A negative sign of $\Delta G^\circ_t(X, A \rightarrow B)$ denotes the preference of the ion for being surrounded by the solvent B. There is also an important effect of the mutual interactions between the two solvents; $G^E_{A,B}$ represents the effects of repulsion (positive values) or attraction (negative values) between solvent molecules.

The values of the excess Gibbs free energy of mixing for the solvents used in this study are reported in Table A.2.

Solvent A	Solvent B	$\Delta G^E_{A,B}$ (x = 0.5) [J mol^{-1}]
water	ethanol	727
water	methanol	300
water	ACN	1316
water	acetone	1140
water	DMF	-339
water	DMSO	

Table A.2: The binary solvent systems studied and their excess Gibbs free energy of mixing

The quasi-lattice theory stipulated that the lattice parameter, Z, does not depend on the ion that is considered as a solute for a given pair of solvents. Barbosa et al. [111] suggested to consider Z = 6, since the effect of employing values between 6 and 12 on the final solubility parameter was found to be very small by other authors [105], while Marcus [112] proposed to calculate it from the lattice parameters of the two solvents.

Finally, Equation A.1 becomes:

$$x_A^L = \frac{1}{1 + \left(\frac{N_{B,B}}{N_{A,A}}\right)^{\frac{1}{2}} \cdot exp(\Delta_{A,B}/2)} \tag{A.15}$$

The theory was applied to calculate the preferential solubility parameters of the ions involved in this study, and the profiles compared with data from literature. [62, 63]. The slight disagreement between the profiles calculated in this study and the literature data was accepted, as the data in [62] and [63] were calculated by using a different theoretical approach. The trend with concentration is satisfactorily reproduced for all ions.

Appendix B

Experimental design and results of peptide nanofiltration (cf. Chapter 6)

Table B.1: Experimental design and results for nanofiltration of PEP_1 solutions through Inopor Nano 750.

Run	$\mathbf{C}_{PEP_1}$ [g l^{-1}]	**%v TFA**	**Pressure [bar]**	**Pump freq. [Hz]**	**%v ACN**	$\mathbf{Rej}_{PEP_1}$	$\mathbf{Rej}_{TFA-H}$	$\mathbf{J}_{v,PEP_1}$ [l m^{-2} h^{-1}]
1	3	0.06	6	35	15	96.9	25.5	17.7
2	1	0.02	2	45	0	83.3	23.8	8.4
3	1	0.02	10	25	0	83.4	18.7	29.0
4	5	0.1	2	25	30	99.9	39.9	11.6
5	5	0.1	10	45	30	99.9	18.2	52.7
6	5	0.1	2	45	0	96.5	11.0	6.6
7	5	0.1	10	25	0	96.0	13.4	23.2
8	3	0.06	6	35	15	97.9	20.6	18.5
9	1	0.1	2	45	30	98.4	3.1	12.4
10	1	0.1	10	25	30	97.2	24.8	44.6
11	1	0.02	2	25	30	96.6	35.2	9.5
12	1	0.02	10	45	30	96.2	30.4	45.2
13	5	0.02	2	25	0	92.1	40.5	4.2
14	5	0.02	10	45	0	92.9	35.7	19.9
15	1	0.1	2	25	0	99.8	4.2	8.5
16	1	0.1	10	45	0	99.8	8.7	34.8
17	5	0.02	2	45	30	95.7	42.4	8.9
18	5	0.02	10	25	30	95.2	53.1	32.3
19	3	0.06	6	35	15	97.0	17.0	18.0

Table B.2: Experimental design and results for nanofiltration of P3 solutions through Inopor Nano 450.

Run	$\mathbf{C}_{P3}$ [g l^{-1}]	**pH**	**P** [bar]	**Pump freq.** [Hz]	%**v** **ACN**	$\mathbf{Rej}_{P3}$ %	$\mathbf{Rej}_{TFA-H}$ %	$\mathbf{J}_{v,P3}$ [l m^{-2} h^{-1}]
1	6	3.5	10	35	30	99.6	25.3	19.4
2	2	2	5	45	10	99.9	12.4	13.7
3	2	2	15	25	10	99.7	30.0	30.6
4	10	5	5	25	50	99.1	13.9	3.7
5	10	5	15	45	50	99.1	15.3	10.8
6	6	3.5	10	35	30	99.7	23.4	17.6
7	10	2	15	45	10	99.9	37.7	40.9
8	10	2	5	25	10	99.9	20.7	12.5
9	10	5	5	45	10	99.8	22.7	6.4
10	10	5	15	25	10	99.5	32.9	14.6
11	2	5	5	45	50	99.3	2.8	5.1
12	2	5	15	25	50	98.8	4.6	11.7
13	6	3.5	10	35	30	99.8	27.0	15.3
14	10	2	5	45	50	99.9	16.9	27.1
15	10	2	15	25	50	99.8	20.7	64.2
16	2	2	5	25	50	99.8	13.7	17.5
17	2	2	15	45	50	99.8	12.9	61.2
18	2	5	5	25	10	99.7	11.5	8.8
19	2	5	15	45	10	99.8	24.7	26.8
20	6	3.5	10	35	30	99.7	25.3	21.7

Table B.3: Experimental design and results for nanofiltration of P2-S-SM solutions through Inopor Nano 750.

Run	$\mathbf{C}_{P3}$ [g l^{-1}]	**pH** **pH**	**P** [bar]	**Pump freq.** [Hz]	%**v** **ACN**	$\mathbf{Rej}_{P2-S-SH}$ %	$\mathbf{Rej}_{TFA-H}$ %	$\mathbf{J}_{v,P2-S-SH}$ [l m^{-2} h^{-1}]
1	3	3.5	6	35	50	34.1	19.8	118.7
2	1	2	2	45	30	19.6	23.1	46.1
3	1	2	10	25	30	14.1	18.6	185.7
4	5	5	2	25	70	98.5	17.9	35.9
5	5	5	10	45	70	98.4	18.3	183.3
6	1	5	2	25	30	3.6	17.2	34.3
7	1	5	10	45	30	9.9	15.5	154.8
8	3	3.5	6	35	50	39.4	20.5	122.9
9	5	5	10	25	30	80.7	15.7	31.4
10	5	5	2	45	30	86.1	12.1	120.0
11	5	2	2	45	70	53.4	26.8	53.6
12	5	2	10	25	70	37.4	21.1	211.1
13	5	2	2	25	30	27.2	15.1	30.3
14	5	2	10	45	30	38.4	13.5	135.3
15	3	3.5	6	35	50	42.4	19.4	116.1
16	1	2	2	25	70	50.7	30.6	61.2
17	1	2	10	45	70	46.6	29.9	208.5
18	1	5	2	45	70	28.9	24.9	49.7
19	1	5	10	25	70	17.1	18.9	190.0
20	3	2	2	25	30	20.3	14.5	29.0
21	3	2	10	45	30	28.9	12.4	124.0
22	1	2	2	35	70	52.1	32.2	64.5
23	1	2	6	25	70	48.7	27.4	164.1

24	1	3.5	10	45	70	47.1	25.2	201.3
25	5	3.5	2	45	70	46.1	23.6	47.2
26	1	2	6	45	30	26.7	19.4	116.1
27	5	2	2	35	30	20.0	14.8	29.5
28	1	5	10	25	30	6.1	12.6	125.9
29	5	5	2	25	30	83.2	12.1	24.2
30	3	3.5	6	35	50	42.3	16.6	99.5
31	1	2	2	25	50	45.5	24.2	48.4
32	2	5	10	25	50	38.7	16.6	165.9
33	3	3.5	6	35	50	45.1	16.7	100.0